AN EXPERIMENTAL AND NUMERICAL STUDY OF PLUG FORMATION IN VERTICAL PIPES DURING CRYOGENIC PIPE FREEZING

by

Mark John Burton

Submitted for the degree of Doctor of Philosophy 1986

UNIVERSITY OF SOUTHAMPTON

DEPARTMENT OF MECHANICAL ENGINEERING

UNIVERSITY OF SOUTHAMPTON

ABSTRACT

FACULTY OF ENGINEERING AND APPLIED SCIENCE

MECHANICAL ENGINEERING

Doctor of Philosophy

AN EXPERIMENTAL AND NUMERICAL STUDY OF PLUG FORMATION IN VERTICAL PIPES DURING CRYOGENIC PIPE FREEZING

by Mark John Burton

Pipe freezing, the method and its application are reviewed together with previous research into this and closely related problems. In particular the research carried out by the Southampton University Pipe Freezing Group is summarised.

The Construction of an experimental rig is described together with details of its instrumentation to measure the temperature profiles and heat flow during pipe freezing.

The experimental results are analysed and a hypothesis to rationalise the observations is put forward. This is that, when pipe freezing water in vertical pipes, plug formation occurs in three phases. During Phase One the boundary layer due to natural convection exists from above the freezing zone to below it. Phase two is commenced when the growing plug has reduced the orifice sufficiently to allow the water returning up the centre of the pipe to mix with the water in the natural convection boundary layer. The water in the centre moving upwards is turned near the centre section of the plug to flow downwards over the lower part of the plug. Natural convection in the upper part of the freezing zone is very significantly reduced to leave a "sump" of cooled water in this volume which freezes more rapidly than the remainder of the plug. Phase three of plug formation covers the axial extension of the plug after initial freeze-off.

The various mathematical modelling techniques for use with moving boundary problems, such as pipe freezing, are reviewed. The development of a one-dimensional finite difference computer model, specific to the pipe freezing problem, is described and results from it are compared to those obtained experimentally.

Acknowledgements

The Author would like to record his thanks to the following people and institutions :

To Dr. D.A.Wigley, his supervisor, for help, advice, encouragement and especially for invaluable general comments on the subject of heat flow and temperature gradients.

To Mr. R.J.Bowen, for providing the initial expertise on the subject of finite difference models and for the many hours spent discussing their application to this particular problem.

To Mr. W.J.Gibbs, for his invaluable assistance in the detail design, construction and operation of various experimental rigs.

To Mr. P.Harris, for his help with the many instrumentation problems experienced.

To S.E.R.C. for providing a maintenance grant as well as other financial support for the experimental program

To Conoco U.K. ltd., for financial support through a CASE studentship, assistance with the literature search and for the provision of an interesting insight into the practicalities of industrial pipe freezing. In particular, thanks to D.Leadbetter, D.Hurden, R.Ganguly and the staff at the Conoco Information Centre.

To the British Oxygen Company, British Petroleum ltd., Cryoservice ltd., the Department of Energy, Liquidair ltd., Mobil ltd., Shell ltd and the Swedish State Power Board.

To Mrs. J.Halliday for typing much of this thesis.

Contents

Contents (continued)

Contents (continued)

Contents (continued)

Contents (continued)

List of Figures

List of Figures (continued)

Nomenclature

A	Area, m^2
C	Specific Heat, kJ/kgK
C_a	Apparent Specific Heat, kJ/kgK
C_L	Liquid Specific Heat, kJ/kgK
C_S	Solid Specific Heat, kJ/kgK
C_W	Pipe Wall Specific Heat, kJ/kgK
C_*	$(C_L + C_S)/2$
D_{iw}	Pipe Inner Diameter, m
D_{ow}	Pipe Outer Diameter, m
Fo	Fourier Number
Fo_e	Modified Fourier Number
G	Temperature Gradient, K/m
H	Enthalpy, kJ/kg
h	Time Step Counter
h_c	Convective Heat Transfer Coefficient, W/m^2K
j	Node Counter
k	Thermal Conductivity, W/mk
k_L	Liquid Thermal Conductivity, W/mk
k_S	Solid Thermal Conductivity, W/mk
k_W	Pipe Wall Thermal Conductivity, W/mk
k_*	$(k_L + k_S)/2$
L	Latent Heat of Fusion, kJ/kg
M	$\alpha\ \delta t/\delta x^2$
m	Number of Nodes in Solid and Liquid
N	$k\ \delta t/\rho\delta x^2$
n	Number of Nodes in Pipe Wall
$\hat{n}$	Normal Vector
Pr	Prandtl Number
Q	Heat Flow Rate, W
q	Heat Flux, W/m^2
Re	Reynolds Number
r_j	Nodal Radius, m
r_1	Inner Radius of a Hollow Cylinder, m

Nomenclature (continued)

r_2	Intermediate Radius of a Hollow Cylinder, m
r_3	Outer Radius of a Hollow Cylinder, m
r_i	Interface Radius, m
r_{it}	Radius of Inner Tube, m
r_{iw}	Inner Radius of Tube, m
r_{ow}	Outer Radius of Tube, m
T	Temperature, K
T_L	Liquid Temperature, K
T_S	Solid Temperature, K
T_W	Pipe Wall Temperature, K
T_f	Freezing Temperature, K
T_o	Temperature on surface of a semi-infinite slab, K
T_∞	Temperature at infinity of a semi-infinite slab, K
$T_{j=1}$	Nodal Temperature (at node 1), K
T_b	Bulk Liquid Temperature, K
T_{ow}	Outer Pipe Wall Temperature, K
T_{iw}	Inner Pipe Wall Temperature, K
T_a	Initial Temperature, K
T_c	Coolant Temperature, K
T_1	Inner Surface Temperature on a Hollow Cylinder, K
T_2	Intermediate Temperature in a Hollow Cylinder, K
T_3	Outer Surface Temperature on a Hollow Cylinder, K
T_{il}	Water Inlet Temperature, K
T_{ou}	Outer Water Bath Temperature, K
T_{in}	Inner Tube Temperature, K
t	Time, s
t_b	Time to Tube Blockage, s
V	Volume, m^3
X	Solid (frozen) Layer Thickness, m
x	distance, m
α	Thermal Diffusivity, m^2/s
α_L	Liquid Thermal Diffusivity, m^2/s
α_S	Solid Thermal Diffusivity, m^2/s

Nomenclature (continued)

α_W	Pipe Wall Thermal Diffusivity, m^2/s
α_{LS}	α_L/α_S
β	Dummy Variable in Definition of the Error Function
ΔT_{ou}	Outer Temperature Difference, $(T_{ou} - T_f)$, K
ΔT_{in}	Inner Temperature Difference, $(T_f - T_{in})$, K
δE	Loss of Sensible Energy from an Element, kJ
δE_L	Loss of Latent Heat, kJ
δt	Incremental Time Step, s
δx	Nodal Spacing, m
δr	Nodal Spacing (radial), m
δr_L	Nodal Spacing in Liquid, m
δr_S	Nodal Spacing in Solid, m
δr_W	Nodal Spacing in Pipe Wall, m
ΔT	Temperature range for Apparent Specific Heat, K
ξ	Transformation, r/r_i
η	Similarity Transformation
θ	Freezing Parameter, $(T_f - T_c)/(T_{il} - T_f)$
λ	Transformation for Solid in Computer Model
ρ	Density, kg/m^2
ρ_L	Density of Liquid, kg/m^2
ρ_S	Density of Solid, kg/m^2
ρ_W	Density of Pipe Wall, kg/m^2
σ	Transformation for Liquid in Computer Model
τ	Time Constant
ϕ	Temperature Penetration Depth, m
ψ	Transformation for Pipe Wall in Computer Model
ω	Boundary layer thickness

Summary

Cryogenic pipe freezing is an industrial technique used to temporarily seal-off pipes and pipelines for repair or maintenance by freezing their contents using some cryogen applied to the outside of the pipe. This thesis covers in detail the results of the Author's four year research programme into the heat and fluid flow aspects of freezing vertical pipes, as well as summarising, in rather less detail, the results of the Southampton University pipe freezing group's research on other aspects of pipe freezing.

Section 1.1 outlines the origins of pipe freezing just after the 2nd world war and its subsequent development as an aid to leak detection. Leaks in long pipelines were pinpointed by freezing a plug in the pipe and hydrostatically pressurising against it. The leak was thus known to be one side or other of the plug and, by using repeated freezes in a kind of 'binary halving' method, the leak could be located. Section 1.2 describes the main features of the three principle methods of pipeline plugging; 'Hot' tapping, 'Cold' tapping and Cryogenic pipe freezing. 'Hot' tapping is the most general of these and it may be applied to pipes whose contents are gaseous or liquid and at a high temperature or pressure. 'Cold' tapping is applicable mainly to gas pipe lines and these must be depressurised. Cryogenic pipe freezing may only be used (with one exception - see section 1.4.6) on pipes completely full of liquid, which should ideally not be too hot. Very high pressures however, can be tolerated; ice plugs have been pressure tested up to 87 MN/m^2 (10,000 psi). The range of fluids that have been frozen includes many oils, chemicals and liquid sludges. Care is needed when freezing some types of pipe using liquid nitrogen because of embrittlement of the pipe wall at very low temperatures. In addition, the initial direct contact of liquid nitrogen creates a large temperature gradient across the pipe wall, which causes significant thermal stresses, although these do not appear to reach the yield stress. To reduce the thermal stress problem, a technique known as controlled temperature freezing

has been developed in which a heat transfer medium such as iso-propanol is interposed between the liquid nitrogen and the pipe to limit both the cooling rate and the minimum temperature. In section 1.3 the relative merits of 'Hot' and 'Cold' tapping and pipe freezing are assessed. Section 1.4 reviews the reported applications of pipe freezing in various branches of industry. The most notable of these are two freezes conducted on the Shell/Esso Dunlin Alpha and Brent C platforms. The Dunlin freeze was made on a 400 mm (16") pipe, 81m below sea level, in a platform leg. The Brent freeze, which was maintained for 21 days, was also performed in a platform leg, this time 55m below sea level on a 500 mm (20") line. Other reported applications include a 1m (40") diameter test freeze, pressurised to 8.5 MN/m^2 (1000 psi) and some smaller freezes on contaminated water for the nuclear power industry. In section 1.5 the possible extension to sub-sea freezing is briefly examined, although no research or development has yet taken place in this direction.

Section 1.6 reviews some of the more relevant experimental work on freezing, conducted outside the Southampton University pipe freezing group. Most of this research concerns problems significantly different from commercial pipe freezing, by nature of their geometry or temperature regime, so the results are not directly applicable. The most interesting work was that conducted by Gilpin [31] into the flow freezing of water. Separation of the boundary layer in the area where the ice walls were diverging on the downstream side of a plug was found to cause increased heat transfer and hence some remelting of the ice. In this way the neck (the narrowest part of the plug) was seen to migrate upstream. Further necks were then established downstream and these in turn also migrated upstream. It should be stressed that in this research, the freezing section was 45 diameters long whereas, in pipe freezing, typical length to diameter ratios are around 2 to 4.

The three major areas of interest to the overall pipe freezing research programme are identified in section 2.0. They are ;

(i) Mechanisms of plug formation and its limiting factors, (ii) Measurement of stresses induced by shock cooling and plug formation and (iii) Determination of the strength of the frozen plug. Section 2.1, which deals with plug formation, is subdivided into three sections covering static water freezes, flowing water freezes and hydrocarbon freezes.

Static water freezes have been performed on 100, 150 and 300 mm (4, 6 and 12") diameter pipes. Freezing times were found to be approximately 13, 30 and 130 minutes respectively and liquid nitrogen consumption was found to be in the region of 60 to 70 litres for the 150 mm pipe and 410 litres for the 300 mm diameter pipe. These results suggest that the time to freeze is approximately proportional to the pipe diameter squared and that the liquid nitrogen consumption is proportional to the diameter cubed.

The Southampton investigation into the freezing of flowing water has concerned itself mainly with establishing the limiting conditions of inlet temperature and flowrate that allow the flow to be stopped. This freeze/no freeze boundary has been determined for 50 mm (2") diameter pipes made from mild steel, stainless steel, UPVC and GRP. The results are shown in figure 2.3; the mild steel and stainless steel boundaries are almost coincident, whereas those for the plastic pipes are an order of magnitude lower. Neck migration and secondary neck formation, of the type observed by Gilpin [31], has been observed in a 100 mm (4") diameter pipe.

Preliminary work on the freezing of hydrocarbons has shown up two problems. The first is that the freezing points, although they are known to be lower than water, are not precisely definable since the material slowly becomes more viscous, finally solidifying, over a temperature range. The second problem is that they all exhibit much stronger natural convection than water, particularly diesel, paraffin and gas oil.

The group's effort in determining pipe wall stresses during freezing (Section 2.2), has so far been expended mainly in the direction of establishing the technique of reliable strain measurement. The principle difficulty was to separate the large thermally induced apparent strains, which have no stress associated with them, from the strain gauge readings. This net strain value could then be used for calculating stress levels. Two 50 mm (2") diameter mild steel pipes have been instrumented to measure strain, one being longitudinally free and the other longitudinally constrained. The hoop and longitudinal peak stress levels observed during initial cooling were around 40% of the yield stress for the unconstrained pipe, rising to 75% for the constrained one. However, residual stresses were much lower when thermal equilibrium was established, with a compressive hoop stress set up in the unconstrained pipe.

Research into the strength and pressurisability of the frozen plug is split up into work on ice plugs and on hydrocarbon plugs. The mechanisms of failure of the two types of plug are quite different. Ice plugs fail at the interface with the pipe wall, where the shear stress is greatest. In contrast, hydrocarbons fail by extruding the relatively warm, and therefore weaker, centre out of the plug.

Various attempts to measure the interfacial shear stress of ice directly by shearing thin layer of ice between two concentric cylinders have been only partially successful as it appears to be very difficult to simulate pipe freezing conditions adequately, in such circumstances. Direct hydrostatic pressurisation of ice plugs has, however, indicated that pressures in excess of 2000 psi may be withheld. The cooling sequence has been shown to be important to the integrity of the plug. For instance, a plug held at a constant temperature of around $-70^{o}C$ was found to move under an applied pressure of 800 psi. Further rapid cooling down to liquid nitrogen temperature weakened the bond between the plug and the pipe wall to

the extent that it would move under an applied pressure of only 120 psi., but subsequent slow rewarming to -140°C over a period of 5.5 hours increased its pressure holding capability to over 2000 psi. The relative expansion of ice and the pipe wall, which causes cracking of the ice and refreezing of the water, is thought to be the cause of these observations. A 300 mm (12") diameter ice plug was successfully tested to 1600 psi.

The strength of frozen hydrocarbons (Section 2.4) was initially investigated qualitatively by withdrawing thin rods from samples of the oils frozen to different temperatures. This enabled a wide range of crude oils and products to be ranked against each other; figure 2.5 illustrates these results. Quantitative results have been obtained by freezing and pressure testing plugs of Diesel, Forties crude and Statfjord crude. The latter of these has been tested in 50 mm (2") diameter pipes to 3500 psi as well as in larger pipes (150 and 300 mm diameter, 6 and 12") to 1500 psi. The relationship between temperature and pressure resistance indicates that the temperature at the centre of the plug must be reduced below -130°C, in order to withhold pressures in excess of 1500 psi.

The development of the 100 mm (4") diameter vertical freezing rig, in which all the authors experimental data was obtained, is traced in chapter 3. The main difficulties experienced with this rig concerned the thermocouple instrumentation. It was necessary to make a large number of temperature measurements at short time intervals, which dictated the use of computerised data acquisition equipment. Because it was hoped to detect quite small temperature differences, rigorous calibration procedures became necessary both for the analogue to digital converters and for the thermocouples themselves. A machine code program had to be written to enable readings to be taken, processed and stored quickly enough. Initially the pipe was frozen as an isolated section 600 mm (24") in length, but after the first set of data was obtained a large tank was fitted to the bottom flange of the pipe to enable the bulk water temperature to

be maintained throughout the freeze. The full effects of natural convection could now be observed using the larger volume of water.

In Chapter 4 the data taken from the rig described above, is analysed and a theory about the mechanism of plug formation in vertical pipes is postulated. The results from the first set of freezes, made without the tank in place, are dealt with first. Ten freezes were performed with initial temperatures varying from 6.5 to 50°C. Figure 4.2 illustrates the variation of time to freeze with initial temperature. Four times have been plotted for each freeze: the times for the centre to reach 0, -60 and -140°C and the time for the plug to attain a length of 100 mm (4") at its centre. Figures 4.3a - 4.7a show the interface positions during freezes from initial temperatures of 10, 20, 30, 40 and 50°C.

Three phases of plug formation can be identified from these results. During phase one the plug grows inwards until it is approximately parallel sided with a central orifice diameter of about 25 to 30 mm. In phase two the top section of the plug starts to freeze inwards faster than the centre and bottom sections and the plug freezes off first somewhere in the upper part of the freezing volume. This is then followed by a very rapid extension downwards. Phase three covers the further more gradual axial extension of the plug.

The pattern of natural convection is thought to change at the transition from phase one to phase two. In phase one a boundary layer starts somewhere above the freezing volume and flows downwards over the whole of the growing plug. By continuity, an upwards return flow of equal volume flowrate must exist in the centre of the pipe. As the plug grows inwards, there comes a time when the boundary layer and the return flow begin to interfere with one another. Phase two begins when the upward flow is reversed at about the narrowest part of the plug and becomes the downward flowing boundary layer. Figure 4.8 shows the convection patterns for phase one and phase two. In phase two a relatively stagnant area exists in the upper part of the plug in

which natural convection is eliminated or at least severely restricted. This allows more rapid plug growth in this area, which is why the plug freezes first near the top section.

The various factors affecting the radial temperature profile are examined in section 4.1.3 and the observations are shown to support the above theory of plug formation. The temperature data has been processed by a computer program to determine the rates of latent and sensible heat loss from the water, ice and pipe wall. As would be expected, the rate of energy loss from the volume above the freezing site increases at the transition from phase one to phase two because its bulk water temperature is no longer being maintained by natural convection from below. By calculating the total heat loss from the pipe and assuming that heat conducted into the pipe outside the freezing section is negligible, the mean heat flux over the area of pipe immersed in liquid nitrogen can be estimated. Peak mean heat fluxes in the range of 60 to 80 kW/m^2 have been observed. Furthermore, all parts of the immersed section of pipe do not cool down at the same rate and it is clear that the transition from film to nucleate boiling occurs first in the lower part of the nitrogen jacket and then moves upwards. This means that the peak local heat fluxes must be considerably higher than the mean values mentioned above.

Section 4.2 covers the analysis of data taken from freezes performed with the large tank in place below the pipe in order to maintain natural convection. Six freezes were performed in this configuration, one each from initial temperatures of 20, 30, 40 and $53^{o}C$ and two from $45^{o}C$. These latter two freezes will be dealt with separately since their results are totally anomalous. The freeze from $53^{o}C$ had to be abandoned because the liquid nitrogen supply ran out, but the indications were that, given sufficient time and nitrogen, this freeze would have proved successful. The times to freeze for the remaining three experiments are shown plotted in figure 4.17, in which the times for the previous series of freezes without the tank are also shown for comparison. It may be seen that with an initial temperature

of 20°C, the time to freeze is almost completely unaffected by the addition of the tank. At higher temperatures, maintenance of the bulk water temperature in the freezing volume considerably slows plug formation. Figures 4.4b - 4.6b illustrate the interface positions during these three freezes. During the freezes from 30 and 40°C, the plug growth on the lower face of the plug is almost completely halted due to the very high rate of convected heat transfer to the ice in this area. The convected heat transfer rate is related to the thickness of the boundary layer, a thin boundary layer giving a high heat transfer coefficient. Because the boundary layer in phase two begins somewhere in the centre of the plug, instead of on the pipe wall above it as is the case during phase one, its thickness over the lower part of the plug is much reduced, which explains the higher heat transfer rate.

As mentioned above, two freezes with an initial temperature of 45°C exhibited an entirely different freezing mechanism from all the other freezes. The basis of this mechanisms appears to be a small stable recirculating convection 'cell', in which the water is relatively isolated from the rest of the water in the rig. Therefore this water cools and freezes very quickly. Two of these 'cells' are then established, one above and one below the short plug that has formed. These cells move slowly up and down the pipe extending the plug axially as shown in figure 4.19 which indicates the interface positions. This phenomenom is not likely to be very important in the freezing of water, since the circumstances under which it occurs appear to be quite limited. However it does indicate another freezing mechanism which may be more prelevant in the freezing of other fluids.

Section 4.3 examines the results of a single freeze performed with modified and improved outer pipe wall thermocouple instrumentation, which enabled local heat fluxes to be estimated by measuring the temperature difference across the pipe wall. The principle findings from this work are that transition from film to nucleate boiling seems to occur at higher pipe surface temperatures

than had been expected and that the peak heat flux after transition could be very high, in the region of 150 kW/m^2.

The chapter dealing with computer modelling opens with a review (Section 5.1) of various methods, both analytical and numerical, of solving moving boundary problems. The numerical approach is identified as being the most general and hence the most realistic way to model the pipe freezing process. The finite difference method is explained in section 5.1.2 and various methods of applying it to moving boundary type problems are examined. Section 5.2 reviews some models written by other authors which have some relevance to the present problem.

The model developed by the current Author is a one-dimensional, pure conduction solution. The assumptions inherent in this are that there is no longitudinal heat flow up or down the pipe and that heat is transferred in the pipe, the ice and the water purely by conduction, i.e. there is no convection in the water. The former may be a reasonable assumption on the centre section of a freeze, the latter is allowable only where the initial water temperature is fairly low, or where the geometry of the pipe is such as to inhibit significant natural convection (as was the case in the first series of experimental tests without the tank in place). A convective outer boundary condition is used, based on data for the pool boiling of liquid nitrogen published by Flynn et al [53] for nucleate boiling and by Hanson and Richards [54] for the film boiling regime.

The physical significance of the equations which allow for the moving interface is discussed in section 5.4, with the object of explaining the slight discrepancy that sometimes exists between the sensible and latent heat lost and the cumulative total of heat convected into the liquid nitrogen. In section 5.4.2., the effect of varying pipe diameter on predicted time to freeze is examined. Wall thickness was set at a constant fraction (1/16th) of the pipes inner diameter, all other factors being kept constant. Figure 5.3

illustrates the results and compares them with available experimental data. As can be seen the agreement with experiment is quite good. The model prediction of time to freeze has also been compared with experimental data for varying initial temperatures, as shown in figure 5.5 (The experimental data is taken from the series of freezes carried out in the short isolated pipe without the tank in place. This arrangement restricts natural convection and gives conditions that are more consistent with the assumptions of the model.). The model consistently gives a slight over-estimate of the time to freeze, but the slope of the line relating time to freeze with initial temperature is in very good agreement with experiment. It is thought that this over estimation of time to freeze may be due to the use of a liquid nitrogen convective heat transfer relationship that gives lower heat fluxes than is suggested by the analysis described in section 4.1.5. Finally, section 5.4.5 describes the effect of varying the five thermal properties on the time to freeze. The properties varied were the latent heat and the thermal conductivities and specific heat capacities of the pipe wall and the ice/water. The results indicate that for freezing a 100 mm diameter, 6.25 mm wall thickness mild steel pipe containing water, the most important thermal property is the ice/water thermal conductivity, followed by the latent heat. Varying the value of these properties by a factor of ten changes in the time to freeze by the same order of magnitude. By contrast, varying the thermal conductivity of the pipe wall by the same amount had almost no effect at all on the time to freeze.

The principle recommendations for further experimental work made in section 7.0, are to investigate the effect of different pipe diameters and orientations on the freezing mechanism of water and to perform similar work on some hydrocarbons. The one-dimensional model should be extended to cover the effects of natural convection at the ice/water interface and a separate model should be written to predict the freezing of fluids which freeze over a temperature range, as is the case with most crude oils and products.

Appendices I and II give the derivation of the radial heat conduction equation both for a constant and linearly temperature dependent thermal conductivity. The detailed derivation of the equations used in the model is given in appendix III. Appendix IV illustrates the alternative control volume approach to formulating finite difference equations.

1.0 Introduction to Pipe Freezing

1.1 Pipe freezing as a leak detection aid

The Cryogenic pipe freezing technique was developed when the need arose to recommission a wartime pipeline in Britain. When a pipeline is to be tested it is pressurised to its test pressure. If leakage is detected, then the traditional methods used to locate the leak are as follows [1]. The first attempt is usually by men on foot, in vehicles or aircraft, traversing the length of the pipeline to look for wet spots in the ground. The success of this method depends upon generally dry ground so rain or marshland render it useless. If a visual inspection of the pipe line route fails to locate the leak then some dye or odoriser may be injected into the pipeline to aid visual inspection on the ground. Neither of these approaches will be of any use in the case of a sub-sea pipeline except that dye might be detectable in shallow water. If the leak remains undetected some form of listening devices may be employed, but they must be applied directly to the pipe and so this requires the pipe to be exposed at intervals along its length.

Before the development of freezing techniques, if the foregoing methods did not locate the leak, then the following highly expensive and time consuming procedure had to be followed. The pipeline would have to be drained down and then exposed at its midpoint. It would be cut here and manifolds attached to allow each half of the pipeline to be filled and re-pressurised. This would allow engineers to determine which half of the pipeline contained the leak. This half of the pipeline would then be cut at its midpoint and so on until the fault is located. At each test the pipeline must be emptied and refilled and a considerable amount of machining and welding performed on the pipe. Once the leak has been detected, there still remains the task of repairing all the breaks that have been made in the pipe.

There is now a viable alternative to this last stage of leak detection in the form of cryogenic pipe freezing. This method proceeds as follows. If a leak is detected and visual and acoustic methods of locating it fail, then the test pressure is maintained. The midpoint of the pipe is exposed and a freezing jacket is clamped around the pipe. Liquid nitrogen is poured into this annulus and an ice plug, capable of withstanding very high pressure, is formed in the pipe. Figure 1.1 is a general illustration of the equipment involved and the ice plug growth. Monitoring the pressures on either side of the frozen plug and the rate at which water is being added to maintain the test pressure will indicate on which side of the plug the leak is occurring. The freezing jacket is then removed and placed on the pipeline at the midpoint of the half that is known to leak. By the time preparations for the second freeze are complete, the first plug should have thawed. By performing 10 freezes on a 20 km pipeline, the location of the leak may be pinpointed to within 20 m.

Throughout the process there is no need to drain and refill the pipe, and no cuts are made that must subsequently be repaired and retested. The equipment required is substantially less than before, the main items being a freezing jacket and a liquid nitrogen tanker. The manpower required is also substantially reduced.

Pipeline companies who have used the pipe freezing technique have reported savings of between 50 and 60%. Brister Inc. (U.S.A.), who were involved in developing the technique, also point out [2] that the technique is useful for isolating sections of a pipeline that have different test pressures due, for example, to changes in elevation. Conoco/Deplancke [3] report using the technique successfully on a 550mm diameter (22") pipeline with dry ice and iso-propanol as the coolant. Since the pipeline was 22.7 km (14 miles) long, conventional techniques would have involved the emptying and filling of the pipe with 5.6 million litres of water. Using three open trough jackets, two pinhole leaks were located to within one mile. Final location of the leaks was by nitrous oxide detector units.

With cryogenic pipe freezing developed for pipeline testing, its potential as a more general tool for pipeline plugging, during repair or modification, was obvious. The cost, due to lost production and revenue, of shutting down some of today's plant or pipelines can be enormous. There are now three major options available to engineers requiring to plug pipes, which all aim to eliminate or reduce downtime.

1.2 Pipeline plugging techniques

1.2.1 'Hot' tapping

The first and most general of these is known as "Hot tapping" or sometimes "Pressure tapping". T.D. Williamson Inc., Tulsa, U.S.A., are major exponents of this technique which is outlined in their papers, references [4] and [5]. Briefly the idea is as follows:

A split tee is bolted or welded around the pipe where it is to be tapped. The branch of the tee is flanged, and to this is bolted a sandwich valve. The tapping machine, which is attached to the top flange of the sandwich valve, contains a cutter of either the trepanning or hole saw type which is lowered through the open valve onto the pipe. The cut is effected and the cutter, which is designed to retain the coupon (i.e. the cut out section of the pipe) and prevent it from falling into the line, is withdrawn through the sandwich valve. The valve is then closed, and the tapping machine removed. The tee and sandwich valve may now be used for one of two purposes. Firstly, a new pipe may be coupled to the valve to establish a bypass. Alternatively, a plugging device may be inserted into the line to halt the flow. Figure 1.2 illustrates the sequence of operations.

There are a variety of plugging devices available [4], and choice is governed by the type of product in the line, pressure and

temperature. One such is an expanding cylinder type, split into segments so that it can be expanded, and surrounded by a resilient cover. Use of this plug requires an oversize tee so that the tap, which in all cases must be greater than the pipe internal diameter, passes through the bottom of the pipe as well. The cylinder is lowered into the tee and expanded, sealing the pipe. This type of device is often used for gas installations; it has high temperature applications but is limited to around 5.2 MN/m^2 (600 psi) pressure.

A second example is the paddle-type plug. This consists of a rubber paddle sandwiched between metal plates, so that when pressure is applied from the top, the rubber is forced to follow the contours of the pipe inner surface, and seal it. These plugs have applications in the medium pressure and temperature ranges.

The third type of plug is the cup type (as illustrated in figure 1.2), designed for high pressure use up to 10.4 MN/m^2 (1200 psi). Here the head swivels into position as the plug is lowered. The cup type seal uses the pressure in the line to help effect a seal.

Since these plugs are usually installed as a temporary measure it is desirable to be able to reseal the pipe after use in a way which allows the removal of the sandwich valve. For this reason, the inside of the top flange of the split tee normally contains a number of segments which can be moved inwards. A grooved completion flange plug is inserted through the sandwich valve. It has a neoprene 'O' ring seal and can be locked in position at the top of the tee by moving the segments mentioned above into the locking groove (as shown in Figure 1.2). With this plug in place, the sandwich valve may be removed.

'Hot' tapping is the only technique which will allow modification or repairs to lines without stopping the flow at all, since it allows the installation of a bypass. To accomplish this requires four taps. The first two, on each side of the working area,

are made and a temporary bypass line is installed between the outlets of the two sandwich valves. Two more taps are now made just inside the bypass connections to allow plugs to be inserted. When using cup type plugs, it is important that, in order to avoid the flow pushing the plug into position, the downstream plug is inserted first and removed last. Figure 1.3 illustrates the set up.

Thus, if no interruption of the product flow is permissible, then there is no alternative to the use of 'hot' tapping. If some stoppage is allowable, then alternatives become available.

1.2.2 'Cold' tapping

'Cold' tapping is a system developed by Total Marine Norsk in conjunction with A/S Konigsberg Vapenfabrikk and Comex Services, specifically to allow repairs to Totals twin 800mm (32in) dia., 365km long Frigg-St.Fergus natural gas pipeline, without the need to flood and re-dry the entire pipeline. With the construction of suitable equipment, the technique could be used on any gas line, and, if the working area of the pipe could be cleaned, the developers see no reason why the process could not be extended for use on oil pipelines [6]. The technique is known as 'cold' tapping because the flow must be stopped and the pressure reduced to ambient. The sequence of operations is shown in figure 1.4. Initially the equipment and procedure are similar to 'hot' tapping, except that the outlets of the split tee, the sandwich valve and the tapping machine are inclined at 45 degrees to the pipeline. Two of these inclined taps are made, one either side of the working section, then the tapping machines are removed. Next, specialised "plug launchers" are attached to the sandwich valves. The plugs in this case are inflatable rubber drums, 1.5m long with 15mm walls [7], that are just smaller in diameter than the inside of the pipe, but when inflated to 3-3.5 MN/m^2 will grip the pipe wall firmly. The plug launchers use the slight flexibility of the deflated plugs to push them around the 45 degree bend in the tees and then about 3m up the pipe away from the damaged area. The plugs

are inflated and the repair site is now isolated. The section of pipe containing the damage plus the sections containing the two taps and valves can now be cut away and replaced using hyperbaric welding. When this is complete, the line, with the plugs still in place, is returned to its operational pressure at approx. 15 MN/m^2, and the plugs which are only inflated to 30 bar will compress and move off down the pipeline and are eventually removed at a pig trap.

1.2.3 Cryogenic Pipe Freezing

The third plugging technique now available is Cryogenic Pipe freezing, developed by BOC, BCB Pipe freezing and Brister (USA), using liquid nitrogen as the coolant, and by I.C.I. using dry ice and iso-propanol. The basis of this system is extremely simple and has already been outlined in section 1.1.

Water has a relatively high freezing point and forms a strong pipe to plug wall bond, and is therefore the easiest fluid to use for a pipe freeze. The range of other fluids that have been successfully frozen in commercial pipe freezes includes light and heavy fuel oils, potassium carbonate, chromic acid, titanium tetrachloride, paints, glycol, brines and liquid sludge [8]. The higher the line pressure, or the less good the plug/pipewall adhesion, the longer the plug should be. Plugs of all types can stand very high pressures, ice plugs have been successfully tested to 87 MN/m^2 (10,000 psi). The plug is not only held in position by adhesion to the pipe wall but also by thermal contraction of the pipe in the jacket area, which will cause the pipe to take up a very shallow "hour glass" type shape. The plug will also form to this shape so that in order to force it out under pressure the thick part of the plug must be extruded through the narrow part of the pipe.

There is some reticence in industry to use this technique because of the possibility of embrittling the pipe or over stressing it. Tests have shown that the properties of the metal subsequent to

pipe freezing are unchanged, although during freezing the impact strength in carbon steels is very low and so this part of the pipe must not be subjected to impact.

Domestic water lines often burst when they freeze in cold weather because ice freezes across in two places trapping unfrozen water. Because of the density inversion anomaly at $4^{o}C$, water expands below this temperature as it cools to freezing point, where it expands further on freezing to ice. The expansion of water trapped within the ice can cause very high pressures, which bursts pipes. This will not happen in the pipe freezing situation provided that an adequate distance is left between any one freeze and a blockage such as another freeze, a valve or a blank.

Stresses are caused in the pipewall during freezing for two main reasons. Firstly, the shock cooling effect, typically at the start of a pipe freeze, where a large temperature gradient exists across the pipe wall. This causes the outside of the pipe to go into tension, and the inside into compression. Secondly, the differential thermal contraction of ice or frozen products compared to the pipe wall material will induce stresses in both the plug and the pipe. Ice in fact contracts faster than steel, so a steel pipe with an ice plug in it will be pulled into compression. These stresses do not appear to rise to a level which would fracture pipes, the situation is improved by the fact that steel has a higher tensile strength at low temperatures.

However, concern about possible damage due to shock cooling has led to the development of controlled temperature freezing. This is important if lined pipes are to be frozen because large temperature variations could cause separation of the pipe and its lining if, as is probably the case, the thermal coefficients of expansion differ markedly [9]. B.C.B. developed a system using an insulated jacket with an inner and outer annulus [10] (figure 1.5). The outer one was filled with liquid nitrogen in the normal way. The inner annulus

contained iso-propanol in direct contact with the pipe to act as a heat transfer medium. This jacket was designed for a vertical pipe, so the inner annulus was open at the top to allow baskets containing dry ice to be lowered into the iso-propanol. This provided fine temperature control. Using this method it was found possible to limit the rate of cooling and the minimum temperature the pipe is subjected to, and to control that temperature to within $1^{o}C$. Engineers faced with similar requirements at a nuclear power plant in the U.S.A. used a jacket full of ethylene glycol which was recirculated by positive displacement pumps through a reservoir. The reservoir was cooled by a coil through which liquid nitrogen was passed and then vented off to atmosphere.

1.3 A comparison of plugging techniques

The three techniques detailed in the previous sections have different applications and limitations. These will now be outlined and compared.

'Hot' tapping is the most general technique. Its major advantage is that it is possible to effect pipe repairs with no interruption to the flow whatsoever. Pressure and temperature limitations are high with plugging possible from $-29^{o}C$ to $430^{o}C$ and up to 10.4 MN/m^2 (1200 psi). 'Hot' tapping may be used in either liquid or gas pipelines. Its major disadvantage is that of cost. The operation is complex and requires much heavy equipment to be carefully aligned. Split tees must be welded on for high pressure applications. The equipment itself is also complex and very expensive. The size of the equipment relative to the pipe itself dictates that there must be plenty of access space around the pipe to manoeuvre and operate it. Because of the mechanical nature of the seal, the pipe must be free from all solid debris in the plugging area. Finally, when the operation is complete, the split tee must be left at the site of each tap, a potential weak point in the pipe.

'Cold' tapping offers only one advantage over 'hot' tapping, in that the section of pipe that was tapped and through which the plug is introduced is also removed and replaced along with the damaged section, leaving an uninterrupted pipe at the conclusion of the operation. It still requires the expensive tapping operation with all the space and access problems that this entails. In addition the flow must be stopped and the line depressurised. If used in an oil line, and this is speculative since the technique was developed specifically for a gas pipeline, the oil would have to be cleared from the plug area to enable the plug to get a good grip of the pipe. The maximum depth at which the technique can be used is 150m because of the need for the normal line pressure (15 MN/m^2) to be able to displace the plugs when the operation is finished. The line must be equipped with pig traps downstream in order to catch the displaced plugs. 'Cold' tapping is thus a specialised technique, and of limited general use.

Compared to 'cold' tapping, Pipe freezing is a much more general process, but it has more limitations in terms of possible applications than 'hot' tapping. Firstly, with one exception, which will be dealt with in section 1.4.6, the pipe must be full of liquid. The flow must be interrupted for the duration of the operation, and the range of flow rates and temperatures that can successfully be frozen is very limited. For large diameter freezes in oil pipelines it may be necessary to pig a slug of water into the freezing site. Notwithstanding these limitations, pipe freezing offers a number of very significant advantages over the other methods. The most important of these is cost. The operation is simple and the equipment is relatively simple. The only difficulty is providing a seal between pipe and jacket, but even this is less critical than the seal around a split tee, since a leak in the former will cause a slight loss in coolant, whereas a leak in the latter causes a permanent leak in the pipe. Liquid nitrogen is now cheap and readily available in large quantities. The problem of access is much relieved. The largest item is the nitrogen supply vessel but fortunately this may be at any orientation within a reasonable distance of the freezing site. The

next biggest item is the freezing jacket which is only a little larger in diameter than the pipe itself, and about 2-3 diameters long. These split into two parts to facilitate fitting around the pipe. Ice plugs can withstand very high pressures, successful tests up to 87 MN/m^2 (10,000 psi) have been recorded. Debris in the pipe, and deformations of the pipe will not affect the integrity of the plug. Finally, removal of the plug is simple as it is merely allowed to thaw. Care should be exercised here to see that the plug is not thawed too quickly because this will cause it to melt away from the pipe wall. The partially thawed plug would then disappear downstream when the flow is re-established and possibly damage the pipeline.

1.4 Reported applications of pipe freezing

1.4.1 Oil and petrochemical industry

At a major U.K. refinery it became necessary to modify a 5 km (3 mile) long, 100mm (4") diameter pipeline carrying methanol [8]. The line was filled with water and two freezes applied 3 m apart to seal off the working area. The pipe was then cold cut and purged with CO_2 before flame cutting out the complete section for modification. The new branch was arc welded into position and hydrostatically tested. The freezes were maintained for 5 days during which time the welds were stress relieved with heating jackets and then radiographed. An additional plug was frozen near the weld site to act as a sacrificial heat sink and protect the sealing plugs.

At the Coryton refinery belonging to Mobil Oil, valve failure on a river water cooling system posed a maintenance problem since with the valve out of action there was no other means of isolating the system from the river [11]. B.C.B. Ltd. applied a 1.8 m long freeze to the water inlet. Work began on replacing the valve 12.5 hours after freezing commenced and the whole operation was completed in 21 hours.

A slightly more unusual freeze concerned the replacement of an automatic control valve in the high pressure steam line that supplied steam to the main safety valve stack [12]. The stack had to remain in operation for safety reasons, so steam was condensed and then frozen to form a plug, isolating the valve and permitting its replacement.

Large pipe diameter does not rule out the use of pipe freezing. Brister Inc. (U.S.A) did a test freeze on a 1m (40") diameter, 9mm wall thickness steel pipe to prove the technique for hydrostatic testing of the Colonial Pipeline Company's loop line in Texas [13]. A 24.6m (80 ft) long section of pipe was used for the test which was successfully frozen in 16.5 hours. The plug temperature was lowered to $-173^{o}C$ and then pressure tested to 8.5 MN/m^2 for 17 hours. At this pressure the longitudinal load on the plug is over 6.9 MN (760 tons).

1.4.2 Other industry

A costly computer shutdown plus the loss of 20,000 litres of treated water, was avoided by the application of a single freeze at a water chilling plant by B.C.B. Limited [8]. The plant supplied water to cool North Thames Gas Board's computer suite. A flow switch had become defective but was replaced within a total of 3 hours and with no interruption in the supply of chilled water.

B.C.B. also point out another important application of pipe freezing [14], that of maintenance of fire sprinkler systems which, by law, have no isolating valves. Pipe freezing is thus the only way of working on these systems without evacuating the whole building.

All the freezes described so far have involved freezing pure water. This does not have to be the case. A 150mm (6") line carrying Calcium brine was successfully frozen at a meat products factory in Bletchley [12] and a 300mm (12") spun cast iron pipe containing raw

sewage was frozen at the Brooked water pumping station [11] avoiding the need to transport thousands of gallons of sewage.

1.4.3 Nuclear power industry

The nuclear power industry has special requirements, such as the necessity to seal off during maintenance large quantities of contaminated water, for which pipe freezing is particularly useful. At the Florida Power & Light Company's St. Lucie 1 power station, it became necessary to fit motor operated valves into a number of 50mm (2") safety injection lines in order to meet N.R.C. regulations [15]. Rather than drain out and decontaminate 270,000 litres of water, several pipe freezes were performed on the 5.6mm wall thickness 304 stainless steel pipes. The freezes were quite conventional using direct application of liquid nitrogen and the modified pipework was hydrostatically tested against the plug to 6.15 MN/m^2 (710 psi) for 10 minutes. The freeze to thaw time for each plug was in the region of 5-6.5 hours.

At another nuclear plant it was decided to freeze a 50mm (2") pipe but because the pipe was made from carbon steel, engineers deemed it wise to control the temperature very carefully [16]. To this end, they fabricated a carbon steel jacket through which a glycol/water solution could be pumped at a pressure of 0.35 MN/m^2 (40 psi). Pumps were of the positive displacement type to enable pumping of high viscosity fluids. The glycol solution was circulated between the jacket and a 250 litre reservoir containing a cooling coil and a stirrer to prevent localised freezing. Liquid nitrogen was passed through the coil and then vented to atmosphere. Thermocouples monitored the temperatures in the jacket and reservoir and on the pipe. Once installed and leak tested, the freeze can be carried out remotely, which was important in this case. The 300mm long freezes were made in less than 2 hours.

1.4.4 Offshore industry

B.C.B. Ltd. report the successful completion of two offshore pipe freezes. The first was on the Shell/Esso Dunlin Alpha production platform in September 1978 [10,17,18]. For operational reasons, it became necessary to remove a spade blank from one side of a 400mm (16") gate valve to the other. Because of other engineering work in progress, the working site was open to the sea via a 400mm diameter riser. The first task was to remove the coating from the riser at the freeze site, and this was done with pneumatic needle guns to avoid the possibility of damaging or work hardening the surface from which cracks could propagate during the freeze. Next, a 25mm depth of water was frozen in the bottom of the jacket to effect a good seal between the pipe and the jacket. B.C.B. used their controlled temperature method, as explained in Section 1.2.3 to apply a 1.2m (4 ft) long seawater freeze in the steel riser. The freeze took place in dry conditions, inside one of the platform legs, 81m (266ft) below sea level where the ambient pressure in the line was 0.87 MN/m^2 (100 psi). A strict temperature limit of $-60^{\circ}C$ was applied, and the dry ice was added slowly so as to achieve a cooling rate of $8-10^{\circ}C/hr$. Temperature control was found to be possible to $\pm 1^{\circ}C$. Once the plug had frozen very little liquid nitrogen was required to maintain it, and the whole operation was completed in 24 hours. Shell estimate that the freeze cost in the region of $46,000.

Shortly after the Dunlin A freeze, Shell called on B.C.B. to do a second freeze, this time on their Brent C platform. This time the freeze was applied to a 500mm (20") pipe, again inside one of the platform's legs below a gas tight floor, 55m below sea level. The controlled temperature freeze was maintained for 21 days to allow time for the line to be cut, a spool piece welded in position and then for the welds to be stress relieved with electric heating jackets and radiographed. Finally the plug was used to hydrostatically test the modification to 4.5 MN/m^2 (520 psi) before it was allowed to thaw.

1.4.5 Freezing of lined pipe

Freezing of lined pipe might be expected to cause difficulties due to the differential contraction between the pipe and the lining. After the Dunlin A and Brent C freezes, Shell-Esso asked B.C.B. to investigate the possibility of a freeze to enable four sets of expansion bellows to be renewed on their Cormorant platform. The four 750mm (30") diameter pipes were plastic coated inside and out. B.C.B. performed some preliminary tests and concluded that, using their controlled temperature method, the integrity of the plastic coating was unaffected and that the adhesive strength between the plug and the lining was sufficient to allow pressure testing to 4.8 MN/m^2 (554 psi) [11,18]. Shell-Esso had to abandon the idea as the field schedule did not allow work to go ahead.

B.C.B. have performed tests on other lined pipes [19]. Firstly a 175mm (7") diameter ebonite lined pipe was frozen down to $-86^{o}C$ and then pressure tested to 5 MN/m^2 (580 psi) for 15 minutes. Subsequent tests by Babcock Corrosion Control Limited, including high frequency high voltage spark tests, established that the integrity of the pipe and its lining was unaffected. A 300mm (12") diameter vycastic (PVC Rs60) lined pipe has also been successfully frozen with no damage to the pipe or its lining.

A concrete lined pipe has been test frozen, under simulated offshore conditions, again by B.C.B [9]. The pipe, 610mm (24") diameter with a nominal 10mm concrete lining, was filled with seawater and mounted in a test rig. The concrete was allowed 10 days to reach saturation before a 0.9m (3ft) long 'control' sample was removed to allow a comparison of the structural integrity of the concrete lining before and after pipe freezing. Thermocouples were set up to monitor the temperature of the pipe wall and the contents during the controlled temperature freeze which took 30.6 hours to complete. The plug was then pressure tested to 1.95 MN/m^2 (225 psi) for 6 hours. No damage to the pipe or its lining was evident.

1.4.6 Freezing of non-liquid filled pipes

Whilst pipe freezing is almost invariably associated with liquid filled pipes, NASA report a method for sealing empty pipes [20]. The principle is to pass CO_2 gas along the pipe to be sealed at a very low flowrate. Liquid nitrogen is applied to the outside and the CO_2 gas inside gradually freezes inwards to seal off the pipe. The idea was developed to allow sensitive items, such as valves with small passages that may become blocked, to be sealed off during flushing of pneumatic and hydraulic systems without disassembly. The 125mm (5") long 19mm (0.75") diameter plugs were said to form in about 10 minutes and withstand applied pressure of 0.43 MN/m^2 (50 psi).

1.5 Extension to sub-sea plugging

Many of the applications for pipeline plugging in the offshore industry involve temporarily sealing a sub-sea pipeline. 'Cold' tapping, of course, was specifically developed for this purpose.

'Hot' tapping on the other hand was originally developed as a land based technique, but it has been used underwater. T.D. Williamson explained [21] that the procedure is essentially similar to that followed on land except that all the equipment must be manoeuvred into position by divers. Lack of diver visibility is a major problem, especially considering that large pieces of machinery have got to be positioned accurately. The split tees used with the 'cold' tapping process are mechanically clamped around the pipe, but tees for use at the high pressures which 'hot' tapping allows must be welded to the pipe. This involves the setting up of a dry habitat in which the welder can work, a procedure known as hyperbaric welding. This is unfortunately an extremely expensive operation, costing somewhere in the region of 1 million dollars per weld.

Cryogenic pipe freezing has not been used in sub-sea conditions, but there do not appear to be any technical reasons why it should not. Indeed, the effort and skill required to do a sub-sea pipe freeze should be considerably less than that required for a sub-sea 'hot' or 'cold' tapping operation. The freezing jacket is much simpler, lighter and cheaper than the split tees plus tapping and plugging machines required for a 'hot' tap and is simply bolted around the pipe, creating no alignment problem. Although hyperbaric welding will still be necessary at the repair site, it will not be so at the plugging sites thus making a considerable saving. No major power supplies are needed on the sea bed, nitrogen could be supplied from self pressurising tanks, located either on the support vessel or lowered to the sea bed, depending on depth. All the cryogenic equipment would have to be carefully designed and insulated for sub-sea use to prevent frozen sea water rendering it inoperative, but this should not prove too difficult. The nitrogen tank gas take-off would be used to blow down and empty the jacket of sea water before liquid nitrogen was admitted.

All this requires manipulation of the equipment by divers, as is the case with 'hot' and 'cold' tapping. Because of the simple nature of the operation, it is possible, in the longer term, that a remotely operated vehicle could be designed to freeze pipes at depths below which divers can work.

1.6 Review of previous experimental research

Although a reasonable amount of research on freezing of fluids has been accomplished, much of it is only loosely applicable to cryogenic pipe freezing because of the particular geometries, or the temperature regime considered. Much work has been published on dendritic ice growth in pipes, in particular by R.R.Gilpin. However, this pipe freezing mechanism will only occur in pipes with no main flow and where the pipe contents are at or very near the freezing temperature. Any liquid superheat will cause natural convection and

this, or forced convection, will preclude the formation of dendrites at the liquid/solid interface. Since pipe freezing is always carried out on a pipe whose contents are appreciably above the freezing temperature, dendrite formation will not be considered here.

1.6.1 Interface Growth and Pressure Drop in Laminar Flow.

Zerkle and Sunderland [22] conducted an investigation to determine the steady state temperature and pressure distributions in laminar flow through a circular tube with some solidification on the inner tube surface. As liquid enters the section of tube whose walls are maintained below the freezing temperature, some solidification will occur. As the liquid proceeds down the tube, its mean temperature will approach the freezing temperature, the solid layer will become thicker, and therefore the mean velocity will increase.

The situation is represented mathematically by a combination of the continuity, momentum and energy equations together with the appropriate boundary conditions. A theoretical analysis based on the solution of these equations is presented using certain simplifying assumptions. The most important of these are: steady state conditions prevail; liquid flow is laminar with a fully developed velocity profile and it is isothermal at the inlet; heat conduction is axial; no convection; viscous losses are negligible; the tube wall has a negligible thermal resistance and a constant temperature along its length.

The three sets of equations are transformed into non-dimensional quantities and a further transformation of $\zeta = r/r_i$ in the nomenclature of this report is applied to remove the unknown interface radius r_i from the temperature distribution equations. Heat transfer rates are determined from the temperature distribution. The interface energy balance equation is employed together with the temperature distribution to calculate the solid phase shell profile, and from this the pressure drop is determined from an integral form of the axial

momentum equation.

The experimental investigation was in two parts. The first was a simple confirmation of the nature and appearance of the solid phase shell with laminar flow of water through a duct. It was conducted in a duct 25mm wide x 75mm deep x 915mm long (1"x3"x36") whose top and bottom were plexiglass and whose copper sides were maintained below freezing point.

The second and more substantial experiment was to enable a comparison to be made between theoretical predictions and experimental measurement of heat transfer rates, liquid/solid interface position and pressure drop. The test section was a 38mm (1.5") dia. thin walled copper tube, jacketed with a 64mm (2.5") steel pipe. Two lengths, 737mm (29") and 2.08m (82") were used. Acetone, whose temperature was automatically controlled by a cooling system, was passed through the annulus at high flow rate. A 4m (13ft) long inlet pipe was used in order to get entry conditions to the test section as close as possible to those assumed in the theoretical analysis. Water was supplied from a constant head tank, and its flowrate controlled by a valve at the outlet of the test section. Temperature measurements of the tube wall plus the bulk temperatures of water entering and leaving the test section were made with thermocouples. A pressure tap just upstream, and a probe on the centre line at the downstream end of the test section allowed the pressure drop to be measured.

Experimental runs were performed with the wall temperature just above freezing with both tubes, at 6.7^{o}C and 17.7^{o}C below freezing for the short tube and at 6.7^{o}C and 12.2^{o}C below freezing for the long tube.

A comparison was made between the measured dimensionless heat transfer rate versus dimensionless axial distance, and that predicted by the theory outlined earlier (figure 1.6). In all cases the observed heat transfer rate is higher than the theoretical

prediction. The authors [22] explain that this is due to the effect of free convection increasing the local heat transfer coefficient at the interface. Comparison of experimental runs, with wall temperatures just above and below freezing, allows the effect of internal solidification on heat transfer rate to be assessed. As the amount of freezing increases, the heat transfer initially also increases, but a further increase in the amount of freezing reduces it again. This last effect is thought to be due to the reduced interface diameter restricting natural convection.

Rearrangement and substitution of the theoretical equations shows that a large axial gradient in the heat transfer rate would be expected to reduce the amount of freezing, i.e. a larger interface diameter. Thus, near the entrance of the freezing section, natural convection will increase the heat transfer rate and also its axial gradient above the theoretical prediction so that the interface radius here will be larger than predicted. Further along the pipe, where the interface diameter is smaller and natural convection is restricted, the interface diameter will reduce to that predicted and will eventually be less than the prediction. So, providing the pipe is long enough natural convection will cause the minimum interface diameter to be smaller than predicted, and this is the reason advanced to explain why the predicted pressure drop is less than that observed.

Finally, an empirical equation for the heat transfer coefficient in a horizontal tube with natural convection, as developed by Oliver [23] is used with the existing theoretical model to demonstrate the effect of free convection on the interface profile, and the result is as summarised above.

Hwang and Ja-Pung Sheu carried out a similar theoretical and experimental analysis [24] but this time considering freezing in the hydrodynamic entrance region of a pipe, thus assuming a uniform velocity profile at the inlet (slug flow). This was achieved experimentally by connecting the freezing section directly to the

constant head tank, and dispensing with the long inlet tube used by Zerkle and Sunderland [22]. The test sections were made of 9.5mm I.D. copper tube, about a quarter of the diameter used by Zerkle and Sunderland, as this was expected to reduce free convection effects by two orders of magnitude at which point they were thought to be negligible. Results show quite reasonable agreement between dimensionless heat transfer rates predicted by theoretical analysis and those measured experimentally, when plotted against dimensionless axial position.

The two papers considered above have only concerned themselves with steady state conditions, that is that the solid-liquid interface as reached at a position where all the heat flows, conductive and convective, are in equilibrium. Haneef and Aziz [25] presented a paper which considered a transient heat flow following a change in wall temperature and the subsequent solidification in a cylinder with no flow through it. The experimental set up used a 122mm I.D. thin wall (1mm) tube made from steel sheet, and brine solution as the coolant. 25 thermocouples measured the temperatures from the tube wall to the centre. The temperature/time history for the outer wall showed a high initial cooling rate from $0.5^{o}C$, tailing off as the temperature approached $-6.3^{o}C$. After 110 minutes the centre of the tube froze. The time histories of thermocouples spaced across a section of the tube are presented as well as a non-dimensional plot of temperature distribution at 55, 80 and 110 minutes. These experimental results are compared with a perturbation solution due to Asfor et al [26]. This solution assumes a constant outer temperature and so the time averaged experimental outer wall temperature of $5.14^{o}C$ is used. Also the solution assumes the liquid to be initially at its freezing temperature and so takes no account of sensible heat effects. To overcome this the sensible heat in the liquid (temperature above freezing x specific heat) is added to the latent heat. Despite these crude simplifications, the agreement between theory and experiment is found to be within 20%.

Sparrow and Broadbent [27] investigated the freezing of n-eicosane paraffin (melting point 36.4°C) in a vertical 50mm diameter copper tube. Water baths were used both to establish the tube and its contents at the desired initial temperature and to maintain the outer wall of the tube at the chosen degree of undercooling during the freezing run. The parameters varied in these tests were the initial degree of superheat in the liquid (0,11.1 and 22.2°C), the subcooling of the tube wall below freezing (9.7, 20.0 and 30.3°C) and the duration of freezing (up to 90 minutes). At the conclusion of each run the remaining unfrozen liquid was removed with a vacuum device. Then the paraffin plug was removed from the containment tube by briefly warming the tube and withdrawing the frozen plug with the aid of nylon threads. It would then be weighed, sectioned and measured. This procedure allowed the interface movement, and the proportion of the total mass frozen to be plotted against time for each of the nine combinations of initial superheat and tube wall subcooling. Examination of the plots, figure 1.7, shows that subcooling has quite a strong effect while initial superheat has very little effect on solidification, particularly at longer times. Part of the reason that the degree of initial superheat does not affect the freezing more is that it decays fairly quickly. In general it was found that due to convection and conduction, initial superheat was dissipated within 10 minutes.

The energy extracted from the paraffin is divided into two and, in the case of non-zero initial superheat, four components. The first is the latent heat of fusion. The second component is the energy released by subcooling the solid (subcooling is the cooling of the solid below its freezing point). With no initial superheat these two components represent the total heat extracted from the sample. When superheat is present two further components must be considered, the sensible energy extracted by cooling the fluid which has frozen to its freezing point, and the sensible energy extracted from liquid which has yet to, or never ultimately, freezes. Of course, once the superheat has dissipated the sum of these last two components is

constant. The plots of the extracted energy split into its four components against dimensionless time, figure 1.8, show that although the latent heat contribution is by far the largest, the sensible heat components can make a significant contribution with high initial superheat and high subcooling.

The papers reviewed so far have dealt with freezing various geometries with very moderate degrees of subcooling, less than $30^{o}C$. Freezing water filled pipes using liquid nitrogen as the coolant will result in subcooling of around $200^{o}C$ and when freezing hydrocarbons the subcooling is still of the order of $100^{o}C$. This means that the results of these papers are of only limited interest to a study of cryogenic pipe freezing. Stelzer [28] on the other hand, investigated the freezing of flow through various steel and brass pipes up to 50mm diameter particularly with reference to the pipe freezing situation, i.e. a short freezing section using liquid nitrogen as the coolant. The parameters varied were water temperature (20, 25 and $30^{o}C$), flowrate (0.25,0.2,0.15 and $0.1 m^{3}/hr.$) and tube size and material (steel:12,30,38 and 51mm dia.; brass:20,30,40 and 50mm dia.).

The results show that the brass tubes are less inclined to freeze than the steel, possibly due to brass' slightly lower thermal conductivity. No successful freezes of the 50mm dia. brass tube are recorded. For the steel tubes in general, increasing tube size, flowrate or inlet temperature all tended to increase the freezing time. However, at the higher flowrates (0.25 and $0.2 m^{3}/hr.$) for an inlet temperature of $20^{o}C$ the maximum freezing times were recorded with the medium size pipes, and at the higher inlet temperatures the smallest pipes proved impossible to freeze, with freezing time falling as tube size increased.

When freezing times are plotted against $\log_{10}$ [Reynolds No. x Prandtl No.] no pattern emerges. But if freezing time is replaced by the logarithm of a modified Fourier number then the results fall into a wide band. Fourier number is a time dependent dimensionless

group often used in the field of transient heat transfer, a low Fourier number implying that a body needs a lot of time to heat and cool. The data is used to establish a correlation between Fourier, Prandtl and Reynolds numbers.

$$Fo_e = 3.33 \times 10^{-5} \, Re^{1.25} \, Pr^{-0.75}, \qquad \ldots(1.1)$$

where

$$Fo_e = \frac{k_s \cdot t_b \cdot (T_{il} - T_c)}{D_{iw}^2 \cdot \rho_s \cdot L} \cdot \frac{\alpha_s \cdot D_{iw}}{\alpha_w \cdot D_{ow}}$$

This correlation is established on measurements made in the range of $5000 \leq Re.Pr \leq 60000$ in steel and brass tubes. It can be seen that the tubes thermal properties and its diameter are included by using the modified Fourier number. A statistical analysis is presented to show the percentage deviation of the measured points from the above correlation, and the maximum deviation is 60%.

1.6.2 Effects of Natural Convection on the Freezing Process

Sparrow and Broadbent [27] concluded from their experiments that, due to the fast decay of superheat, natural convection was not important in the freezing process they were investigating. However, if the superheat is maintained, then natural convection will continue to play an important role in the heat transfer process. Sparrow and Broadbent investigated the freezing of an isolated sample of paraffin in contrast to the pipe freezing situation where the superheat may be maintained by a combination of conduction and convection of heat from the areas either side of the freezing zone. Zerkle and Sunderland [22] indicated the discrepancy, between experimental results and a theoretical prediction based solely on conduction, due to the effects of natural convection.

Sparrow et al [29] conducted experiments to investigate freezing in which the dominant heat transfer process was natural

convection. To accomplish this, a sample of n-eicosane paraffin was contained in a 152mm dia. tube, insulated top and bottom and itself placed in a constant temperature water bath. Freezing was commenced by lowering a cooled tube into the centre of the paraffin. The cooling tubes temperature was maintained by a thermostatically controlled flow of water. Parameters varied were the outer temperature difference (ΔT_{ou}), that is the outer water bath temperature minus the paraffin freezing temperature (0, 17.8 and 35.6°C) the inner temperature difference (ΔT_{in}), i.e. the freezing temperature minus the inner cooled tube temperature (13.9 and 27.8°C) and the duration of freezing. At the conclusion of each test, the cooled tube, together with the adhered solid paraffin, was removed from the remaining liquid. The solidified paraffin was separated from the tube, weighed, photographed and measured.

The first series of runs with $\Delta T_{ou}=0^{\circ}C$ (no superheat) revealed the steady growth of a parallel sided annulus of solid around the cooled tube. Dendrites could be seen on the surface. The next series of tests were for $\Delta T_{ou}=17.8^{\circ}C$, $\Delta T_{in}=27.8^{\circ}C$. The results of these tests, when compared to the zero superheat case, reveal three important differences. Firstly, freezing does not continue indefinitely, but instead reaches an equilibrium state, and the quantity of frozen material is much reduced. Secondly, the annulus of solid is no longer parallel sided, but gently tapered outwards towards the bottom. Finally, the dendrites observed in the initial test are not seen when superheat is present. For the next series of tests ΔT_{ou} was maintained at 17.8°C but ΔT_{in} was halved to 13.9°C. As expected, the mass of frozen material was further reduced compared to the previous series, and the time required to reach the equilibrium freezing position decreases. A final series of tests was conducted by doubling ΔT_{ou} to 35.6°C and maintaining ΔT_{in} at 13.9°C. The resulting annulii of frozen paraffin were very thin indeed, and the time to reach equilibrium was about 60 minutes.

A rationale of these results is presented by the authors [29]. The conductive heat flow through the frozen layer is approximated by:

$$(q)\text{cond} = (k_s \Delta T_{in})/(r_{it} . \ln(r_i/r_{it})) \quad ...(1.2)$$

and the convective heat flux at the interface by:

$$(q)\text{conv.} = (r_i/r_{it}) . h_c . \Delta T_{ou} \quad ...(1.3)$$

They are shown in figure 1.9 as a function of r_i/r_{it}. Since (q)cond decreases with increasing r_i/r_{it} and (q)conv increases with increasing r_i/r_{it}, they will eventually intersect where (q)cond = (q)conv. The r_i/r_{it} at which this occurs represents the equilibrium value. Initially (q_i)cond is greater than (q)conv and the difference is equal to the rate of removal of the latent heat of fusion at the interface. Thus the interface grows outwards until equilibrium is reached. The tapered nature of the frozen annulus is explained by the fact that since liquid will flow down the cool interface, the convective heat transfer at the bottom would be expected to be less than at the top. Thus the (q)conv line for the bottom of the interface will intersect the (q)cond curve at a higher value of r_i/r_{it}. An increase in ΔT_{in} will move the (q)cond curve upwards and thus intersection will occur at higher r_i/r_i, and finally an increase in Δ Tou will move the (q)conv line upwards and the intersection will occur at lower r_i/r_{it}.

Sparrow and Souza Mendes [30] used the same equipment as above to measure natural convection heat transfer coefficients. They conducted three series of runs, all with $\Delta T_{ou} = 5.6^{o}C$ and with ΔT_{in} equal to 8.3, 11.1 and $16.7^{o}C$ respectively. If the variation of solid phase conductivity with temperature is assumed to follow the law $k_s = A+B.T$, then the conductive heat flux can be written as in equation (1.2) but using k_s as evaluated at $T = (T_f+T_{in})/2$. Equating this heat flux with the convective heat flux allows the convective heat transfer

coefficient to be written:

$$h_c = k_s(\Delta T_{in}/\Delta T_{ou})/(r_i.\ln(r_i/r_{it})) \qquad ...(1.4)$$

For the three different values of ΔT_{in}, the equilibrium radius was measured at six axial positions, and h_c calculated from equation (1.4). At any given axial position the experimental values of h_c were very nearly equal. This is as expected as the minor differences in geometry caused by different frozen layer thicknesses would not be expected to cause large variations in the liquid temperature or velocity distributions. The measured heat transfer coefficients varied from approx. 61 W/m^2K near the top of the interface to approx. 38.5 W/m^2K near the bottom.

1.6.3 Freezing of fluids in the transition and turbulent Regimes.

Gilpin [31] observed the formation of ice in a 33mm dia., 1.5m long glass tube. This tube was cooled along its length by a methanol/water mix. Reynolds numbers up to 14000 could be obtained in this pipe. A freezing parameter $\theta = (T_f-T_c)/(T_{il}-T_f)$ was defined, and the maximum value used was θ =30. The first test was conducted at Re=3025 and θ=2.6. It was found that the flowing water would not nucleate ice growth until the wall temperature was below -3 or -4^oC, thus it was sometimes necessary to nucleate ice growth artificially by some method such as lowering the coolant temperature momentarily or introducing silver iodide into the water stream as a nucleant. For the first two hours of this test the ice growth was much as expected with the ice thickness increasing uniformly from inlet to outlet. At two hours the ice growth appeared to have almost reached steady state. However, at about 4 hours a sharp expansion formed near the outlet and this then started to migrate upstream. The ice downstream of this expansion was completely melted away until at 14 hours, a second ice growth was nucleated near the outlet. At 16 hours steady state was reached with the first expansion point at 45cm from the inlet and a

moderate amount of ice forming again near the outlet.

It was found that increasing the freezing parameter θ by lowering the coolant or water temperature increased the number of cycles of expansion and contraction observed. At θ=11.8 and Re=3025 six cycles are seen.

Gilpin explained the migration of these expansions in the following manner. A sudden expansion, such as would be found at the outlet of the freezing section when solidification is fairly well advanced, causes flow separation and intense turbulence. This causes the heat transfer rate from the water to the ice and tube walls in this area to be dramatically increased, thus tending to melt away the downstream side of the ice wall and causing the expansion point to migrate upstream. As the separation points move upstream, the thickness of the ice through which they are moving decreases and thus the temperature gradient is steeper. It is postulated that a given change in heat transfer coefficient due to flow separation thus causes a smaller change in ice thickness and that steady state is reached when a local heat balance can be achieved everywhere on the ice surface.

When the initial flow is turbulent, the transient formation of the series of separation points is different, but the final steady state condition is similar to that observed with an initially laminar flow. Separation points are formed in a fairly random spacing all along the pipe. As time passes they tend to move together and regularise their spacing.

The separation point spacing is found to be largely independent of Reynolds number, but to decrease sharply with increasing temperature ratio θ up until θ=15. For θ>5 the spacing is constant, approximately equal to 6D for this pipe. The neck diameter at the separation points appears to depend only on Re for θ<5, and for θ>5 it depends both on Re and θ.

The question of predicting complete freeze-off of the pipe is considered but this is difficult because the conditions for freeze-off depend, amongst other things, on the pressure/discharge characteristic of the whole system. It is noted that freeze-off is more likely to occur in the earlier transient stage of ice formation when smaller neck diameters were observed, since pressure drop across the neck depends on the diameter to the fourth power. It is further noted that freeze off in a pipe containing this sort of ice structure is particularly destructive since unfrozen water may be trapped between two frozen necks, which will then try to expand as its temperature falls below $4^{o}C$ and may well rupture the pipe.

Thomason and Mulligan [32] performed experiments on freezing a 116cm long copper tube with turbulent flow inside it. Their experiments consisted of a series of tests in which the freezing conditions were made more and more severe, that is that each test had either a lower coolant temperature, a lower water inlet temperature or a lower initial water flowrate, or a combination of these, compared to the previous test. The earlier runs quickly reached steady state with some ice formation in the pipe, much as expected. As freezing conditions became more severe, some oscillations in flowrate, pressure drop and wall temperature were observed, which tended to damp out until steady state was reached. Still more severe conditions caused an almost perfectly periodic undamped oscillation which had a period of approximately 35 min. Reducing inlet conditions further caused wild fluctuations with the pipe approaching freeze-off conditions at some points in time. Further slight reduction in inlet conditions caused steadier progression to freeze-off with some oscillating behaviour still observable, and the most extreme freezing conditions resulted in a smooth non-oscillatory progression to freeze blockage.

No explanation for this behaviour is offered but it is postulated that the turbulent separation and relaminarisation reported in [31] is the most likely cause.

1.6.4 Freezing of Oil Filled Electrical Cables.

A common type of high voltage underground transmission line is one in which three insulated conductors are run inside an oil filled low-carbon steel pipe. If the cable is to be exposed for any reason, the pipe must be cut and the standard method is to freeze the oil either side of the cut.

Hall and Chevray [33] conducted tests using 200mm (8") and 250mm (10") pipes containing cables, filled with a variety of different types of oil and using various freezing methods. Three types of oil were used, two manufactured by the Sun Oil Company, Sun #6, a medium/high viscosity oil and Sun #4, a low viscosity oil, and finally a low viscosity polybutene-OSH cable oil manufactured by the Cosden Oil Company. The first freezing method tried, was to immerse the pipe in a bath of methanol, and to wrap 60ft of tube carrying liquid nitrogen around the pipe. The 4ft long bath was found to attain a stable temperature of $-60^{\circ}C$ in 5 hours. Next, a second wrap of nitrogen tubing was added and the bath now stabilised at $-90^{\circ}C$ in 8 hours. Neither of these techniques achieved low enough temperatures to freeze the low viscosity oils and provide a factor of safety. Since pure methanol freezes at $-97^{\circ}C$ a further reduction in bath temperature would have required the use of methanol/water mixture (70% by weight methanol freezes at $-139^{\circ}C$), but this mixture was felt difficult to maintain under field conditions. A solid gelatin type heat transfer medium was tried but was found to give unreliable results. Finally, direct immersion of the pipe in liquid nitrogen was tried and this gave satisfactory results.

Using the 200mm (8") pipe filled with Sun #4 oil, a solid freeze was obtained in 4.75 hrs with a liquid nitrogen consumption of 440 litres. Heating the oil to $56^{\circ}C$ prior to freezing, to simulate a cable that had just been on load, increased the freezing time by 21% to 5.75hrs. The same oil in the 250mm (10") pipe at ambient temperature was found to take 10-11 hours to freeze. Freezing the Cosden Oil

in the 200mm (8") pipe took 5.9 hours and 615 litres of liquid nitrogen. A comparison with the Long Island Lighting Company's data for freezing the high viscosity Sun #6 oil, which freezes in an 200mm (8") pipe in 2.75 hrs, shows the longer freezing times associated with the lower viscosity oils.

Ichiyanogi et al [34] conducted field trials on a 250mm (10") diameter pipe containing three 275kV cables and filled with oil. The freezing apparatus had some novel features and is worthy of comment. Firstly, the liquid nitrogen does not directly contact the pipe. The jacket forms two halves of an annulus as normal, but in this case they are completely closed by a half tube which closely fits around the pipe to be frozen. Copper packing around the pipe provides good thermal contact and when the freeze times using this jacket are compared with those obtained in [33] using direct liquid nitrogen contact, it appears that very little, if any, freezing performance is lost. Secondly, the liquid nitrogen was introduced into the jacket from a tube inside the jacket containing many nozzles. This was so that gaseous nitrogen could be fed down the tube, and Joule-Thompson effect of the gas emerging from the nozzles would be sufficient to maintain a freeze formed earlier with liquid nitrogen, thus providing a saving on liquid nitrogen consumption. Finally, since some freezes were conducted with an oil flow to simulate a leak in the pipe, the use of a sub-chamber, positioned just upstream of the freezing chamber, was investigated. Gaseous nitrogen exhausting from the freeze chamber was fed into the sub-chamber and then exhausted from there at a higher temperature, thus using more of the sensible heat in the nitrogen gas.

Results show that with no oil flow, an initial oil temperature of $5^{o}C$ and just a 1m long freezing chamber (no sub-chamber), a solid freeze was effected in 10.5 hrs. Increasing the initial oil temperature to $15^{o}C$ increased the freezing time to 14 hrs. Using the same equipment with an oil temperature of 5C, a 20 litres/hr flowrate increased the freezing time to 16.0 hrs and a 40 litre/hr

flowrate to 18.0 hrs. An initial oil temperature of 40°C flowing at a rate of 60 litres/hr proved impossible to freeze with this set up. Addition of a 1m long sub-chamber allowed the oil to be frozen in 31 hours. A 2m long sub-chamber shortened this freezing time to 21 hrs.

A crude thermal circuit type model is presented by the authors [34], which draws analogies with electrical components, which predicts the freezing times mentioned above to within 30%.

Finally, checks were carried out to confirm that the act of freezing the cable, and cutting and splicing in the general area of the freezing jacket, did not damage the cables electrical insulation properties, and this was found to be so.

2.0 Review of Pipe Freezing Research at Southampton University

It can be seen from chapter 1 that the amount of serious research performed on the subject of pipe freezing is relatively limited, being aimed mainly at determining the freezing characteristics of a particular geometry with no attempt to generalise the results to predict freezing in other situations. Furthermore, only the freezing mechanism has been investigated and whilst this is of central importance to pipe freezing, other highly relevant areas such as the strength of the frozen plug, its mode of possible failure under pressure and the stress induced in the pipe itself by pipe freezing have hardly been touched on.

In 1981 therefore, a research program was started in the Department of Mechanical Engineering at the University of Southampton under the direction of Dr. D.A.Wigley, to investigate all aspects of cryogenic pipe freezing. Work undertaken by the group, now in its fourth year, can be split logically into three areas.

(i) Mechanisms of plug formation and its limiting factors including the effects of:

- Pipe wall thickness, diameter and jacket length
- Thermal conductivity and diffusivity of the pipe wall
- Thermal conductivity and diffusivity of the frozen plug
- Heat transfer from liquid to solid interface by forced convection and free convection
- Boundary layer separation during flow freezes

(ii) Measurement of stresses induced by freezing and plug formation including the effects of:

- Cooling rate
- Longitudinal constraint
- Welds, notches and other flaws

(iii) Determination of the strength and pressurisability of the frozen plug including the effects of:

- Temperature/time histories for the freezing of ice
- Temperature/adhesion relationships for hydrocarbons
- Interlaminar shear strength of frozen hydrocarbons
- Segregation in multicomponent fluids

The progress made in each of these areas will now be reviewed, excluding the major contribution made by the author since this work will be covered in detail in later chapters.

2.1 Mechanisms of Plug Formation and its Limitations

Initial tests were carried out by Williams [35] using a mild steel pipe of 100mm (4") nominal bore and 6mm (1/4") wall thickness. Copper/constantan thermocouple wire was threaded through long 1mm dia. stainless steel tubes and twelve such thermocouples were lead through and sealed in the steel blank that was itself bolted to the end flange of the pipe. A stiff wire carriage held these thermocouples in position while keeping the freezing area as free as possible. Another twelve thermocouples were attached to the outside surface of the pipe. They were all connected to two twelve channel chart recorders. Since the recorders used common cold junctions the 'hot' junctions on the rig had to be electrically insulated from one another with thin layers of araldite. Connections were provided on the pipe so that a flow of water could be set up in order to test the effect of fluid flow on freezing.

2.1.1 Static water freezes

Initially static water freezes were attempted in order to check the instrumentation and verify existing ideas on plug formation. The twelve thermocouples that could be placed in the water at any one time were found to give inadequate cover of the freezing volume, but fortunately the results of the freezes were so repeatable that the

temperature time plots for four freezes with the thermocouples in different positions could be superimposed on one another. By keeping one position as a reference and adjusting the start times of each run by up to 1 minute so that the reference thermocouple started to cool at the same time, temperature time plots were obtained for forty four positions.

Results indicate that under these conditions the pipe will freeze in 12 to 13 minutes. On application of the liquid nitrogen, ice grows along the bottom of the pipe immediately, closely followed by a slightly smaller amount at the top. There are two possible reasons for this. One is that natural convection is causing the bottom to freeze more quickly than the top and the other is that there will be a time delay before the liquid nitrogen level reaches the top of the pipe and indeed there may be times subsequently when the top of the pipe becomes exposed due to imperfect liquid nitrogen level control. In view of the low degree of superheat in the water initially, it is considered that the latter is the dominant effect. Freezing was continued after the plug first closed, it widened to the full width of the jacket and then began to undergo further cooling without much increase in its volume. By 45 minutes into the freeze, 3/4 of the ice was almost at liquid nitrogen temperature. In the initial stages, slight bumps in the ice were detected near the nitrogen inlet and outlet possibly due to higher liquid and gas flowrates in these areas.

Maximum cooling rates of $54^{o}C$/minute were measured on the outer surface of the pipe within the freezing jacket. In the centre of the jacket ice was found to advance upwards from the bottom at an average rate of 4-5mm/minute and 3mm/minute from the top downwards. Near the edge of the freezing jacket the rates are found to be 1.5 and 1mm/minute respectively.

In order to obtain some indication of the existence of a solid plug in situations where internal instrumentation is not

practical, as is the case in all commercial pipe freezes, it was hoped to be able to correlate the closing of the plug with some effect observable from the traces of external thermocouples. Unfortunately no real evidence was found to suggest this may be a possibility.

In the ICI publication 'Drikold' [36] it was indicated that a flow of water through a tee piece, to which the dead leg being frozen was attached, could affect the freezing rate in that dead leg. Williams' rig was arranged so that this effect could be measured. In contrast to the ICI results no measurable differences in either cooling rate or plug formation were observed. It is possible however, that either the flow rate past the end of the freezing section was insufficient, or else the distance between the freezing zone and the tee was too great (500mm) for the plug to be affected.

Results of tests performed by Emtage [37] showed that freezing water in a 150mm (6") diameter mild steel pipe took around 28 to 31 minutes and used 60 to 70 litres of nitrogen. Similar tests of a 300mm (12") diameter mild steel pipe, reported by Wigley [38], indicated a time to freeze of 130 minutes and a liquid nitrogen consumption of approximately 410 litres. Comparing results for freezes in 100,150 and 300mm diameter pipes, suggests that time to freeze is very approximately proportional to pipe diameter squared and liquid nitrogen consumption is very approximately proportional to the cube of pipe diameter. The latter is not unexpected since liquid nitrogen consumption will be dependent on the total amount of heat to be removed which, if the length to diameter ratio of the jacket is constant, is proportional to diameter cubed.

2.1.2 Flowing water freezes

ICI published [36] a curve showing the maximum flowrate, for a given inlet temperature, that could successfully be frozen in a 50mm (2") mild steel pipe using the 'Drikold' freezing mixture (dry ice and iso-propanol), this is shown as curve (iv) in figure 2.1. Using

liquid nitrogen as the coolant it was expected that a considerable improvement could be obtained. Williams' rig was modified to provide a flow through the freezing section and a series of tests were performed at various flowrates and inlet temperatures. A graph, similar to the ICI one, was obtained. The maximum flowrate that was frozen in these tests was approximately 15 litres/sec and the maximum inlet temperature about $30^{o}C$. Of course, the results are not directly comparable with those of ICI because the pipe diameters were different. In general it was found that any freeze that was not complete in 20 minutes would never freeze and should be abandoned.

During some of the unsuccessful freezes significant oscillation of the recorded temperatures were observed at some positions. A considerable quantity of ice was formed quite quickly, but then it apparently began to melt again before once again re-freezing. Figure 2.2 shows the approximate ice front position after 13 and 27 minutes. It is interesting to compare this behaviour with that observed by Gilpin [31] and Thomason [32], outlined in section 1.6.3. They recorded temperature oscillations and ice migration when the flow was in the the transient to turbulent regime, and the pipe Reynolds number of 5300 for this test fits in with this. However in their tests the melting was observed on the downstream side of the plug, leading to the supposition that separated and therefore turbulent flow caused by the diverging section on the downstream side of the plug was causing enhanced heat transfer from the warm water and melting it. In this case however, it appears that the remelting occurred mainly upstream of the minimum diameter point and if this was so then the above theory cannot be used in this case. It is possible that the position of the ice front was mis-interpreted because, unlike in the earlier static water freezes it was not found to be possible to superimpose the results of several freezes in order to obtain the temperature history at more points. Thus the temperature information available is very much more sparse. None of the freezes, in which this retreat of the ice front was observed, were subsequently successful.

During each test the inlet and outlet water temperatures were recorded. A knowledge of the temperature difference and the flowrate allows an approximate 'cooling power' to be calculated (ignoring transient effects such as the removal of the latent and sensible heat from the advancing ice), and thus the liquid nitrogen consumption necessary to maintain this cooling power, assuming only the latent heat of vaporisation of the liquid nitrogen is used (i.e. assuming the gas leaves the jacket at $-195.8^{\circ}C$). Since the amount of nitrogen actually used was known to be less that this calculated figure it is clear that some of the sensible heat in the nitrogen gas is also used for cooling.

Eden [39] followed up these flow freeze tests with further experiments to investigate the effect of pipe diameter and jacket length during this type of freezing. A new rig, more suited to the freezing of flowing water, was built using 50mm I.D. (2") mild steel pipe with a wall thickness of 4mm (0.157"). Perspex end covers allowed plug formation to be viewed. Twelve thermocouples were located inside the pipe in much the same manner as in Williams' rig. The temperature at inlet was varied by mixing the hot and cold water from the laboratory supply. The range of temperatures available and tested by this means was $8^{\circ}C$ to $40^{\circ}C$. A jacket with a length to diameter ratio of 2.8 was used initially.

The results from the rig in this configuration are summarised by curve (i) in figure 2.1. This represents the freeze/no freeze boundary for combinations of flowrate and inlet temperature. ICI's results from their 'Drikold' tests are shown as curve (iv) for comparison. Next the internal thermocouple instrumentation was removed, the series of tests repeated and the boundary re-established for this new arrangement. This is shown as curve (ii) in figure 2.1 It can be seen that removal of the internal thermocouples significantly increases the maximum flowrate that can successfully be frozen. This is thought to be due to the thermocouples in their stainless steel tubes initiating or increasing turbulence in the

freezing zone, thus causing enhanced heat transfer between the flowing water and the ice interface which retards plug growth.

The final set of results shown in figure 2.1 as curve (iii) refer to the pipe with no thermocouples, but with a jacket of length to diameter ratio 7.9. This, it might be thought, would again increase the maximum flowrate that can be frozen for any given inlet temperature. But the fact that curves (ii) and (iii) are almost coincident implies that this is not the case. This is a surprising result and is rather at odds with that observed by Ichiyanogi et al [34], whose freezing experiments with flowing oil in electrical cables, summarised in section 1.6.4., showed that the addition of a sub chamber just upstream of the main freezing chamber, thereby increasing the cooling span, allowed significantly higher flowrates and inlet temperatures to be frozen. It should, however, be remembered that the flowing oil tests were conducted at very low flowrates (60 l/hr.) in relatively large diameter pipes (250mm, 10"). This means that heat is removed from the bulk of the oil by natural convection. By contrast, the flow freezes conducted on water filled pipes had much higher flowrates (140 - 2200 l/hr.) in smaller pipes (50mm, 2" diameter). Under these conditions heat is removed primarily from the boundary layer, leaving the bulk water temperature largely unchanged.

In all the unsuccessful freezes some oscillation of the ice front position was again observed, though this time directly via the viewing ports. Although in some cases the initial pipe Reynolds number was well within the laminar region, it is possible that as the plug closes and the local Reynolds number, defined by the neck diameter, rises and turbulent separation of the boundary layer then occurs causing the retreat of the ice front.

Collier [40] extended the flow freeze investigation to explore the effect of different pipe materials on the freeze/no freeze boundary. A 50mm (2") diameter stainless pipe was tested in a similar

manner to the above and the boundary is shown as curve (ii) in figure 2.3. It can be seen that the curve is similar to the mild steel case, particularly at low temperatures and high flowrates, although at high inlet temperatures and low flowrates the boundary for stainless steel is measurably lower due to its lower thermal conductivity. Next an unplasticised PVC pipe was tested. From curve (iii) in figure 2.3 it can be seen that the maximum flowrate that can be frozen at any given temperature is reduced by around a factor of ten compared to a mild steel pipe. From visual observations made down the pipe during freezing it is known that plug growth in the UPVC pipe is entirely different to that in the steel pipe. It grows from the bottom upwards with a series of sloping layers building up from alternate sides of the pipe which gradually consolidate before the plug closes very near the top. These effects are probably due to a combination of forced and free convection. This work was completed by Castle [41] who performed a similar series of tests on a glass fibre reinforced plastic pipe. Results, plotted as curve (iv) of fig 2.3, can be seen to be broadly similar to those from the UPVC pipe. This is as expected since the thermal conductivities of the two materials are also similar, 0.25 W/mK for UPVC and 0.5 W/mK for GRP.

A more detailed investigation into the freezing mechanism for ice plugs in flowing water was also undertaken by Castle [41]. A 100mm (4") diameter mild steel pipe was fitted with a 300mm long freezing jacket and a perspex extension pipe just downstream to allow the plug formation to be viewed. Plug formation was observed to occur initially much as expected, with a neck forming near the centre of the freezing jacket. However, at a certain critical neck size, the neck started to migrate towards the upstream end of the plug. The critical neck size was found to depend on the water flowrate, being smaller for higher flowrates. Some thickening of the ice near the downstream end of the plug was subsequently observed, and in freezes with high flowrates this preceded the formation of a secondary downstream neck. Fig 2.4 shows the progress of a typical unsuccessful freeze. Successful freezes were similar except that the neck continued to

reduce in diameter as it migrated upstream leading ultimately to plug closure. Debris trapped in recirculating flows, downstream of necks, indicated areas of separated and turbulent flow.

The phenomena observed here are thought to be due to adverse pressure gradients in the downstream part of a partially formed plug, causing separated and turbulent flow and hence higher heat transfer to the ice, as suggested by Gilpin [31] (section 1.6.3). Secondary downstream necks start to form where the boundary layer reattaches and the heat transfer rate falls again.

During flow freeze tests on the 50mm diameter mild steel pipe using the long (L/D=7.9) freezing jacket (Eden [39]), two pipe failures occurred, in both cases just after the plug had closed. This suggests that the mechanism of failure was the trapping of unfrozen water between the primary and downstream secondary necks which both close off. This trapped water will try to expand as it cools from $4^{o}C$ and freezes, but is unable to do so, and a rupture of the pipe may be caused. The initial Reynolds number for the first failure was approximately 3200, and for the second, 1600 both within or approaching the transition regime at which Gilpin [31] observed ice migration and multiple necking in the ice. It is also interesting to note that the minimum spacing of the necks observed by Gilpin was six diameters. When using the shorter (L/D=3.0) jackets on the 100mm pipe (Castle [41]) no conditions were found in which the secondary downstream neck would close off.

2.1.3 Hydrocarbon freezes

To initiate the investigation into the freezing of hydrocarbons, Williams [35] performed four attempted freezes of diesel oil in a 100mm diameter (4") mild steel pipe. It was expected that diesel would take longer to freeze for two reasons. Firstly separate experiments, detailed in section 2.3, show that diesel oil, when cooled, exhibits very strong natural convection. This causes heat

from surrounding parts of the rig to be carried to the freezing zone and thus retard plug formation. Secondly, it was known that the freezing point of diesel, though not well defined, is considerably below that of water and so more sensible heat must be removed before a plug is formed. Of the two effects, it is thought that the first is the most important. During these freezes, it was noticeable that the whole rig was cooled below ambient temperature, indicating that strong natural convection currents were carrying cooled oil all around the rig. Lagging the whole rig produced only a minor improvement in cooling rate.

Lack of repeatability meant that temperature time plots for different runs could not be superimposed and so only twelve data points in the oil were available with each freeze. Thus plotting the position of the interface calls for a certain amount of estimation, particularly as the freezing point is not well defined, but it can be said that freezing diesel in this rig takes 4-5 times as long as freezing water.

Continuing the hydrocarbon freezing experiments, Kennedy [42] used a 50mm diameter (2") stainless steel pipe to test various fluids. Initial tests with water showed that a plug took around 10-12 minutes to form and used around 8 litres of liquid nitrogen.

Tests with paraffin showed that the plug took around 60 minutes to freeze and consumed about 20 litres of liquid nitrogen. Observation of the growing plug through perspex end plates showed very strong natural convection currents until the paraffin became opaque after about 10 minutes. Plug closure was judged to have occurred when a small hydrostatic head, caused by topping up the paraffin on one side of the plug, could be withheld. Two tests conducted with the pipe set at 9 degrees to the horizontal showed faster freezing times (40 and 49 minutes) and a slightly lower liquid nitrogen consumption. When the pipe is inclined, natural convection will occur mainly on one side of the plug. The fluid on the higher side will stay relatively

warm and not mix with that in the freezing area, thus less heat has to be removed to achieve plug closure and the freezing time is cut. By contrast, adding a 900mm long perspex extension tube to one end of the 1200mm long stainless steel pipe significantly increased the freezing time. In this configuration plug formation took 75 minutes and used 24 litres of liquid nitrogen. Cooler, more opaque, paraffin could be seen flowing away from the freezing section in the bottom of the perspex tube while warmer, clearer, paraffin return towards it in the top of the tube.

Three freezes of gas oil were found to take around 45 to 48 minutes using only the stainless steel tube. Adding the perspex extension gave freezing times of 49 and 58 minutes. In all cases the axial extension of the frozen plug after initial plug closure was found to be slower and less extensive than was the case with paraffin. Liquid nitrogen consumption was in the range of 16 to 24 litres.

Freezes of a 20/50 motor oil took between 18 and 18.5 minutes using 12 to 14 litres of liquid nitrogen. The addition of the perspex extension tube added only about a minute to the freezing time. This oil was much more viscous than either paraffin or gas oil and it is thought that this inhibited natural convection. Thus cooling of the oil either side of the freezing jacket was very much reduced. Three freezes of Statfjord crude oil were achieved with the perspex extension fitted in times of 16 to 17.5 minutes.

2.2 Measurement of stress and strain induced during pipe freezing

One of the major factors that holds industry back from accepting pipe freezing for more routine and widespread use, is the lack of information on the possibly harmful effects to pipework caused by thermally induced stresses during freezing. Therefore it was decided that the pipe freezing group should develop the ability to measure strains during pipe freezing, and to use it to analyse the

stresses and determine whether they are harmful to the pipe.

2.2.1 Development of strain measuring technique

The problem with measuring strain in an environment with large thermal variations, is that of separating out the strains that one wishes to measure from other temperature induced effects.

Any solid material when cooled, will undergo thermal contraction according to its coefficient of thermal expansion. Provided the material is unconstrained, no stress is associated with this strain. Therefore this thermal strain must be subtracted from any strain measurements before using them for calculating stress.

The normal way of doing this is with a dummy gauge attached to an unconstrained piece of material, similar to the test piece. The dummy gauge is kept in the same thermal environment as the test piece, and connected into the measuring bridge circuit so that the difference in resistance between the two gauges is measured. Unfortunately, initial work by Pratt [43] indicated that it was impossible to keep the dummy gauge at exactly the same temperature as the active one, so this method of compensation had to be abandoned for pipe freezing strain measurement.

Of course the unconstrained thermal contraction could be calculated from a knowledge of the pipe walls coefficient of expansion, and its temperature. This calculated figure could then be subtracted from the measured strain to leave the strain due to the stress distribution in the pipe. There are two reasons why this is not practical. Firstly the variation in temperature affects the gauge constant, which is the factor used to determine the strain from a change in gauge resistance. Secondly, there will be differential thermal contraction between the gauge material, its substrate and the pipe wall.

Fortunately, attempts to measure the unconstrained thermal contraction of small tubes yielded results repeatable enough for them to be used as calibration runs, the data from which is subtracted from all future freezing experiments on those tubes.

The only disadvantages with this method of compensation are the need to measure the temperature at or very near the gauge and the considerable tedium of looking up the calibration strain for each gauge corresponding to the temperature measured and subtracting it from the apparent strain. However, if computerised data gathering equipment is used, then the compensation routine can be incorporated into the software.

Gostick [44] developed the technique applied to small (150mm long x 25mm diameter) tubes with a single pair of strain gauges (one longitudinal and one radial). The calibration run was accomplished by suspending the tube to be calibrated on the axis of a larger diameter tube, itself cooled by being immersed in liquid nitrogen. The slow cool down thus achieved ensured that, to all practical purposes, no temperature gradients existed across the tube wall. The strain and temperature results from this calibration run were input into a least squares curve fitting program to obtain a polynomial expression which would subsequently be used to obtain the calibration strain for a measured temperature. To get a good curve fit it was found necessary to split the data into two ranges, ambient to $-90^{o}C$ and $-90^{o}C$ to liquid nitrogen temperature.

When the calibration strain has been subtracted, the remaining strain is due to two factors. The first factor is the temperature gradient across the pipe wall. When a pipe is frozen normally, particularly where liquid nitrogen impinges directly on it, strong temperature gradients exist initially across the tube wall. Since the cold outer part of the pipe will be trying to contract more than the warm inner, the stress and strain will be tensile on the outside and compressive on the inside. The remaining strain is due to

the formation of solid material on the inner wall which may cause either a compressive or tensile stress in the tube wall, depending on the relative expansion coefficients of the tube and the solid material. For example, ice has a higher coefficient of expansion than steel and so it will try and contract away from the steel, causing compressive stresses and strains in the tube wall.

To measure the strains due to plug formation only, Gostick slowly cooled a water filled tube. To measure the strain caused by shock cooling, a tube filled with propan-2-ol (freezing point -89.5^{o}C) was immersed directly in liquid nitrogen. The results show that rapid cooling develops strains that are an order of magnitude higher than those observed with slow cooling.

2.2.2 Application of strain measuring technique to pipe freezing

Once the strain measurement technique had been developed and tested on the very small diameter tubes, further tests were carried out on a 50mm (2") diameter pipe, similar to that used in the flow freeze tests described in section 2.1. The pipe was instrumented with 16 strain gauges (8 longitudinal and hoop pairs) and 16 thermocouples (8 soldered to the outside of the pipes near each strain gauge pair and 8 glued to the inside of the pipe opposite them). Before this pipe could be frozen in the normal way and the strain measured, the calibration routine detailed in the previous section had to be performed. Due to the size of the pipe a new way of obtaining a slow, and temperature gradient free, cool down had to be devised. The technique, developed by the author, was to support the pipe inside a long insulated tube, so that gas can pass all around and through it. Nitrogen gas was passed through the insulated tube, and the temperature of the gas was gradually lowered until it reached approximately -190^{o}C. The flow of this gas could be assisted by a fan at the outlet end if necessary. The very cold gas was generated by boiling off liquid nitrogen in a pool at the inlet end of the tube.

In order to further cool the gas it was passed over a heat exchanger, itself cooled by the incoming liquid nitrogen. Temperature control was achieved by varying the liquid nitrogen inlet flowrate, so that more or less air at ambient temperature was mixed with the nitrogen gas. The nitrogen was boiled off by immersing a set of copper tubes into the nitrogen pool, which were heated by the building hot water supply and designed so that they would not freeze up. Once the pipe had reached its minimum temperature, the nitrogen supply was stopped and the pipe allowed to return slowly to ambient temperature.

The computer was used to collect data from the strain gauges and thermocouples during both the cooling and warming phases of the run. It was necessary to collect data whilst the pipe was warming up since the strains measured at this time differed by up to a few tens of microstrains from those measured at the same temperatures during the cooling phase. The raw data was stored on floppy disk for further analysis. After each calibration run, a second computer program was used to fit 6th order polynomials to the temperature/strain data. This was done separately for the cooling and warming phases. In order to get a good curve fit it was again found necessary to split up the run into two further sections : ambient to $-90^{o}C$ and $-90^{o}C$ to minimum temperature. Thus for each calibration run with each strain gauge, four sets of polynomial coefficients were produced which were then stored on disk. The third and final program read all the polynomial coefficients produced by up to six calibration runs and used them to produce an average curve of strain against temperature. This curve was then fitted to a 6th order polynomial, splitting up the temperature range, as before, into 4 sections. This final set of coefficients was output on paper to be incorporated into the software that measured the strain during the actual freezing runs with the pipe.

Experiments on the 50mm pipe, calibrated as described above, were performed by Ashfield [45]. The maximum strains recorded (at the start of the freeze when the temperature gradients were greatest) were

around 350 microstrain, equivalent to about 100 MN/m^2 (14000 psi), which is approximately 40% of the room temperature yield stress.

A further run was performed with a layer of cotton wool surrounding the pipe inside the freezing jacket. This was to slow the cooling rate in order to limit the temperature gradient across the pipe. It did indeed do this but surprisingly the peak hoop strain was still around 350 microstrain. The peak longitudinal strain was, however, lowered to less than 100 microstrain.

Wallbank [46] instrumented and calibrated a similar pipe, and mounted it in a rig designed to be 50 times as stiff as the pipe and effectively restrain its longitudinal contraction. The first runs were performed with the pipe empty. The hoop and longitudinal stresses showed initial tensile peaks due to the shock cooling, the peak stress, this time, rising to around 75% of the yield stress at one position. Then the longitudinal stress dropped to a lower level. Due to Poissons Ratio effects the hoop stress went compressive at this point. When the pipe was frozen full of water the behaviour was similar except that the hoop strain went more strongly compressive due to the additional effect of the ice contracting and pulling the pipe inwards.

2.3 Determination of the strength of frozen ice plugs

Another facet of pipe freezing to be investigated has been the strength of the frozen ice plug. Initial pressure tests were conducted by Williams [35] on the 100mm diameter (4") freezing rig. Self pressurisation of freezing ice between the plug and the flange plate showed that the plug failed at between 5 and 6.2 MN/m^2 (720 and 900 psi) which correspond to an interfacial shear stress of 0.41 and 0.52 MN/m^2 (60 and 75 psi). These figures agree well with the that quoted by Hall [47] of 0.45 MN/m^2 (65 psi).

An attempt was made by Abbot [48] to measure the interfacial shear strength of an ice plug directly. Water was frozen between concentric stainless steel cylinders and then the outer cylinder was supported while the inner one was loaded with weights until failure occurred. Unfortunately problems with the experimental technique, particularly that of maintaining the temperature of the apparatus during loading, meant that the results of the earlier experiments showed far too much scatter to be interpreted. Once the rig had been modified to overcome these difficulties the frozen annulus of ice was found to be too strong for the loading system, available at that time, to shear.

Gibbs and Harris, the group's technical support, continued similar experiments, but this time using an Instron tensile testing machine to load the ice annulus. The shear strengths measured varied considerably, from 0.3 to 2.0 MN/m^2 (43 to 270 psi). Plugs were frozen in three ways, cooling the inner tube, the outer tube, and cooling both tubes so that the ice met in the middle. The first of these three produced plugs of the highest strength. This is thought to be because the outer tube, which cools last, will contract and compress the already frozen ice. If the plug is frozen from the outside inwards, the inner tube will cool last and will tend to contract away from the ice, thus weakening the bond.

Due to the difficulty of interpreting the results, the shearing ice annulus tests described above were of limited practical use. So for subsequent work, a return was made to hydrostatically pressure testing plugs formed in pipes in the conventional way. A 50mm (2") diameter, 4mm (0.16") wall thickness, stainless steel pipe was fitted with welded flanges to allow hydrostatic testing to high pressures. It was instrumented with a central string of twelve thermocouples, spaced at 25mm (1") intervals on a nylon cord. A 250mm (10", 5 x diameter) open trough type jacket was fitted to allow the use of either liquid nitrogen or solid carbon dioxide (dry ice) and methanol as a coolant.

Dry ice was added to the methanol quickly, so as to obtain as fast a freeze as possible. Consequently, only three pressure tests were made during the plug cool down. After 20 minutes, when the plug was about 175mm (7") long it moved slightly with an applied pressure of 500 psi. By 57 minutes the plug had grown to nearly 250mm (10") long and moved at 1400 psi. 80 minutes into the freeze and the plug withheld a pressure of 2000 psi. No more dry ice was added after this time and the pressure was held for a further 5.5 hours. A second freeze was made using dry ice as a coolant, but this time adding it more slowly to allow more pressure tests during the cooling period. The results obtained showed good agreement with the first test.

A third test was started using dry ice as the coolant. After 90 minutes the plug was moving under an applied pressure of 800 psi. All the dry ice and methanol was removed at this point and liquid nitrogen was added. After 110 minutes, when the central temperatures had fallen to around $-150^{\circ}C$, a pressure test showed that the plugs pressure holding capability had fallen to 200 psi. As the plug approached liquid nitrogen temperature the plug strength reduced further, 120 psi being sufficient to move it at one point. After 2.5 hours no more liquid nitrogen was added and within another hour the central temperatures started to rise. As they did so the plug strength improved. 5.5 hours into the test the central temperatures had warmed to about $-140^{\circ}C$ and a pressure of 2000 psi was withheld for over 2 hours.

In a test using only liquid nitrogen as the coolant, the pressure holding capability during cool down fell from a maximum value of 750 psi to 400 psi, as nitrogen temperature was reached. As the plug warmed up the strength again increased until 2000 psi was withheld at a central temperature of around $-140^{\circ}C$.

The results described above must be interpreted with some care. It is possible that repeatedly moving a plug slightly , during pressure testing, may affect the results of tests made subsequently.

Nevertheless, some rationale of the results can be offered. The thermal coefficient of expansion for ice is greater than that for steel, so that during cool down the ice will tend to contract away from the pipe wall thus weakening the bond. Loud cracking sounds heard during cool down may indicate that the plug is fissuring and breaking away from the pipe wall. If this is the case, then water may be able to leak into the gap between the pipe wall and the plug and freeze. So when the pipe and plug reach thermal equilibrium at liquid nitrogen temperature, the frozen ice will be relatively unstressed. When allowed to warm up the ice will try to expand faster than the pipe which means that the pipe/plug interface will be in compression, thus increasing the strength of the bond.

The reduction in plug strength reported above was not observed during freezing of a 300mm (12") diameter pipe filled with water. In this larger pipe temperature equilibrium was never reached, minimum central temperatures recorded being around $-170^{o}C$ and pressure holding capability rose to in excess of 1600 psi.

2.4 Determination of the strength of frozen hydrocarbon plugs

Many pipes that are presently frozen commercially contain some sort of hydrocarbon product or crude. Often however, particularly with larger pipes, a slug of water is pigged into the freezing zone and this is then frozen because it is assumed that an ice plug will be stronger. It is therefore considered particularly important to develop a knowledge of the freezing characteristics and plug strength of hydrocarbons so that hopefully the product or crude itself may be reliably frozen, thus avoiding the necessity of introducing the water.

One of the problems concerning the freezing of hydrocarbons is that, unlike water based fluids, they have no well defined freezing point but rather a stiffness (or viscosity) against temperature

gradient. In order to compare qualitatively the adhesive properties of several different frozen hydrocarbons, a simple rig was built and operated by Howell [49]. The principle was to establish a temperature gradient along the length of a heavily insulated steel bar that had a row of 10mm dia., 20mm deep holes drilled in its top. In each of these holes was a sample of the liquid under test, and suspended in the centre of each of these were thin tubes containing a single thermocouple. Thus the samples of oil would be cooled or frozen to a range of temperatures that would be measured by the thermocouples. When temperature equilibrium had been reached, the thermocouple tubes were withdrawn with a spring balance and the force required to do so recorded.

The hydrocarbons tested in this rig were Forties, Kuwait and light Arabian Crudes, Gas and Diesel oils, a proprietary SAE 15/50 grade motor lubricating oil, turbine oil and paraffin. The curves of pull force against temperature thus obtained are shown in figure 2.5. The range of temperatures of which the different oils were found to freeze varied from $-45^{o}C$ for turbine oil to $-150^{o}C$ for Gas oil. The sharpness, or otherwise, of the freezing points is also clear from this figure.

It was possible that, in multicomponent fluids such as crude oil, some segregation of the various fractions during freezing, would occur. Since the arrangement of the experiment described above would inhibit any possible segregation, a second rig was designed to check whether this factor was important. A long thin glass fibre reinforced plastic trough was constructed, heavily insulated on its bottom and sides, and fitted with aluminium chills at each end. One end was maintained at liquid nitrogen temperature and the other at ambient. The trough was filled with the test fluid and a temperature gradient established along it. A row of the thin stainless steel tubes, with the thermocouples as before, were located in the oil by a drilled perspex cover. Once temperature equilibrium had been established, the tubes were withdrawn from the oil using a spring balance. The results

obtained for all the oils in which a temperature gradient was successfully set up were similar to those obtained in the previous rig, showing that segregation was not affecting the interface strength if, indeed, it was occurring at all. However, as intimated above, with some oils it proved impossible to establish a stable temperature gradient along the trough due to strong natural convection currents carrying the heat from one end of the trough to the other. The oils in which this was found to occur were Diesel (which was already known to convect strongly - see section 2.1), Gas oil and Paraffin.

Since the results obtained above are of a purely qualitative nature, an experiment was conducted by Brown [50] with the object of quantifying them. A series of steel tubes, pressurisable using a pump and manifold system, was mounted vertically in an aluminium block. The aluminium block was cooled at one end by liquid nitrogen and it was hoped that a range of freezing temperatures would be obtained in the tubes in a similar way to the qualitative tests described above. Unfortunately, in practice it was found that only the bottom two tubes, nearest the nitrogen, became cold enough to freeze a pressurisable plug, and therefore all tests were performed in these tubes. A string of thermocouples were mounted on the axes of each tube in such a way that plug movement would not damage them.

Two hydrocarbons were tested in this rig, Forties crude and Diesel oil. The results are shown in figures 2.6 and 2.7 together with Howell's results [49] from the pull force rig with these fluids, scaled at 20 psi = 1 kgf pull force. This scaling factor overlaps the data for the Forties Crude and shows the pressure tests on the diesel to be a lower temperature continuation of the previous results. However, care should be taken when interpreting these results since it is not possible to know where the plug failed and therefore what the temperature was at the point of failure. The temperatures recorded by the central string of thermocouples should be the warmest in the plug, but they will vary considerably along its length.

The next series of hydrocarbon pressure tests were performed on a 150mm (6") diameter mild steel pipe, filled with Statfjord crude oil, using conventional direct contact liquid nitrogen cooling. Pressure tests were started when the central temperature had fallen to $-60^{o}C$ and were repeated thereafter for each further $10^{o}C$ fall. Figure 2.8 shows the relationship between central temperature and maximum pressure recorded. It can be seen that once the central temperature is below $-125^{o}C$, pressures in excess of 1000 psi can be withheld.

Use of a 50mm (2") diameter stainless steel pipe allowed higher test pressures to be used. After 30 minutes of freezing Statfjord crude, with central axis temperatures in the range -110 to $-130^{o}C$, a pressure of 2000 psi was withheld. When the central temperatures reached -150 to $-170^{o}C$ after 40 minutes, an applied pressure of 3500 psi was held with no sign of movement.

Finally, Statfjord crude was frozen in a 300mm (12") diameter mild steel pipe and successfully tested to 1500 psi after 18 hours and 40 minutes. The relationship between central temperature and pressure holding capability was found to be very similar to that of the tests in the 150mm (6") diameter pipe.

2.5 Heat flow during plug formation

The main area of interest of the Author was identified as the heat transfer and fluid flow effects on plug formation. It was decided that a highly instrumented rig would allow plug formation to be measured as well as the radial and longitudinal temperature gradients in the tube wall, the solid and the liquid. The experimental programme would provide correlations for a computer model of the pipe freezing situation which would be developed in parallel. The development of the model is essential if the results are ever to be generalised to any combination of geometry, pipe material and fluid type that it might be desired to freeze. The following chapters will deal with the progress of the experimental and modelling programmes to date.

3.0 Development of the experimental programme

Consideration was given to the type of rig that should be built to get the experimental programme underway. Since none of the experiments performed by the group at this time had allowed the freezing plug to be viewed, this was considered an important first step.

The idea initially was to construct a transparent freezing rig which would allow total visibility of the plug as it formed. However, there were several problems to overcome. The first and greatest is that any transparent material that could be used to construct the rig had a far lower thermal conductivity than the metallic pipes on which pipe freezing is usually performed. Thus it is likely that the plug formation observed would not be typical of more normal pipe freezes. The second problem is that transparent materials were likely to be extremely brittle at liquid nitrogen temperatures and when combined with the considerable thermal stresses caused by shock cooling, this was a major difficulty. The other problems concern visibility, firstly through the boiling nitrogen, which may be solved by using a non boiling heat transfer liquid such as I.P.A. but this would limit the temperature applied to the outside of the pipe to around $-100^{o}C$, again not typical of industrial pipe freezes. Finally, plug formation in the pipe would itself inhibit visibility from the side. Consideration of these problems prompted the conclusion that a transparent pipe freezing rig was impracticable if the plug formation in it was to be at all typical of freezes performed on metallic pipes.

An alternative was sought, and the solution decided upon was a short, relatively large diameter steel pipe which would freeze in a manner similar to that of a normal industrial pipe freeze, but would allow a reasonable amount of visibility via perspex end plates. The dimensions selected were 100 mm (4") diameter and 600 mm (24") long, with a 200 mm (8") long freezing jacket positioned centrally. It was

decided that the pipe would be frozen vertically as this orientation allows more natural convection, a phenomenon which it was intended to investigate, and also has the advantage that the freeze would be axi-symmetric, thus making interpretation of the results easier. Vertical freezes, although perhaps in a minority, are still relevant in an industrial sense since refineries and similar plant contain many potential vertical freezing sites. Fabrication of this rig would be straightforward compared to a totally transparent rig and no problems of pipe fracturing at low temperatures were expected, or subsequently encountered.

On the debit side, the need to keep the pipe short to allow good visibility meant that thermal circulation above, and particularly below the freezing zone, would be more restricted than in the real case, and also the total volume of water to be cooled by convection would be less, thus the pipe would be expected to freeze more quickly.

The first version of the rig was built from mild steel. Since ice has a lower density than water, some water will be displaced as freezing takes place, and to prevent a catastrophic pressure build up two 1" dia. relief tubes were taped into the main pipe 4" from each end. The later version of the rig, on which all the data discussed in chapter 4 was obtained, was built from stainless steel.

3.1 Addition of thermocouple instrumentation

The addition of thermocouple instrumentation to this rig presented some problems. The method in use within the pipe freezing group up until this time consisted of leading individual thermocouples, shielded inside 1mm I.D. stainless steel tubes, down from one end of the pipe. With the large number of thermocouples to be fitted to this rig, this method was impracticable due to the large thermal mass of all the stainless steel tubes, their interference with visibility and their effect on the natural convection currents within the freezing zone.

A better method was devised, consisting of a frame of four thin wall, .25" diameter stainless tubes arranged so that they just slide down the inside wall of the pipe. The thermocouple wires are led down the inside of these tubes and out into the main pipe through small holes drilled along their length. They are fixed in their appropriate position by being fastened to tough fishing line strung between the tubes. This arrangement has considerably less thermal mass, and since it keeps the wires tightly bunched inside tubes led up the sides of the pipe, interferes with fluid flow and visibility to a much smaller extent. Additional thermocouples were soldered to the outside and glued with epoxy resin to the inside of the pipe wall.

The raw data, as microvoltages, from the thermocouples were fed through CIL PCI 1002 analogue to digital converters and thence in digitised form to a Commodore PET microcomputer. The computer uses a fitted curve, expressed as a quartic equation to convert from microvolts to temperature. The temperature of the cold junctions inside the A/D converter is monitored with a platinum resistance thermometer and this temperature is also sent to the computer whose software has a cold junction compensation routine.

A program was written that could read data from up to eight of these PCI 1002 A/D converters thus giving the capacity to read 96 thermocouples, though it was later modified to read a 1-off, 96 channel PCI 6380 derived converter. The program provided output on screen, printer and cassette tape.

3.2 Rig modifications

Some preliminary tests of the rig indicated a number of problems that would have to be solved before useful information could be gathered. These problems and the solutions employed will now be dealt with one by one, not necessarily in chronological order.

The method of suspending thermocouples from the tubular frame proved successful though some care proved necessary when handling the assembly due to its rather delicate nature. However, the practice of glueing the internal pipe wall thermocouples to the pipe was shown to be unsatisfactory, since they frequently became detached. Presumably, the differential thermal contraction of mild steel and Araldite was to blame for this. It was found that, with care, and suitable cleaning of the pipe, it was possible to solder thermocouples to the inside. Subsequent experience showed that the Araldited thermocouples had not been reading the inner pipe wall temperature but rather some temperature between the wall and the surrounding water.

3.2.1 Analogue to digital conversion problems

After this initial modification, more tests were performed. It was clear that the instrumentation was still unsatisfactory because, after the initial rapid cooling, some inner thermocouples within the freezing jacket area were indicating temperatures lower than the corresponding outer thermocouples. This would indicate heat flowing out of the liquid nitrogen into the pipe, which is clearly impossible.

It was decided that the operation of the analogue to digital converters should be looked at more closely. Two types of thermocouple A/D converter are in use, both manufactured by CIL Limited. One is a 12 channel device known as the PCI 1002 and the other is a 96 channel instrument especially manufactured for us but based on the PCI 6380 series with a 12 channel multiplexer on each of the 6380's eight input channels. This device is arranged as a processor card plus eight thermocouple input cards, each with twelve thermocouple inputs. Each of these input boards has its own cold junction compensation platinum resistance thermometer. The circuitry of the PCI 1002 and the input cards on the 96 channel machine are very similar. In both cases the cold junctions are formed by leading a constantan wire from the thermocouple socket to a copper terminal

block mounted on the circuit board. The platinum resistance thermometer is mounted on the other side of the circuit board.

It is, of course, necessary to calibrate the converters before use if accurate results are to be obtained. The cold junction is calibrated by replacing the resistance thermometer with two accurate resistors of 100 ohms (zero degrees centigrade on a standard platinum resistance thermometer) and 130.0 ohms ($100^{o}C$), and adjusting the gain and zero potentiometers until the output of the cold junction channel is zero and FSD respectively. There is an overall gain potentiometer for all 12 input channels which is set by feeding 10mV exactly into one of the pairs of input terminals and adjusting that channel for FSD. Each channel has a zero adjust potentiometer, and these are set by using a thermocouple in an ice bath. This last process relies upon the accuracy of the cold junction compensation, or rather compensates for any inaccuracy at that cold junction temperature, such as could be caused by non linearity in the amplifiers. Of course, if the cold junction temperature were to change, then the error could be different and the thermocouple in ice would no longer read $0^{o}C$.

Herein lies a problem. In order to perform the calibration routine, the cards must be removed from their boxes to allow access to the potentiometers situated on them; thus they are in a completely different thermal environment when they are calibrated, to when they are in operation. Most electronic circuits are temperature sensitive to a greater or lesser degree, and this fact gives rise to unavoidable inaccuracies in reading data from the thermocouples. To combat this problem as much as possible, the converters are left permanently switched on so that they reach a quasi-steady temperature which will only vary with ambient temperature, and when cards are exposed for calibration they are left for at least 30 minutes in this position before any adjustments are made.

One idea that was tried was to convert one of the input cards to a system using external cold junctions that could be placed in an ice bath. This has the advantage of simplifying the calibration routine, and thus reducing the inaccuracies due to internal temperature fluctuations. However, because the thermocouples may be electrically connected, via the pipe wall for instance, each one must be provided with a separate and electrically insulated cold junction. Since it was planned to install nearly 120 thermocouples on the rig, this method was considered too cumbersome and was abandoned.

During the experimentation with the converters, the output of a thermocouple pair (cold junction in ice, 'hot' junction in liquid nitrogen) was being monitored by a highly accurate DVM. It was noticed that when this pair was connected to the input terminals of a PCI 1002 channel, the voltage read by the DVM fell from 5525 microvolts (195.2^{o}C) to 5471 microvolts (192^{o}C). No change was observed if both junctions were in ice. This indicated that the input impedances of the PCI 1002 channels were too low, and both our instruments of this type were sent away to be modified accordingly.

Another hardware problem that was noted at this time was an instability in the 96 channel device of some 30-40 microvolts, equivalent to about 2^{o}C at liquid nitrogen temperature. This was not evident in the PCI 1002's and turned out to be due to a different type of A/D converter chip. This chip was replaced by a newer version and the devices internal software modified to allow the selection of a digital filter which averages the results of 16 readings before putting anything on the IEEE bus. This cured the problem but did have the disadvantage of making the reading time longer.

A check was made on the linearity to the input amplifiers by feeding their input with a range of voltages from an accurate microvolt source and noting the output to the computer. The linearity was found to be better than $\pm$3 bits, or around $\pm$0.5^{o}C at LIN temperature. This inaccuracy was felt to be insignificant when the

standard thermocouple wire in use was only guaranteed to within ± 2% of the standard tabulated voltages, i.e. around ± 4°C at LIN temperature.

3.2.2 Thermocouple calibration

As mentioned above, the standard grade thermocouple wire is accurate only to within ±2% due to variations of composition of the conductors. This margin of error is far too large to allow useful measurements of small temperature gradients at low temperatures to be made. Accordingly a method of calibrating the thermocouple over its entire operating range was sought. Furthermore, to allow for any variation between different channels in the A/D converters, it was decided to calibrate the thermocouple using the A/D channel with which it would eventually be used.

Because of the large number of thermocouples to be used, it was decided that they must be calibrated 12 at a time. The basic method settled on was to cool all 12 and some other temperature sensing element down to liquid nitrogen temperature and then allow them all to slowly warm back to ambient temperature.

The original idea was to use a platinum resistance thermometer as the 'reference' element, and a sheathed thermometer was set in a small brass block which was itself set into a larger lead block to give a greater thermal mass. A similar brass and lead block was bolted against this one trapping the 12 thermocouples against the resistance thermometer in the centre. Two problems were experienced with this set up. One was that of finding a resistance thermometer with robust enough connections to stand the shock cooling to LIN temperature. Eventually a type was found that was satisfactory in this respect, but unfortunately this device allowed too much heat down its outer case which set up a temperature gradient along the brass block and hence also along the line of thermocouples.

A re-think was called for and it was decided that, while it was important that all thermocouples should read the same while they were at the same temperature, the actual temperature read was not needed to such a high degree of accuracy. This is because we are interested more in heat flow, i.e. temperature differences, than in absolute temperature.

This allowed the use of a thermocouple pair with one junction in an ice bath as the 'reference' temperature sensing element. A highly accurate DVM was used to measure the voltage output of this pair when the 'hot' junction was immersed in ice, dry ice and methanol, liquid oxygen and liquid nitrogen. The standard thermocouple tables were used to determine the difference between the voltage measured and the standard value at each temperature, that is the offset voltage. Next a curve fitting computer program produced a smooth curve of offset voltage against temperature from $15^{o}C$ to $-196^{o}C$. The maximum value of this offset voltage was 12 microvolts at LIN temperature, equivalent to around $0.66^{o}C$. The tabulated voltage at each full degree centigrade between 15 and -196 was then added to the smoothed offset voltage for that temperature. This sum was used as the independent variable input and the corresponding temperature as the dependent variable input to the curve fitting program again, thus producing a 6th order polynomial expression for the curve, based on the tabulated thermocouple data, but adjusted for this particular thermocouple. This thermocouple, together with its polynomial was accepted as the 'standard' to which all the others would be calibrated.

A new device was built to perform the calibration which consisted of a small brass cylinder (.75" dia., 1" long) into the top face of which were drilled 13 equally spaced 2mm dia. holes, subsequently filled with soft solder. When twelve thermocouples were to be calibrated the cylinder was heated to melt the solder, and then the 12 thermocouples, plus the one reference one, inserted into the holes. The cylinder was then allowed to cool. The solder ensures

good thermal contact between the brass and the thermocouples, so they were all at the same temperature. The brass cylinder and its attached thermocouples were then heavily insulated by placing them in the centre of a large styrofoam cylinder.

The 12 thermocouples were connected to the A/D converter channels with which they were eventually to be used. These had been carefully calibrated according to the procedure described in section 3.3.1 before the calibration run was started. The reference thermocouple pair was connected to a Datron DVM, itself connected by the IEEE bus to a PET computer. Figure 3.1 illustrates the calibration set up. The brass cylinder in its insulation was cooled to LIN temperature by direct immersion which did not take too long because LIN was able to leak through the joint in the insulation and contact the brass. When LIN temperature was reached the computer program was started and the apparatus removed from the nitrogen to begin warming up.

The computer continuously monitored the temperature of the brass block as it warmed up via the reference thermocouple and the DVM. As each full degree centigrade was reached it took a reading via the A/D converters of the output voltages of the 12 thermocouples being calibrated. The block reached $15^{o}C$ after 15 hours or so, and the computer then stopped taking readings. It now had stored, for each thermocouple, 211 voltage readings from $15^{o}C$ to $-195^{o}C$ and these were used as the independent variable, with temperature being the dependent one in a least squares curve fitting routine. This routine fitted a sixth order polynomial to the data for each thermocouple, and the coefficients of these polynomials were stored on disk together with the identification of each thermocouple and its A/D converter channel number.

The above procedure was performed three times for each set of 12 thermocouples. A second program was then run which read the three sets of coefficients stored on disk from the three calibration

runs. With these it calculated the three slightly different temperatures corresponding to a voltage of +600 microvolts, and averaged these temperatures. 600 microvolts and this average temperature provided the first point on the final calibration curve for that particular thermocouple. Further points were derived by calculating the average temperature at 500 microvolts, 400 microvolts..., down to -5600 microvolts. These points were once again fed into the least squares curve fitting subroutine and a 6th order polynomial produced as the final calibration of that thermocouple, and these were then stored on disk.

Thus to calibrate 120 thermocouples required thirty experimental runs each of which took effectively 24 hours. This was obviously a time consuming process but was considered essential if useful results were to be obtained.

3.2.3 Software modifications

The original tests were done with just 52 thermocouples on the rig and even with this number the time taken by the existing software to read, process and present the data was too long. With 120 individually calibrated thermocouples now to be installed on the rig, a complete rethink of the way the data was to be handled was necessary.

Obviously some form of hard copy of results was essential, but the dot matrix printers available were so slow that they would seriously inhibit the rate at which readings could be taken. Some form of storage of data that could then be printed out when convenient was called for. The tape storage in use up until this time was still too slow, so disk storage was selected.

Since no real time hard copy would be produced, it was desirable to have a real time screen presentation of data. The best way of presenting the thermocouple temperatures would be so that the

temperature appears on the screen in a position corresponding to its position in the pipe. Unfortunately, the resolution of the PET screen does not allow this, and the only way a hundred and twenty temperatures could be displayed at once was in closely spaced rows and columns. An alternative was decided upon which allocated one screen position to each thermocouple according to its position in the rig. If the thermocouple was reading above $0^{o}C$ then no figure would be put in that thermocouple's position. When the temperature registered was in the range 0 to $-20^{o}C$ a '1' would be inserted, -20 to $-40^{o}C$, as '2' and so on until -180 to $-200^{o}C$ produces a '9'. With an averaging routine to fill in the gaps between figures a representative picture of the shape of the plug and its approximate temperature distribution would be built up and modified each time the thermocouples were read. A full print out of temperatures packed onto the screen was produced before a run commenced to enable defective thermocouples to be detected.

Up until now all programs had to be written in BASIC, but even the operation of just reading the A/D converters in BASIC took a time that was significant when compared to the rate at which temperatures were changing. Thus, because of the delay between reading the first and last thermocouple, the output would not be a series of instantaneous 'pictures' of the temperature distribution, but rather each 'picture' would contain readings made at significantly different times according to the order in which they are read. This would obviously make analysis more difficult and was undesirable. To combat this problem and to allow a reasonable number of readings to be made every minute, a machine code program was developed, capable of reading the A/D converters, selecting the appropriate calibration coefficients to convert the output of each thermocouple to a temperature including cold junction compensation, and finally producing a screen presentation of the type described above. This machine code program was run as a subroutine in a basic program which handled the timing of the readings plus the initialisation of the disk file and writing data to it.

The machine code program was organised into three sub-programs. A short machine code program called these three subprograms as subroutines as well as saving and reinstating the zero page RAM. This last is necessary since BASIC makes extensive use of nearly all zero page, yet zero page is well worth using in a machine program as pointers or storage locations that are to be heavily utilised. The reason that zero page is so useful lies in the addressing modes on the 6502 processor chip which allow indirect addressing using zero page addresses as pointers and short form addressing of zero page itself which decreases execution time.

The first subprogram consists of IEEE handshake routines to obtain raw data from the A/D converters and store those as a 260 byte block in RAM. The second subprogram uses each thermocouple's own calibration coefficients in turn to process the voltage data into temperature. This subprogram includes floating point arithmetic routines and uses the same number representation as BASIC, that is a four byte mantissa and a single byte exponent. In the rest of the machine code, numbers are represented in abbreviated form consisting of 2 bytes in order to save space and processing time. Subroutines in this second subprogram convert from one form to the other. The final subprogram handles the screen presentation including all the averaging for spaces in between thermocouples.

In order to produce hard copy of results, a separate BASIC program has been written which allows the temperature distribution at selected times to be printed out.

3.2.4 Improvements to ice plug visibility

Early experimental runs with the rig revealed a stream of bubbles given off at the ice/water interface. The reason for this is not clear, presumably it is dissolved air coming out of solution but in any case it does cause a visibility problem when it collects under the top viewing plate. A method had to be devised of clearing it and

the first idea tried was an arrangement of water jets directed to sweep the bottom surface of the perspex plate, together with a drain to bleed off the air and water so displaced. Although this method cleared the bubbles it was strongly suspected that it caused a lot of turbulence in the area that temperature measurements were taking place, thus affecting the results. The alternative settled on was a simple, mechanical wiper with a shaft lead through the top plate, incorporating an 'O' ring seal. This method allowed clearance of the bubbles with a minimum of fluid disturbance.

Although unimportant in this particular work, the evolution of air bubbles is significant where the plug is to be used for hydrostatic pressure testing. The formation of air pockets may have safety implications due to their compressibility and hence their ability to store energy. Even if this is not the case, they may make interpretation of the test more difficult especially if they tend to redisolve in the water as the pressure is raised.

3.2.5 Liquid nitrogen level maintenance

In order for the experimental results to be meaningful and repeatable, it was essential that the nitrogen level in the jacket be maintained at a constant level for all runs. The earliest and simplest method tried was a float with a marker stick in a perforated tube. Unfortunately the boiling off of the LIN and the restricted exhaust of N2 gas creates a small positive pressure inside the jacket which tends to blow the float out of the top of the perforated tube. The next idea, a float switch connected to a light bulb did work but proved unreliable, possibly due to freezing up of the float. The solution finally adopted was to use a carbon resistor as a probe. Current was continuously fed through the resistor thus heating it up so that even in cold nitrogen gas its temperature was well above that of liquid nitrogen. However, when the LIN level rose and immersed the resistor, the improved heat transfer coefficient in the liquid as opposed to the gas, caused the temperature of the resistor, and hence

also its resistance, to fall sharply. When this occurred the voltage across it fell also. By using a variable resistor and a voltage comparitor driving an LED indicator, a circuit was built and adjusted so that the LED was on when the resistor was immersed and off when it was not so. By using two such circuits with two resistors spaced half an inch apart vertically a level detection device with high and low level indicators was obtained. It was then possible to maintain the nitrogen level fairly accurately by turning off the supply valve when both indicators were on (level above upper resistor) and on again when both were off (level below lower resistor).

Although this method of level detection worked well, it required much concentration in use to keep the nitrogen level between the two resistors, which meant it was difficult to monitor the rest of the experiment. Accordingly, an automatic control circuit was designed to add to the sensing circuit that operated a solenoid LIN supply valve. A manual by-pass valve was also fitted so that the jacket could be filled quickly at the start of each test, but this was closed as soon as the first LED lit up, and thereafter LIN level control was totally automatic. Some trouble was experienced with the solenoid valve icing up during the initial cool down and to prevent this the practice of briefly closing the valve every five seconds or so for the first minute and a half, was adopted. This apart, the system has proved very reliable in practice.

3.2.6 Freezing jacket development

Some effort has been expended in the direction of nitrogen jacket development. The jackets supplied to us by the pipe freezing industry at the outset of this project were made of two layers of aluminium with an insulant in between. They were made in two halves that bolted together around the pipe. Although these jackets were very robust, something that is important in commercial applications, they were heavy and wasted a lot of nitrogen through heat leaks and their own high heat capacity. A jacket was made entirely from

styrofoam which is light, a very good insulant and has low heat capacity. The jacket was made in two halves that were fastened together with large jubilee clips. The joints of this jacket proved very difficult to seal. The sealant in use at the time was a mastick or putty type material which tended to crack up at low temperatures. A change was made to Denso-Tape, a cloth tape impregnated with a waxy substance. This improved the situation but did not cure all the leaks, the lower jacket to pipewall joint proving particularly troublesome. A new jacket was designed, made in six pieces. The edge of each piece was hot wire cut into a tongue or a groove. When these tongue and groove joints were assembled with Denso-Tape between them they form a very effective seal. Furthermore, because the bottom plate of the jacket is assembled onto the pipe first, the critical lower jacket to pipe wall joint can be carefully sealed with Denso-Tape inside and out. This jacket has proved almost completely leakproof, its only disadvantage being that due to its method of construction it uses a lot of styrofoam.

3.2.7 Addition of tank

After the first series of runs with the rig in the format described above it was clear that the full effect of natural convection was not being observed. This was because the natural convection circulation currents, set up at the start of the freeze, quickly cooled the water below the freezing zone and thus reduced the effect of these currents on the progress of the freeze. In a real pipe with many metres of length below the freezing zone, this reduction in bulk temperature would be slower and less extensive. It was obviously important to examine the full effects of natural convection but in the laboratory it was impractical to attach a long length of pipe below the freezing section. So to simulate the effect of a long pipe within the space available a glass fibre tank of approximately 200 litres capacity was modified so that the test section of pipe could be bolted directly to its top. In this way natural convection between the pipe and the tank below would maintain

the bulk temperature of the water within the pipe much longer. Increasing the volume of water above the freezing section was not thought to be so important since after freeze-off, natural convection in this area is much less important. This is because from a convection point of view, the situation in the top of the pipe is a stable one with warm water above cold water and ice.

Additional pipework was added to enable the water in the tank and test pipe to be circulated by a pump through a heat exchanger, thus enabling the bulk temperature of the water to be raised or lowered by heating or cooling the heat exchanger. The pump was always turned off and isolated during freezing so as not to affect plug formation.

The problem of how to get light up the pipe to enable plug formation to be viewed with the tank in place was solved using a higher intensity light shining through a perspex window in the side of the tank onto a mirror angled at 45^{o} and set below the pipe.

3.2.8 Modifications to outer pipe wall thermocouples

The results analysed in chapter four were obtained with the rig in the configuration as described so far. Full analysis of the results revealed that the thermocouples located on the outer wall of the pipe within the liquid nitrogen jacket were reading temperatures considerably lower than the true temperature of the outer wall of the pipe. These were simply soldered to the surface of the pipe wall and it was thought that the resultant surface irregularity was causing a local breakdown of the vapour barrier during film boiling and hence wetting, by liquid nitrogen, of the area immediately surrounding the thermocouple tip. In addition, the thermocouple wire were led away directly into the liquid nitrogen. This meant that a high temperature gradient existed along the wire very close to the tip, causing heat to be conducted away and the tip to be further cooled. In order to combat these problems, horizontal grooves, about 2 mm deep and 25 mm long, were cut in the pipe wall where each thermocouple was to be

located. The tip of each thermocouple was soldered into one end of a groove and the wire laid in the groove which was filled in with a plastic metal compound. When set, the solder and plastic metal were filed flush with the pipe so as to present a smooth pipe wall to the liquid nitrogen in the area of the thermocouple tip.

3.3 Future Experimental Work

The 100 mm rig described in this chapter will be used for the freezing of crude oils since it has not been possible to date to carry out a realistic test freeze on a more highly convective fluid such as these because of the restricted length of pipe available.

A new rig is being designed and built which will allow the freezing of pipes up to 250 mm (10") diameter in either the vertical or horizontal orientations. Large tanks will be provided to simulate the effect of surrounding pipe work. A pump will allow the fluid to be circulated through the freezing area in either direction to test the effect of forced convection on the freezing mechanism. Steam heat exchangers will provide the necessary heat input to maintain the inlet temperature during these flow freezes.

Some work must be undertaken on controlled temperature freezes, using solid carbon dioxide and iso-propanol as the coolant, since industrial users, conscious of the embrittling effect of liquid nitrogen, may often opt for this type of freezing. This work would be linked with a similar extension in the numerical modelling programme (chapter 5).

Finally some flow visualisation work is planned. The mechanism of plug formation postulated in chapter 4, which is controlled by changes in the pattern of natural convection, is all inferred from temperature measurements. It is hoped to be able to visually confirm these convective effects by freezing a thin vertical "slice" of water in a transparent sided vessel, injecting dye or

electrolysing the water to form tiny hydrogen bubbles as a tracer. The use of a fluid like freon in a rig of this type may allow the visualisation of plug formation with very highly convective fluids.

4.0 Analysis of Results

Before analysing the results in detail it is worthwhile considering the limits on the accuracy of the data. The thermocouple temperatures should have been accurate to around $\pm 1^{\circ}C$. An exception to this was the thermocouples positioned on the outside of the pipe wall within the freezing jacket. When the heat lost from the pipe was compared with heat apparently flowing across the pipe wall, the latter was found to be much larger. The only explanation that could be found for this is that the outer thermocouples, which were simply soldered to the pipe wall, were reading too low. It is thought that a combination of the solder blob breaking down the vapour barrier during film boiling and heat flow up the wire into the liquid nitrogen, caused the thermocouple to become a local cold spot particularly during the early stages of a freeze. This problem was corrected for the final freeze, as described in section 4.3, but for the remainder of the data analysed in this chapter, this inaccuracy applied.

The thermocouples should have been spaced radially at either 12.5 mm or 6.25 mm intervals, but in fact their position was probably only accurate to about ± 1 mm. In the case of the thermocouples in the water and nearest to the pipe wall this positional inaccuracy was probably much worse. These thermocouples were unsupported at their tips and hence prone to being bent out of position as the thermocouple cage assembly was lowered into the pipe. Some of them may have been touching the pipe wall while others may have been up to 2mm distant from it.

When the thermocouples were positioned on the cage it was assumed that plug formation would be axi-symmetric and so thermocouples that were apparently adjacent were positioned on opposite sides of the pipe to reduce the over crowding of wires. From the results it appears that the freezes were not totally axi-symmetric especially in the cases of higher initial temperatures. This was probably due to the nitrogen feed and exhaust creating cold spots on

certain parts of the pipe.

The calibration of the thermocouples took place over the range from -195°C to 15°C. Thus any temperature readings above 15°C can only be regarded as approximate and the further away from its calibrated range a thermocouple was, the greater the inaccuracy was liable to be. The initial temperatures for warm water freezes were set by using a simple program to read a thermocouple on the centre section near the pipe wall and adjusting the water temperature until this thermocouple was stable at the required temperature.

4.1 Results from freezes made without tank

The first series of tests, conducted without the tank below the pipe, consisted of ten freezes with initial temperatures varying from 6.5°C to 50°C in approximately 5°C steps. Timing and data recording were started when the nitrogen supply was first turned on. A full jacket (nitrogen 150mm deep) was obtained in approximately 90 seconds and the nitrogen supply was terminated after 20 minutes. After this time however, the rate of nitrogen boil off is very low and hence its level declined only slowly. The freezes were conducted in the following order of approximate initial temperatures; 50, 40, 30, 20, 10, 6.5, 15, 25, 35 and 45°C. This was done so that any drift in the instrumentation calibration over the period in which the freezes were performed would be easier to spot, and thus misleading deductions would be avoided.

When reading the remainder of this chapter, reference should be made to figure 4.1 which shows the layout of the pipe, the position of thermocouples within it, the location of cross sections and the subdivision of the pipe into upper, middle and lower volumes.

4.1.1 Times to freeze

Four times have been recorded for each freeze, these are ; time for plug to close (i.e. the time for the centre reach $0^{o}C$), time for the centre to cool to $-60^{o}C$, time for the centre to cool to $-140^{o}C$ and finally time for the plug to extend to a length of 100mm (4" or 1 diameter) along its central axis. These are shown in table 4.1 below and plotted in figure 4.2. It should be noted that these times have been estimated by an approximate interpolation process with data points spaced 30 seconds, or sometimes 15 seconds, apart.

Initial Temperature	Times (minutes - seconds)			
	$0^{o}C$	$-60^{o}C$	$-140^{o}C$	100mm plug
$6.5^{o}oC$	13-30	14-45	17-00	14-30
$10^{o}C$	14-30	15-20	18-30	16-30
$15^{o}C$	14-30	15-20	18-00	16-45
$20^{o}C$	15-15	16-00	18-30	17-30
$25^{o}C$	15-30	16-15	19-00	17-45
$30^{o}C$	16-30	17-15	20-00	19-15
$35^{o}C$	17-15	17-30	20-00	19-30
$40^{o}C$	17-30	18-10	21-00	20-30
$45^{o}C$	17-45	18-20	21-00	20-30
$50^{o}C$	19-15	19-50	22-15	23-00

Table 4.1

From the above table it can be seen that the times to freeze increased in a very approximately linear fashion with increasing initial temperature, although the $50^{o}C$ data indicates that the freezing times may increase more steeply above this temperature.

Also plotted on figure 4.2 are the time intervals between attaining $0^{o}C$ and $-60^{o}C$, $-60^{o}C$ and $-140^{o}C$ and $0^{o}C$ and a 100mm plug. It is evident that after freezing the centre temperature dropped to

$-60^{o}C$ very quickly, in all cases in less than 75 seconds and more typically in around 45 seconds. Furthermore it can be seen that this temperature drop was slightly faster with higher initial temperatures. A fuller discussion of this observation will be left until the radial temperature profiles have been examined in section 4.1.3.

The cool-down time from $-60^{o}C$ to $-140^{o}C$ was much slower, typically around 2 minutes 40 seconds and shows no relationship to initial temperature. By contrast, the time for the plug to extend to 100mm rose from 1 minute with an initial temperature of $6.5^{o}C$ to 3.75 minutes with an initial temperature of $50^{o}C$. This was due to strong natural convection currents in the bottom section of the pipe retarding plug growth downwards.

4.1.2 Interface positions

The estimated ice/water interface positions have been plotted in figures 4.3a - 4.7a for initial temperatures of 10, 20, 30, 40 and $50^{o}C$. The solid lines represent the interface at 4 minute intervals, while the dotted lines are drawn at certain intermediate times to illustrate plug growth more clearly. Figures 4.3b - 4.6b are shown on the same pages for comparison but will be discussed separately in section 4.2.2. Plug growth appears to have occurred in three phases, the first of which advanced the ice front until the remaining orifice is around 25mm (1") diameter.

The progress of the first phase of plug formation was very dependent on initial temperature. At $10^{o}C$ the position of the ice front after 4 minutes showed approximately 10mm of ice over almost the full length of the freezing section. At $50^{o}C$ the 4 minute position shows that ice was only just established over the lower 50mm (2") of the freezing section and this was due to much higher convected heat transfer from the water to the pipe wall. During phase one the convection currents started some distance above the freezing section and flowed down the wall as a boundary layer, past the freezing

section, finally separating from the wall in the lower section of the pipe to turn and flow back up the centre. The velocity of the downward flowing boundary layer has been observed to be of the order of 0.01 m/s by seeding the water with small particles. Velocities of this type are too low to cause significant pressure changes when flowing over the contracting and expanding parts of the partially formed plug. Therefore boundary layer separation of the type observed by Gilpin [31] when freezing flowing water (section 1.6.3) should not be observed in this case.

The establishment of an ice front was followed by a period of fairly rapid movement of the ice front inwards. The higher the initial temperature the more plug growth was biased towards the lower part of the pipe.

This observation can be rationalised using the boundary layer analysis of natural convection on a flat vertical plate [51]. This assumes a constant wall temperature, a constant bulk water temperature and, in between, a boundary layer of thickness ω, where ω is a function of x, the vertical distance down the plate. If the temperature profile across the boundary layer is assumed to be a quadratic function of distance then the local heat transfer coefficient is inversely proportional to the boundary layer thickness. Intuitively it can be seen that the thinner the boundary layer the higher the average temperature gradient across it must be. Since the heat transfer coefficient is proportional to the heat flux at the pipe wall, it must be proportional to the temperature gradient in the water where it meets the pipe wall. Therefore a thinner boundary layer means a higher heat transfer coefficient. The analysis due to Squire [52] shows that the boundary layer thickness is proportional to the 4th root of x, which implies that the boundary layer becomes thicker as it flows down the plate. The heat transfer coefficient, being inversely proportional to boundary layer thickness, decreases down the plate and therefore convected heat transfer, assuming a constant plate to bulk water temperature difference, will also decrease. The inside

of the pipe and the growing ice plug do not form a constant temperature flat plate, but in the early stages of plug formation the flat plate analysis should still be applicable as a first approximation.

Ice growth is governed by a balance between heat convected into the interface from the water and heat conducted away through the ice. The difference between these two is made up by latent heat removal at the interface. Where the convective heat transfer is high, i.e. at the top of the plug, the release of latent heat must be small, but when the convective heat transfer falls, then the removal of latent heat will be much higher. This is the reason why initial ice growth was biased towards the bottom of the freezing section and intuitively it can be seen that the effect will be more marked in hotter freezes where natural convection is stronger.

The other factor which controls interface growth is the conducted heat transfer away from the ice/water interface. For a given convective heat transfer, plug growth will depend on the ice temperature gradient at the interface. Obviously a fall in wall temperature tends to increase the temperature gradient but the thickening of the ice tends to reduce it. Given a temperature difference across the ice and a certain ice thickness, the gradient at the interface is affected by the rate of cooling of the ice. The transient effect on the radial temperature profiles will be explained in section 4.1.3. It is sufficient here to note that a high cooling rate reduces the temperature gradient at the interface.

The net effect on the 100mm dia. pipe was that the plug growth slowed considerably after an ice thickness of 25mm had been achieved, and became very slow indeed with an ice thickness of around 35mm. At this thickness the remaining orifice was 30mm dia. The slowing of the ice growth on the centre and bottom sections, where growth had been initially more rapid, allowed the ice front on the top section to catch up until the plug attained a roughly parallel section

over most of the volume immersed in liquid nitrogen. Above and below this parallel sided part of the plug the ice front tapered away to the pipe wall. This position was reached during all the freezes with initial temperatures from 6.5°C to 50°C initial temperature, although with the hotter freezes the parallel section was shorter. This concluded the first phase of plug formation; the time taken varied, according to initial temperature, from 10 minutes at 10°C to 16 minutes at 50°C.

The second phase of plug growth was initiated when the pattern of natural convection changed. Throughout phase one there was a convective boundary layer flowing down the pipe wall, over the plug and onto the pipe wall below again. Obviously there must have been an upward current in the middle, of equal volume flow rate. Whilst the neck of the plug was wide, the upwards return flow was slow since the velocities are in inverse proportion to the areas. As the neck closed inwards the central return flow must have accelerated considerably if the same boundary layer flow was maintained. To illustrate this numerically, consider the very simplified situation of a 10mm thick boundary layer flowing down the side of a 100mm dia. pipe with a mean velocity of 10mm/sec. The mean return velocity up the centre will be 5.6 mm/sec. If we now consider the same arrangement but with a plug partially frozen, leaving an orifice of 30mm diameter, then the mean return velocity will be 80 mm/sec. It is clear that as the neck diameter closes, there must come a time when the boundary layer flow existing in phase one is restricted or modified. It is thought that below a neck diameter of around 30 mm the upward flowing warm water in the centre is turned in the lower part of the parallel section, to flow downwards over the lower surface of the plug. The transition from the first to the second phase of plug formation is illustrated in figure 4.8. This leaves a "sump" of stagnant water between the sections 1 and 2 (see figure 4.1) which cools quickly because it is not mixing with any warmer water. In the experimental freezes water temperature on section 1 was seen to fall sharply, coinciding with a less sharp fall on section 2. Possibly there was still some mixing

between the water at the centre of the freeze and the relatively warm water below it, because the lowest centreline temperature was now on section 1. Although the water at the centre of the freeze on the section 2 was warmer, it was here that the ice first advanced, presumably because the surrounding ice on this section was colder due to lower longitudinal heat conduction. However it appears that continued slight mixing with the water below prevented the centre section from completely closing. With the remaining orifice at section 2 almost closed the water temperature above it fell further and the ice front on the section 1 accelerated inwards and closed off the plug. The closing of the ice on section 1 was followed immediately by an extension of the plug down past section 2. Within 30 seconds of the plug closing on section 1 the ice at the centre of the section 2 had cooled substantially, typically to around $-40^{\circ}C$, while the centre temperature on section 1 had only cooled one or two degrees below zero. On freezes with an initial temperature of $20^{\circ}C$ or below the plug closed first at the intermediate section between sections 1 and 2. With cooler water in the lower sections of these freezes there would have been less heat convected upwards to inhibit section 2 from freezing. The second phase of plug formation concluded with the rapid extension of the plug downwards to the intermediate section between sections 2 and 3. The plugs took around 4 to 5 minutes to complete this phase irrespective of initial temperature. This observation will also be rationalised after the radial temperature gradients have been examined in section 4.1.3.

The third and final phase of plug formation covers the axial extension of the plug upwards and downwards so that the full length of the freezing section was frozen. It might be expected that natural convection would have caused the plug to grow downwards more slowly than it did upwards. The experimental results did not show this. This is because the bulk temperature of the water was very much lower at the bottom than at the top. So although heat transfer at the top of the plug was principally by conduction, the heat flow across the interface was of the same order of magnitude as that convected from

the cooler water at the bottom.

4.1.3 Radial temperature profiles

The various influences on the radial temperature profile will now be examined. If a homogeneous piece of material of constant cross section has a constant heat flux through it then the temperature profile will simply be a straight line from the high temperature to the low temperature side. The ice formed during pipe freezing is clearly not of constant cross sectional area. If the ice is considered to be a hollow cylinder with heat flowing only radially outwards (i.e. one dimensional heat flow) then it is simple to show (appendix I) that the steady state solution to the temperature distribution is as follows :

$$T_2 = T_1 + (T_3 - T_1) \cdot \frac{\ln (r_2/r_1)}{\ln (r_3/r_1)} \qquad \ldots(4.1)$$

where : subscripts 1 and 3 refer to inner and outer temperatures and radii and subscript 2 refers to some intermediate temperature (unknown) and radius.

The temperature distribution given by this formula will be referred to in the remainder of this section as the steady state distribution, and is characterised by a steadily decreasing temperature gradient from the inside of the cylinder outwards. The reason for this is clearly that the heat flux is decreasing towards the outside of the cylinder (as opposed to the total heat flow which is constant) due to increasing cross sectional area. It should be noted that equation 4.1 cannot be used when r_1 is zero because a solid cylinder cannot have a steady state temperature difference between its centre and the outside.

Now consider the linear (non-radial) case again, for which the steady state temperature profile is a straight line. If the

specimen is cooling the temperature profile will assume a transient form in which the gradient increases from the warm side to the cool (see figure 4.10b). To explain this, take a small section from the specimen and consider the heat flow into and out of it, as shown in figure 4.9. A temperature difference exists across the section so it has a warm side and a cool side. On the warm side, heat is conducted in (Q), flows across the section and leaves on the cool side. Since the section is cooling down, sensible heat is being released internally (δQ) and this will also flow across the section and out of the cool side. Therefore, when the section is cooling, the heat flow rate on the cool side is higher than on the warm side, which implies that the temperature gradient must increase from the warm to the cool side. This is known as the transient temperature distribution.

The steady state temperature profile for a hollow cylinder can be considered convex and the transient profile for a flat slab similarly may be considered concave (figures 4.10a and 4.10b). The terms "concave" and "convex" are only used for clarity and are not absolute since a temperature distribution is either concave or convex depending on how it is viewed. If a hollow cylinder, cold on the outside and warmer on the inside, such as the ice annulus of a partially formed plug, is cooled then the transient temperature distribution will be a combination of convex and concave parts according to the rate of cooling at each section. Where the cooling rate is low the radial effect will dominate and the temperature profile will be convex, but where the cooling rate is higher the transient effect is more important and the profile will be concave.

So far the assumption has been made that heat conduction is only occurring radially. The effect of longitudinal heat conduction must now be examined since this will occur in the growing ice annulus of a pipe freeze, especially on the sections near the ends of the freezing zone. Figure 4.11 shows a typical longitudinal section of a partially formed plug and beside it a typical longitudinal temperature profile at radius r_1. The three radial cross sections have also been

marked (1),(2) and (3). Consider a small but finite control volume on section 3 at radius r_1. Heat is flowing longitudinally upwards and radially outwards (from right to left). Since the longitudinal temperature gradient is decreasing upwards at this point there must be more heat flowing longitudinally into volume (Q_1)than out of it (Q_2), i.e. there is a net longitudinal heat flow into the volume (Q_1-Q_2). Ignoring for the moment any possible transient effects, if the volume is at a steady temperature there must be an equal net heat flow out of it in the radial direction. This means that more heat must be leaving radially on the left (Q_3+{Q_1-Q_2})than is entering on the right (Q_3)and therefore the radial temperature gradient must be increasing from right to left. Thus the effect of longitudinal heat conduction is similar to the transient effect in that it makes the radial temperature profile more concave.

One further effect that must be examined is that of a temperature dependent thermal conductivity. The thermal conductivity of ice rises from 2.09 W/mK at 0°C to 2.445 W/mK at -100°C. This means that for a given heat flow rate the temperature gradient will be lower in the colder parts of the plug. Thus the effect is to make the radial temperature profile more convex.

The radial temperature profiles for the centre section are plotted at 2 minute intervals in figures 4.12a - 4.12h. These show the fast fall in wall temperature initially accompanied by the rapid loss of sensible heat from the ice near the wall. This rapid loss of sensible heat causes the early temperature profiles in the ice to be nearly straight or slightly concave. As the rate of cooling falls the profiles assume a convex shape nearer to the steady state profile. When the plug closes the central core of the ice cools very fast and the profiles become concave near the centre once again.

Careful examination of figures 4.12a-4.12h reveals that the temperature gradient near the centre of the pipe immediately prior to plug closure was steeper for the freezes with higher initial

temperatures. In section 4.1.2 it was explained that at this stage of plug formation convection heat transfer was still limiting plug growth on the centre section causing the top section to close first. This convection was much greater with higher initial water temperatures, so the transient effect was less important and the temperature profile in this area closer to the steady state. This is the reason for the steeper central temperature gradients and also serves to explain why the $0^{o}C$ to $-60^{o}C$ cooling times are faster with the higher initial water temperatures as noted in section 4.1.1.

Initial Temp. oC	6.5	10	15	20	25	30	35	40	45	50
Temp.grad. oC/mm	2.5	4.8	4.0	7.2	8.3	10.5	11.4	9.0	8.5	10.8
0 to -60oC time secs	75	50	50	45	45	45	15	40	35	35

Table 4.2

Table 4.2 shows the correlation between the central temperature gradient just prior to freezing and the time to cool the centre from $0^{o}C$ to $-60^{o}C$. It should be remembered that both quantities are only estimated; the cooling time by interpolation between data points and the temperature gradient by assuming a straight line temperature profile between the thermocouple placed centrally in the water and another 6mm radially distant in the ice. Nevertheless the trend can be seen and the anomalously short cool down time with the $35^{o}C$ freeze corresponds to the highest temperature gradient. The higher the adjacent temperature the greater the driving force for the transient cool down of the centre when latent heat removal and convective heat transfer cease as the plug closes.

The observation made in section 4.1.2, that phase two of the plug formation took approximately the same time irrespective of initial water temperature, can now be rationalised. The higher convective heat transfer inhibits plug growth inwards where there is enough water to allow effective natural convection. It also allows higher temperature gradients to build up giving colder ice surrounding the unfrozen water and it is this effect that accelerates plug growth in areas where the remaining water passage is too thin for effective natural convection to occur. These two effects work in opposition and leave the total time for phase two of the plug formation roughly independent of initial water temperature.

Because the transience and longitudinal heat conduction cause only relatively small deviations from the steady state temperature profile, it is helpful to compare the steady state with the experimental temperature profile when examining these effects. Because of problems due to non-axisymmetrical freezing mentioned in section 4.0, it is necessary to chose sections whose thermocouples are on the same side of the pipe. On the experimental rig, sections 1,2 and 3 (figure 4.1) each had five thermocouples at 12.5 mm intervals (i.e. at the centre, 1/4, 1/2, 3/4 and full pipe radius points) on the same side of the pipe. A computer program was written to compare the experimental temperature profile obtained from these thermocouples with the steady state profile. Equation 4.2, a modified form of equation 4.1 to allow for the temperature dependence of the thermal conductivity, was used to calculate the steady state profile (derived in appendix II).

$$\frac{B.(T_2^2-T_1^2)}{2} + A.(T_2-T_1) - \frac{B.(T_3^2-T_1^2)}{2} + A.(T_3-T_1).\frac{\ln(r_2/r_1)}{\ln(r_3/r_1)} = 0 \quad \ldots(4.2)$$

where the thermal conductivity, $k = A + B.T$

T_3 was set equal to the temperature of the outermost thermocouple. Once the ice had advanced past the third thermocouple in at the half radius point, T_1 was set equal to the temperature of this thermocouple. T_2 was calculated as the steady state temperature of the point at 3/4 the pipe radius and this was compared with the experimental value measured at this point. When the ice plug had advanced past the thermocouple at 1/4 the pipe radius, this thermocouple's temperature was set equal to T_1 and steady state temperatures were calculated for both the 1/2 and 3/4 radius points and compared with experimental values. Figure 4.13 illustrate how the comparison of steady state and experimental profiles were made. Figures 4.14a - 4.14h show the results of this comparison for the centre section. A positive difference indicates that the experimental temperature was higher than the steady state value and therefore the profile was more concave than the steady state profile. This may be caused by the loss of sensible heat (i.e. a transient effect) or by longitudinal heat conduction. A negative difference indicates a more convex profile.

The freezes from cooler initial temperatures (up to 20°C) all showed marked peaks and troughs in their variation from steady state profiles. Looking first at the curve for the 3/4 radius point with an initial temperature of 6.5°C, the conclusion of phase one of plug formation can be seen when the curve falls from highly transient (i.e. rapid ice formation and cooling) to the steady state value. Phase two begins with a rise of the curve as the centre section freezes inwards again, followed by a dip as convected heat from below the plug restricts ice growth. Finally another peak as the centre section freezes over and cools rapidly. For freezes from water temperatures of 25°C and above, the curves are much smoother but all show an increasingly transient profile until 2-3 minutes after plug closure. With the exception of the freeze from 40°C all profiles remain nearer to steady state than the cold water freezes. This is as expected since the increase in convected heat flowing through the ice and the corresponding reduction in the loss of sensible and latent

heat will make the temperature profile closer to steady state.

The curves for the 1/2 radius points on the centre section follow the same peaks and troughs as the 3/4 radius points, but since they are nearer the interface and hence cooling more rapidly in the latter stages of a freeze, they are more transient.

A similar analysis was done for the top and bottom sections but there was some doubt as to the accurate positioning of the outermost thermocouples in the water on these two sections. This was due to considerable temperature differences between these thermocouples and those on the same section but soldered to the inside of the pipe wall. On the centre section these two thermocouples agreed to within $4^{o}C$ but much greater differences were seen on the top and bottom sections (up to $20^{o}C$). Because the soldered thermocouples were not in the same radial plane it was not possible to substitute their readings for those of the outermost ones in water.

4.1.4 Rate of energy loss

Another computer program has been written to analyse the experimental results, which used the entire temperature distribution in the pipe to produce an energy account. The analysis, which can only be considered an estimation to illustrate the longer term trends, was based on the simplifying assumption that the temperature profiles between adjacent thermocouples were straight lines. The interface position was estimated by a linear interpolation process on each section. Then the interface positions on two longitudinally adjacent sections were used to give an average position for the whole interface between those two sections. The calculation of the loss of sensible heat from the water and the pipe wall was affected by the uncertainty in temperature measurements above $15^{o}C$, but the trends observed are still valid. The calculation of the loss of sensible heat from the wall was also affected by the error in the outer wall temperature reading mentioned in section 4. The effect of this was to make the

loss of sensible heat from the wall appear more rapid than was really the case.

The 600 mm (24") long pipe was considered in three 200mm (8") long volumes. These will be referred to as the upper, middle and lower volumes (figure 4.1). The middle volume was the one to which the freezing jacket was attached and therefore all the energy that left the pipe did so through this volume. Some heat flowed in through the upper and lower volumes but this should be very small compared to that which left from the middle. Energy passed from the upper and lower volumes to the middle mainly by conduction along the pipe wall and by convection in the water.

The energy lost was split into four component parts, latent heat of fusion of the ice and sensible heat lost from water, ice and the pipe wall. These were added together to give a total heat loss for each volume. Figures 4.15a - 4.15f show the results for freezes with initial temperatures of 6.5, 10, 20, 30, 40 and 50^{o}C. The heat lost from the middle volume is shown in component form and in total, while that lost from the upper and lower volumes are shown only as totals. All graphs have been plotted as percentages of the energy that would be lost if the entire pipe and its contents were frozen down to liquid nitrogen temperature.

It can been seen that figures 4.15a - 4.15f all show the same pattern, with the freezes from higher initial temperatures having a longer timescale. This supports the view that all tests had a similar plug formation mechanism.

The nitrogen supply was turned off after 20 minutes in all tests and this is reflected in the fall in the pipes sensible heat curve at this time. The peak in the total heat removed from the middle volume is remarkably consistent for each test at about 90% with the exception of the 50^{o}C freeze which reached around 88%. It is probable that the total heat removed would have been greater if the

liquid nitrogen supply had been continued beyond 20 minutes. The maximum sensible heat removed from the pipe varied from 86% (6.5°C) down to 84% (50°C) and from ice, 83% down to 72%.

Looking now at the curves for the upper volume of the pipe, it can been seen that the energy removed at 30 minutes varied from 15% (6.5°C) down to 10% (50°C). Each curve can be seen to have two parts. During phase one of plug formation the gradient was low reflecting the low net heat loss, because the bulk water temperature maintained convection from the middle and lower volumes. Then at the beginning of phase two the convection of water from the lower volume more or less ceased and the upper volume was isolated from the rest of the pipe. Although heat transfer from the relatively warm water sitting above the cool freezing zone would be very slow, the net heat loss rate will increase because lost heat is not replaced by convection from below. All the curves for the upper volume show an increase in gradient at the commencement of phase two with the exception of the freeze from 50°C where the increase occurred a little later. With the warmer water freezes the higher convection from the lower volume reduces the initial (phase one) heat loss rate more than is the case with cooler freezes.

The curves for heat removed from the lower volume of the pipe show the reverse trend. Heat was lost from this volume by convective heat transfer throughout the freeze. Freezes from initial temperatures of 6.5 and 10°C showed a fairly constant rate of net heat loss from this volume. However with warmer initial temperatures, the superheat decayed quite quickly because of natural convection between this and the higher volumes, so the net heat loss from the lower volume was initially higher. This explains the reduction in the gradient of the curves for the lower volume, after a few minutes of freezing time had elapsed, as seen in figures 4.15c - 4.15f.

4.1.5 Rate of heat transfer to liquid nitrogen

The analysis used in section 4.1.4 was employed again to calculate the total heat loss from the whole pipe at every recorded time interval. The incremental increases were calculated and divided by the length of the time interval (15, 30 or 60 seconds) to give the total heat flow rate out of the pipe. From these it was possible to estimate the heat flux (heat flow per unit area) into the liquid nitrogen by dividing the total heat flow rate by the area of liquid nitrogen in contact with the pipe. The nitrogen level was maintained at 150 mm (6") deep and since the heat transfer coefficient for liquid nitrogen is substantially higher than that for gaseous nitrogen it is reasonable to assume that virtually all the heat leaves through the part of the pipe immersed in liquid nitrogen. Indeed in the later stages of each freeze the temperature gradient across the pipe wall reversed at the section of pipe that was surrounded by nitrogen gas at the top of the freezing jacket. This indicates that heat was flowing inwards from the cold gas, then downwards by conduction through the ice and the pipe wall and finally back out to the liquid nitrogen. Each point was then plotted on a graph. The scatter was quite considerable (typically ± 5 kW/m^2, sometimes more), but it was possible to smooth the data by eye and draw a line for the heat flux into the liquid nitrogen. Figure 4.16 shows these estimates of the heat flux for freezes from 10, 20, 30, 40 and 50°C.

Taking as a first example the curve for an initial temperature of 20°C. At the start of the freeze the curve rises steeply and this corresponds to the jacket filling with liquid nitrogen. After 2 minutes the jacket was full, the curve levels off and the heat flux had now apparently reached 63 kW/m^2. A later experiment conducted with modified outer wall instrumentation suggested that this figure was somewhat high due to the over estimation in the fall in outer wall temperature. It was possible to estimate the outer wall temperature by noting that the inner wall temperature was around -5°C and that the heat flux was, at maximum,

about 60 kW/m^2. Dividing the heat flux by the thermal conductivity of stainless steel (approximately 13 W/mK) gives the temperature gradient and multiplying by the pipe wall thickness (6 mm) gives a steady state temperature difference across the wall of about 27^oC. Because the wall was cooling down it would have had a transient temperature profile across it, so the temperature difference should have been less than 27^oC. So the outer wall temperature should not have been lower than -30^oC where the inner temperature was around 5^oC. (The thermocouples indicated outer wall temperatures of between -68^oC and -163^oC which is an indication of how inaccurate this part of the instrumentation was.) With an outer wall temperature of -30^oC there was a temperature difference to the liquid nitrogen of approximately 165^oC, which, according to the data of Flynn et al [53], was well within the film boiling regime. The curve indicates that the heat flux then fell steadily, reaching 30 kW/m^2 after 6 minutes. It is not possible to say whether this fall in heat flux really occurred, again because of the error in outer wall instrumentation. Sensible heat from the pipe wall, which the inaccurate instrumentation indicated was lost mainly in the first two or three minutes, would in fact continue to be lost steadily over this period, so the fall in heat flux was certainly not as great as indicated by the curve. At about 6 minutes into the freeze, the film boiling collapsed and nucleate boiling took over. This transition is characterised by a sharp increase in the heat flux into the nitrogen. As the outer wall cooled further the heat flux dropped rapidly and as it did so the cooling rate also fell. From the curves and the temperature data it appears that the film to nucleate boiling transition occurred in two stages. The lower 100 mm of immersed pipe undergoes the transition first and the top 50 mm or so at some time later. In the heat flux curve for the 20^oC freeze a second transition peak can be seen at 10 minutes as the top part of the freezing section underwent the film to nucleate boiling transition. It should be emphasised that the above is a local event deduced from average readings of heat flux and has not been directly observed.

The curve for an initial temperature of 10°C is very similar (figure 4.16). The first peak is unusually high, at least partly due to overfilling with liquid nitrogen. The boiling regime transition again appears to have occurred in two stages, both a little earlier than with the 20°C freeze. Also visible on this curve, because the time interval between data points was shorter, are a number a smaller peaks at 13,15.5,18 and 20 minutes. These correspond to rises in the liquid nitrogen level. It is possible that the rises in heat flux were due, not so much to the actual rise in nitrogen level as, to the disturbance of the existing nitrogen pool associated with filling the jacket with a mixture of high pressure gas and liquid from the dewar.

The curves for freezes from 30 and 40°C indicate that the pipe was taking progressively longer to undergo transition from film to nucleate boiling. This is as expected since the cooling rate was also lower due to increased convected heat transfer from the water. The 30°C curve again has a small enough data recording interval to show the small peaks associated with topping up of the jacket. The 40°C curve has a data interval so large that the secondary transition peak (i.e. the transition of the top part of the freezing section) is lost, if indeed it did occur.

The 50°C curve is difficult to rationalise. The initial peak is much lower although from the temperature data it appears that the jacket was more or less full after 2 minutes. After a small but sharp drop, the heat flux gently rose prior to dipping again before the transition peak. Thereafter the curve is similar to all the others with a secondary transition peak at 12 minutes. No explanation can be found at present for the behaviour of the curve in the film boiling regime, particularly since accurate outer wall temperatures were not available from these tests.

4.2 Results from freezes made with tank

The second set of freezes were performed with the pipe standing on a large glass fibre tank as described in section 3.3.7. This was to allow the full effect of natural convection to be observed by increasing the volume of water below the pipe and by maintaining the original bulk water temperature more closely. Six freezes were conducted with the rig in this configuration and these were at 20,30,40,53°C and two freezes at 45°C. The results of the two freezes at 45°C were so anomalous that they will be considered quite separately in section 4.2.4. Thus sections 4.2.1 - 4.2.3 will be concerned only with the results of the remaining four freezes.

4.2.1 Times to freeze

The same four times have been recorded in this series of tests as were used previously. They were time for the centre to cool to 0, -60 and -140°C and the time for the plug to grow to 100 mm (4") long at its centre. These are shown in table 4.3 and are plotted in figure 4.17 which also includes the same data from the earlier tests for comparison. Also plotted in figure 4.17 are the time intervals between the centre attaining 0°C and -60°C, -60°C and -140°C and between the plug first closing and achieving a length of 100 mm.

Initial Temperature	Times (minutes - seconds)			
	0°C	-60°C	-140°C	100mm plug
20°C	15-30	16-30	19-00	18-00
30°C	21-30	23-45	30-00	30-00
40°C	31-00	36-00	46-00	50-00
53°C	-------- No freeze achieved -------			

Table 4.3

Comparing the results here with those from the freezes without the tank, as shown in table 4.1, it can be seen that the addition of the tank made very little difference with an initial water temperature of 20°C. The plug closure time was increased by 15 seconds and the other three recorded times by 30 seconds. With an initial temperature of 30°C the plug took 5 minutes longer to close, 6.5 minutes longer to reach -60°C, 10 minutes longer to reach -140°C and 10.45 minutes longer to attain a length of 100 mm. For a freeze from an initial temperature of 40°C the increases in the freezing times were 13.5, 17.45, 25 and 29.5 minutes respectively. The reason for the increase in freezing times was the maintenance of the bulk water temperature below the plug throughout the freeze. By the time the freezes without the tank attained a central temperature of -140°C, the bulk water temperature below the plug had cooled to around 10-12°C from initial temperatures of 20,30 and 40°C. With the tank added the bulk temperature only fell to 18, 27 and 34°C respectively despite the fact that the elapsed freezing times were much higher. The longer water temperatures increased the heat transfer by natural convection and reduced the removal of latent heat, thus slowing plug growth.

The freeze with an initial temperature of 53°C was abandoned after 48 minutes when the liquid nitrogen supply was exhausted. At this time the plug had grown inwards just over half the radius.

4.2.2 Interface positions

Figures 4.4b - 4.6b show the estimated interface positions for freezes performed with the tank from initial temperatures of 20, 30 and 40°C. Figures 4.4a - 4.6a, plotted opposite, show freezes from the same initial temperatures but without the tank in place. The presence of the tank in the 20°C freeze did not affect plug formation very much. The ice growth in phase one was a little more biased towards the bottom because the bulk water temperature was maintained and therefore natural convection was stronger. The axial extension of the plug in phase three was somewhat retarded on the bottom compared

to the case with no tank.

Comparing figures 4.5a and 4.5b, it can be seen that at 30°C the addition of the tank has quite drastically altered plug growth. The maintenance of higher bulk temperatures in the upper part of the freezing section increased convected heat transfer in this area to the extent that no ice was formed above the level of the liquid nitrogen during phase one (remember that the convection boundary layer is thinner near the top of the freezing section so higher bulk water temperatures are particularly effective in restricting or preventing plug growth in this area.). Phase one was completed in approximately 16 minutes, but compared to the freeze with no tank the length of the parallel section was much reduced, mainly at the top. When phase two started it appears that the boundary layer formed on the ice about half way between sections 2 and 3. Plug growth from this level downwards was almost non-existent until the plug closed and this is again was because a high bulk water temperature combined with a thin boundary layer caused a very high convected heat transfer rate from water to the ice. After plug closure the bottom advanced downwards into the lower part of the freezing section rather than inwards into it. On top of the plug ice froze upwards at about the same rate as in the case with no tank, but starting from a lower level.

Looking now at the freeze from 40°C (figure 4.6b), the transition from phase one to phase two occurred after about 20 minutes. At around this time plug growth on section 1 accelerated while growth on section 2 and particularly section 3 slowed almost to a halt. The central remaining orifice at transition was rather larger than with other freezes, at about 40 mm diameter. It is possible that because of this large remaining orifice, transition from one phase to the next was not clear cut and considerable heat was still being convected up the centre. Plug growth on section 1 slowed again between 24 and 28 minutes, but after this phase two was firmly established and a sump of water, cooled by conduction, formed. The plug then closed off the remaining 25 mm diameter quite rapidly.

Again ice growth below the plug was mainly downwards rather than radially inwards after closure. Plug growth upwards after freezing off was initially quite rapid but slowed very considerably after 40 minutes.

4.2.3 Rate of energy loss

Using the same analysis as in section 4.1.4 the rates of heat extraction, for freezes from initial temperatures of 20,30,40 and 53°C, have been plotted in figures 4.18a - 4.18d. All the curves have a similar form to those in figures 4.15a - 4.15f suggesting similar plug formation mechanisms. As well as having longer time scales compared to the freezes without the tank, the hotter freezes (30, 40 and 53°C) all showed measurable short term fluctuations in their rate of heat loss, particularly in the early stages of plug formation. It would be unwise to attach too much significance to this because the first stages of plug formation, when the ice layer was quite thin, were visually observed not to be totally axi-symmetric. However this observation itself suggests that convection patterns were changing during this period.

The curves for the middle volume (figure 4.1) of the 20°C freeze are very similar to the curves for the freeze from the same temperature without the tank. They are only slightly elongated in the time direction as would be expected considering the freezing times and interface positions. Nitrogen supply was maintained throughout the freeze instead of being terminated at 20 minutes as was the case with the earlier freeze. The total heat removed therefore rose from 90 to 95% in the middle volume.

The net heat flow from the upper volume rose sharply at the transition from phase one to phase two of plug formation in the same manner as the freeze without the tank. The net heat loss from the lower volume after showing a small initial rise was then much more restricted by the convection of warm water from the tank below. Most

of the subsequent rise in net heat lost can be attributed to ice formation in the top part of the lower volume rather than to any fall in the bulk water temperature.

The heat loss curves for the upper and lower volumes during freezes from 30 and 40°C show broadly similar characteristics. The net heat loss from the lower section was even lower due to stronger natural convection. The curves for the upper volume do not show the phase one/phase two transition so clearly. The reason for this is that plug formation was more strongly biased towards the bottom part of the middle volume and heat transfer from water above the plug is by conduction during phase two. Therefore the plug must advance up the pipe before significant heat is lost from the upper volume. Note that the nitrogen supply was turned off in the 30°C freeze after 30 minutes, hence the fall of some of the curves after this time.

The heat loss curves for the unsuccessful freeze with an initial temperature of 53°C (fig 4.18d) show that, given sufficient time and liquid nitrogen, this freeze could probably have been completed. All curves were rising when the supply of nitrogen was exhausted after 48 minutes, indicating a net heat flow out of the pipe. The form of the curves does not suggest that the heat flow tails off to a situation of equilibrium between heat convected into the pipe and heat removed from it.

4.2.4 45°C Anomaly

Two freezes were conducted with an initial temperature of 45°C, the second one to check whether the unexpected results of the first were repeatable. The plug formation mechanism for these two freezes was completely different from all the other freezes. Figure 4.19 shows the estimated interface positions at 4 minute intervals, the first freeze on the left and the second on the right. The first freeze begins normally, with a thin layer of ice down the length of the freezing section at 4 minutes. However by 8 minutes, a band of

water just at the level of the liquid nitrogen surface and about 25 mm (1") deep had cooled to freezing temperature. The temperatures in this region all fluctuated very close to freezing, so it is very difficult to draw a definite ice front position. For this reason the 8 minute interface has been drawn dotted at the extremities of this cold area. At twelve minutes there was definitely a solid ice plug established from the top of the gas space in the freezing jacket down to about 40 mm above the bottom of the nitrogen pool. Thereafter the plug extended both upwards and downwards with the ice front remaining nearly horizontal. After freezing for 24 minutes the plug reached from the bottom of the nitrogen pool to 50 mm above the top of the jacket.

With the second freeze, most of the volume of water surrounded by the liquid nitrogen had cooled to freezing point by 4 minutes. Again because the boundary was hard to define, a dotted line has been drawn where the water temperature rose a degree or so above freezing. Notice that in this freeze the indistinct area of ice/water was much deeper than before. By 8 minutes into the freeze a definite plug, approximately 125 mm (5") long, had been established, but its position had moved up the pipe some 50 mm. This means that some water, in the area surrounded by the gas space in the jacket, had cooled and frozen. Also, in the volume level with the lower part of the jacket, some water/ice that cooled to around freezing point, and then warmed back up to the bulk water temperature. A further 4 minutes saw the top ice front move up about 15 mm and the bottom down 1 or 2 mm. In the interval from 12 to 16 minutes the plug extended upwards some 45 mm while the bottom again underwent some remelting and the ice front retreated about 15 mm. The top interface then remained almost stationary for the next 8 minutes while the bottom ice front moved swiftly downwards, reaching the bottom of the liquid nitrogen by 20 minutes and nearly the bottom of the pipe by 24 minutes. Although the ice now reached well down below the jacket, the water immediately adjacent to the pipe wall remained unfrozen. Obviously heat was now flowing into the pipe below the jacket, through the water, across the

lower ice interface, then by conduction up through the ice and finally back out of the pipe into the nitrogen. After 1 hours freezing time only the top 70 mm of water in the pipe remained unfrozen.

It is thought that this anomalous behaviour was due to the formation of small stable "convection cells". In these the water circulated around a relatively small volume and was largely isolated from adjacent water. The dotted interface boundaries, at 8 minutes in the first freeze and 4 minutes in the second, show the extent of the "cell" when it first formed. Because the water did not mix with that in the rest of the pipe and the tank, it cooled very quickly and then froze. Two cells then appear to have been created, one above and one below the plug. The lower cell in the first freeze moved downwards as the ice freezes above it until ice reached the bottom of the nitrogen pool. A steady state situation then existed at the bottom of the plug, which grew no more. In the second freeze the formation of the lower cell appears to have been delayed because convected heat from below the freezing section remelted some of the plug. However, after 18.5 minutes the cell formed and the lower ice front moved down the pipe. Unlike the first freeze equilibrium was not reached with the lower ice front level with the bottom of the nitrogen, but instead the convection cell was maintained and ice grew all the way to the bottom of the pipe. The exact nature of these cells is unknown, this will probably only be determined by some flow visualisation work.

Figures 4.20a and 4.20b show the heat loss from these two freezes. They show considerably different patterns of heat loss with only the curves for the upper volume (as defined in figure 4.1) being similar. All curves show quite sharp changes in gradient indicating transitions in the fluid and heat flow patterns. Whilst plug formation of this type appears to be confined to a very narrow band of water temperatures, it is possible that similar mechanisms may occur with certain oils and possibly over a wider temperature range.

4.3 Results from modified outer wall instrumentation

The thermocouples on the outside of the pipe within the freezing jacket were modified as described in section 3.3.8 so that the true pipe temperatures in this area could be measured. Unfortunately it was found that in the interval since the instrumentation was used to collect the data analysed earlier, many of the soldered thermocouple tips had deteriorated and now indicated an open circuit. A full analysis of these latter results was not possible therefore, but an indication of local and average heat flux through the pipe wall and into the nitrogen could be obtained.

The local heat flux through the pipe wall was estimated by calculating a thermal conductivity from the formula $k = 12.9 + 0.013\ T$ where T was taken to be the average temperature across the pipe wall. The temperature gradient was approximated to the temperature difference divided by the wall thickness (6.25 mm) and this was multiplied by the thermal conductivity to give the local heat flux. This approximation ignores the effect of sensible heat loss from the pipe wall which would make the heat flux greater for a given temperature difference across the pipe wall. The local heat flux was calculated at five levels in this way; at 25,50,75,100 and 125 mm (1,2,3,4 and 5") above the bottom of the jacket in which the nitrogen level was 150 mm (6") deep.

Table 4.4 shows the results of these calculations. The average heat flux shown in the right hand column of table 4.4 may be compared with the curves for heat flux plotted in figure 4.16. The latter were calculated from sensible heat lost in a given time rather than from temperature gradients across the pipe wall. The data from which they were obtained came from tests conducted without the tank in place and before the outer wall thermocouples were modified. The error in the outer wall temperature measurement may account for the peaks in the mean heat flux seen at around 2 minutes in figure 4.16. This peak is not seen in the data presented in table 4.4 where the

outer wall temperature measurement is believed to be correct. Up until around 4 minutes the average heat flux remained at around 45 kW/m^2 whereas in the previous tests the heat flux apparently fell from about 60 to 30 kW/m^2, so there is some measure of agreement here if the instrumentation error associated with the earlier data is taken into account. In the period from 6 to 8 minutes two peaks of 75 and 82 kW/m^2 occurred due to film to nucleate boiling transitions. These were just a little higher than the transition peaks observed in the earlier data but they did occur in the same time interval. When calculating average heat flux by measuring loss of sensible and latent heat in a given time interval, the height of such peaks will be dependent on the length of the time interval used, a long interval tending to show lower smoother peaks. In the nucleate boiling period from 8 minutes onwards the two sets of data show reasonable agreement, the results from the later test showing slightly higher heat flux.

Time (mins)	Heat flux (kW/m2) Depth above bottom of jacket					Average Heat Flux (kW/m2)
	25	50	75	100	125	
2	82	38	40	37	29	45
3	88	42	37	36	24	45
4	88	41	42	36	31	48
5	82	53	49	47	28	52
6	75	52	71	50	33	56
6.5	65	152	70	52	32	75
7	55	71	93	55	30	60
7.5	52	47	86	169	54	82
8	48	40	53	69	129	68
8.5	47	35	45	53	87	53
9	47	32	46	49	48	44
10	47	28	33	40	33	36
12	43	22	25	31	24	29
14	44	18	22	27	19	26
16	43	16	18	22	16	23

Table 4.4

Inspecting the columns of table 4.4 which give the local heat flux at 50,75,100 and 125 mm from the bottom of the jacket reveals three points worthy of comment. Firstly the peaks in local heat flux at the collapse of film boiling (transition) are very much higher than might be expected from the data of Flynn et al [53]. Secondly the transition from film to nucleate boiling occurs first at the bottom of the jacket and moves up the jacket over a period of about two minutes. It is not possible to say that the transition occurs in two distinct events, bottom and centre sections first, top section last, but it is possible that this did occur in the earlier freezes. Finally, the local heat flux at a point 25 mm above the bottom of the jacket does not appear to undergo a transition peak in the same way as the heat flux measured at the other points. Instead it falls from an initially high value of 80-90 kW/m^2 to maintain a flux of around 45 kW/m^2, even after the heat flux above this point had fallen to around 20 kW/m^2. The wax impregnated cloth tape, used to seal the inside of the freezing jacket to the pipe, covered the pipe wall up to a point only just below the thermocouple in question. It is possible that the insulation provided by the tape allowed nucleate boiling to take place well before the actual pipe wall had cooled to the transition temperature and that the rough and slightly porous nature of the tape allowed enhanced heat transfer in the nucleate boiling regime. This raises the question as to whether certain pipe wall coverings may be able to increase the rate of heat transfer and thus lower freezing times.

The degree of agreement with the results shown in table 4.4 and those obtained earlier by the different method (figure 4.16), give grounds for some confidence that the measurement of outer wall temperature is now reasonably accurate. It was worthwhile, therefore, to attempt some correlation between surface heat flux and the temperature difference between the pipe wall and the boiling nitrogen. In figure 4.21, heat flux has been plotted against temperature difference on log-log scales. For comparison the correlations of Flynn et al [53] and Hanson and Richards [54] have also been shown.

The major difference between Flynn's results and those derived from the pipe freezing experiment is that the collapse of film boiling appears to occur at very much higher surface temperature differences, starting at around 150°C in the authors experiment compared to 50°C from Flynn. The heat flux in the nucleate range also appears to be considerably higher than that measured by Flynn et al. These observations have significance to the results of the one-dimensional computer model (chapter 5) which uses a heat flux/temperature difference relationship based on the results of Flynn et al for the nucleate and transition regimes and those of Hanson and Richards for the film boiling regime. The discrepancy between the authors estimate of heat flux and that measured by Flynn et al may be due to differences in surface roughness or orientation in the two experiments. The results of the latter were obtained on a horizontal as opposed to a vertical tube and the surface temperatures were measured on the horizontal plane. Brentari and Smith [55], review a wide range of published data for pool boiling heat transfer to cryogenic liquids. From this it is clear that in the nucleate boiling regime, surface roughness, orientation and even chemistry, exert a considerable influence on the value of the heat flux obtained from a given surface to pool temperature difference. The data of Flynn et al gives almost the lowest heat fluxes of all the data reviewed. The data of Lyon [56], whose experimental programme included a wide range of surface orientations and treatments, shows peak nucleate heat fluxes in excess of those estimated by the present author. Lyon's results indicate that the heat flux from a vertical cylinder is slightly less than for a similar horizontal cylinder, but conversely, experiments by Class et al [57] gave higher a heat fluxes for vertical surfaces compared to horizontal.

4.4 Conclusions

A mechanism of plug formation has been postulated, namely that plug formation occurs in three distinct phases. In phase one a natural convection boundary layer flows from some short distance above

the freezing section, down over the growing plug and back onto the pipe wall below. Phase two, which usually begins when the remaining orifice is around 30 mm diameter, has a different convection pattern. Due to the restriction of the neck formed by the plug, the returning upward flow is turned at approximately the mid-point of the plug and flows downwards over the lower part of the plug only. Water in the upper part of the freezing section which is unable to convect downwards cools more quickly, causing the plug to freeze first in the upper part of the freezing section. Phase three covers the extension of the plug in the axial direction.

The effect of sensible heat loss, radial geometry, longitudinal heat flow and temperature dependent thermal conductivity, on the radial temperature distribution, are explained in section 4.1.3. The experimentally determined profiles were examined in this light. Variations in the transient element of the profiles, were shown to support the three phase theory of plug formation.

The percentage of sensible and latent heat lost from the centre section has been calculated. In freezes where there was no tank in place below the pipe, restricting the effect of natural convection, the total heat lost from the freezing area was very consistent at around 90% that would be lost by freezing the whole volume down to liquid nitrogen temperature. When the tank was in place, the percentage of heat removed with an initial temperature of 20°C was higher, at 95%, due to the fact that in this series of tests the nitrogen supply was not terminated after 20 minutes as before. The rate of heat removal was approximately the same as for freezing with the same initial temperature, but without the tank in place. For initial temperatures higher than 20 °C, the net rate of heat removal was much reduced due to the bulk water temperature in the freezing section being maintained by convection from the tank below. These calculations and the measurement of freezing times indicate that natural convection only significantly affects the time to freeze if the initial temperature is above 20°C. Below this temperature it

appears that the geometry of the pipework surrounding the freezing site, in a vertical plane, is unimportant.

Excepting two freezes conducted from an initial temperature of 45°C, measurements of interface position, radial temperature profiles and heat loss rates all support the three phase theory of plug formation, although no direct observation of the convection currents has been made. There was some detailed variation in the mechanism between freezes however, particularly with the freezes from high initial temperatures with the tank attached.

The approximate local heat flux into the liquid nitrogen has been deduced from measurements of the temperature difference across the pipe wall. The average heat flux over the whole freezing area has been found to be in reasonable agreement with the rate of loss of sensible and latent heat from the pipe. The local heat flux and the temperature difference between the pipe wall and the liquid nitrogen have been correlated. Although there is considerable scatter, it appears that there are several differences between this and some existing experimental data. The collapse of film boiling appears to start at much higher temperature differences than the data of Flynn et al [53] would suggest and the heat flux in the nucleate regime is significantly higher. Heat flux in boiling heat transfer is dependent on geometry, surface finish and on the direction of change of surface temperature (i.e. whether it is cooling or warming) so comparisons are not strictly valid.

Finally, although almost all the freezes performed in this work appeared to have the same mechanism of plug formation, two freezes, with an initial temperature of 45°C and with the tank in place below the pipe, froze by a completely different mechanism. From the data available, the precise process was not clear, but it appeared to involve the formation of small convection cells in which the water recirculated without exchanging heat with the surrounding water. The water in these cells was cooled rapidly leading to very long plugs

formed very quickly. Whilst the importance of this phenomenom appears limited in relation to the freezing of water (freezes from temperatures 5°C either side of the critical 45°C showed the normal freezing mechanism), it does indicate the possibility of other freezing mechanisms which may be of importance in the freezing of crude oils and hydrocarbon products.

5.0 Computer Modelling

To make pipe freezing a widely accepted technique in industry it is necessary to be able to predict success or failure to freeze, time to freeze, liquid nitrogen consumption and plug temperature profiles, before any freezing equipment is installed on site.

Since experimentation is expensive, the number of different pipe freezing situations (i.e. particular pipe geometries, materials, pipe contents, flowrates) that can be tested is limited. This is particularly so with the larger pipe sizes (greater than 300 mm diameter) where potential savings in maintenance costs are most attractive. It is necessary therefore, to find some way of generalising the results of a few experiments to predict the outcome of any potential pipe freeze, and allow its technical and economic factors to be assessed. Due to the complication of the problem, no simple, all embracing, laws are likely to emerge, so the only alternative is to attempt a more or less rigorous analysis of the heat and fluid flow as applied to pipe freezing, and to use the experimental results to verify the analysis.

5.1 Review of mathematical modelling techniques

Heat flow modelling techniques can be split into two broad areas, analytical and numerical. The former solves equations for the whole solution domain whereas the latter splits the domain into smaller sections and solves the equations for each section as it relates to its immediate neighbours.

For the analysis of pipe freezing, the particular solutions employed are known as 'Phase Change' or 'Moving Boundary' problems. The general method of all these solutions is to solve the energy equation for the liquid and solid phases and to apply suitable boundary conditions to these solutions. If convection in the liquid

is assumed to be absent, then the energy equation in one dimension reduces to :

$$\frac{d}{dx}\left(k.\frac{dT}{dx}\right) = \rho C.\frac{dT}{dt} \qquad \ldots(5.1)$$

The boundary conditions that are applied to this equation are :

$$T_S(X,t) = T_L(X,t) = T_f \qquad \ldots(5.2)$$

$$k_S \cdot \left.\frac{dT}{dx}S\right|_{X,t} = k_L \cdot \left.\frac{dT}{dx}L\right|_{X,t} + \rho L.\frac{dX}{dt} \qquad \ldots(5.3)$$

Also some assumption must be made about the temperature or heat flux at the outer boundaries of the liquid and solid phases or just one outer boundary if the solution domain is semi-infinite.

Equation (5.1) equates the gradient of heat flux against position at any particular section (or in finite terms, the difference between heat flowing into and out of a thin section) to the rate of change of sensible heat in that section. Equation (5.3) equates the difference between heat flowing away from the interface on the solid side and the heat flow into it on the liquid side with the release of latent heat due to the interface movement.

5.1.1 Analytical Solutions

Analytical solutions of these equations can be subdivided into exact and approximate solutions. Because of the complication introduced by the moving interface, very few exact solutions available. The most comprehensive is due to Neumann and generalised by Carslaw and Jaeger [58]. This is a one dimensional solution for freezing, due to a step change in the surface temperature (T_o), of a semi-infinite slab of liquid (freezing point T_f), initially at a

constant temperature above the freezing point.

If, as in this case, the thermal properties are assumed to be constant with temperature, then equation (5.1) reduces to :

$$\frac{d^2T}{dx^2} = \frac{1}{\alpha}.\frac{dT}{dt} \qquad \ldots(5.4)$$

where $\alpha = k/C$

This is a differential equation with two independent variables, time t and position x. If the similarity transformation shown in equation (5.5) is applied, then the differential equation and all the boundary and initial conditions can be expressed in terms of a single independent variable η. The solution of (5.4) expressed in terms of η is shown in equations (5.6) and (5.7).

$$\eta = \frac{x}{2\sqrt{\alpha_S t}} \qquad \ldots(5.5)$$

$$T_S = T_o + A.\mathrm{erf}\,\eta = T_o + A.\mathrm{erf}\,\frac{x}{2\sqrt{\alpha_S t}} \qquad \ldots(5.6)$$

$$T_L = T_\infty - B.\mathrm{erfc}\,\frac{x}{2\sqrt{\alpha_L t}} \qquad \ldots(5.7)$$

where erf = the error function, $\mathrm{erf}\,\eta = \frac{2}{\sqrt{\pi}}\int_0^{\eta} e^{-\beta^2}\,d\beta$

and $\mathrm{erfc}\,\eta = 1-\mathrm{erf}\,\eta$

From (5.2), (5.6) and (5.7) it follows that the interface position X is proportional to the square root of time t, or :

$$X = 2\gamma\sqrt{\alpha_S t} \qquad \ldots(5.8)$$

The temperature gradients at the interface can be obtained by differentiating equations (5.6) and (5.7). These, together with (5.8), substituted into (5.3) yield :

$$k_S A e^{-\gamma^2} - k_L B\sqrt{\alpha_{SL}} e^{-\alpha_{SL}\gamma^2} = \alpha_S \rho L \gamma \sqrt{\pi} \qquad \ldots(5.9)$$

where $\alpha_{SL} = \alpha_S/\alpha_L$

Substituting (5.8) into (5.6) and (5.7) and equating $T_S=T_L=T_f$ (at $x=X$) allows A and B to be determined :

$$T_o + A.\text{erf} = T_\infty - B.\text{erfc}\gamma\sqrt{\alpha_{SL}} = T_f$$

$$\text{i.e.} \qquad A = \frac{T_f - T_o}{\text{erf}\gamma} \qquad \ldots(5.10)$$

$$\text{and} \qquad B = \frac{T_\infty - T_f}{\text{erfc}\gamma\sqrt{\alpha_{SL}}} \qquad \ldots(5.11)$$

Finally, substituting (5.10) and (5.11) into (5.9) gives :

$$\frac{e^{-\gamma^2}}{\text{erf}\gamma} - \frac{k_{SL}\sqrt{\alpha_{SL}}(T_\infty - T_f)e^{-\alpha_{SL}\gamma^2}}{(T_f - T_o)\text{erfc}\gamma\sqrt{\alpha_{SL}}} = \frac{L}{C_S(T_f - T_o)} \qquad \ldots(5.12)$$

This equation may be numerically solved for γ, and then the final solution becomes :

$$T_S = T_o + \frac{(T_f - T_o)}{\text{erf}\gamma}.\text{erf}\left(\frac{x}{2\sqrt{\alpha_S t}}\right) \qquad \ldots(5.13)$$

$$T_L = T_\infty - \frac{(T_\infty - T_f)}{\text{erfc}\gamma\sqrt{\alpha_{SL}}} \cdot \text{erfc}\left(\frac{x}{2\sqrt{\alpha_L t}}\right) \qquad \ldots(5.14)$$

Cho and Sunderland [59] modified the Neumann solution above to allow a limited variation of thermal conductivity with temperature.

The Stefan problem is a special case of the Neumann problem in that the liquid is assumed to be initially at the phase change temperature, i.e. $T_\infty = T_f$. With this assumption (5.12) becomes :

$$\text{erf}\,\gamma \simeq \frac{2}{\sqrt{\pi}}\cdot\gamma \qquad \ldots(5.15)$$

$$\text{therefore} \qquad \gamma^2 = \frac{C_S(T_f - T_o)}{2L} \qquad \ldots(5.16)$$

$$\text{and} \qquad X = \frac{k_S(T_f - T_o)t}{\rho L} \qquad \ldots(5.17)$$

Equation (5.17) is clearly very much simpler than (5.12) but it is no longer an exact solution due to the approximation in (5.16). However, for water with small degrees of sub-cooling ($T_f - T_o \leq 5^\circ C$), the agreement with the exact Neumann solution is found to be good.

The Neumann solution is an exact solution of a very limited and idealised phase change problem. Solutions of this type are only possible where similarity transformations can be found, such that the differential equation, its boundary and initial conditions can all be expressed as functions of a single independent variable. This will not be possible for finite domains, domains in which both phases are initially present, non-uniform initial temperatures, and boundary conditions that are a function of time.

To deal with these situations, various approximate solution methods have been developed. One such is the Quasi-stationary approximation where the movement of the interface is assumed not to affect the temperature distribution for short times. This is then a transient conduction problem with no phase change, the phase change being solved for with the interface boundary conditions. The Quasi-steady approximation is a further simplification in which the transient term in the conduction equation is assumed negligible. A major disadvantage of this approximation is that the initial conditions cannot be satisfied. However, the mathematics is so simple that it is still used fairly widely.

Another approximate solution is the "Heat Balance Integral Method" in which a temperature penetration depth $\phi(t)$ is assumed, beyond which the temperature is still at its initial value, and there is therefore no heat transfer. The energy equation is satisfied on a volume averaged basis within the temperature penetration depth.

$$\int_0^{\phi(t)} \alpha \cdot \frac{d^2T}{dx^2} dx = \int_0^{\phi(t)} \frac{dT}{dt} dx \qquad \ldots(5.18)$$

In pipe freezing the geometry is radial and finite, the outer boundary condition is a function of time (and position if more than one dimension is considered), the thermal properties vary greatly over the temperature range, and convection in the liquid may or may not be an important effect depending on the fluid and the degree of superheat. It can be seen, therefore, that even the most powerful analytical solution will be inadequate for an accurate prediction of plug formation. Accordingly, attention will now be turned to the range of numerical techniques that may be employed.

5.1.2 Numerical Solutions

Numerical solutions to heat transfer problems fall into two classifications, finite element and finite difference methods. Finite element techniques have proved very powerful in the field of structural analysis, but their use in the modelling of transient heat conduction has been very much more limited. This is particularly so when a change of phase is involved because of problems caused by the discontinuity in thermal properties at the interface.

Finite difference methods have been developed and used much more widely for phase change problems, so despite certain advantages that finite element methods have in tracking the irregular geometries that occur in plug formation, this is the path which has been pursued in the Author's work.

It is now instructive to examine the finite difference technique in some detail. The basis of the method is the discretisation of the governing differential equation over a network of points, or nodes. This is done by replacing derivatives at a point (in space or time) with an average derivative over a region. To illustrate the technique, consider a one-dimensional slab of material with five nodes spaced evenly across its width, two on the boundaries and three in the volume as shown below.

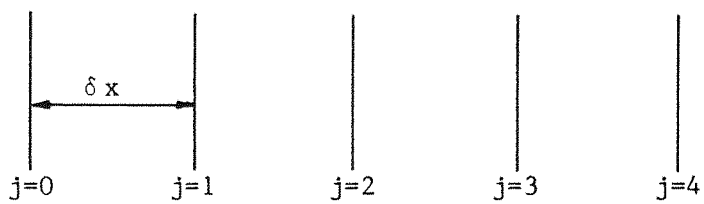

The equation governing heat conduction is :

$$\frac{d^2T}{dx^2} = \frac{1}{\alpha}\cdot\frac{dT}{dt} \qquad \ldots(5.19)$$

This equation must be satisfied throughout the volume, and this can be modelled by arranging for an approximation to be satisfied at each internal node. The outer nodes are governed by the boundary conditions. To achieve this the two differentials must be discretised as follows. Taking node 1 first, the differential dT/dx may be approximated by $(T_{j=1}-T_{j=0})/\delta x$ where δx is the distance between nodes. This is known as the backwards difference approximation, the forwards difference approximation being $(T_{j=2}-T_{j=1})/\delta x$. It is obvious that a more accurate approximation will be $(T_{j=2}-T_{j=0})/2\delta x$ and this is the central difference approximation. To obtain the central difference approximation to the second derivative it is necessary to consider two extra nodes, j=1/2 and j=3/2, located half way be 0 and 1, and 1 and 2 respectively. The central difference approximations to dT/dx, at these two intermediate points, are $(T_{j=1}-T_{j=0})/\delta x$ and $(T_{j=2}-T_{j=1})/\delta x$. The approximation to the second derivative is the change in dT/dx over the distance δx, divided by δx, i.e. $(((T_{j=1}-T_{j=0})/\delta x)-(T_{j=2}-T_{j=1})/\delta x))/\delta x$.

$$\left(\frac{d^2T}{dx^2}\right)_{j=1} = \frac{T_{j=0} + T_{j=2} - 2.T_{j=1}}{\delta x^2} \qquad \ldots(5.20)$$

For the differential of temperature with respect to time the forward difference approximation can used, so :

$$\left(\frac{dT}{dt}\right)_{j=1} = \frac{T^{h+1}_{j=1} - T^{h}_{j=1}}{\delta t} \qquad \ldots(5.21)$$

where h and h+1 denote present and next time steps

The discretised form of equation (5.19) can be written :

$$\frac{T^{h}_{j=0} + T^{h}_{j=2} - 2.T^{h}_{j=1}}{\delta x^2} = \frac{1}{\alpha}.\frac{T^{h+1}_{j=1} - T^{h}_{j=1}}{\delta t} \qquad \ldots(5.22)$$

Rearranging gives :

$$T^{h+1}_{j=1} = MT^{h}_{j=0} + (1-2M).T^{h}_{j=1} + MT^{h}_{j=2} \qquad ...(5.23)$$

where $M = \alpha\delta t/\delta x^2$

Similar equations can be written for nodes 2 and 3. The left hand sides represent the unknowns, i.e. the temperature distribution at the present time step, and the right hand side the known parameters, i.e. the temperature distribution at the previous time step. This is called an explicit formulation because each node's temperature is determined explicitly from known parameters. This is obviously very convenient but there is a problem. It is fairly simple to show that, for the approximate numerical solution to be convergent and stable, M must be positive and less than 1/2, i.e. $\delta t \leq (\delta x^2/2\alpha)$. Thus if the spatial grid is kept small to minimise the discretisation errors then the time step must be very small indeed. To avoid these stability problems the implicit formulation may be used. In the explicit formulation the derivatives of temperature with respect to time were written in terms of known temperatures at time step h. Now consider that the temperature distribution at time step h is unknown and that the last known temperature distribution is at step h-1. The position derivatives are still discretised in terms of the unknown temperature distribution (step h) and the time differential is discretised by the backwards difference approximation :

$$\left(\frac{dT}{dt}\right)_{j=1} = \frac{T^{h}_{j=1} - T^{h-1}_{j=1}}{\delta t} \qquad ...(5.24)$$

This leads to the implicit form of equation (5.23) where the temperatures at time h are calculated from a knowledge of temperatures at time h-1 :

$$-M.T^{h}_{j=0} + (1+2M).T^{h}_{j=1} - M.T^{h}_{j=2} = T^{h-1}_{j=1} \qquad ...(5.25)$$

Notice that in the equation for each node there are now three unknown temperatures. This necessitates their solution as a set of simultaneous equations. For nodes adjacent to the boundaries (in this case nodes 1 and 3) the number of unknowns is reduced to two since the boundary temperatures ($T_{j=0}$ and $T_{j=4}$) are defined by the boundary conditions. The complete set of equations for this example is :

$$(1+2M).T^{h}_{j=1} - M.T^{h}_{j=2} = T^{h-1}_{j=1} + M.T^{h}_{j=0} \quad ...(5.26a)$$

$$-M.T^{h}_{j=1} + (1+2M).T^{h}_{j=2} - M.T^{h}_{j=3} = T^{h-1}_{j=2} \quad ...(5.26b)$$

$$- M.T^{h}_{j=2} + (1+2M).T^{h}_{j=3} = T^{h-1}_{j=3} + M.T^{h}_{j=4} \quad ...(5.26c)$$

The above equations may be represented by the matrix equation :

$$[A].[T] = [B] \quad ...(5.27)$$

where [A] is a 3x3 matrix containing the coefficients
[T] is a 3x1 matrix full of the unknown temperatures
and [B] is a 3x1 matrix representing the known parameters of each equation.

[A] is a tridiagonal matrix, i.e. excepting elements on the central diagonal and the two adjacent diagonals, all other elements are zero. This makes solution of equation (5.27) by Gaussian elimination particularly simple and efficient. Obviously as the number of nodes increases then the sizes of matrices [A],[T] and [B] increase accordingly.

It can be seen from the above that the price of avoiding the stability problems of the explicit formulation is the need to solve a set of simultaneous equations that may be very large if there are many

nodes. For one dimensional problems, the fully implicit formulation is quite practical because the resulting tridiagonal matrix can be solved fairly easily. However for problems in two or three dimensions, the matrix [A] will not be tridiagonal, furthermore a two dimensional network of 10x10 nodes will require the gaussian elimination of a 100x100 non-tridiagonal matrix, a time consuming task even with fast computers. To alleviate this problem the Alternating Direction Implicit method has been devised [60]. Assuming the temperature distribution is known at time h-1 then the temperatures at time h-1/2 are calculated by writing the x derivatives in the implicit form (in terms of the unknown temperatures) and the y derivatives in the explicit form (in terms of temperatures at time h-1, which are known). This reduces the number of unknown temperatures in any one equation to three, and if the nodes are numbered correctly reduces the matrix [A] to a tridiagonal one. Having calculated the temperature distribution at time h-1/2 then the temperatures at time h are calculated by reversing the order and writing the y derivatives in implicit and the x derivatives in explicit form. This method has been shown to be unconditionally stable [61].

Having established the general principles of solving transient heat conduction problems by finite difference schemes, attention will now be focused on methods of dealing with a change of phase whose boundary is moving. If the two phases had similar thermal properties and no latent heat was evolved on freezing, then there would be no difficulties, but this is never the case. The change in thermal properties can be accommodated in any finite difference scheme simply enough (provided the change with temperature is smooth), by changing the values of the individual coefficients in matrix [A]. Accounting for the evolution of the latent heat is not so simple since the interface then represents a discontinuity, i.e. a heat source. Various methods have been tried including :

(i) Apparent Specific heat

(ii) Enthalpy Formulation

(iii) Isotherm migration

(iv) Boundary Immobilisation

The first of these represents the latent heat as an apparent heat capacity. The specific heat capacity is defined as the rate of change of enthalpy with temperature. Since freezing at the interface involves the liberation of energy (the latent heat), and thus a change in enthalpy with no change in temperature, then the specific heat capacity becomes infinite. If however, the phase change is assumed to take place over a small but finite temperature range $2\Delta T$, then the specific heat capacity can be redefined to incorporate the latent heat as follows :

$$C_a = C_s \qquad T < T_f - \Delta T \qquad \ldots(5.28a)$$

$$C_a = \frac{(C_s + C_L)}{2} + \frac{L}{2\Delta T} \qquad T_f - \Delta T \leq T \leq T_f + \Delta T \qquad \ldots(5.28b)$$

$$C_a = C_L \qquad T > T_f + \Delta T \qquad \ldots(5.28c)$$

C_a is then used in the discretised equations to solve for temperature. Since C_a is a function of temperature, some iteration is involved. The C_a's at each node are calculated from the latest approximation to the temperature distribution, and then used to obtain the next approximation. Since in many practical situations, thermal properties k and C vary with temperature, this procedure is necessary in any case. The method is relatively simple to program and lends itself well to two and three dimensional problems. However, it has been noted [62] that the range $2\Delta T$ is critical, both to the accuracy and the stability of the results, with a large ΔT causing inaccuracy and a small ΔT, instability.

An alternative to the temperature formulations discussed so far, is the enthalpy formulation. Equation (6.1) may be rewritten as

follows :

$$\frac{d}{dx}\left(\frac{k}{\rho}.\frac{dT}{dx}\right) = \frac{dH(T)}{dt} \qquad \ldots(5.29)$$

where the enthalpy H(T) is defined by :

$$H(T) = \int_0^T C(T)dT + L \qquad T \geq T_f \qquad \ldots(5.30a)$$

and

$$H(T) = \int_0^T C(T)dT \qquad T \leq T_f \qquad \ldots(5.30b)$$

Although H(T) is multivalued at $T=T_f$, temperature as a function of enthalpy is single valued, and this allows the solution of (5.29) assuming freezing over a finite range of temperatures (the diffuse model) or freezing at a discrete temperature, using the H-T relationship described by equations (5.30). The enthalpy formulation version of (5.23) is :

$$H_j^{h+1} = H_j^h + N.(T_{j+1}^h - 2.T_j^h + T_{j-1}^h) \qquad \ldots(5.31)$$

where $N = k.\delta t/\rho\delta x^2$

The enthalpy distribution can be calculated explicitly from (5.31) and then the temperature distribution may be deduced using equations (5.30). This is a simple solution provided the limit, placed upon the time step by the use of the explicit formulation, is acceptable. If the implicit formulation is used then a series of non-linear algebraic equations result. Shamsundar [62] notes that the discrete enthalpy model (freezing at a discrete temperature) converges on the real solution, but if it is used to predict heat flux, the solution oscillates either side of the correct solution. This oscillation may be reduced by using a smaller spatial step δx.

The Isotherm Migration Method is a scheme whereby the temperature is made an independent variable and one of the space variables becomes a dependent variable. There are several advantages associated with this procedure. The movement of the boundary is calculated explicitly, there is no need to interpolate it from temperature or enthalpy distributions. There is no need to re-evaluate thermal properties at each time step since the grid lines are constant temperature and hence constant property lines. If the nodes are equally spaced in the x,T plane, then in the x,y plane they will be closely spaced in the areas of high temperature gradient and widely spaced where heat flow is lower. However, against these advantages must be set the disadvantages that implicit methods are inapplicable [62], certain boundary and initial conditions may cause the position of an isotherm to be multivalued [60] and a small time starting solution will be required [63].

The final technique to be discussed here is the Boundary Immobilisation Method [61]. In this scheme the temperature distribution in the liquid and the solid are calculated separately with the interface equations (5.2, 5.3) linking the two solutions. Each solution domain is divided uniformly into a fixed number of nodes. As freezing proceeds the spacing of the solid nodes will widen, while the liquid nodes will compress together. Consider the solution for the solid phase (that for the liquid is similar), where a transformation is applied such that $\lambda = x/X(t)$ where $X(t)$ is the solid phase thickness at time t. The following transformations (5.32) can then be applied to (5.1) to give equation (5.33).

$$\frac{d^2T}{dx^2} = \frac{1}{X^2}\cdot\frac{d^2T}{d\lambda^2} \qquad \ldots(5.32a)$$

$$\frac{dT}{dt} = \frac{\partial T}{\partial t} - \frac{\lambda}{X}\cdot\frac{\partial X}{\partial t}\cdot\frac{\partial T}{\partial \lambda} \qquad \ldots(5.32b)$$

$$\alpha \cdot \frac{d^2T}{d^2} = X^2 \cdot \frac{\partial T}{\partial t} - \lambda X \cdot \frac{\partial X}{\partial t} \cdot \frac{\partial T}{\partial \lambda} \qquad \ldots(5.33)$$

The third term in (5.33) involving (dX/dt) can be seen as a pseudo-convective term due to the movement of the grid lines through the solid as X increases. It can also be seen that when λ is zero (i.e. on the outer boundary) this term disappears, and it rises to its maximum value at the interface (λ = 1) where the movement of the grid lines is fastest. The three temperature derivatives are discretised in the normal way, but it can be seen that the position of the phase boundary X(t) and its velocity dX/dt are also required. These may be approximated by applying a transformed version of (5.3) to the temperature distribution at the previous time step. The solution to (5.33) could then be used to find a better approximation to X(t) and dX/dt, and the iteration continued until the true interface position is converged upon. For some solutions, this iteration loop may not be necessary since a small error in the approximation of X(t) at one time step will be compensated for in the next.

The disadvantage of the method is the considerable complication of the governing equations especially when they are written in radial coordinate form. The problem becomes even worse when solving problems in two or three dimensions since the spatial variables are no longer orthogonal. Also a small time starting solution is required since the transformation λ is not defined at X=0. Nevertheless, the method has certain attractions for the modelling of pipe freezing. Since the liquid domain is solved separately, it is easier to include the effects of forced or free convection, either by a rigorous analysis of the liquid velocity and temperature distribution, or by assuming the liquid to be at a bulk temperature and using semi-empirical heat transfer coefficients to calculate heat flow at the solid/liquid interface. In this case equation (5.3) may be replaced by :

$$k_s \cdot \frac{dT}{dx}\Big|_1 - h_c \cdot (T_b - T_f) = \rho L \cdot \frac{dX}{dt} \qquad \ldots(5.34)$$

5.2 Review of Some Finite Difference Phase Change Models

In section 5.1.2 the difficulty of dealing with temperature dependent thermal properties in finite difference models was mentioned. Bonacina and Comini [64] introduced a numerical scheme for the solution of this type of nonlinear heat conduction equation, without the normal recourse to successive iterations. A three time level formulation was used in which the derivative of temperature with respect to time was written as a central difference approximation, rather than the normal forwards or backwards approximation. The differential of temperature with respect to the spatial dimensions x and y, are written in terms of temperatures averaged over the three time levels. Therefore this formulation involves two known temperature distributions, at time steps h-1 and h, and the unknown temperature distribution at time step h+1. The thermal properties are calculated on temperatures existing at the middle time level (step h), which are known a priori, and so there is no need to iterate the results. The problem considered by this paper [64] is that of two dimensional heat conduction with no phase change. The numerical solution is effected by a type of alternating direction implicit method, as outlined in section 5.1.2. The authors [64] note that the method is unconditionally stable and convergent.

Bonacina et al [65] extended the above work to include a phase change. The method used was that of Apparent Heat Capacities applied to the one dimensional liquid/solid case. Forty one equally spaced nodes divided up the solution domain, which was 0.5m wide. Time steps varied between 200 and 600 seconds, but were constant for each run. The phase change was assumed to take place over a temperature range of $0.5^{\circ}C$. In order to facilitate the comparison of the results with an analytical solution, the model was run first with the initial water temperature set at $0^{\circ}C$. Thermal properties were

assumed to be different for each phase but constant with temperature. Results were presented for 5,10,20,40 and 80°C of tube wall sub-cooling and in all cases the numerical solution agreed with the analytical result to within 1%. Next the model was modified to assume an initial temperature of 10°C and a tube wall temperature of -20°C. Eighty one nodes were now spaced over the solution domain which was 1m wide and the phase change range was assumed to be 2°C. In this case, where the liquid has some initial superheat, the phase change range was found to be critical. It had to be large enough for 2-3 nodes to be undergoing the phase change simultaneously. Too large an interval on the other hand, was found to give a strong divergence from the true solution. The accuracy of this numerical solution was checked by comparison with the semi-infinite solution with superheat (Neumann Solution). Obviously this is only valid up until the time when the inner node of the numerical model starts to change temperature significantly, but up until this point the two solutions were found to agree to within 3%.

Talwar and Dilpare [66] performed a numerical analysis in which the geometry and conditions are close to that found in the pipe freezing situation. The phase change was again approximated by assuming a freezing range and incorporating the latent heat into an apparent specific heat. The model was a two dimensional radial formulation, in which a certain length (the freezing section) of the outer boundary was held at a temperature below the freezing point, while the remaining length of the outer boundary was held at the initial temperature. An interesting feature of the program was that it selected its own time step, commensurate with maintaining the stability of its explicit solution. The results of the model were compared with those from experimental tests, designed to conform as closely as possible to the conditions assumed in the model. Two cases were tried, One with an external temperature in the freezing section of -100°C and the other with a temperature of -45°C. The differences between actual and predicted times to freeze were 23% and 16% respectively, with the predicted times being the shorter.

Voller and Cross [67] proposed an algorithm for reinterpreting the results of the enthalpy model. As has already been noted (5.1.2), if the enthalpy method is applied to a situation where the phase change takes place over a small interval or at a discrete temperature, then the resulting solution oscillates about the true solution. The basis of this new interpretation is to predict the points of agreement between the two solutions. The normal enthalpy method is used to obtain a "working" temperature distribution. From this the enthalpy of each element can be inferred (elements are of length δx and centred on their respective nodes). When an element has a temperature which indicates that it is at the phase change temperature and that half the latent heat has been removed, then the associated node may be assumed to be the position of the interface at this time. This precise time is determined by linear interpolation between temperatures at two successive time intervals. If node i is exactly on the interface at time (h+Z). t (where $0 \leq Z \leq 1$) then the temperature at all other points may be obtained, again by linear interpolation, i.e. $T_j^{h+Z} = T_j^h + Z(T_j^{h+1} - T_j^h)$. This method may be extended to two dimensional problems.

Shamsundar and Sparrow [68] presented a two dimensional model based on an integral form of the energy equation. For substances which freeze at a discrete temperature, the enthalpy H and the heat flux k.dT/dx change discontinuously, so the differentials dH/dt and d(k.dT/dx)/dx (in equation 5.29) are indeterminate at the interface. An arbitrary control volume is defined, which may or may not contain the moving interface. The integral energy equation for this control volume is :

$$\frac{d}{dt}\int_V H dV = \int_A k.\text{grad } T.\hat{n} dA \qquad \ldots(5.35)$$

The authors [68] demonstrated that this equation can be reduced to multi-dimensional forms of (5.29) and (5.3). Equation (5.35) was non-dimensionalised, discretised using an implicit

formulation and solved in the normal way.

Sparrow and Chuck [69] used the boundary immobilisation method to model one dimensional planar or radial freezing where the solid exists in two phases, thus including a second phase change temperature and interface. A convective boundary condition was applied at the solid/liquid interface. The space, temperature and time parameters were non-dimensionalised. The space dimension was transformed in a manner similar to that described in section 5.1.2, in order to immobilise the solid/solid and solid /liquid phase change interfaces. The temperature fields in the two solid phases were solved for separately using implicit formulations. To avoid the need to iterate between these two solutions, the interface equations were represented by explicit formulations as follows. Assume the temperature fields were known at time h. The interface velocities at time h were calculated from a knowledge of the temperature gradients either side of the interfaces. Let X^h represent the interface position at time step h.

$$X^{h+1/2} = X^h + \left(\frac{dX}{dt}\right)^h . \frac{\delta t}{2} \qquad \ldots(5.36)$$

The interface velocity at time h+1/2 was approximated by assuming the nodal temperatures at h and h+1/2 to be equal, but the temperature gradients were re-evaluated using the nodal spacing at h+1/2 calculated from $X^{h+1/2}$. Finally the interface position at h+1 was calculated from :

$$X^{h+1} = X^h + \left(\frac{dX}{dt}\right)^{h+1/2} . \delta t \qquad \ldots(5.37)$$

Since the backwards discretisation for the time differential used in the implicit temperature field equations can also be regarded as a central difference approximation based on time step h+1/2, the interface velocity at h+1/2 was used in the equations. Thus the

procedure for each time step was to obtain the boundary position at h+1 and velocity at h+1/2, as outlined above, and then to use these values in the implicit equations to solve for the temperature fields in each phase.

5.3 A One Dimensional Pipe Freezing Model

A full representation of the pipe freezing situation requires a two, or in the case of a horizontal pipe, a three dimensional model. However, as a starting point, it was decided that a one dimensional model should be written so that experience of finite difference modelling techniques could be obtained, without tackling programs of the immense complexity that some multi-dimensional models require.

The configuration chosen for the model is equivalent to assuming that a pipe freeze is axi-symmetric, which in the case of a vertical freeze is a reasonable assumption, and that heat flows only radially out of the pipe not axially along it. Obviously this last assumption is not valid, but if the freezing jacket is sufficiently long then at its centre the axial temperature gradients will be very small and so the assumption is at least a good approximation to conditions on this central section.

Such a model has enabled the determination of the effects of varying the pipe material, diameter and wall thickness and freezing with different degrees of initial superheat present in the liquid. The relative importance of the thermal properties of the pipe wall and the water/ice have also been explored. The model is validated by comparison with experimental results from the author's 100mm diameter vertical pipe rig.

Initially a program was written, based on a one dimensional version of the three time level, apparent specific heat model of Comini et al [64, 65], because this method is easy to extend to two

dimensions. However instability was experienced, as is often the case when using this type of model for the freezing of liquids which have a discrete freezing point. Thus it was decided to abandon this approach in favour of using a boundary immobilisation model similar to that of Sparrow and Chuck [69].

The author's model includes three phases, one with fixed boundaries and two with moving boundaries, the former to represent the pipe wall and the latter to represent the ice and the water. In the time domain the model is also split into three solutions, a starting solution involving only the pipe wall and water, a main solution for when ice and water are present and a finishing solution to cover the period between the completion of the ice growth and the achievement of the coolant temperature at the centre of the pipe. All three solutions are implicit finite difference formulations. In the case of the starting and finishing solutions, which involve no moving interface, a single tridiagonal matrix is formed, representing the finite difference equations for the pipe wall and the water or ice, and solved for the complete temperature distribution. The main solution is split into two parts, the pipe wall and the ice being represented by one tridiagonal matrix and the water by another.

5.3.1 General Arrangement of the Computer Program

This section will only deal with the broader aspects of the program logic. A more detailed derivation of the governing equations and their implementation in the model will be found in Appendix III.

The program begins with the input of the relevant parameters. The pipe diameter, wall thickness, initial temperature (which is assumed to be constant across the pipe) and coolant temperature are all set at this point. Also variable are the time step and the number of nodes in the pipe wall (maximum of 21) and the ice and water phases (both equal and maximum of 51). This obviously fixes the physical spacing of the nodes in the pipe wall, whereas in

the ice and water phases the actual spacing will vary as the interface moves from the pipe wall to the centre.

The thermal properties (conductivity and heat capacity) of the pipe wall, ice and water are all represented as linear or quadratic functions of temperature. Since the thermal properties are a function of temperature and the formulation being used is an implicit one, then it is necessary to iterate in order to achieve a solution for the temperature distribution. This is because the implicit finite difference equations involve the thermal properties at the time step for which the temperatures are unknown. Therefore the temperature distribution is represented in a two dimensional array with three columns. The first column represents the latest approximation to the temperature distribution, the second column represents the approximation at the previous iteration and the third column the temperature distribution at the previous time step. The method of solution is as follows. The thermal properties at each node are obtained, based on the temperature distribution at the previous time step. The coefficients of the tridiagonal matrix are calculated from these thermal properties and the previous temperature distribution. The matrix is then solved and the resulting temperature distribution is compared with the previous approximation. If all the nodal temperatures agree to within $0.1^{o}C$ then the check is passed. In the case of the first iteration the previous approximation is taken to be the distribution at the previous time step, so in this case the check will be failed. The thermal properties are now recalculated using the latest approximation and the solution repeated. This procedure is carried out until the check is passed at which point the solution may proceed to the next time step.

The procedure for the main solution is slightly more complex than the above. In early versions of the program, the first operation was to obtain the new boundary position and velocity explicitly in terms of temperature gradients, thermal conductivities and the latent heat of fusion. Then the temperature distribution in the water was

solved for as above and when that was complete the procedure was repeated for the ice and the pipe wall. There were therefore two separate iterative loops, the second of which was only started when the first had successfully converged. This method was found to introduce an inconsistency between the heat flow balance at the phase change interface and the rate of boundary movement. Since interface movement was calculated from temperature gradients at the previous time step, there was no guarantee that the new temperature distribution would imply the same boundary movement. The solution to this problem was to change to a single iteration loop for the whole solution and to recalculate the boundary movement from the latest approximation to the temperature distribution at each iteration. The water and the ice/pipe temperature distributions are still calculated separately, but new approximations for both are made before the check subroutine is called and the program either starts another iteration or proceeds to the next time step. In addition the check subroutine was modified so that the test was only passed if the latest approximation to the boundary velocity agreed with the previous one to within 0.01 percent. The effect of this modification was tested by performing two runs using identical parameters, one of which included the recalculation of the boundary movement at each iteration and one which did not. The difference in the predicted time to freeze was insignificantly small (943 and 944 seconds), but there were small but measurable differences in the temperature profile so the modification was left in place. The reason why the two solution were so close, is that although at any one time step the temperature gradients at the interface and the interface movement do not match, the boundary movement will match the temperature distribution of the previous time step. Therefore the boundary movement, over the period of a complete freeze, is more or less unchanged.

The equations governing the main solution with the moving boundary require a non-zero ice layer thickness. It has been found by experience that for the solution to start successfully the initial ice thickness must be at least 0.25mm in the case of a 100mm diameter

pipe. The starting solution is allowed to continue until the water begins to sub-cool, that is the water at the pipe wall interface passes below $0^{o}C$. After this time a check is made at each time step to see whether the loss of energy due to the sub-cooling of the water is greater than loss of latent and sensible heat associated with the formation of a 0.25mm thick ice layer. The starting solution continues until this is found to be so. Before the start of the main solution a subroutine calculates the initial ice thickness so that the above two energies are equal. Because of the latent heat, the energy loss associated with a given amount of ice is greater than that for the same amount of water. Therefore the point at which the temperature distribution crosses the $0^{o}C$ axis will move towards the pipe wall. Another subroutine expands the water temperature distribution to allow for this and recalculates all the nodal temperatures to take account of the different nodal spacing. The program switches to the finishing solution when the new boundary radius, calculated at the beginning of each time step, becomes negative.

When this program was first written, the outer pipe wall boundary condition was a time dependent temperature function of an exponential type. The outer temperature was set by the time dependent function given in equation 5.38 below :

$$T_w = T_a - (T_c - T_a).(1-\exp(-t/\tau)) \qquad \ldots(5.38)$$

where : T_w = Outer Wall Temperature
T_a = Initial Temperature
T_c = Coolant Temperature
t = time
τ = time constant

The time constant τ is determined approximately from experimental results from the 100mm rig. The boundary condition for the centre line of the pipe should be that of zero heat flux. This is

slightly difficult to incorporate into a finite difference scheme, but a reasonable approximation can be made by setting the central temperature at each time step equal to the adjacent node's temperature at the previous time step. The solution is terminated when this central temperature is within $1^{o}C$ of the coolant temperature.

5.3.2 Development of the One Dimensional Model

The outer boundary condition described above was thought to be unsatisfactory for two reasons; firstly, it was based on experimental data from a 100mm diameter rig, so the time constant for the exponential function would not be valid for larger or smaller pipes. Secondly, analysis of the experimental data, performed after the early program had been written, indicated that the measured external temperatures were not a true indication of the pipe wall outer temperature. The problem is described in more detail in section 3.4, but briefly it was clear that the measured outer wall temperatures were too low, and this was thought to be due to local wetting by liquid nitrogen of the soldered thermocouple during film boiling, as well as heat transfer along the wires. The solution was to use a convective outer boundary condition based on published data for the heat flux into the nitrogen from the pipe wall. Unfortunately the heat flux, as well as varying with temperature, also varies greatly for different geometries and surface roughnesses. The transition regime between nucleate boiling and film boiling is particularly uncertain, the actual value of the heat flux depending on whether the specimen is warming up or cooling down and its rate of change of surface temperature. However in spite of these difficulties, it was felt that an outer boundary condition based upon some estimate of the heat flux-temperature curve, would be more valid than a boundary condition derived from a rather arbitrary temperature-time relationship.

In the early stages of development the procedure was as follows. An outer wall heat flux was calculated from the latest

approximation to the outer wall temperature. This, together with the last approximation to the adjacent nodes temperature, was used to calculate the new approximation to the outer wall temperature which was then used as the boundary condition for the next approximation. However a check revealed that the heat flux into the nitrogen (the outer wall heat flux) did not match flux out of the pipe as implied by the temperature gradient between the two outermost nodes. No account has been taken of the sensible heat lost by the section of pipe between the outer wall and half way between the two outermost nodes. However, if the number of nodes is high enough, this is a relatively small error and cannot, by itself, account for the inaccuracy. The cause of the problem proved to be more fundamental. The procedure described above set only an outer wall temperature for the new solution, it did not pre-determine the outer temperature gradient. The solution proceeded to the next time step when all the nodal temperatures agreed with their previous approximations to within $0.1^{o}C$. The pipe wall may typically have a temperature difference across it of 2 or $3^{o}C$, so with 20 nodes the temperature difference between adjacent nodes was only of the order of $0.1^{o}C$. Once the outer wall temperature was set, very small variations in the adjacent nodes temperatures could cause very large variations in the outer wall heat flowrate. To solve this problem the boundary condition subroutine was modified so that only the outer heat flowrate was set, based upon the previous approximation to the outer wall temperature. This value was used to modify the tri-diagonal matrix so that the relationship between the present temperatures for the outer two nodes and the outer wall temperature at the previous time step was defined. This procedure guaranteed that the temperature gradient at the outer wall of the pipe corresponded with the heat flowrate into the liquid nitrogen, including allowing for the loss of sensible heat from the outermost section of pipe.

The next development was to add subroutines to the program to keep totals for the loss of sensible and latent heat and to compare this with the total heat conducted out of the outer boundary as

obtained from the outer boundary condition subroutine. The sensible heat loss from the water, ice and pipewall as well as the latent heat were all totalled separately and they were printed as a fraction of the total of each energy that would be lost in cooling the pipe and its contents from the initial temperature to the coolant temperature. The purpose of this extension to the program was to act as a check to the correct operation of the model, and to provide additional information for the interpretation of the results. Originally, the sensible heats were all calculated assuming linear temperature distributions between each node, which is not the same as assuming the nodal temperature exists across the whole element, since the elements are radial. The difference for fine meshes is very small and since one of the objects of these subroutines is to check the solution which implicitly assumes that the nodal temperature exist over the whole element, it was decided to simplify the calculation and make this assumption when calculating sensible heat loss. The loss of sensible heat was calculated for each element from its initial temperature, i.e. the cumulative loss of heat rather than that for the last time step. Specific heat capacities were given as quadratic functions of temperature, so by integrating these functions with respect to temperature between the initial and present temperatures and then multiplying by the elements mass, the loss of sensible heat is obtained. The latent heat was simply calculated from the volume of ice frozen up to the present time step.

The interface between the pipe wall and the ice creates two problems. One is a change in materials and hence in thermal properties. The other is that the grid spacing changes at this point. The original approach was to use a divided difference equation to take account of the different nodal spacing and to use thermal properties averaged between ice and the pipe wall material. This method assumes that the governing equation, 5.39 applies at the interface, but since there is a discontinuity in the temperature profile at this point, this will not be the case because the differentials with respect to radius are undefined.

$$\frac{d}{dr}\left(k.\frac{dT}{dr}\right) + \frac{k}{r}.\frac{dT}{dr} = \rho C.\frac{dT}{dt} \qquad \ldots(5.39)$$

It can be shown (Appendix IV) that discretisation using a control volume approach yields the same finite difference equations. This method makes no assumptions about continuous temperature profiles, but merely expresses the energy balance between net heat flow out of a volume and its loss of sensible heat. So, to solve the inner pipe wall interface problem, a radial control volume was set up between radii half the ice nodal spacing less and half the pipe wall nodal spacing more than the pipe inner radius. The average temperature gradients between the inner pipe wall and its two adjacent nodes were taken as the temperature gradients on the boundaries of the volume and the inner pipe wall temperature was assumed to exist throughout the volume.

5.4 Results and Discussion from One Dimensional Model

The performance of the model during the various series of runs was assessed by comparing the loss of sensible and latent heat with the cumulative total of heat convected into the liquid nitrogen. Most of the runs showed that the discrepancy was within 2% and many were better than this, although in one case the totals differed by 4%.

The cause of this slight discrepancy is thought to lie in boundary immobilisation transformation as applied to the differential of temperature with respect to time. Equation 5.40 gives the total differential of temperature with respect to time in terms of the transformed spacial coordinate λ. λ is defined by equation 5.41 so that nodes, whose radius varies as freezing progresses, have a constant value of λ.

$$\frac{dT_S}{dt} = \frac{\partial T_S}{\partial t} + \frac{\partial \lambda}{\partial r_i}.\frac{\partial r_i}{\partial t}.\frac{\partial T_S}{\partial \lambda} \qquad \ldots(5.40)$$

and

$$\lambda = \frac{r - r_i}{r_{iw} - r_i} \qquad \ldots(5.41)$$

By differentiating equation 5.41 with respect to r_i and substituting into 5.40 the total time derivative may be rewritten :

$$\frac{dT_S}{dt} = \frac{\partial T_S}{\partial t} + (\lambda - 1).\frac{\partial r_i}{\partial t}.\frac{1}{(r_{iw} - r_i)}\frac{\partial T_S}{\partial \lambda} \qquad \ldots(5.42)$$

To understand the physical significance of equation 5.42, consider a finite time step δt and boundary movement δr_i. Figure 5.1 illustrates the present and previous temperature profiles and the present and previous position of a node within the ice layer. The finite difference approximation to the time derivative in the governing equation (5.39) is $\delta T_t / \delta t$. The change in temperature of the node is δT_p, but the nodes position is a function of r_i, the interface radius. The difference between δT_t and δT_p can be approximated by multiplying the gradient of the temperature profile by the change in radius of the node. From the definition of the non-dimensional spacial ordinate λ, it can be seen that the movement of a node in one time step δt may be expressed as $-(\lambda - 1).\delta r_i$. The following relationship between δT_t and δT_p can now be written :

$$T_t = T_p + (\lambda - 1).\delta r_i.\frac{dT}{dr} \qquad \ldots(5.43)$$

Dividing equation 5.43 by δt throughout gives :

$$\frac{\delta T_t}{\delta t} = \frac{\delta T_p}{\delta t} + (\lambda - 1).\frac{\delta r_i}{\delta t}.\frac{dT}{dr} \qquad \ldots(5.44)$$

Applying the transformation λ, defined by equation 5.41, to the derivative of temperature with respect to radius, yields equation

(5.45) which is very similar to 5.42 but expressed in terms of a finite time step δt.

$$\frac{\delta T_t}{\delta t} = \frac{\delta T_p}{\delta t} + (\lambda - 1).\frac{\delta r_i}{\delta t}.\frac{1}{(r_{iw}-r_i)\delta\lambda}.\frac{\delta T}{} \qquad \ldots(5.45)$$

The temperature drop of a node divided by the time step ($\delta Tp/\delta t$) may be seen as the finite difference approximation to the partial differential of temperature with respect time seen in equation 5.42. The right hand term will approximate well the difference between $\delta T_t/\delta t$ and $\delta T_p/\delta t$, provided that the temperature gradient does not change appreciably over the distance $(1-\lambda).\delta ri$.

The are two main reasons why the equation derived above may not give a good approximation to the heat balance at each node. The first is large variations in the temperature gradient, such as occur in the water near the ice interface. The other is a discontinuity in the temperature profile, as found at the ice/water interface.

Dealing first with the effect of a varying temperature gradient, reference to figure 5.2 shows that with a positive 2nd differential of temperature with respect to radius, the loss of sensible heat at each time step will be under estimated. This will make the heat flowrate smaller in relation to the actual amount of sensible heat lost. Conversely, a negative 2nd differential, such as exists in the water near the ice interface, will cause the heat flowrate to be larger in relationship to the sensible heat loss.

The phase change interface introduces further complications. If the node spacing is small and the interface movement fairly rapid, then a node in the ice may be in a position that was unfrozen at the previous time step. Two inaccuracies are possible in this situation. The first is an error in approximating the previous temperature at the new nodal position, due to a sharp change in the temperature gradient

at the ice/water interface. The second error will be introduced by assuming that the specific heat capacity of ice applies over the whole temperature change, when some weighted average between the specific heats of water and ice should be used. The change of temperature gradient at the phase change interface depends on the ratio of sensible heat loss from the water to latent heat loss. The thermal conductivity of ice is approximately four times that of water, so for the same heat flow the temperature gradient in the ice will be about a quarter of that in the water. From the results however, it appears that the rate of latent heat loss generally exceeds three times the rate of sensible heat loss from the water and so the heat flux on the ice side of the interface is over four times that on the water side. Therefore the temperature gradient is usually greater in the ice than it is in the water which causes an over estimation of the sensible heat loss. By itself this would cause the total heat convected into the liquid nitrogen to exceed the actual sensible heat lost, but this effect is offset by the fact that the specific heat capacity of ice is approximately half that of water. The overall effect of these two errors again depends on the ratio of the rate of sensible heat loss from the water to the rate of latent heat loss. When the latter exceeds the former by a factor of more than approximately 7, the net heat conducted out of each element will be apparently greater than its sensible heat loss. During most freezes this situation does not apply and the total heat conducted out appears to be slightly less than the total sensible heat lost.

There is one error, unrelated to the moving boundary approximation problems described above. This occurs at the transition from the starting solution, where only water is present in the pipe, to the main solution, when both water and ice are present. It has been explained in section 5.3.1 how the thickness of the initial ice layer is determined, by balancing the sensible and latent heat lost in forming the ice with the sensible heat associated with all the water that is subcooled below $0^{o}C$. Because of the latent heat, the ice layer is thinner than that layer of subcooled water and so the

temperature distribution in the water has to be expanded towards the pipe wall. This reduces the sensible heat lost from the water and therefore causes the heat convected into the liquid nitrogen to exceed the total sensible heat lost up until that time step. Typically this inbalance is around 6% of the heat lost at that time for a 100 mm diameter pipe. The cumulative total of heat loss at the transition between the two solutions, for this size of pipe, is around 10% of the total heat to be removed. The total error then, is of the order of 0.5% of the total heat removed. The magnitude of this error decreases with increasing pipe diameter because the fraction of sensible heat removed at the conclusion of the starting solution is smaller for large pipes. This small error, which causes the heat convected into the liquid nitrogen to exceed the sensible and latent heat lost from the pipe, to some extent compensates for the larger error due to inbalances in the moving boundary approximation, which tends to have the opposite effect.

All the results to be discussed in the remainder of this chapter are affected to some degree or other by these errors. It is possible to estimate their maximum effect on time to freeze by comparison of the heat removed and heat convected columns of the printed output. These figures give the cumulative totals of heat convected into the liquid nitrogen and sensible plus latent heat lost, at intervals selectable by the program user. The method used to estimate the error is as follows: The heat removed at the instant the plug closed is read off, typically about 94% of the total heat removed by cooling the ice and pipe down to liquid nitrogen temperature. The heat convected column is then searched to find at what time 94% of the total heat had been convected into the liquid nitrogen. This time is then taken as the limit of the error. Take, as an example, a model run performed to find the time to freeze of a 305 mm (12") diameter mild steel pipe. Predicted time to freeze was 7315 seconds (121.9 minutes) and the heat removed at this time was 93.5 %. Using linear interpolation on the heat convected column showed that 93.5% of the total heat had been convected into the liquid nitrogen in 7822 seconds

(130.7 minutes). The actual predicted time to freeze should fall somewhere between 122 and 131 minutes.

Other limitations on the accuracy of the model include its assumption of heat transfer only by conduction. Experimental work, analysed in chapter 4, showed that natural convection affected plug formation at all fluid temperatures tested, but it is thought that the time to freeze was not significantly affected with initial temperatures below 20°C. Also the time taken to fill the jacket with liquid nitrogen is not allowed for in the model, which assumes liquid nitrogen in contact with the pipe from the very start of the freeze.

5.4.1 Varying Time Step and Nodal Spacing

The accuracy of any finite difference approximation is affected by the length of its time step and the physical distance between nodes. To be more exact, what is important is the relationship between time step and the total duration of the event being modelled (in this case the freezing of a pipe) and the ratio between nodal separation and the overall dimensions of the solution domain (the pipe radius). It is clear that for a small pipe which freezes quickly, the time step must be smaller and the nodes closer together than for a large pipe, if accuracy is to be maintained. Small time steps and fine nodal spacing generally increase accuracy by reducing discretisation errors, but at some cost in terms of the solution time and the computer memory necessary to run the solution, although for one dimensional models the latter is a minor consideration.

To investigate the effect of different time steps on the predicted time to freeze, several runs were performed on a "standard" freeze of a 101.6 mm (4") internal diameter, 6.25 mm (1/4") mild steel pipe, using various time steps from 0.25 seconds upwards. Time steps of 0.25, 0.5 and 1.0 seconds all gave the same predicted time to freeze. When using time steps longer than 1 second it was found that

sometimes the successive iterative approximations to the temperature profile did not converge closely enough for the solution to proceed. These results indicate that, for this size of pipe, time steps of around 1 second do not introduce significant discretisation errors. In all the work described subsequently, involving 100 mm internal diameter pipes, a time step of 0.5 seconds has been used to ensure convergence of the solution. For larger pipes, the time step was kept small enough to ensure that the total number of time steps taken was at least as great as that taken in the solution of a 100 mm diameter pipe.

Different nodal spacings have been tried to determine their effect on predicted time to freeze. The number of nodes in the pipe wall and in the ice/water domains are set separately. The finest mesh used had 21 nodes in the pipe wall and 51 nodes each in the ice and water, a total of 121 (two nodes are on the boundaries and hence included in two domains). Coarser meshes have been tried for comparison as shown in Table 5.1 below.

Number of Nodes		Time to Freeze	Heat Convected
Pipe Wall	Ice/Water (each)	(seconds)	(percent)
21	51	943	99.1
11	26	929	98.1
5	11	891	95.9
3	6	839	93.2

Table 5.1

The final column of table 5.1 shows the percentage of the total sensible heat lost that has apparently been convected into the liquid nitrogen and may be regarded as some measure of the accuracy of the solution. Bearing in mind the large increase in solution time associated with, say, halving the finest mesh shown above, this mesh (21 and 51+51 nodes) has been used in all the solutions discussed

subsequently.

5.4.2 Varying Pipe Diameters

The first series of runs with the model was to predict times to freeze and times to cool the centre to -60 and -140°C for mild steel pipes of various diameters. The diameters used varied from 51 mm (2") to 1219 mm (48"), the wall thickness was set at 1/16th of the pipe diameter in each case and the initial water temperature was 12°C. There were 51 nodes each in the ice and water and 21 in the pipe wall. The time step used varied from 0.25 seconds (51 mm dia.) to 5.0 seconds (1219 mm dia.). The results are illustrated in figure 5.3. The maximum error for the time to freeze, calculated as above, is also shown. The model prediction for the time to cool the centre to -140°C is shown as a dotted line. Experimental data, where available, has also been included for comparison. The line indicating the limit of error refers to the error caused by inaccuracies in the moving boundary approximation and the discrepancy in the sensible heat removed from water at the conclusion of the starting solution as discussed in section 5.4. It does not take into account the error due to the simplifying assumptions of the model.

The effect of pipe diameter on the possible error can be clearly seen. The "limit of error" time to freeze rises from 101% of the predicted time at 51 mm diameter, to 111% at 1219 mm diameter. The experimental results of Williams [35] and Emtage [37] show slightly shorter freezing times than predicted, that of Eden [39], slightly longer. The quoted result of Eden came from a series of flow freeze tests, the fastest freezing being taken as the approximate freeze time for a 50 mm diameter static freeze. It is very probable that even the lowest flowrates would increase the freezing time, so the predicted freezing time for this diameter may in fact be an over estimation. The experimental result quoted by Wigley [38] for a 304 mm (12") diameter pipe takes just 10 minutes longer to freeze than the predicted time, although the "limit of error" time is only 2 minutes

less than the experimental time. For freezes of 152 mm diameter and above, the predicted time to freeze is proportional to the pipe diameter squared.

The model was also used to estimate liquid nitrogen consumption. Two values were calculated, the first used the total heat removed to cool a section of pipe and water, three diameters long, down to liquid nitrogen temperature. The total heat was then divided by the latent heat of vaporisation of nitrogen (199.6 kJ/kg [70]) to give the mass of nitrogen required and this in turn was divided by the density (0.8073 kg/l) to give the volume. The assumption implicit in this estimate is that heat is removed by the nitrogen using only the latent heat and none of the sensible heat (i.e. nitrogen gas leaves the jacket at liquid nitrogen temperature, $-195.8^{o}C$). The other value calculated for liquid nitrogen consumption assumed that nitrogen gas left the jacket at a temperature equal to that of the outer pipe wall. In this case the maximum possible sensible heat has been used. The liquid nitrogen consumption for each time step was calculated on this basis using the specific heat capacity of nitrogen (approximately 1.04 kJ/kgK [70]), the latent heat of vaporisation, the outer wall temperature and the heat convected into the liquid nitrogen in that interval. The results indicate that the reduction in liquid nitrogen consumption, if the maximum sensible heat of the gas is used, falls from around 18% for a 150 mm pipe to 11% for a 1200 mm pipe. The reduction in the maximum usable sensible heat is as expected, because when compared to the total freezing time, the outer wall of the pipe cools more quickly with larger pipes. Accurate experimental data for liquid nitrogen consumption is difficult to obtain, but the indications are that the predicted nitrogen consumption is around 50-60% of actual nitrogen consumption. This is probably because the model takes no account of nitrogen leaks, losses in the delivery pipe (flashing off), heat leaks through the jacket and the heat removed from the jacket as it is cooled down initially.

5.4.3 Varying Pipe Wall Thickness

The second series of runs on the model set out to explore the effect of varying the pipe wall thickness on time to freeze. The standard conditions chosen were as follows : Internal diameter 101.6 mm, initial temperature 12°C, a mild steel pipe, a time step of 0.5 seconds, 50 nodes each in the ice and water and 20 in the pipe wall. The wall thickness was varied from 3.17 mm (1/8") to 50.8 mm (2"). Figure 5.4 shows the results. It may be seen that the time to freeze is approximately linearly related to wall thickness, rising from 15.15 minutes to 21.5 minutes as the wall thickness is increased from 3.17 to 50.8 mm.

5.4.4 Varying Initial Temperatures

The next series of runs on the model was to provide correlation between the model and the series of experimental tests as described in section 4.1. Pipe diameter was 101.6 mm (4"), wall thickness was 6.25 mm (1/4"). Initial temperatures used were 0.5, 5, 10, 15, 20, 25, 30, 35, 40, 45 and 50°C. The same nodal spacing and time step was used as in the previous series of runs.

Figure 5.5 illustrates the results of these runs and those of the corresponding series of experiments. It can be seen that the model consistently over estimates the time to freeze. The gradient of the line (i.e. the effect of increasing initial temperature on the time to freeze) is in very good agreement with the experiments. The over-estimation of the predicted times to freeze can probably be attributed to the nitrogen heat flux/temperature difference relationship used in the model. The relationship used was taken from combination of two sets of experimental data as shown in figure 5.6. In the film boiling regime the data of Hanson and Richards [54] has been used whereas in the transition and nucleate regime that of Flynn et al [53] was employed. Analysis of experimental results described in section 4.1.5 suggests that transition from film to nucleate

boiling occurs at much higher pipe wall temperatures than the above data would suggest and the heat flux in the nucleate regime appears to be significantly higher. Adoption of a heat flux/temperature difference relationship based on the experimental results of the author would reduce the predicted times to freeze of the model.

The prediction of the cooling rate after the centre of the plug has frozen off will be considered in two stages, 0 to $-60^{o}C$ and -60 to $-140^{o}C$. In the experimental freezes, typically the centre cooled to $-60^{o}C$ in about 45 seconds after freezing. The trend was for this figure to decrease slightly with increasing initial temperature (35 seconds at $45^{o}C$). The model prediction varied from 22 to 24 seconds, which is a considerable under estimation. The explanation for this probably lies in longitudinal heat conduction in the plug which would be quite considerable just after the plug closed and which the model does not take into account. The longitudinal heat conduction would decline rapidly as the plug extends axially and therefore the cooling time from -60 to $-140^{o}C$ should be much less affected by it. The average experimental cooling time between these temperatures was 161 seconds (varying between 135 and 190 seconds) and showed no particular trend with increasing initial temperature. The predicted cooling time from -60 to $-140^{o}C$ fell from 163 seconds with an initial temperature of $0.5^{o}C$ to 159 seconds with $50^{o}C$, and thus shows very good agreement with experiment.

Figure 5.6 shows the position of the interface, plotted against time, for the experimental freeze from an initial temperature of $10^{o}C$. The interface radius on section 2 (figure 4.1) has been used for the purposes of this graph because, although the plug did not close first on this section, the longitudinal heat conduction was least and so the conditions were closest to those assumed by the model. For comparison the predicted interface position has been plotted with a dotted line. The time scale of the predicted interface position has been multiplied by a factor of 0.877 so that plug closure of the model coincides with the freezing-off of section 2 in the

experiment. It can be seen that the interface velocity in the model was fairly constant, being slightly faster initially and accelerating again just before plug closure. The model predicted that ice growth will begin about 30 seconds after the start of the freeze. This assumes that the jacket is full of nitrogen from the start, and for this reason ice growth was not seen in the experimental run until about 90 seconds into the freeze. Thereafter the experimental interface velocity rose to become higher than predicted. It should be remembered that the model assumed heat transfer from the water to the ice by conduction whereas natural convection was in reality the controlling factor. The experimental interface velocity fell almost to zero at the conclusion of phase one of plug formation before increasing sharply at the start of phase two. In this period the interface velocity was once again considerably higher than predicted. This was possibly due to a large temperature gradient on the ice side of the interface which was allowed to build up when the interface velocity was very low.

5.4.5 Varying Thermal Properties

To determine their relative importance, the program was modified to allow multiplying factors to be applied to the various thermal properties. These were the thermal conductivity and specific heat of the pipe wall, the thermal conductivity and specific heat of the ice/water and the latent heat of fusion. A 'standard' freeze was chosen as the basis from which to compare all the other results. This was a 101.6 mm (4") diameter pipe of 6.23 mm (1/4") wall thickness at an initial temperature of $12^{o}C$. The thermal properties were as for mild steel and ice/water. Runs were made with each of the five thermal properties in turn multiplied by factors of 10, 2, 0.5 and 0.1. The predicted times to freeze were divided by the time to freeze of the 'standard' freeze and plotted on log-log graph paper as figure 5.8. The slope of the lines indicate the relative significance of each property. Thus the ice/water thermal conductivity is shown to be the most important property affecting time to freeze. By contrast the

conductivity of the pipe wall has hardly any affect at all. This is not to say that the pipe wall conductivity is always unimportant in pipe freezing, but this is so for freezes similar to this 'standard' freeze. It can be seen that the time to freeze is just beginning to rise as pipe conductivity falls to 1/10th that of mild steel. If the pipe and its contents are seen as two thermal resistances in series through which heat must flow, then the heat flowrate will be relatively unaffected by quite large variations in the low resistance. Only when the thermal resistance of the pipe becomes significant compared to that of its contents, as would be the case with a plastic pipe for instance, do variations in the pipe conductivity become important. This is the reason why the gradient of curves for both the ice/water conductivity and the pipe conductivity decrease as the conductivities increase and each becomes a less significant thermal resistance compared to the other. After the liquid solid thermal conductivity the next most important thermal property for this 'standard' freeze is the latent heat of fusion. This is followed by the specific heat capacities of the ice/water and finally the pipe wall. The latent heat of fusion may be viewed as an effective heat capacity since it represents heat that must be removed to lower the temperature, the only difference being that it is removed at one particular temperature rather than over a range. For the standard freeze, at the point of freeze-off, approximately 2700 kJ/m of latent heat have been removed, 2200 kJ/m of sensible heat from the solid/liquid and 1200 kJ/m from the pipe wall. This reflects the order of importance on the time to freeze but it should be remembered that latent heat and sensible heat from the ice/water has to flow further than sensible heat from the pipe wall, which is removed comparatively easily, so the slopes of the lines are not purely a result of the relative magnitudes of each term.

5.5 Conclusions and Future Modifications to the One Dimensional Model

A one-dimensional pure conduction finite difference model has been written. It is specific to pipe freezing in that it includes a separate domain to model the pipe wall and uses a convective outer boundary condition based on the boiling of liquid nitrogen. It has not been validated against an analytical solution because, to the authors knowledge, no such solution exists which includes the above two features. The operation of the model has been checked by comparing the balance of heat flow and energy lost both for each individual node during development of the program and for the whole solution during each run. The results of these checks indicates that, with the reservations described in section 5.4 (which amount to small inaccuracies usually less than 2% of the total heat removed) the model is operating satisfactorily. The validity of the model itself has been assessed by comparison with experimental data. At smaller diameters (100 and 150 mm) the model over-estimates time to freeze by around 15-20%, with a diameter of 300 mm the model under estimates by a little under 10%. It is thought that the boiling heat transfer correlation used in the model gives lower heat fluxs than observed experimentally, so the model would be expected to over estimate freezing times. The model predicts well the slope of the line for time to freeze against initial temperature, provided the initial data is drawn from the experiments conducted without the tank in place beneath the pipe. In this configuration the bulk temperature of the water falls quickly because very little heat is convected into the freezing section. This fits the simplifying assumptions of the model (pure, radial one-dimensional conduction) better than when the bulk temperature is maintained by convection from below. The relative importance of the thermal properties have been examined by multiplying each by factors between 0.1 and 1.0 and observing the effect on predicted time to freeze. Varying the latent heat caused the largest variation in freezing time while changing the pipe wall conductivity had almost no effect. This suggest that for freezes in metallic

pipes, the actual pipe material is relatively unimportant. The experimental flow freezes conducted by Eden [39] and Collier [40], in mild and stainless steel pipes (section 2.1.2), support this conclusion.

The first modification that should be made to the model is to test the effect of a better estimate of the outer wall temperature to heat flux relationship. This would be obtained from the results of the experimentation carried out with improved instrumentation (section 4.3). This will hopefully decrease the error between experimental and predicted times to freeze.

With the exception of the above, it is felt that the principal limitation to the accuracy of the model is its simplifying assumption of heat transfer only by conduction. Experimental results have shown (section 4.2) that for water temperatures in excess of 20°C the time to freeze will be very significantly affected by natural convection if the bulk water temperature in the freezing area is maintained. To incorporate this effect it will be necessary to replace the conduction solution for water with a convective inner boundary condition for the ice/water interface. The solution would probably be arranged to revert to an all conduction solution once the ice plug has reduced the central orifice to about 30 mm diameter, since this is the point at which experiment suggests that convection breaks down.

Finally, the program could be modified to model the effect of different coolants such as dry ice and propanol. Commercial freezes are sometimes carried out using such coolants in order to reduce pipe stresses caused by rapid cooling and avoid the brittle failure risk caused by very low temperatures. It would be very useful therefore to be able to predict the reduction in cooling rates caused by the necessity to avoid the use of liquid nitrogen.

6.0 Conclusion

A literature survey has revealed that, with very few exceptions, there is no published experimental work on freezing that is directly applicable to pipe freezing. Papers by Stelzer [28], on the flow freezing of water using liquid nitrogen, and by Hall and Chevray [33] and Ichiyanogi et al [34], on the freezing of oil filled electrical cables, are relevant, but other published work differs significantly in geometry, temperature regime or plug material.

A wide range of experiments carried out by the Southampton group including the author have investigated the feasibility of formation of both ice and hydrocarbon plugs in pipes from 50 to 300 mm (2 to 12") diameter and measured their freezing times. The 300 mm diameter pipe took 130 minutes to freeze when filled with water and around 18 hours when filled with Statfjord crude oil. For freezes in flowing water, the limiting combination of inlet temperature and flowrate for a successful freeze have been measured for 50 and 100 mm (2 and 4") diameter mild steel pipes and for 50 mm diameter stainless steel, UPVC and GRP pipes. Almost no difference in freezing characteristics was seen between stainless and mild steel pipes, but when using plastic pipes the maximum flowrate for a given inlet temperature that can be successfully stopped is reduced by an order of magnitude.

The integrity of ice and hydrocarbon plugs has been investigated by hydrostatic testing in 25, 50, 150 and 300 (1,2,6 and 12") diameter pipes. Ice plugs have been tested to 2000 psi in the 50 mm pipe and 1600 psi in the 300 mm diameter pipe. Statfjord crude oil plugs have withstood 3500 and 1500 psi respectively in the same pipes. Maximum test pressures have been limited so far by the design pressure of the pipes and fittings rather than by the adhesion and strength of the plugs. Instrumentation techniques have been developed to measure the stress levels induced in the pipe wall during pipe freezing. These have been applied to the freezing of a 50 mm diameter pipe

containing water using direct contact liquid nitrogen cooling. When the pipe was unconstrained the peak stress levels during initial cooling reached about 40% of the yield stress. When a 1m long section of pipe was restrained longitudinally and frozen using a 0.2m long freezing jacket, the peak stress level observed rose to approximately 75% of the yield stress.

The major work of the author, on which this thesis is based, concerns the heat and fluid flow aspects of ice plug formation in vertical pipes. Two parallel paths have been pursued. Firstly an experimental programme in which the approach taken was to measure the temperature distribution in the pipe during freezing as accurately as possible and to infer from this the heat flow which in turn indicates the pattern of natural convection. Secondly a numerical model has allowed the prediction of times to freeze for a wider range of freezing conditions than could possibly be tested experimentally. The results of the experimental programme have been used to validate the computer model.

The major achievement to come out of the experimental programme has been the postulation of a three phase plug formation mechanism for freezing under conditions which have not previously been investigated. In phase one the natural convection boundary layer flows from some distance above the freezing area to some distance below it and a return flow of equal volume flowrate must exist up the centre. When the remaining orifice in the pipe is around 30 mm diameter, the upward current in the middle interferes with the downward flowing boundary layer. The phase two convection pattern now takes over, in which the upward centre flow is turned to become the downward boundary layer about midway up the freezing section. This eliminates, or at least severely restricts, the natural convection in the upper part of the freeze and effectively isolates the water in this area from surrounding water. The bulk temperature of this water falls quickly and the consequent reduction in heat flux into the upper part of the partially formed plug causes this section to freeze off

first. The plug then extends downwards into the lower part of the freezing section. During phase three of plug formation, the plug further extends axially upwards and downwards.

The changes in convection pattern postulated above, have not been directly observed, due to the experimental difficulty involved. However, measurements during freezes from a range of initial temperatures from 6.5 to 53°C, of interface position, radial temperature profiles and rate of loss of sensible and latent heat, all supported the above theory of plug formation. The three phase plug formation mechanism was observed to operate in both the geometries in which the pipe was frozen. In the first of these, the pipe was blanked off a short distance either side of the freezing section, which restricts the effect of natural convection. In the second geometry, natural convection was encouraged by attaching a large tank just below the freezing section, thus vastly increasing the volume of water in the rig and hence maintaining the bulk water temperature for longer.

Testing in the two different geometries described above, has shown that although local natural convection within the freezing section exerts a controlling influence on plug formation, significant heat exchange with water more distant from the freezing site does not occur in vertical pipes unless the water temperature is above 20°C. As, from the point of view of natural convection these represent the extremes, the layout of pipework surrounding the freezing site is unimportant unless the water exceeds this temperature. However, it has also been demonstrated that with warm water of only 30°C and above, the geometry effect becomes very important to freezing time and liquid nitrogen consumption.

The local heat flux into the liquid nitrogen has been estimated from measurements of the temperature difference across the pipe wall. The wide range of results quoted in the literature indicate that measurements of heat flux in pool boiling is highly

specific to the exact conditions under which measurement was made. Peak nucleate boiling heat fluxes of around 150 kW/m^2 as estimated by the author, are within the range of values quoted by other authors e.g. by Lyon [56]. However this figure is significantly higher than the results of Flynn et al, whose data was used in the boundary condition for the author's computer model.

Two freezes with the tank in place, starting with an initial temperature of $45^{o}C$, indicated an entirely different plug formation mechanism. This is thought to involve small isolated convection "cells" in which water is virtually isolated and can thus be cooled very quickly. It was difficult to determine the exact freeze-off time for these two freezes, but they appeared to be in the order of 4 to 8 minutes.

The numerical model, developed in parallel with the experimental programme, has enabled predictions to be made for times to freeze for a variety of pipe diameters, wall thicknesses, pipe materials and initial temperatures. Although it is a relatively simple one-dimensional, pure-conduction formulation, it does represent a significant advance, in that the geometry and boundary conditions are set up specifically for pipe freezing, i.e. one fixed interface between the pipe and the ice, a moving interface between the ice and the water and an outer boundary condition based on the convective heat transfer characteristics of pool boiling liquid nitrogen. This type of outer boundary condition has been found to lead to instability under certain circumstances and steps have had to be taken to over come this problem.

Wherever possible the predicted times have been compared with experimental data obtained, either from the authors own work, or from work conducted by other members of the Southampton University pipe freezing group. The degree of agreement between the experimental data and the model prediction, over a range of pipe diameters from 50 to 300 mm (2 to 12"), was most encouraging considering the simplifying

assumptions made in the model (no axial heat transfer and no natural convection). The model has been found to over-estimate times to freeze by up to 20%, which is thought to be mainly attributable to the nucleate and film boiling heat flux to temperature difference relationship used. This was based on data from Flynn et al [53] and Hanson and Richards [54] which gives a significantly lower heat flux in the nucleate regime when compared to approximate data obtained from the authors experimental rig. The transition from film to nucleate boiling appears to occur at higher surface-to-pool temperature differences than the data used in the model would suggest.

Specifically, the model has been validated against the authors own experimental work by comparing the predicted times to freeze for a range of initial temperatures against those obtained experimentally with the freezing section blanked off. This geometry was used for the comparison because, at present, the model does not include the effects of natural convection which are very important at temperatures above $20^{o}C$ and where the geometry allows the bulk water temperature in the freezing section to be maintained by natural convection from below. Although over estimating all times to freeze as explained above, the model predicted very well the slope of the line relating initial temperature and freezing time.

7.0 Recommendations for future work

The three phase model of ice plug formation built up during this work is based solely on the freezing of a vertical 100 mm (4") diameter pipe. The first priority must, therefore, be to see how increasing the pipe diameter affects the freezing mechanism. For instance, how will the pipe diameter affect the central orifice diameter at which transition from phase one to phase two occurs.

Having extended our understanding of ice plug formation in vertical pipes, a similar investigation should be launched to determine the freezing mechanisms for horizontal pipes.

Two freezes in the authors experiments indicated that different mechanisms of plug formation are quite possible. It is very possible that the freezing of a more highly convective liquid such as crude oil will exhibit such an alternative mechanism. Therefore a program of freezing these fluids in similar, highly instrumented, rigs must be undertaken.

Some form of flow visualisation or even flow measurement work is highly desirable to confirm the three phase hypothesis which, at present, is based only on temperature measurements. Flow measurement will, however, probably prove extremely difficult due to the slow velocities involved in natural convection and the lack of access to the freezing volume.

The one-dimensional model should be modified to replace the conduction solution for the water by an empirical or analytical convective heat transfer coefficient at the ice/water interface. This would allow the effect of natural or forced convection to be modelled in a limited way. The outer boundary condition should be modified to use boiling heat transfer data obtained experimentally from pipe freezing rigs, since this should be more applicable than data for different geometries and materials.

Modelling of the freezing of hydrocarbons presents an entirely different proposition. In one way the problem is easier than for water, because the changes in mechanical and thermal properties do not occur at a discrete temperature, but gradually over a temperature range. These characteristics would allow the use of a single solution for both the liquid and solid since an apparent specific heat method can be used in which the latent heat is incorporated into the specific heat capacity over some range of temperatures. Against this simplification, must be set the need to model more rigorously the natural convection within the liquid.

References

1 G.J.Howard, The Ice-O-Lator: A proven way to determine pipeline leaks. 10th Int. Pipeline Technology Exhib. & Conference, conference papers p327-330 Houston USA Feb 23rd-25th 1982.

2 Brister Inc., Quick freeze plug reduces testing and repair costs. Pipeline Industry Mar 1977 p37-39.

3 R.P.Deplancke, How the frozen plug method found an elusive pipeline leak. Petroleum & Petrochemical International Jan 1972 p46-47.

4 J.S.Reef, 'Hot' tapping and plugging of pressurised lines. Plant Engineering Apr 18th 1974 p111-113.

5 M.B.Pickell, Pipeline-plugging methods keep pace with industry needs. Oil & Gas Journal Mar 3rd 1980.

6 Total, Total's 'cold tapping' system comes on stream. Pipes & Pipelines International Sep-Oct 1983 p21-24.

7 British Gas Corp., Cold tapping aims to halve pipeline repair time. Offshore Engineer Jul 1982 p53-54.

8 C.W.Bishop, Pipe freezing plugs cost of maintenance downtime. Processing Nov 1978 p29,31.

9 BCB Pipe Freezing, Pipe freezing technique proved for Services concrete-lined pipelines. International Petroleum Times Mar 1st 1980 p22.

10 A.M.Keay, Ice plug method used on Dunlin A. Offshore Jul 1979 p30,35.

11 C.W.Bishop, Freeze technology cuts maintenance downtime. Water Services Feb 1980 p114-115.

12 D.Martin, Freezing out maintenance downtime. Process Engineering Jan 1978 p57.

13 Brister Inc., Freeze plug test 40 inch pipe for Colonial loop line. Pipeline News Mar 1978 p44.

14 C.W.Bishop, Pipe freezing...Latest Maintenance 'tool' for pipeline engineers. Pipes & Pipelines International Dec 1977 p16,17,40.

15 Anon, Pipe freezing speeds safety injection line changes at St.Lucie 1. Power July 1982 p80-81.

16 T.C.Elliot, Establishes freeze seal system for pipe repair in radiation area. Power Jul 1976 p120.

17 Anon, Pipe freezing Valuable in Repair/Maintenance. Pipeline & Gas Journal Apr 1980 p25

18 D.Buckman, Ice plugs isolate pipe sections. Ocean Industry Apr 79 p172-176.

19 D.Buckman, Quick freeze plug performed successfully on lined pipe. Pipeline Industry Feb 1980 p52,54.

20 Anon, Dry-Ice plug seals hydraulic piping for flushing. Hydraulics and Pneumatics Aug 1973 p97-98.

21 E.Seaton, Subsea plugging speeds repair of offshore crude pipeline. Oil & Gas Journal Feb 18th 1980 p108-110.

22 R.D.Zerkle and J.E.Sunderland, The effect of liquid solidification in a tube upon laminar-flow heat transfer and pressure drop. Jnl. of Heat Transfer May 1968 p183-190.

23 D.R.Oliver, The effect of natural convection on viscous flow heat transfer in horizontal tubes. Chemical Engineering Science v17 1962 p335-350.

24 G.J.Hwang and Ja-Pung Sheu, Liquid solidification in combined hydrodynamic and thermal entrance region of a circular tube. Canadian Jnl. of Chemical Engineering Feb/Apr 1976 p66-71.

25 M.Haneef and A.Aziz, Experimental study of inward freezing in circular and square pipes. Applied Energy Dec 1982 p243-251.

26 O.R.Asfar, A.Aziz and M.A.Soliman, A uniformly valid solution for inward cylindrical solidification. Mechanics Research Communications v6 1979 p325-332.

27 E.M.Sparrow and J.M.Broadbent, Freezing in a vertical tube. Jnl. of Heat Transfer May 1983 p217-225.

28 J.F.Stelzer, Flow blocking of water currents by freezing. Proc. 15th Congress of Refrigeration on Progress in Refrigeration Science and Technology. Venice Italy Sep 23rd-29th 1979 Vol 2 p453-459.

29 E.M.Sparrow, J.W.Ramsey and R.G.Kemink, Freezing controlled by natural convection. Jnl. of Heat Transfer Nov 1979 p578-584.

30 E.M.Sparrow and P.Souza Mendes, Natural convection heat transfer coefficients measured in experiments on freezing. Int. Jnl. Heat & Mass Transfer v.25 No.2 1982 p293-297.

31 R.R.Gilpin, Ice formation in a pipe containing flows in the transition and turbulent regimes. Jnl. of Heat Transfer May 1981 p363-368.

32 S.B.Thomason and J.C.Mulligan, Experimental observations of flow instability during turbulent flow freezing in a horizontal tube. Jnl. of Heat Transfer Nov 1980 p782-784.

33 R.E.Hall and R.Chevray, Freezing of low and medium viscosity type cable filling oils. IEEE trans. Power Apparatus and Systems Nov/Dec 1975 p1994-2001.

34 N.Ichiyanagi et al, The freezing method for the oil stop in POF cable repair. IEEE trans. Power Apparatus and Systems Nov/Dec 1979 p2037-2046.

35 D.Williams, An investigation into cryogenic pipe freezing using liquid nitrogen. Univ. of Southampton Internal Project Report 1982.

36 Anon, 'Drikold', the freezing technique for pipeline isolations. Published by ICI.

37 J.A.Emtage, An investigation into the freezing of a six inch pipe using liquid nitrogen. Univ. of Southampton Internal Project Report 1985.

38 D.A.Wigley, Final report on phase 1 of the Southampton University Pipe Freezing Project. Univ. of Southampton Report No. ME/85/9 July 1985.

39 C.Eden, Freezing flowing water in a pipe using liquid nitrogen. Univ. of Southampton Internal Project Report 1983.

40 S.M.Collier, Determination of the freezing characteristics of water in pipes at various combinations of flowrate and temperature. Univ. of Southampton Internal Project Report 1984.

41 P.A.Castle, Freezing flowing water in GRP and mild steel pipes using liquid nitrogen. Univ. of Southampton Internal Project Report 1985.

42 H.J.A.Kennedy, Formation of plugs frozen in a 2" internal diameter pipe water and liquid hydrocarbons. Univ. of Southampton Internal Project Report 1985.

43 P.R.Pratt, An investigation of the stresses caused by plug formation during pipe freezing. Univ. of Southampton Internal Project Report 1982.

44 M.Gostick, Computer based instrumentation for cryogenic pipe freezing. Univ. of Southampton Internal Project Report 1983.

45 M.A.Ashfield, Determination of the stresses and strains induced in pipewalls by cryogenic pipe freezing. Univ. of Southampton Internal Project Report 1984.

46 P.C.M.Walbank, The strains induced and the effect of flaws during the pipe freezing process. Univ. of Southampton Internal Project Report 1984.

47 R.M.Hall, Liquid nitrogen pipe freezing. B.O.C. Derby, Internal memorandum

48 B.Abbot, An investigation into the strength of an ice to metal bond, typical of a frozen pipe. Univ. of Southampton Internal Project Report 1984.

49 P.D.Howell, An investigation into the freezing characteristics of liquid hydrocarbons. Univ. of Southampton Internal Project Report 1983.

50 D.Brown, Pressure testing plugs frozen in pipes containing water and liquid hydrocarbons. Univ. of Southampton Internal Project Report 1984.

51 G.F.C.Rogers and Y.R.Mayhew, Engineering thermodynamics work and heat transfer. 2nd Edition p551-554 : Longman 1967.

52 S.Goldstein, Modern developments in fluid dynamics 1 and 2. p641 : Oxford, Clarendon Press 1938.

53 T.M.Flynn, J.W.Draper and J.J.Roos, Advances in Cryogenic Engineering v.7 1962 p 539-545.

54 W.B.Hanson and R.J.Richards, Heat transfer to a boiling liquefied gas. Unpublished laboratory note 56-1, NBS-CEL, Boulder, Colorado 1956.

55 E.G.Brentari and R.V.Smith, Nucleate and film pool boiling design correlations for O_2, N_2, H_2, and He. Int. Advances in Cryogenic Engineering, 325-341, Plenum Press 1965.

56 D.N.Lyon, Peak nucleate-boiling heat fluxes and nucleate-boiling heat-transfer coefficients for liquid N_2, liquid O_2 and their mixtures in pool boiling at atmospheric pressure. Int. Jnl. Heat and Mass Transfer, 7, 1097-1116.

57 Class et al, Boiling heat transfer to liquid hydrogen from flat surfaces. Advances in Cryogenic Engineering, 5, 254-261.

58 H.S.Carslaw and J.C.Jaeger, Conduction of heat in solids. Oxford : Clarendon Press 1959.

59 S.H. Cho and J.E.Sunderland, Phase change problems with temperature dependent thermal conductivity. Jnl. Heat Transfer 1974 v96 p214-217.

60 B.A.Boley, An applied overview of moving boundary problems. In, Moving Boundary Problems, Ed. D.G.Wilson et al, Academic Press Inc. 1978.

61 V.J.Lunardini, Heat transfer in cold climates. Van Nostrand Reinhold 1981.

62 N.Shamsundar, Comparison of numerical methods for diffusion problems with moving boundaries. In, Moving Boundary Problems, Ed. D.G.Wilson et al, Academic Press Inc. 1978.

63 G.H.Meyer, The numerical solution of multidimensional Stefan problems - A survey. In, Moving Boundary Problems, Ed. D.G.Wilson et al, Academic Press Inc. 1978.

64 C.Bonacina and G.Comini, On the solution of Nonlinear heat conduction equation by numerical methods. Int. Jnl. Heat and Mass Transfer 1973 v16 p581-589.

65 C.Bonacina, G.Comini, A.Fasano and M.Primicerio, Numerical solution of phase change problems. Int. Jnl. Heat and Mass Transfer 1973 v16 p1825-1832.

66 R.Talwar and A.L.Dilpare, A two dimensional solution to freezing/melting in cylindrical coordinates.
ASME Pap n 77-WA/HT-11 for meeting Nov 27th - Dec 2nd 1977.

67 V.Voller and M.Cross, Accurate solutions of moving boundary problems using the enthalpy method. Int. Jnl. Heat and Mass Transfer 1981 v24 p545-556.

68 N.Shamsundar and E.M.Sparrow, Analysis of multidimensional conduction via the enthalpy model. Jnl. Heat Transfer 1975 p333-340.

69 E.M.Sparrow and W.Chuck, An implicit/explicit numerical solution scheme for phase-change problems. Numerical Heat Transfer 1984 v7 p1-15.

70 R.R.Conte, Elements de Cryogenie. Masson & Co. 1970.

Appendix I

The one-dimensional (radial) steady state heat conduction equation

To derive the steady state heat conduction equation for heat flowing one-dimensionally (radially) through a hollow cylinder, consider any cross section of the cylinder, a section of which is shown below.

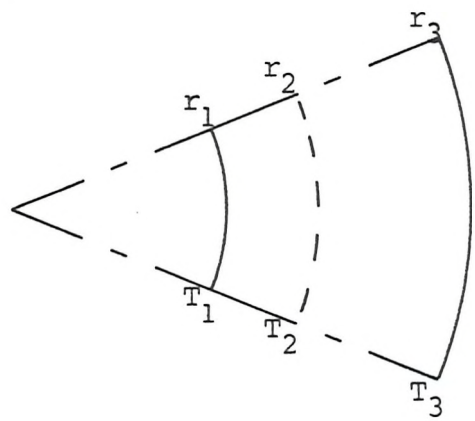

T_1, the temperature of the inner surface (radius r_1), and T_3, the temperature of the outer surface (radius r_3), are known. T_2 is the temperature at some intermediate section r_2.

The radial heat flow Q at all radii is constant

$$Q = -2\pi r.k.\frac{dT}{dr} = \text{constant (c)} \qquad \ldots(I.1)$$

$$dT = \frac{-c}{2\pi k}.\frac{dr}{r} \qquad \ldots(I.2)$$

Integrating equation I.2 between r_3 and r_1 allows the constant c to be determined.

$$T_3 - T_1 = \frac{-c}{2\pi k}.\ln(r_3/r_1) \qquad \ldots(I.3)$$

$$c = \frac{-2\pi k.(T_3-T_1)}{\ln(r_3/r_1)} \qquad \ldots(I.4)$$

Integrating equation I.2 between r_2 and r_1 and substituting equation I.4 for c allows the unknown temperature T_2 to be determined.

$$T_2-T_1 = \frac{2\pi k.(T_3-T_1)}{\ln(r_3/r_1)} \cdot \frac{\ln(r_2/r_1)}{2\pi k} \qquad \ldots(I.5)$$

Rearranging equation I.5 gives :

$$T_2 = T_1 + (T_3-T_1).\frac{\ln(r_2/r_1)}{\ln(r_3/r_1)} \qquad \ldots(I.6)$$

Appendix II

The one-dimensional (radial) steady state heat conduction equation with a temperature dependent thermal conductivity

To investigate the effect of a temperature dependent thermal conductivity on the one-dimensional (radial), steady state, heat conduction equation, consider the thermal conductivity k to be a function of temperature as defined in equation II.1.

$$k = A + B.T \qquad \ldots(II.1)$$

The heat flowrate at any radius is constant (c), so :

$$2\pi r.(A + B.T).\frac{dT}{dr} = c \qquad \ldots(II.2)$$

$$(A + B.T).dT = \frac{c}{2\pi}.\frac{dr}{r} \qquad \ldots(II.3)$$

Integrating equation II.3 between r_3 and r_1 allows the constant c to be determined.

$$A.(T_3-T_1) + (B/2).(T_3^2-T_1^2) = \frac{c}{2\pi}.\ln(r_3/r_1) \qquad \ldots(II.4)$$

$$c = \frac{2\pi.(A.(T_3-T_1) + (B/2).(T_3^2-T_1^2))}{\ln(r_3/r_1)} \qquad \ldots(II.5)$$

Integrating equation II.3 between r_2 and r_1 and substituting equation II.5 for c :

$$A.(T_2-T_1)+(B/2).(T_2^2-T_1^2) = (A.(T_3-T_1)+(B/2).(T_3^2-T_1^2)).\frac{\ln(r_2/r_1)}{\ln(r_3/r_1)}$$

...(II.6)

or,

$$\frac{B}{2}.T_2^2 + A.T_2 - A.T_1+\frac{B}{2}.T_1^2+(A.(T_3-T_1)+\frac{B}{2}.(T_3^2-T_1^2)).\frac{\ln(r_2/r_1)}{\ln(r_3/r_1)} = 0$$

...(II.7)

This is a quadratic equation in T_2 and may be solved accordingly.

Appendix III

Derivation of equations for the one-dimensional finite difference model

A radial segment of the pipe and its contents is shown below. There are three regions, the pipe wall (subscript W), the ice (subscript S) and the water (subscript L).

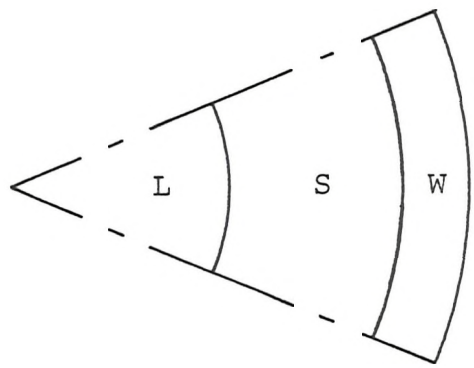

There are three governing equations :

$$\rho C_W \cdot \frac{dT_W}{dt} = k_W \cdot \frac{d^2T_W}{dr^2} + \frac{k_W}{r} \cdot \frac{dT_W}{dr} \qquad \ldots(III.1)$$

$$\rho C_S \cdot \frac{dT_S}{dt} = k_S \cdot \frac{d^2T_S}{dr^2} + \frac{k_S}{r} \cdot \frac{dT_S}{dr} \qquad \ldots(III.2)$$

$$\rho C_L \cdot \frac{dT_L}{dt} = k_L \cdot \frac{d^2T_L}{dr^2} + \frac{k_L}{r} \cdot \frac{dT_L}{dr} \qquad \ldots(III.3)$$

There are four boundary conditions :

$$\left.\frac{dT_W}{dr}\right|_{(r=row)} = f(T_{ow}-T_c) \qquad \ldots(III.4)$$

where $f(T_{ow}-T_c)$ represents the heat flux - temperature curve as obtained from the boiling heat transfer curve for liquid nitrogen.

$$T(r_i) = T_f = 0^oC \qquad \ldots(III.5)$$

$$k_L.\left(\frac{dT_L}{dr}\right)_{r_i} - k_S.\left(\frac{dT_S}{dr}\right)_{r_i} = -\rho L.\frac{dr_i}{dt} \qquad \ldots(III.6)$$

$$\left.\frac{dT_L}{dr}\right|_{r=0} = 0 \qquad \ldots(III.7)$$

Note that no boundary condition is needed for the pipe wall/ice interface since the solution encompasses this boundary.

The following transformations are applied to the governing and boundary conditions, equations III.1 to III.7 :

In the pipe wall, $\psi = \dfrac{r - r_{ow}}{r_{ow}-r_{iw}}$ ...(III.8)

In the ice, $\lambda = \dfrac{r - r_i}{r_{iw}-r_i}$ ...(III.9)

In the water, $\sigma = r/r_i$ ...(III.10)

The derivatives with respect to radius are transformed as follows :

$$\frac{dT_W}{dr} = \frac{\partial\psi}{\partial r}.\frac{\partial T_W}{\partial\psi}$$

$$\frac{dT_W}{dr} = \frac{1}{r_{ow}-r_{iw}} \cdot \frac{\partial T_W}{\partial \psi} \qquad \ldots(III.11)$$

$$\frac{d^2T_W}{dr^2} = \frac{\partial \psi}{\partial r} \cdot \frac{\partial}{\partial \psi}\left(\frac{\partial \psi}{\partial r} \cdot \frac{\partial T_w}{\partial \psi}\right)$$

$$\frac{d^2T_W}{dr^2} = \frac{1}{(r_{ow}-r_{iw})^2} \cdot \frac{\partial^2 T_W}{\partial \psi^2} \qquad \ldots(III.12)$$

Similarly :

$$\frac{dT_S}{dr} = \frac{1}{r_{iw}-r_i} \cdot \frac{\partial T_S}{\partial \lambda} \qquad \ldots(III.13)$$

$$\frac{d^2T_S}{dr^2} = \frac{1}{(r_{iw}-r_i)^2} \cdot \frac{\partial^2 T_S}{\partial \lambda^2} \qquad \ldots(III.14)$$

$$\frac{dT_L}{dr} = \frac{1}{r_i} \cdot \frac{\partial T_L}{\partial \sigma} \qquad \ldots(III.15)$$

$$\frac{d^2T_L}{dr^2} = \frac{1}{r_i^2} \cdot \frac{\partial^2 T_L}{\partial \sigma^2} \qquad \ldots(III.16)$$

The transformation ψ, used for the pipe wall is not a function of time and therefore the differential of T_W with respect to time is not affected by the transformation. The differentials of T_S and T_L must be transformed however, because λ and σ are time dependent functions (since r_i is a function of time).

$$\frac{dT_S}{dt} = \frac{\partial T_S}{\partial t} + \frac{\partial \lambda}{\partial r_i} \cdot \frac{\partial r_i}{\partial t} \cdot \frac{\partial T_S}{\partial \lambda} \qquad \ldots(III.17)$$

Partially differentiating equation III.9 with respect to interface radius, r_i :

$$\frac{\partial \lambda}{\partial r_i} = \frac{(r_{iw}-r_i).(-1) - (r-r_i).(-1)}{(r_{iw}-r_i)2}$$

$$\frac{\partial \lambda}{\partial r_i} = \frac{\lambda - 1}{(r_{iw}-r_i)} \qquad \ldots(III.18)$$

Substituting III.18 into III.17 gives :

$$\frac{dT_S}{dt} = \frac{\partial T_S}{\partial t} + \frac{(\lambda - 1)}{(r_{iw}-r_i)} \cdot \frac{\partial r_i}{\partial t} \cdot \frac{\partial T_S}{\partial \lambda} \qquad \ldots(III.19)$$

Similarly :

$$\frac{dT_L}{dt} = \frac{\partial T_L}{\partial t} - \frac{\sigma}{r_i} \cdot \frac{\partial r_i}{\partial t} \cdot \frac{\partial T_L}{\partial \sigma} \qquad \ldots(III.20)$$

Equations III.11 to III.16, III.19 and III.20 are substituted into equations III.1 to III.7 to give the transformed governing equations and boundary conditions as follows :

In the pipe wall,

$$\rho C_W \cdot \frac{\partial T_W}{\partial t} = \frac{k_W}{(r_{ow}-r_{iw})^2} \cdot \frac{\partial^2 T_W}{\partial \lambda^2} + \frac{k_W}{r.(r_{ow}-r_{iw})} \cdot \frac{\partial T_W}{\partial \psi} \qquad \ldots(III.21)$$

In the ice,

$$\rho C_S \cdot \frac{\partial T_S}{\partial t} + \frac{\rho C_S \cdot (\lambda - 1)}{(r_{iw} - r_i)} \cdot \frac{\partial r_i}{\partial t} \cdot \frac{\partial T_S}{\partial \lambda} = \frac{k_S}{(r_{iw} - r_i)^2} \cdot \frac{\partial^2 T_S}{\partial \lambda^2} + \frac{k_S}{r \cdot (r_{iw} - r_i)} \cdot \frac{\partial T_S}{\partial \lambda} \qquad \ldots(III.22)$$

In the water,

$$\rho C_L \cdot \frac{\partial T_L}{\partial t} - \frac{C_L \cdot \sigma}{r_i} \cdot \frac{\partial r_i}{\partial t} \cdot \frac{\partial T_L}{\partial \sigma} = \frac{k_L}{r_i^2} \cdot \frac{\partial^2 T_L}{\partial \sigma^2} + \frac{k_L}{r \cdot r_i} \cdot \frac{\partial T_L}{\partial \sigma} \qquad \ldots(III.23)$$

On the outside of the pipe wall,

$$\frac{1}{(r_{ow} - r_{iw})} \cdot \frac{\partial T_W}{\partial \psi} = f(T_{ow} - T_c) \qquad \ldots(III.24)$$

At the ice/water interface,

$$\frac{k_L}{r_i} \cdot \frac{\partial T_L}{\partial \sigma} - \frac{k_S}{r_{iw} - r_i} \cdot \frac{\partial T_S}{\partial \lambda} = -\rho L \cdot \frac{\partial r_i}{\partial t} \qquad \ldots(III.25)$$

At the centre of the pipe,

$$\frac{1}{r_i} \cdot \frac{\partial T_L}{\partial \sigma} = 0 \qquad \ldots(III.26)$$

Equations III.21 to III.26 are discretised using finite difference approximations for the differentials. A system of nodes is set up so that there are m+1 evenly spaced nodes each in the ice and the water and n+1 nodes in the pipe wall. The total number of nodes is 2m+n+1 because two of the nodes are on boundaries between the pipe and the ice and the ice and water. Node 1 is at the centre of the pipe, node m+1 is on the ice/water interface, node 2m+1 is on the inside of the pipe wall and 2m+n+1 is on the outside. Note that although the nodes are evenly spaced in the pipe wall, ice and water, the spacing in each will be different from the others.

For $j = 2m+2$ to $2m+n$ (in the pipe wall), discretising equation III.21 leads to :

$$\rho C_W \cdot \frac{(T_j^h - T_j^{h-1})}{\delta t} = \frac{k_W}{(r_{ow}-r_{iw})^2} \cdot \frac{(T_{j+1}^h + T_{j-1}^h - 2.T_j^h)}{\delta\psi^2} + \frac{k_W}{r.(r_{ow}-r_{iw})} \cdot \frac{(T_{j+1}^h - T_{j-1}^h)}{2.\delta\psi}$$

Equating $\delta\psi = 1/n$ and $r = r_{iw}+((j-2m-1)/n).(r_{ow}-r_{iw})$, then collecting terms in T :

$$T_{j-1}^h \cdot \left(\frac{-n^2.k_W}{(r_{ow}-r_{iw})^2} + \frac{n.k_W}{2r_{iw}.(r_{ow}-r_{iw})+2.((j-2m-1)/n).(r_{ow}-r_{iw})^2} \right) +$$

$$T_{j+1}^h \cdot \left(\frac{-n^2.k_W}{(r_{ow}-r_{iw})^2} - \frac{n.k_W}{2r_{iw}.(r_{ow}-r_{iw})+2.((j-2m-1)/n).(r_{ow}-r_{iw})^2} \right) +$$

$$T_j^h \cdot \left(\frac{\rho C_W}{\delta t} + \frac{2n^2.k_W}{(r_{ow}-r_{iw})^2} \right) = T_j^{h-1} \cdot \frac{\rho C_W}{\delta t} \qquad \ldots(III.27)$$

For j = m+2 to 2m (in the ice), discretising equation III.22 gives :

$$\rho C_S \cdot \frac{(T_j^h - T_j^{h-1})}{\delta t} + \frac{\rho C_S \cdot (-1)}{(r_{iw}-r_i)} \cdot \frac{\partial r_i}{\partial t} \cdot \frac{(T_{j+1}^h - T_{j-1}^h)}{2.\delta\lambda} =$$

$$\frac{k_S}{(r_{iw}-r_i)^2} \cdot \frac{(T_{j+1}^h + T_{j-1}^h - 2.T_j^h)}{\delta\lambda^2} + \frac{k_S}{r.(r_{iw}-r_i)} \cdot \frac{(T_{j+1}^h - T_{j-1}^h)}{2.\delta\lambda}$$

Equating $\delta\lambda = 1/m$ and $r = r_i + ((j-m-1)/m).(r_{iw}-r_i)$, then collecting terms in T :

$$T_{j-1}^h \cdot \left(\frac{\rho C_S (2m-j)}{2.(r_{iw}-r_i)} \cdot \frac{\partial r_i}{\partial t} - \frac{m^2 k_S}{(r_{iw}-r_i)^2} + \frac{mk_S}{2r_i.((r_{iw}-r_i)+2.((j-m-1)/n).(r_{iw}-r_i)^2} \right) +$$

$$T_{j+1}^h \cdot \left(\frac{\rho C_S (j-2m)}{2.(r_{iw}-r_i)} \cdot \frac{\partial r_i}{\partial t} - \frac{m^2 k_S}{(r_{iw}-r_i)^2} - \frac{mk_S}{2r_i.((r_{iw}-r_i)+2.((j-m-1)/n).(r_{iw}-r_i)^2} \right) +$$

$$T_j^h \cdot \left(\frac{\rho C_S}{\delta t} + \frac{2m^2 k_S}{(r_{iw}-r_i)^2} \right) = T_j^{h-1} \cdot \frac{\rho C_S}{\delta t} \qquad \ldots(III.28)$$

For j = 2 to m (in the water), discretising equation III.23 gives :

$$\rho C_L \cdot \frac{(T_j^h - T_j^{h-1})}{\delta t} - \frac{\rho C_L \cdot \sigma}{r_i} \cdot \frac{\partial r_i}{\partial t} \cdot \frac{(T_{j+1}^h - T_{j-1}^h)}{2 \cdot \delta\sigma} =$$

$$\frac{k_L}{ri^2} \cdot \frac{(T_{j+1}^h + T_{j-1}^h - 2 \cdot T_j^h)}{\delta\sigma^2} + \frac{mk_L}{r \cdot r_i} \cdot \frac{(T_{j+1}^h - T_{j-1}^h)}{2 \cdot \delta\sigma}$$

Equating $\delta\sigma = 1/m$ and $r = r_i \cdot (j-1)/m$, then collecting terms in T :

$$T_{j-1}^h \cdot \left(\frac{\rho C_L \cdot j}{2r_i} \cdot \frac{\partial r_i}{\partial t} - \frac{m^2 k_L}{r_i^2} + \frac{m^2 k_L}{2i \cdot r_i^2} \right) +$$

$$T_{j+1}^h \cdot \left(\frac{-\rho C_L \cdot j}{2r_i} \cdot \frac{\partial r_i}{\partial t} - \frac{m^2 k_L}{r_i^2} - \frac{m^2 k_L}{2i \cdot r_i^2} \right) +$$

$$T_j^h \cdot \left(\frac{\rho C_L}{\delta t} + \frac{2m^2 k_L}{r_i^2} \right) = T_j^{h-1} \cdot \frac{\rho C_L}{\delta t} \qquad \ldots(III.29)$$

The outer boundary condition (equation III.24) is discretised to give :

$$\frac{n}{(r_{ow} - r_{iw})} \cdot (T_{2m+n+1}^h - T_{2m+n}^h) = f(T_{2m+n+1}^h - T_c) \qquad \ldots(III.30)$$

The temperature of node m+1, at the ice/water boundary, is always 0^oC (equation III.5). Equations III.27 and III.28 include the ice/water interface radius, r_i, and velocity, $\partial r_i/\partial t$. This is determined from the discretised form of equation III.25. Firstly the interface velocity at the last time step (h-1) is calculated from equation III.31 below :

$$\frac{k_L}{r_i}\cdot\frac{(T_{m+1}^{h-1}-T_m^{h-1})}{\delta\sigma} - \frac{k_S}{(r_{iw}-r_i)}\cdot\frac{(T_{m+2}^{h-1}-T_{m+1}^{h-1})}{\delta\lambda} = -\rho L\cdot\left(\frac{\partial r_i}{\partial t}\right)^{h-1}$$

$$\left(\frac{\partial r_i}{\partial t}\right)^{h-1} = T_m^{h-1}\cdot\frac{mk_L}{Lr_i} - T_{m+1}^{h-1}\cdot\left(\frac{mk_L}{Lr_i} + \frac{mk_S}{L(r_{iw}-r_i)}\right) + T_{m+2}^{h-1}\cdot\frac{mk_S}{L(r_{iw}-r_i)}$$

...(III.31)

The interface radius at the intermediate time step h-1/2 is approximated by equation III.32.

$$r_i^{h-1/2} = r_i^{h-1} + \left(\frac{\partial r_i}{\partial t}\right)^{h-1}\cdot\frac{\delta t}{2} \qquad ...(III.32)$$

The interface velocity at the intermediate time step is then calculated from equation III.31, but replacing r_i^h with $r_i^{h+1/2}$. The temperature distribution at step h-1 is still used. The interface position at the unknown time step h is calculated from equation III.33 :

$$r_i^h = r_i^{h-1} + \left(\frac{\partial r_i}{\partial t}\right)^{h-1/2}\cdot\delta t \qquad ...(III.33)$$

The interface radius at time step h, and the velocity at step h-1/2 are used in equations III.27 and III.28.

The boundary condition for the centre of the pipe, equation III.7, is approximated by setting the centre temperature to the temperature of the node adjacent to the centre at the previous time step, i.e.:

$$T_{j=1}^h = T_{j=2}^{h-1} \qquad ...(III.34)$$

The ice/pipewall interface presents a problem. Because there is a discontinuity in the temperature gradient at this point,

which means that the first and second differentials of temperature with respect to radius are undefined, the normal type of finite difference equation, based on a governing equation of the type given in equation III.1, cannot be used in this case. Consider the three nodes 2m, 2m+1 and 2m+2 as shown below. The distance between 2m and 2m+1 (in the ice) is δr_s, and the distance between 2m+1 and 2m+2 (in the pipe wall) is δr_w. A control volume is defined between the nodal midpoints as shown in the figure. The temperature of the node at j=2m+1 is assumed exist across the whole control volume. In any one time step, the sensible heat lost is equal to the difference between heat conducted out and heat conducted into the volume.

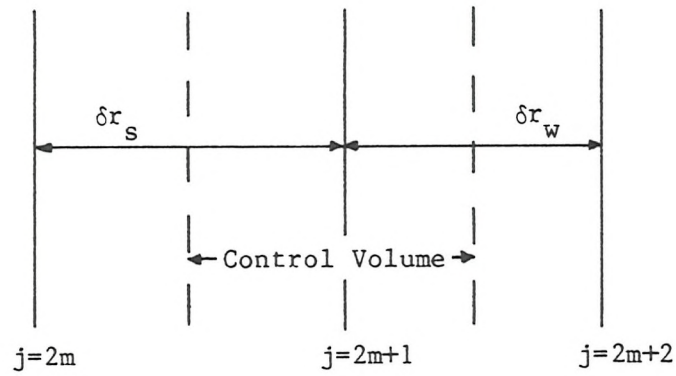

The loss of sensible heat in one time step may be written as :

$$\left(\rho_s C_s \pi.(r_{iw}^2-(r_{iw}-\delta r_s/2)^2) + \rho_w C_w \pi.((r_{iw}+\delta r_w/2)^2-r_{iw}^2)\right) .(T_{2m+1}^{h}-T_{2m+1}^{h-1}) \qquad \ldots(III.35)$$

The heat flow into the volume may be approximated by assuming the temperature gradient on the boundary to be equal to the mean gradient between nodes 2m and 2m+1. So heat flow in to the volume in one time step equals :

$$\left(2\pi.(r_{iw}-\delta r_s/2).k_s.(T^{h}_{2m+1}-T^{h}_{2m})/\delta r_s\right).\delta t \qquad ...(III.36)$$

Similarly heat flow out in one time step equals :

$$\left(2\pi.(r_{iw}+\delta r_w/2).k_w.(T^{h}_{2m+2}-T^{h}_{2m+1})/\delta r_w\right).\delta t \qquad ...(III.37)$$

So, by continuity equations III.35, III.36 and III.37 may be combined to give :

$$\left(\rho_s C_s.(r^2_{iw}-(r_{iw}-\delta r_s/2)^2) + \rho_w C_w.((r_{iw}+\delta r_w/2)^2-r^2_{iw})\right)$$
$$.(T^{h}_{2m+1}-T^{h-1}_{2m+1})/\delta t =$$
$$2\left((r_{iw}-\delta r_s/2).k_s.(T^{h}_{2m+1}-T^{h}_{2m})/\delta r_s -\right.$$
$$\left.(r_{iw}+\delta r_w/2).k_w.(T^{h}_{2m+2}-T^{h}_{2m+1})/\delta r_w\right) \qquad ...(III.38)$$

Collecting terms in T :

$$T^{h}_{2m}.\left(\frac{2.(r_{iw}-\delta r_s/2).k_s}{\delta r_s}\right) +$$
$$T^{h}_{2m+1}.\left(\frac{\rho_s C_s.(r^2_{iw}-(r_{iw}-\delta r_s/2)^2) + \rho_w C_w.((r_{iw}+\delta r_w/2)^2-r^2_{iw})}{\delta t} -\right.$$
$$\left.\frac{2.(r_{iw}-\delta r_s/2).k_s}{\delta r_s} - \frac{2.(r_{iw}+\delta r_w/2).k_w}{\delta r_w}\right) +$$
$$T^{h}_{2m+2}.\left(\frac{2.(r_{iw}+\delta r_w/2).k_w}{\delta r_w}\right) =$$
$$T^{h-1}_{2m+1}.\left(\frac{\rho_s C_s.(r^2_{iw}-(r_{iw}-\delta r_s/2)^2) + {}_w C_w.((r_{iw}+\delta r_w/2)^2-r^2_{iw})}{\delta t}\right)$$
$$...(III.39)$$

Where : $\delta r_s = (r_{iw}-r_i)/m$

and $\delta r_w = (r_{ow}-r_{iw})/n$

For each time step, the computer program uses equations III.31-III.33 to estimate values for the interface position and velocity. Equation III.29 is written with j from 2 to m and these equations, together with the boundary condition equations III.5 and III.34, are used to form an (m-1)x(m-1) tri-diagonal matrix. This is solved by gaussian elimination to obtain the temperature distribution in the water. In a similar manner, equation III.28 is written for j equals m+2 to 2m, equation III.39 and equation III.27 for j equals 2m+2 to 2m+n, together with boundary conditions III.5 and III.30, to form an (m+n-1)x(m+n-1) tri-diagonal matrix that is then solved to obtain the temperature distribution in the ice and pipe wall. The new temperature distribution is used to obtain better estimates of the thermal properties at each node and the ice/water interface position and velocity. The solution is repeated until the new temperature distribution agrees with the previous approximation to $0.1^{o}C$.

The solution outlined above requires that water and ice are present. When there is no ice, ($r_i=r_{iw}$), equations III.28 and III.39 are not valid, and are indeterminate since they involve terms of $1/(r_{iw}-r_i)$. When there is no water, ($r_i=0$), equation III.29, which has terms of $1/r_i$, is invalid. Therefore a different solution is required when ice and water do not exist together.

Consider the situation illustrated below where two regions exist; the pipe wall (subscript W) and the water (subscript L). The governing equations III.1 and III.3, together with boundary conditions given by equations III.4 and III.6, still apply.

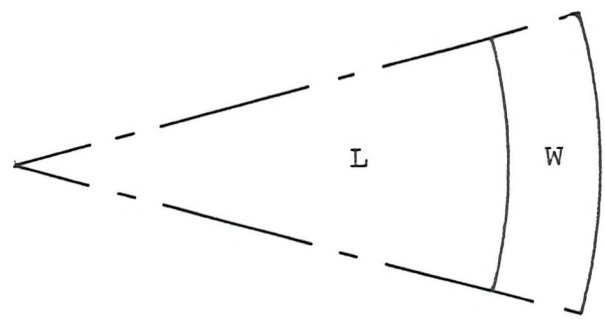

The two regions are divided by m+n+1 nodes, so that node 1 is on the centreline, node m+1 is on the pipe wall to water boundary and node m+n+1 is on the outside of the pipe wall. The nodes are evenly spaced in each of the two regions. No transformations are necessary since there is no moving interface, so the governing equations and boundary conditions may be discretised directly.

In the pipe wall (from equation III.1), for j=2 to m :

$$\rho C_W \cdot \frac{(T_j^h - T_j^{h-1})}{\delta t} = k_W \cdot \frac{(T_{j+1}^h + T_{j-1}^h - 2.T_j^h)}{((r_{ow}-r_{iw})/n)^2} + \frac{k_W}{r} \cdot \frac{(T_{j+1}^h - T_{j-1}^h)}{2.((r_{ow}-r_{iw})/n)}$$

Equating $r = r_{iw}+((j-m-1)/n).(r_{ow}-r_{iw})$, then collecting terms in T:

$$T_{j-1}^h \cdot \left(\frac{-n^2.k_W}{(r_{ow}-r_{iw})^2} + \frac{n.k_W}{2r_{iw}.(r_{ow}-r_{iw})+2.((j-m-1)/n).(r_{ow}-r_{iw})^2} \right) +$$

$$T_{j+1}^h \cdot \left(\frac{-n^2.k_W}{(r_{ow}-r_{iw})^2} - \frac{n.k_W}{2r_{iw}.(r_{ow}-r_{iw})+2.((j-m-1)/n).(r_{ow}-r_{iw})^2} \right) +$$

$$T_j^h \cdot \left(\frac{\rho C_W}{\delta t} + \frac{2n^2.k_W}{(r_{ow}-r_{iw})^2} \right) = T_j^{h-1} \cdot \frac{\rho C_W}{\delta t} \qquad \ldots(III.40)$$

In the water (from equation III.3), for j=2 to m :

$$C_L \cdot \frac{(T_j^h - T_j^{h-1})}{t} = k_L \cdot \frac{(T_{j+1}^h + T_{j-1}^h - 2.T_j^h)}{(r_{iw}/m)^2} + \frac{k_L}{r} \cdot \frac{(T_{j+1}^h - T_{j-1}^h)}{(r_{iw}/m)}$$

Equating $r = r_{iw} \cdot (j-1)/m$, then collecting terms in T :

$$T^{h}_{j-1} \cdot \left(\frac{-m^2 k_L}{r_{iw}^2} + \frac{m^2 k_L}{2j \cdot r_{iw}^2} \right) + T^{h}_{j+1} \cdot \left(\frac{-m^2 k_L}{r_{iw}^2} - \frac{m^2 k_L}{2j \cdot r_{iw}^2} \right) +$$

$$T^{h}_{j} \cdot \left(\frac{\rho C_L}{\delta t} + \frac{2m^2 k_L}{r_{iw}^2} \right) = T^{h-1}_{j} \cdot \frac{\rho C_L}{\delta t} \qquad \ldots(III.41)$$

At the boundary of the pipe wall and the water, a control volume based equation similar to equation III.39 is used :

$$\left(\rho_L C_L \cdot (r_{iw}^2 - (r_{iw} - \delta r_L/2)^2) + \rho_w C_w \cdot ((r_{iw} + \delta r_w/2)^2 - r_{iw}^2) \right)$$

$$\cdot (T^{h}_{2m+1} - T^{h-1}_{2m+1})/\delta t =$$

$$2 \left((r_{iw} - \delta r_L/2) \cdot k_L \cdot (T^{h}_{2m+1} - T^{h}_{2m})/\delta r_L - \right.$$

$$\left. (r_{iw} + \delta r_w/2) \cdot k_w \cdot (T^{h}_{2m+2} - T^{h}_{2m+1})/\delta r_w \right)$$

Collecting terms in T :

$$T_{2m} \cdot \left(\frac{2 \cdot (r_{iw} - \delta r_L/2) \cdot k_L}{\delta r_L} \right) +$$

$$T_{2m+1} \cdot \left(\frac{\rho_L C_L \cdot (r_{iw}^2 - (r_{iw} - \delta r_L/2)^2) + \rho_w C_w \cdot ((r_{iw} + \delta r_w/2)^2 - r_{iw}^2)}{\delta t} - \right.$$

$$\left. \frac{2 \cdot (r_{iw} - \delta r_L/2) \cdot k_L}{\delta r_L} - \frac{2 \cdot (r_{iw} + \delta r_w/2) \cdot k_w}{\delta r_w} \right) +$$

$$T_{2m+2} \cdot \left(\frac{2 \cdot (r_{iw} + \delta r_w/2) \cdot k_w}{\delta r_w} \right) =$$

$$T_{2m+1} \cdot \left(\frac{\rho_L C_L \cdot (r_{iw}^2 - (r_{iw} - \delta r_L/2)^2) + \rho_w C_w \cdot ((r_{iw} + \delta r_w/2)^2 - r_{iw}^2)}{\delta t} \right)$$

$$\ldots(III.42)$$

Where : $\delta r_L = r_i/m$

The boundary condition at the centre of the pipe is still given by equation III.34 and the outer boundary condition is given by equation III.43 below (which is very similar to equation III.30) :

$$\frac{n}{(r_{ow}-r_{iw})}.(T^h_{m+n+1}-T^h_{m+n}) = f(T^h_{m+n+1}-T_c) \qquad ...(III.43)$$

Equations III.40-III.43 are used to obtain the temperature distribution in the water and the pipe wall when no ice is present. The equations to obtain the temperature distribution in the ice and the pipe wall when no water is present, which is an analogous problem, are obtained by replacing subscript L by subscript S in the above equations.

Appendix IV

Derivation of finite difference equations using the control volume approach

In appendix III the finite difference equations III.27, III.28 and III.29 were derived from governing equations (III.1, III.2 and III.3) which related the first and second derivatives of temperature with respect to radius and the first derivative of temperature with respect to time at a point. The purpose of this appendix is to demonstrate that the same equations are forthcoming from a control volume approach. The principle of this method is to balance the net heat flow into or out of the control volume, with its gain or loss of sensible heat in a given time step.

Consider the three nodes j-1, j and j+1 in the water, (the derivation for the ice and pipe wall is very similar), as shown below. A control volume is set up between the nodal midpoints as shown in the diagram. The nodal radii are r_{j-1}, r_j and r_{j+1} and the nodal spacing is δr_L.

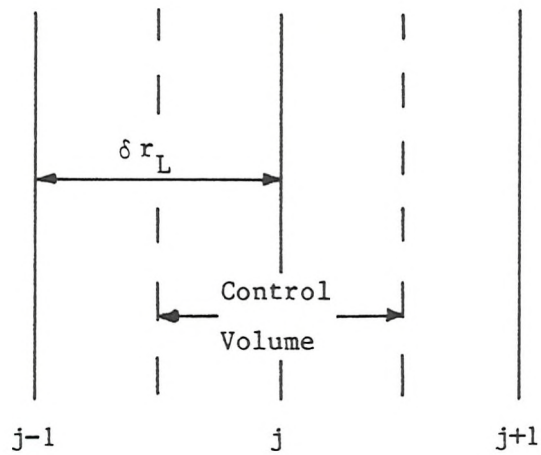

By assuming the temperature gradients on the boundaries of the control volume to be equal to the average temperature gradients

between the central node and its neighbours, the net heat flow out in one time step can be written :

$$\delta t \cdot \left(2\pi (r_j + \delta r_L/2) \cdot k_L \cdot \frac{(T_{j+1} - T_j)}{\delta r_L} - 2\pi (r_j - \delta r_L/2) \cdot k_L \cdot \frac{(T_j - T_{j-1})}{\delta r_L} \right) \quad \ldots(IV.1)$$

The nodal temperature, T_j, is assumed to apply across the whole volume. It should be noted that, because the node j is moving, the fall in nodal temperature ($T_j^h - T_j^{h-1}$) is not equal to the fall in temperature of the control volume. A correction factor must be added to the previous temperature of node j to compensate for its movement across the temperature distribution.

The movement of node j in one time step equals :

$$\frac{r_j}{r_i} \cdot \frac{dr_i}{dt} \cdot \delta t$$

By multiplying the movement of the node by the temperature the temperature correction is obtained. The correction to be added to the previous nodal temperature is therefore :

$$\frac{r_j}{r_i} \cdot \frac{dr_i}{dt} \cdot \frac{dT}{dr} \cdot \delta t$$

or using a finite difference approximation for dT/dr :

$$\frac{r_j}{r_i} \cdot \frac{dr_i}{dt} \cdot \frac{(T_{j+1}^h - T_{j-1}^h)}{2 \cdot \delta r_L} \cdot \delta t$$

So the change in temperature at radius r_j, which is assumed to apply over the whole control volume equals :

$$T_j^h - T_j^{h-1} + \frac{r_j}{r_i} \cdot \frac{dr_i}{dt} \cdot \frac{(T_{j+1}^h - T_{j-1}^h)}{2 \cdot \delta r_L} \cdot \delta t$$

The loss of sensible heat from the control volume in the last time step, δt, may therefore be written :

$$2\pi \cdot r_j \cdot \delta r_L \cdot \rho_L \cdot C_L \cdot \left(T_j^h - T_j^{h-1} - \frac{r_j}{r_i} \cdot \frac{dr_i}{dt} \cdot \frac{(T_{j+1}^h - T_{j-1}^h)}{2 \cdot \delta r_L} \cdot \delta t \right) \quad \ldots(IV.2)$$

The loss of sensible heat (equation IV.2) may be equated with the net heat flow out (equation IV.1) to give :

$$2 \cdot (r_j + \delta r_L/2) \cdot k_L \cdot \frac{(T_{j+1}^h - T_j^h)}{\delta r_L} - 2 \cdot (r_j - \delta r_L/2) \cdot k_L \cdot \frac{(T_j^h - T_{j-1}^h)}{\delta r_L} =$$

$$2 \cdot r_j \cdot \delta r_L \cdot \rho_L \cdot C_L \cdot \left(T_j^h - T_j^{h-1} - \frac{r_j}{r_i} \cdot \frac{dr_i}{dt} \cdot \frac{(T_{j+1}^h - T_{j-1}^h)}{2 \cdot r_L} \cdot \delta t \right) \quad \ldots(IV.3)$$

Collecting terms in T :

$$T_{j-1}^h \cdot \left(\frac{2 \cdot r_j \cdot k_L}{\delta r_L} - k_L - r_j \cdot \rho_L \cdot C_L \cdot \frac{r_j}{r_i} \cdot \frac{dr_i}{dt} \right) +$$

$$T_j^h \cdot \left(\frac{-4 \cdot r_j \cdot k_L}{\delta r_L} - \frac{2 \cdot r_j \cdot \delta r_L \cdot \rho_L \cdot C_L}{\delta t} \right) +$$

$$T_{j+1}^h \cdot \left(\frac{2 \cdot r_j \cdot k_L}{\delta r_L} + k_L + r_j \cdot \rho_L \cdot C_L \cdot \frac{r_j}{r_i} \cdot \frac{dr_i}{dt} \right) = T_j^{h-1} \cdot \left(\frac{2 \cdot r_j \cdot \delta r_L \cdot \rho_L \cdot C_L}{\delta t} \right)$$

$\ldots(IV.4)$

Dividing equation IV.4 by $2.r_j.\ r_L$ throughout gives :

$$T^h_{j-1}.\left(\frac{\rho_L.C_L.r_j}{2.\delta r_L.r_i}.\frac{dr_i}{dt} - \frac{k_L}{\delta r_L^{\,2}} + \frac{k_L}{2.r_j.\delta r_L}\right) +$$

$$T^h_j \ .\left(\frac{\rho_L.C_L}{\delta t} + \frac{2.k_L}{\delta r_L^{\,2}}\right) +$$

$$T^h_{j+1}.\left(\frac{\rho_L.C_L.r_j}{2.\delta r_L.r_i}.\frac{dr_i}{dt} - \frac{k_L}{\delta r_L^{\,2}} - \frac{k_L}{2.r_j.\delta r_L}\right) = T^{h-1}_j \ . \ \frac{L.C_L}{\delta t} \qquad \ldots(IV.5)$$

Now, equating $\delta r_L = r_i/m$ and $r_j = r_i.(j-1)/m$ gives :

$$T^h_{j-1}.\left(\frac{\rho_L.C_L.(j-1)}{2.r_i}.\frac{dr_i}{dt} - \frac{m^2.k_L}{r_i^{\,2}} + \frac{m^2.k_L}{2.(j-1).r_i^{\,2}}\right) +$$

$$T^h_j \ .\left(\frac{\rho_L.C_L}{\delta t} + \frac{2.m^2.k_L}{r_i^{\,2}}\right) +$$

$$T^h_{j+1}.\left(\frac{-\rho_L.C_L.(j-1)}{2.r_i}.\frac{dr_i}{dt} - \frac{m^2.k_L}{r_i^{\,2}} - \frac{m^2.k_L}{2.(j-1).r_i^{\,2}}\right) =$$

$$T^{h-1}_j.\frac{\rho_L.C_L}{\delta t} \qquad \ldots(IV.6)$$

Comparison of equation IV.6 with equation III.29 will show that the same equation has been derived using the control volume approach as was obtained using the differentials at a point governing equation. A similar analysis could be done to demonstrate that the

equations for ice and pipe wall can also be derived from consideration of the heat balance in control volumes. In fact, in the program, the equation for the inner pipe wall node is derived from a control volume method because the differentials of temperature with respect to radius are undefined at this point.

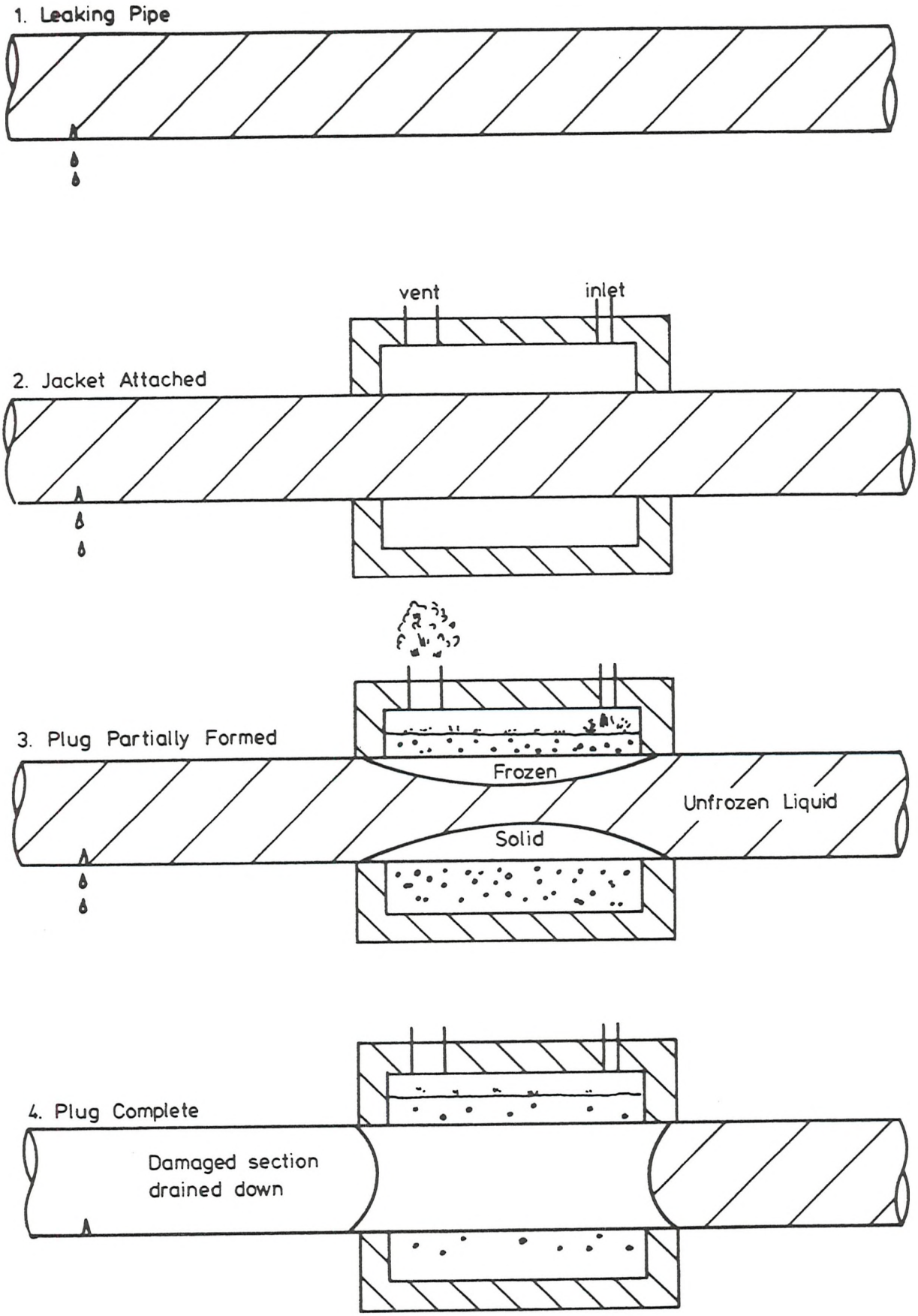

Fig. 1.1 The Pipe Freezing Technique

1. Split Tee welded in place

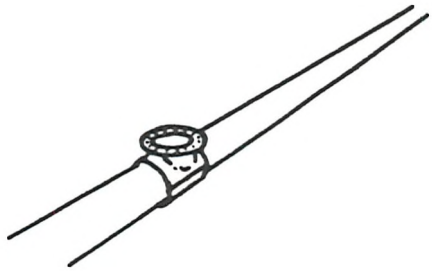

2. Sandwich valve and Tapping machine attached, Pipeline is Tapped.

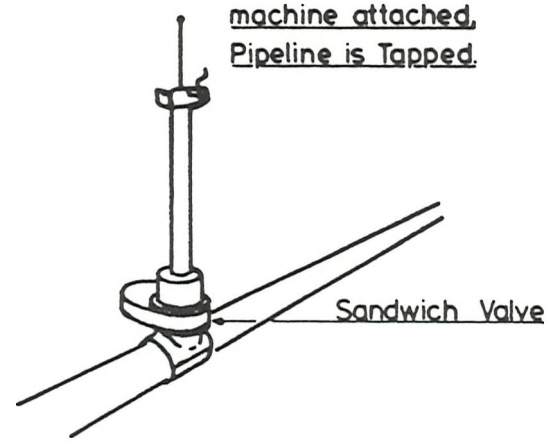

3. Stopple Plugging machine attached

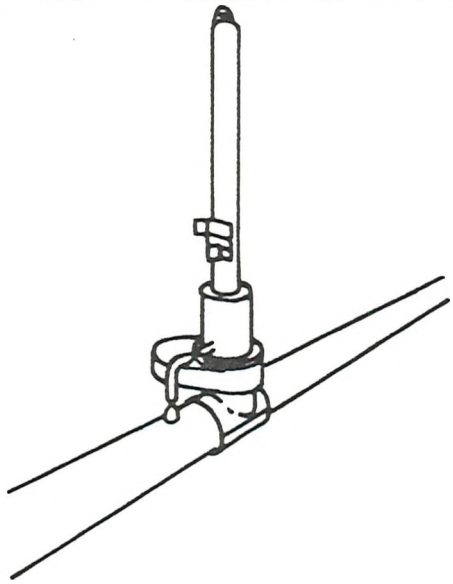

4. Plugging Head lowered into pipe

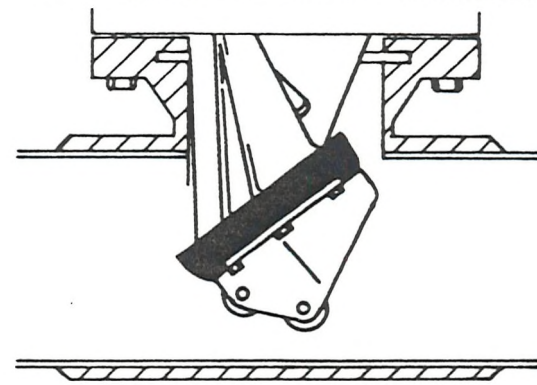

5. Plugging Head in place

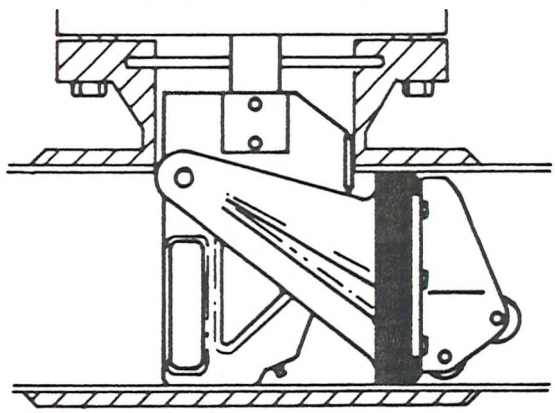

6. Completion Flange Plug inserted

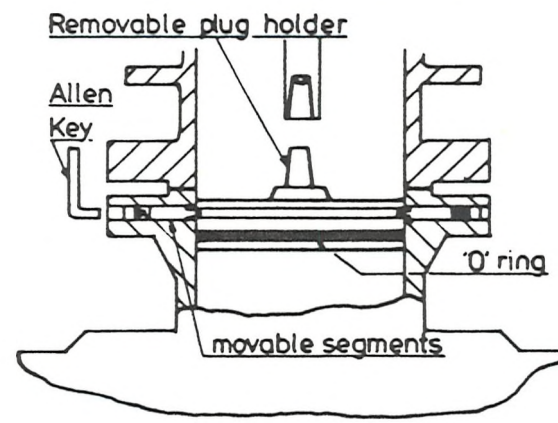

Fig. 1.2 The 'Hot' Tapping Technique

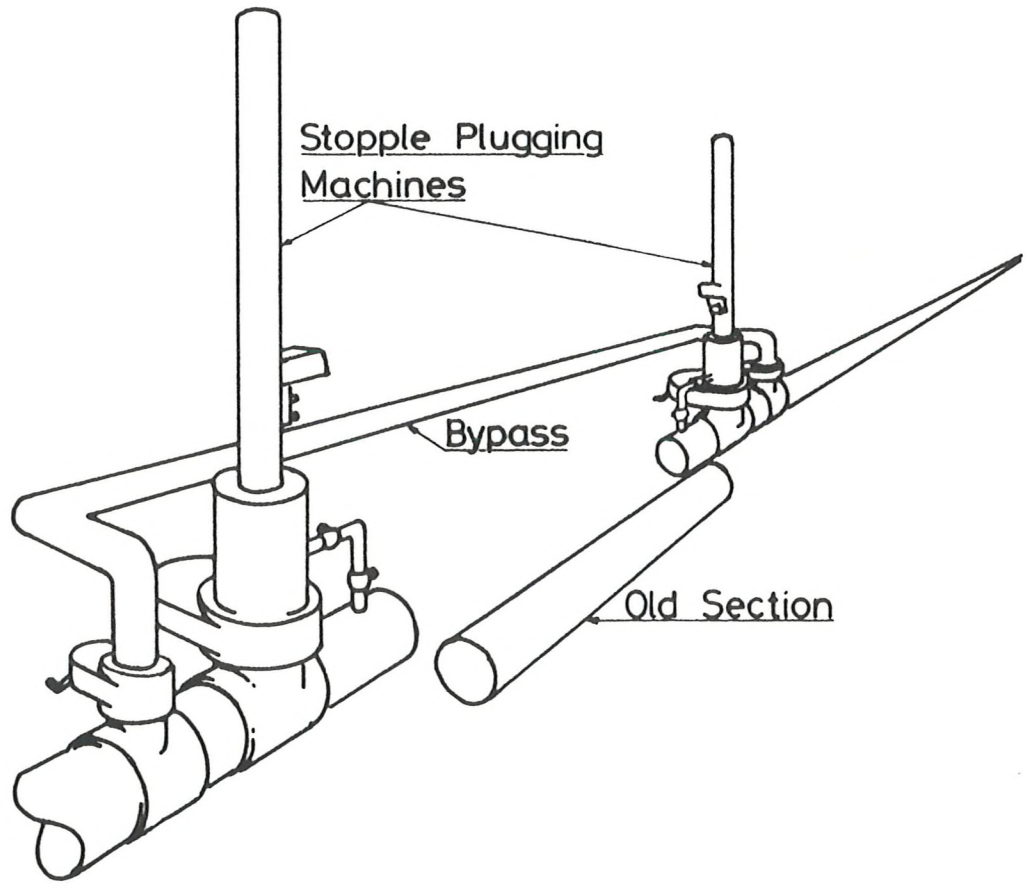

Plugging and Bypass Setup

Fig. 1.3

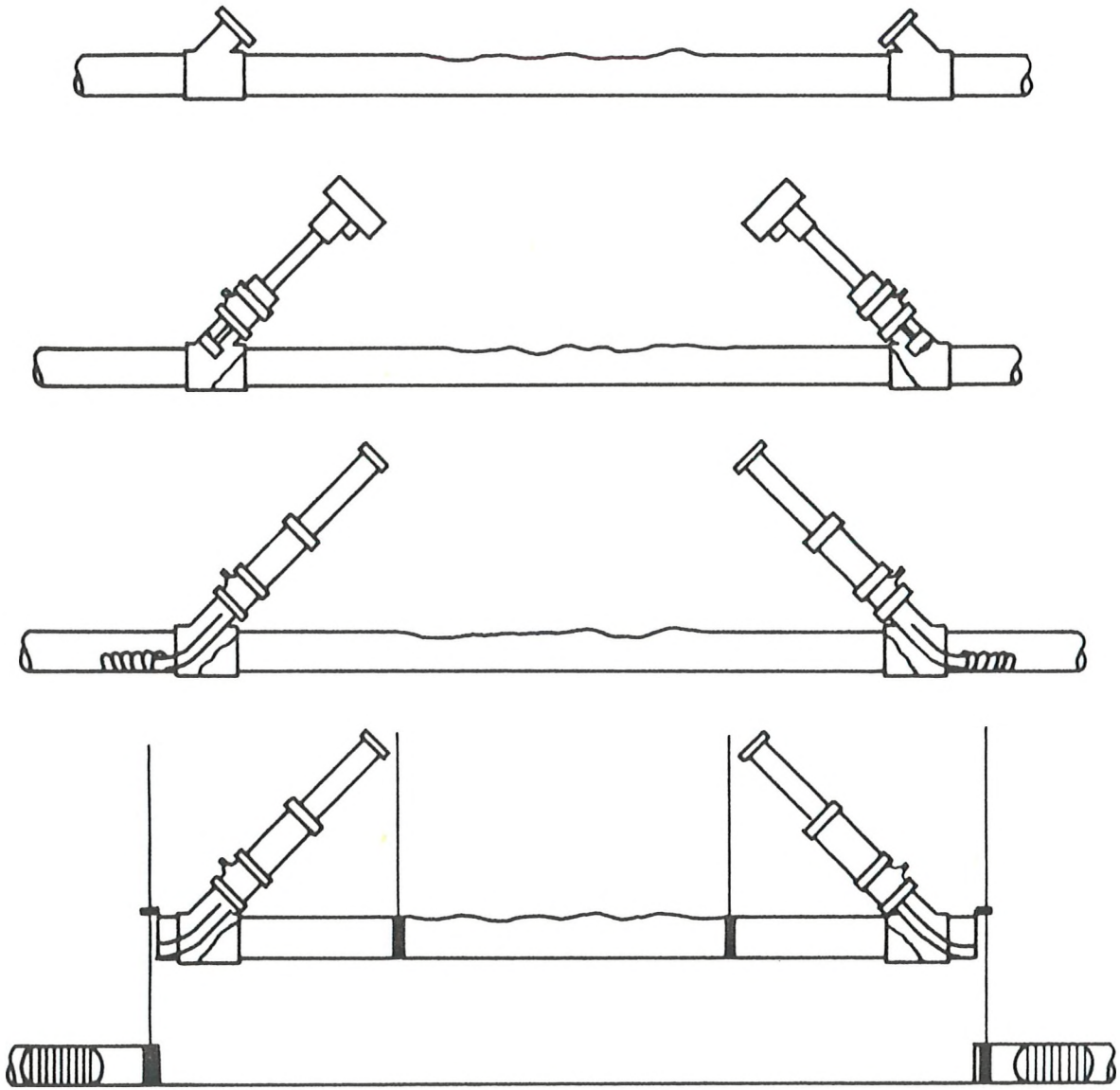

1. Flow stopped and pressure reduced to ambient.
   Split Tees clamped to pipe.

2. Sandwich valves and tapping machines attached.
   Pipe Tapped.

3. Plug launchers attached.
   Deflated plugs inserted into pipe.

4. Plugs inflated.
   Damaged section cut and raised.
   New section welded in.

Fig. 1.4 The 'Cold' Tapping Technique

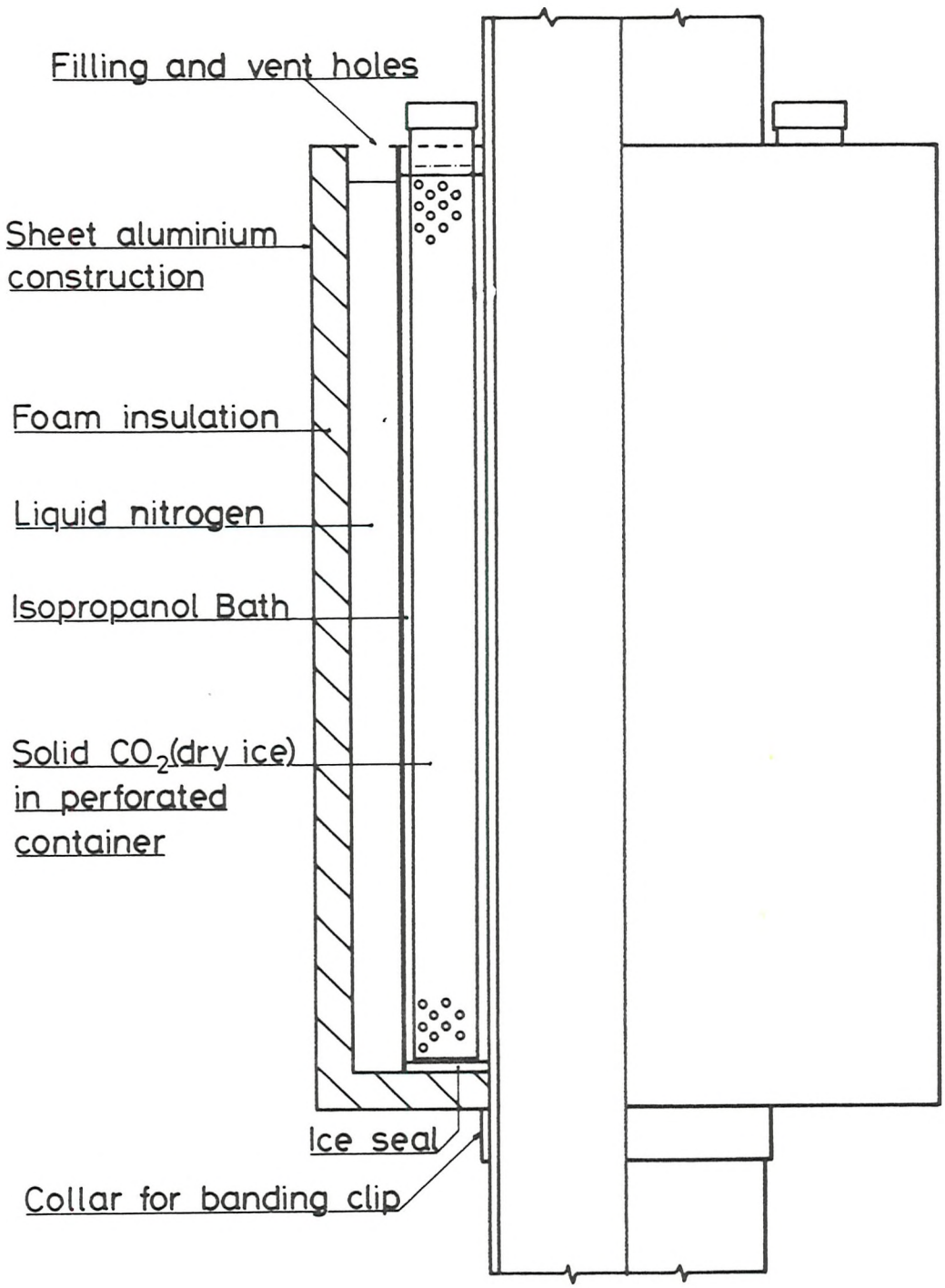

Controled Temperature Jacket for Vertical Pipes

Fig. 1.5

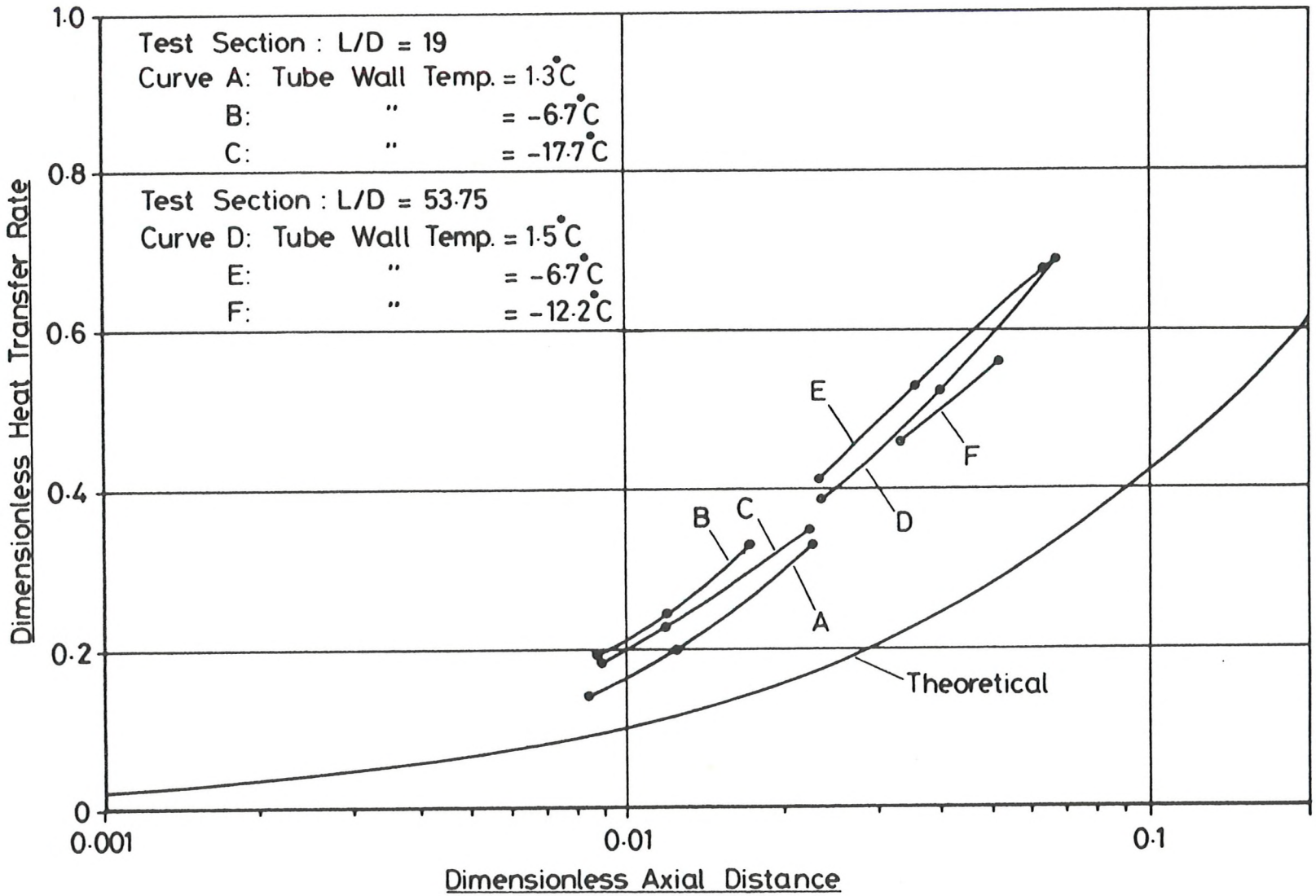
Test Section : L/D = 19
Curve A: Tube Wall Temp. = 1·3°C
B: " = -6·7°C
C: " = -17·7°C
Test Section : L/D = 53·75
Curve D: Tube Wall Temp. = 1·5°C
E: " = -6·7°C
F: " = -12·2°C
Dimensionless Heat Transfer Rate
1·0
0·8
0·6
0·4
0·2
0
0·001
0·01
0·1
Dimensionless Axial Distance
A
B
C
D
E
F
Theoretical

Fig. 1.6 [22]

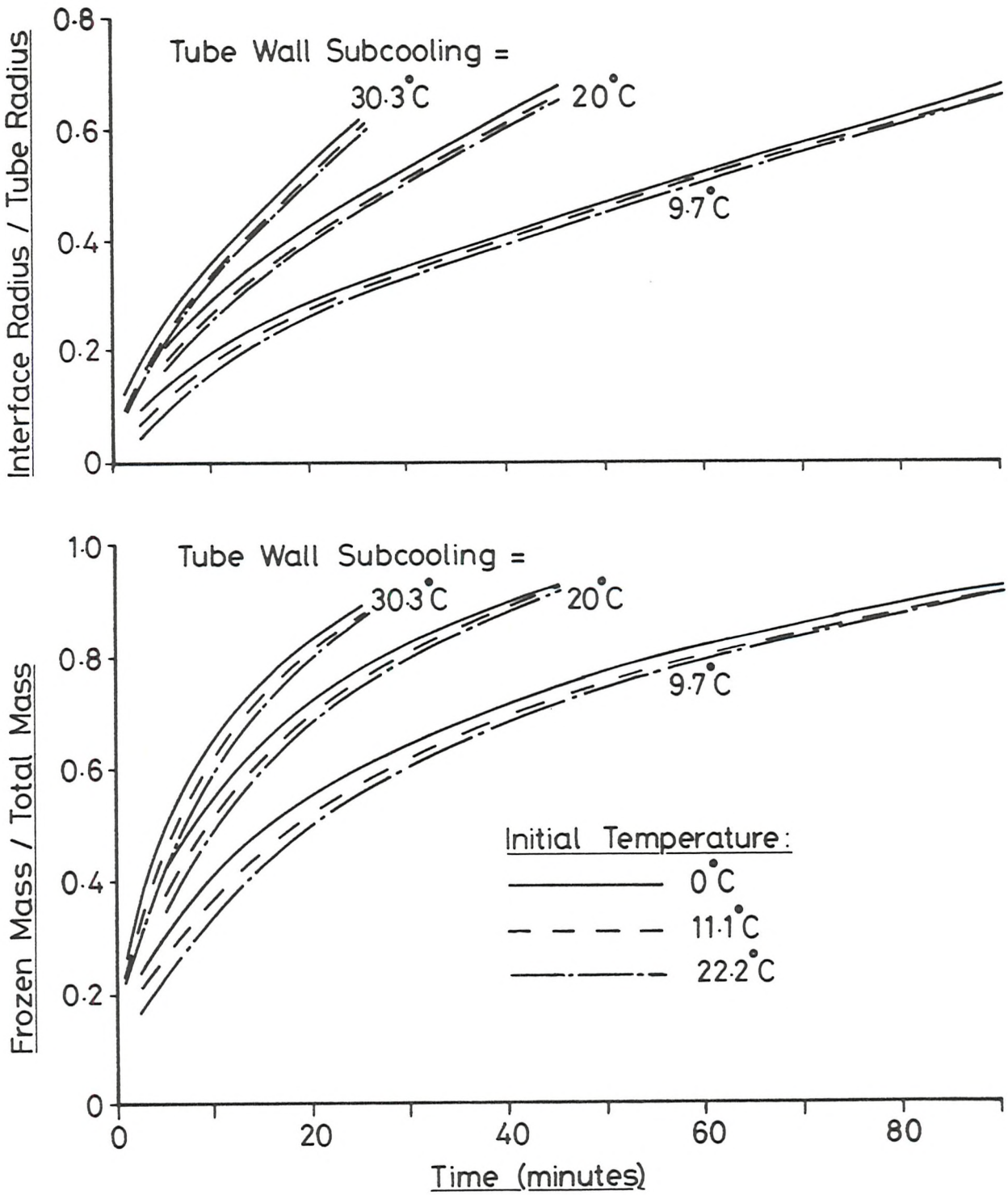

Fig. 1.7 Freezing of n-eicosane paraffin [27]

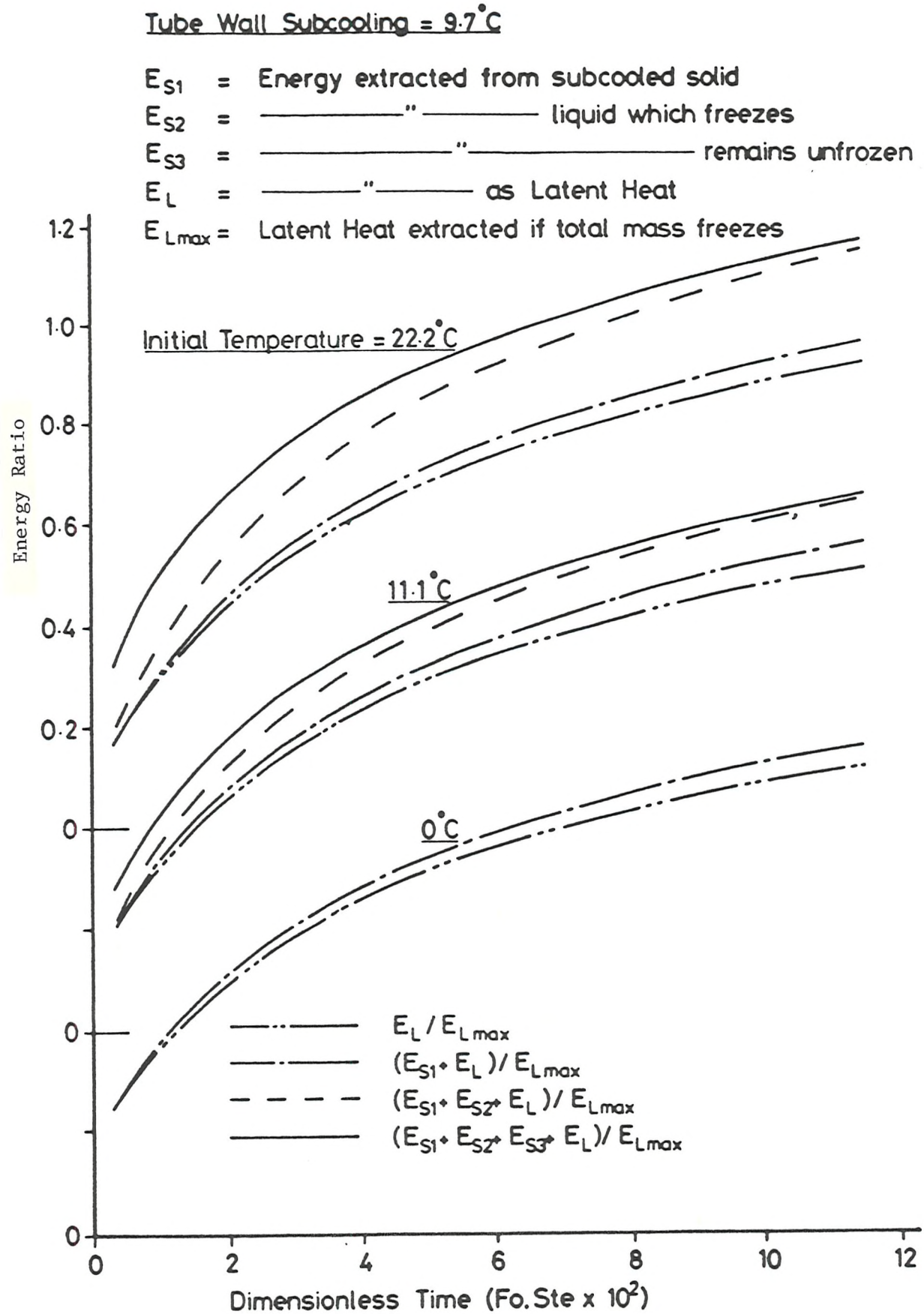

Fig. 1.8 Energy extracted during freezing of n-eicosane paraffin

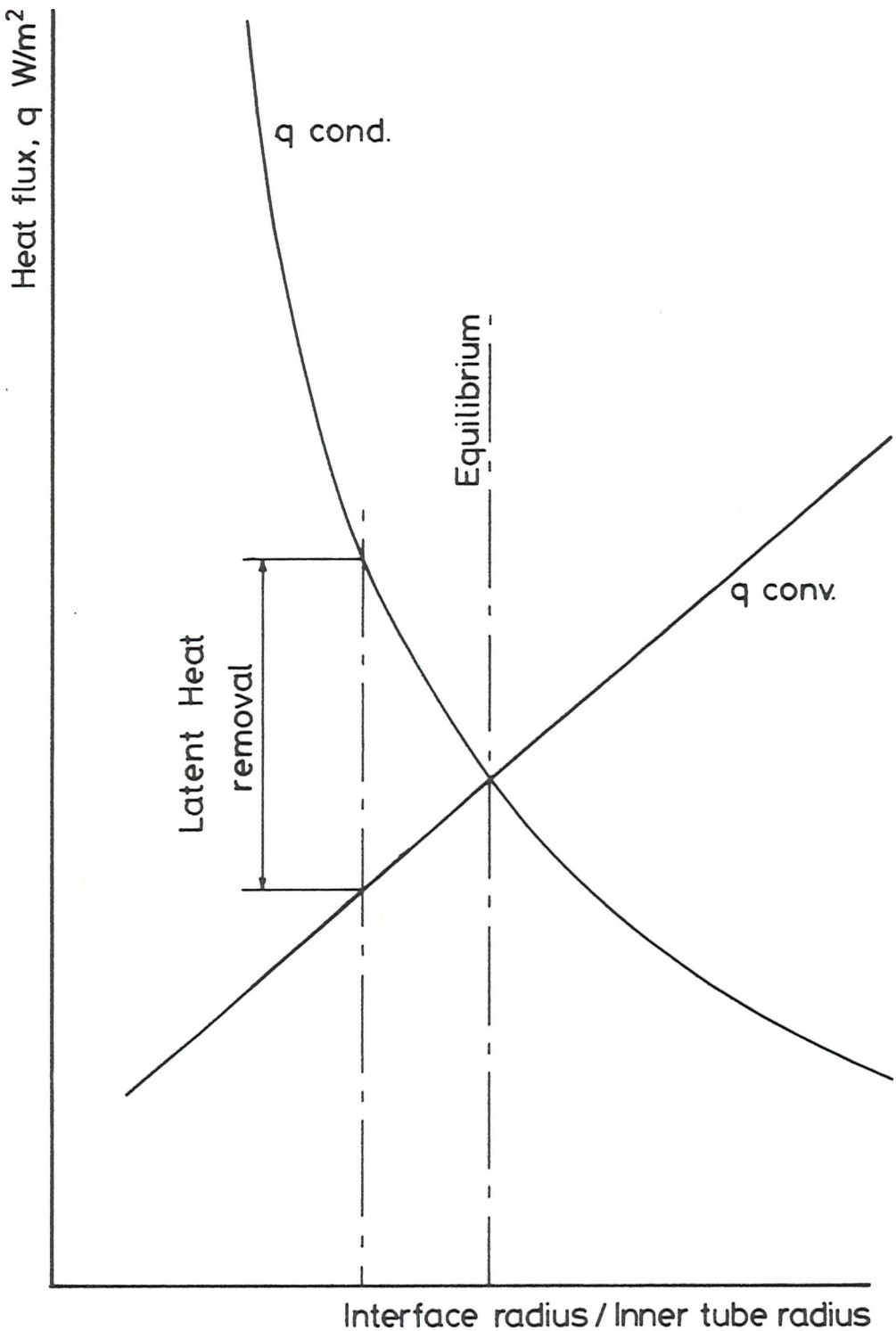

Fig. 1.9 Conduction and convection heat fluxes as a function of solid layer thickness

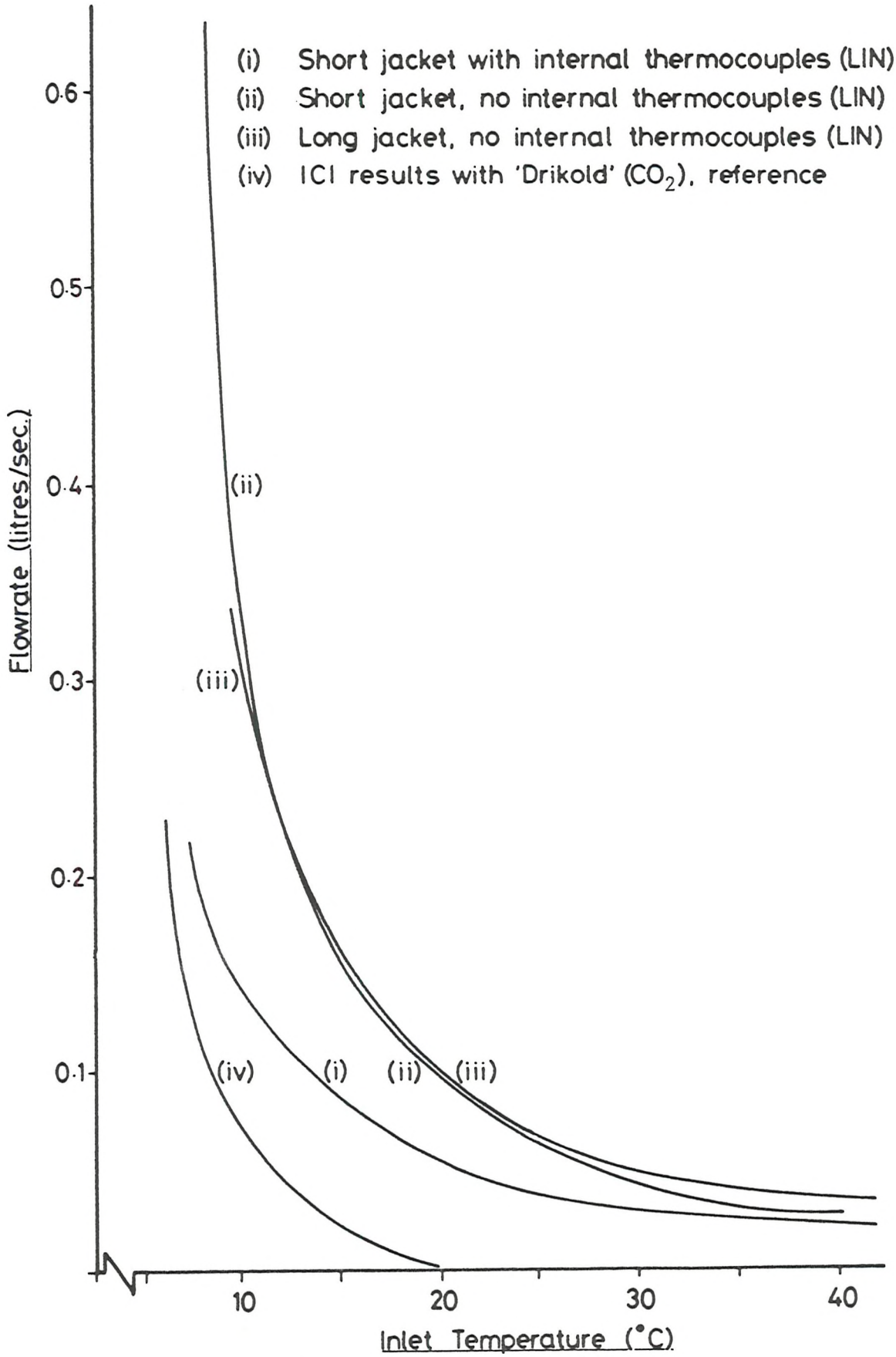

Fig. 2.1 Freeze/No Freeze boundaries for a 50 mm diameter mild steel pipe

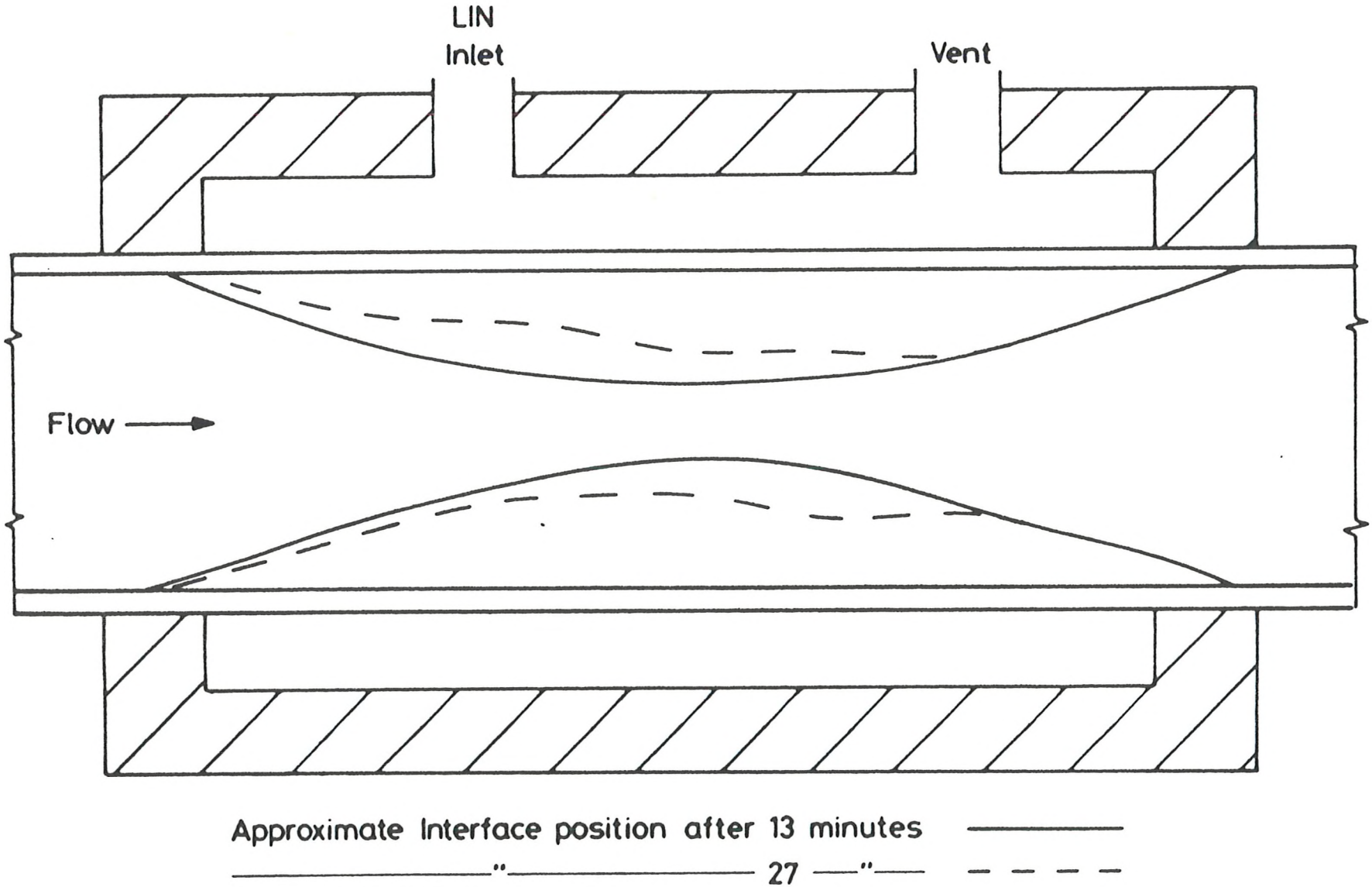

Fig. 2.2 Ice front retreat during flow freezing a 100 mm diameter horizontal pipe

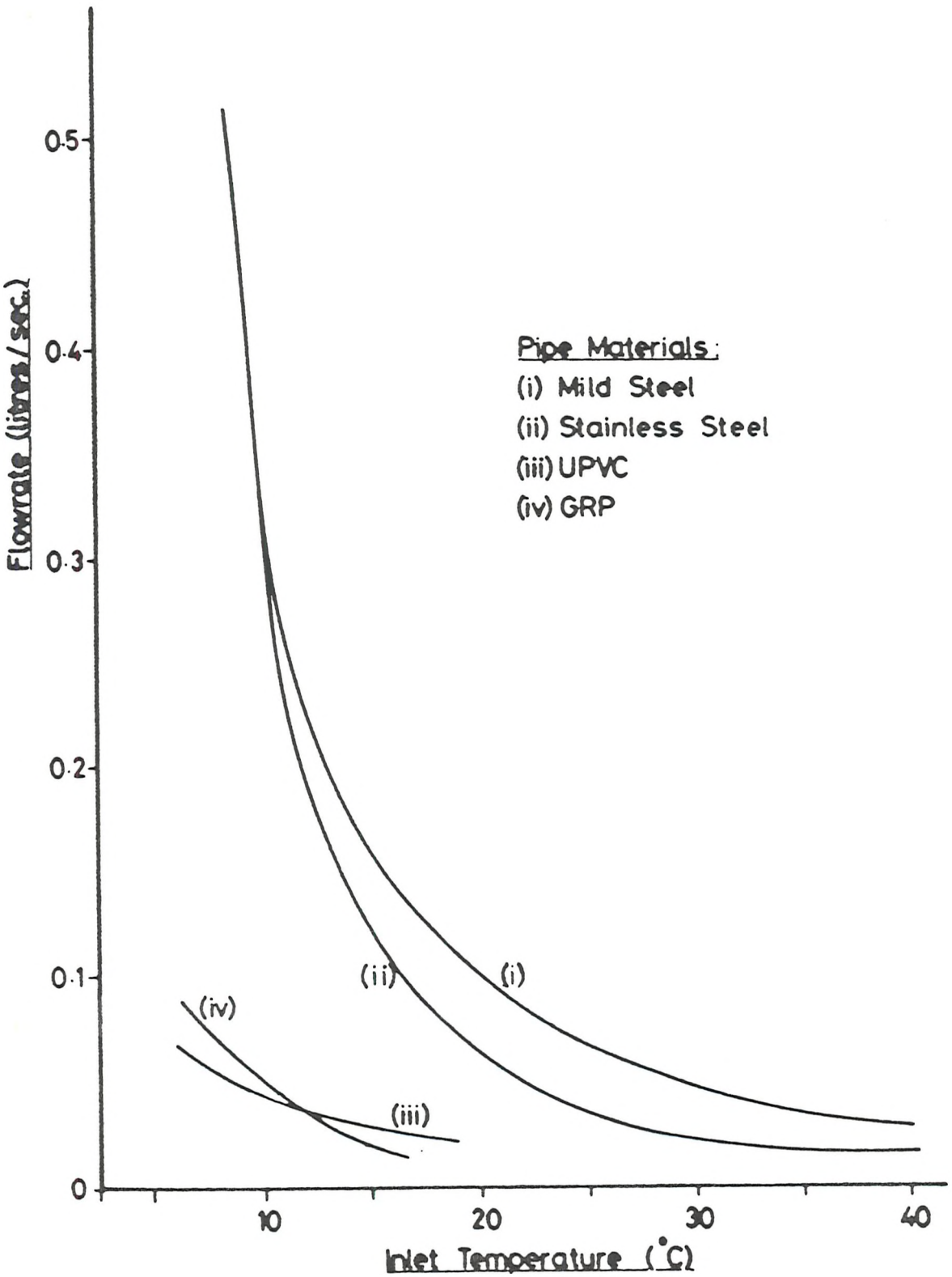

Fig. 2.3 Freeze/No Freeze boundaries for 50 mm diameter pipes of various materials

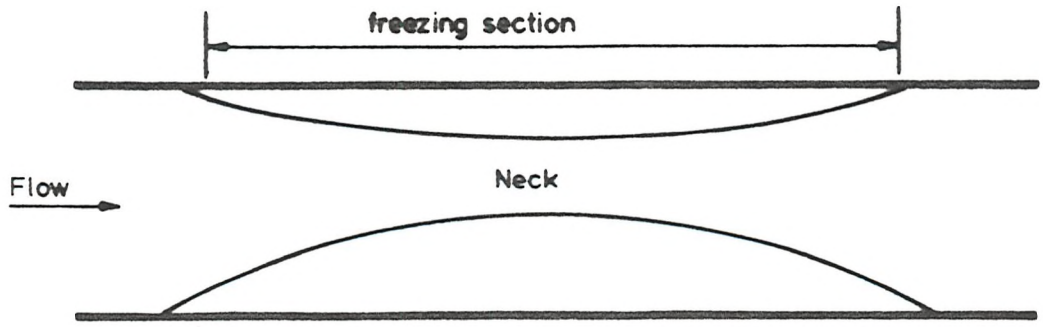

plug forms uniformly within freezing section

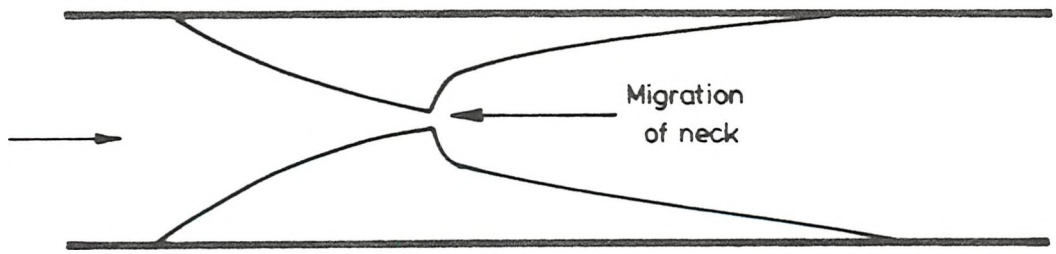

at critical neck size, neck starts to migrate;
rapid melting occurs downstream.

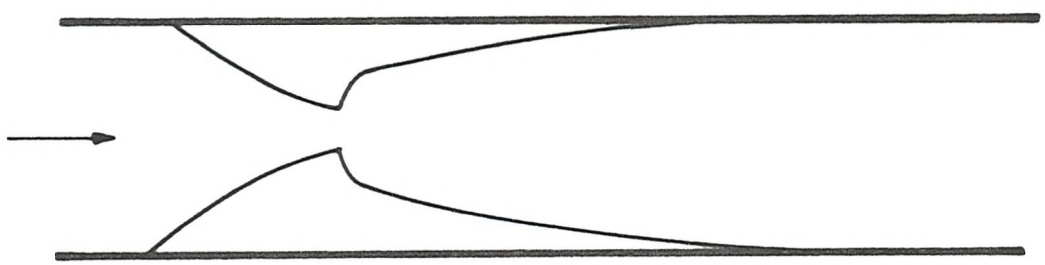

neck widens as migration continues.

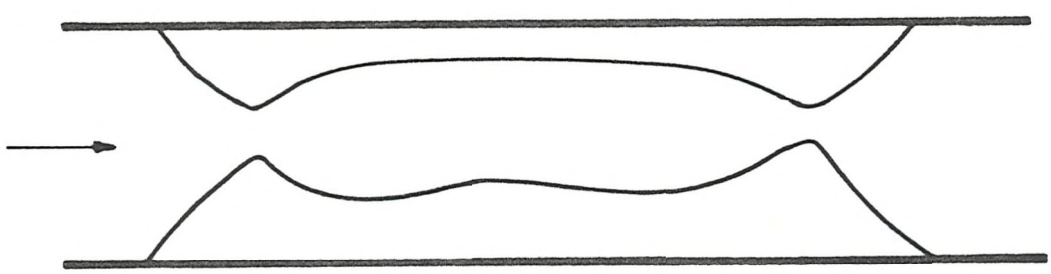

migration ceases at certain neck size; secondary
neck may form at high flowrates.

Fig. 2.4 Neck migration during an unsuccessful flow freeze

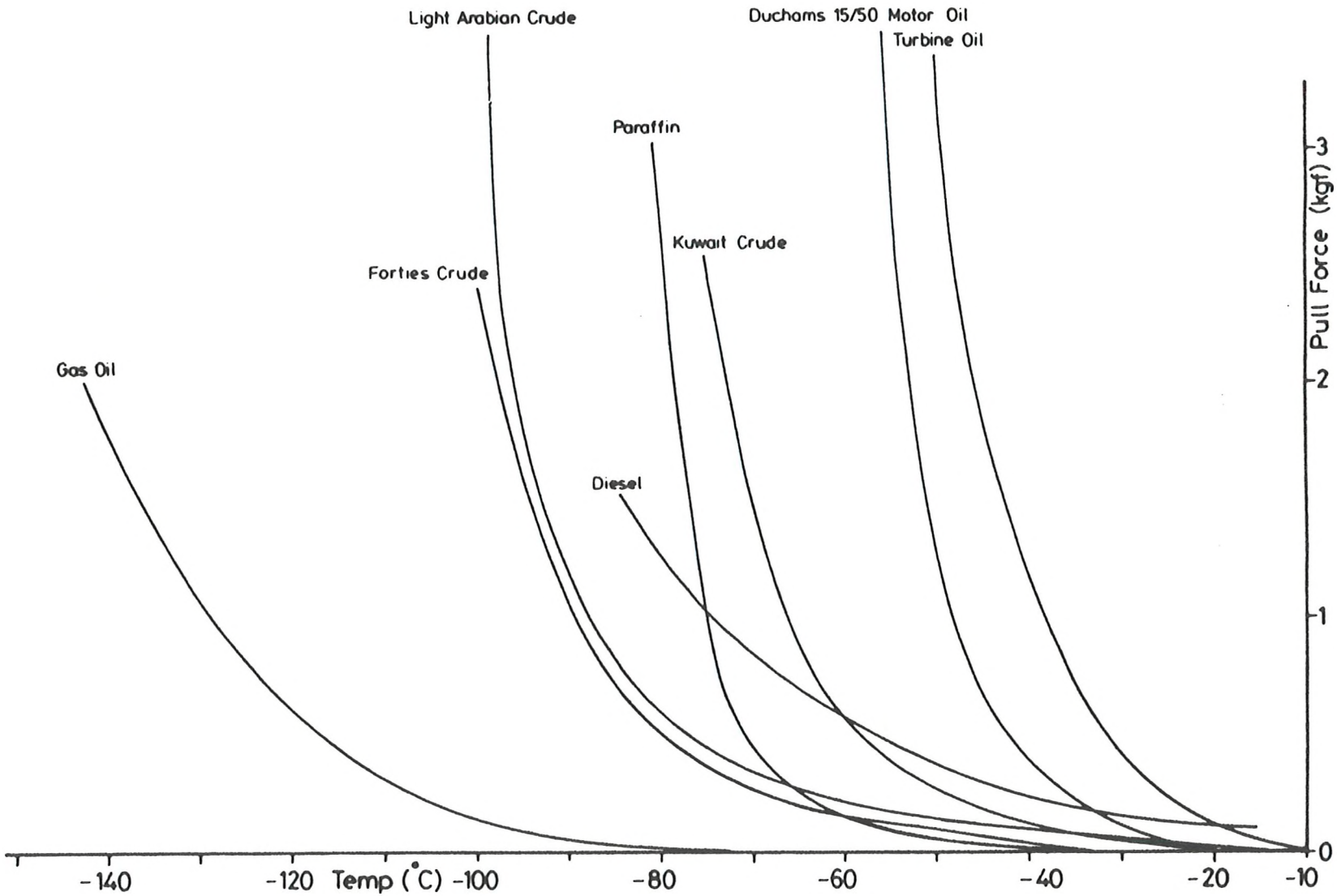

Fig. 2.5 Pull force v Temperature curves for various hydrocarbons

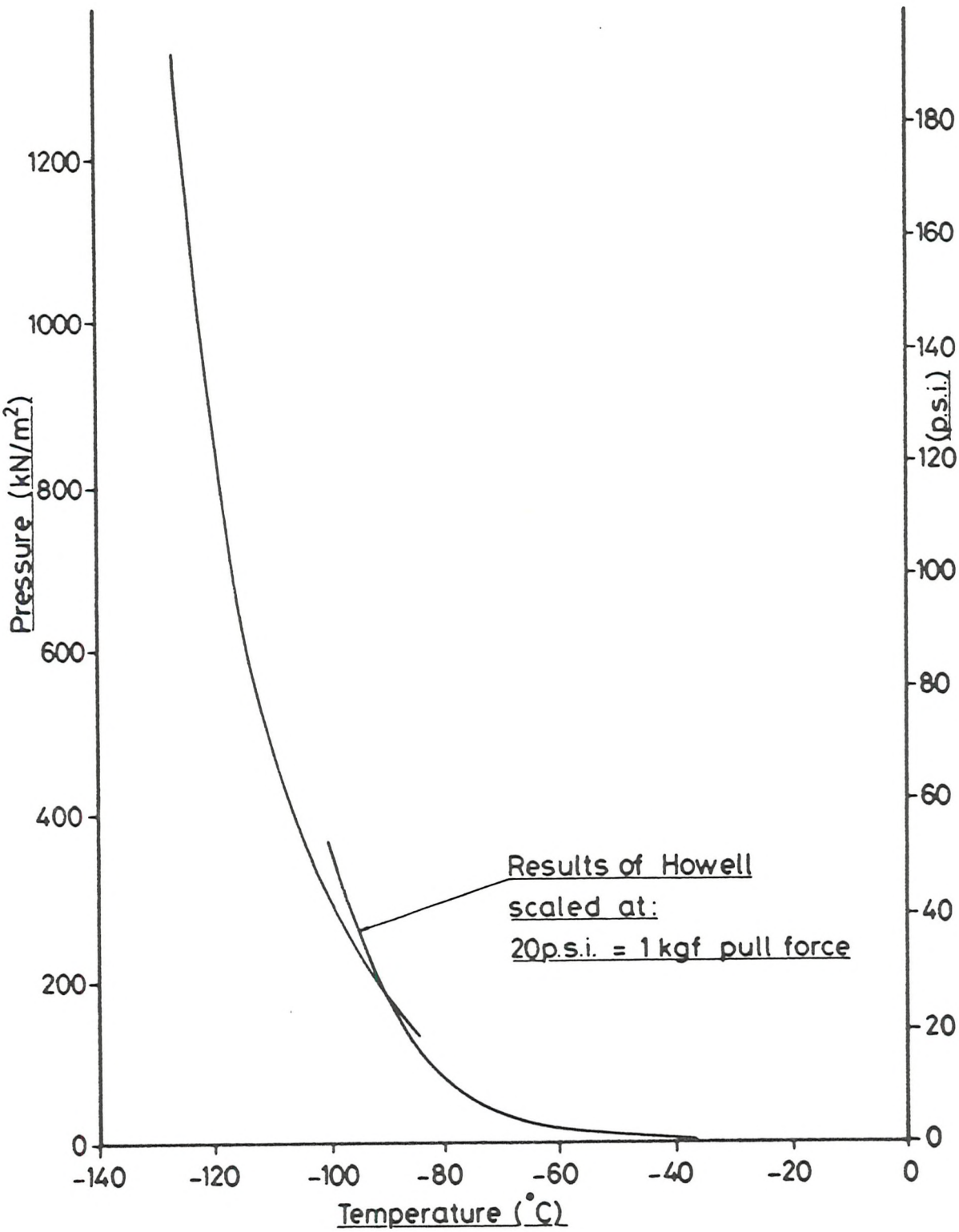

Fig. 2.6 Pressure test results of a 25 mm diameter Forties Crude plug

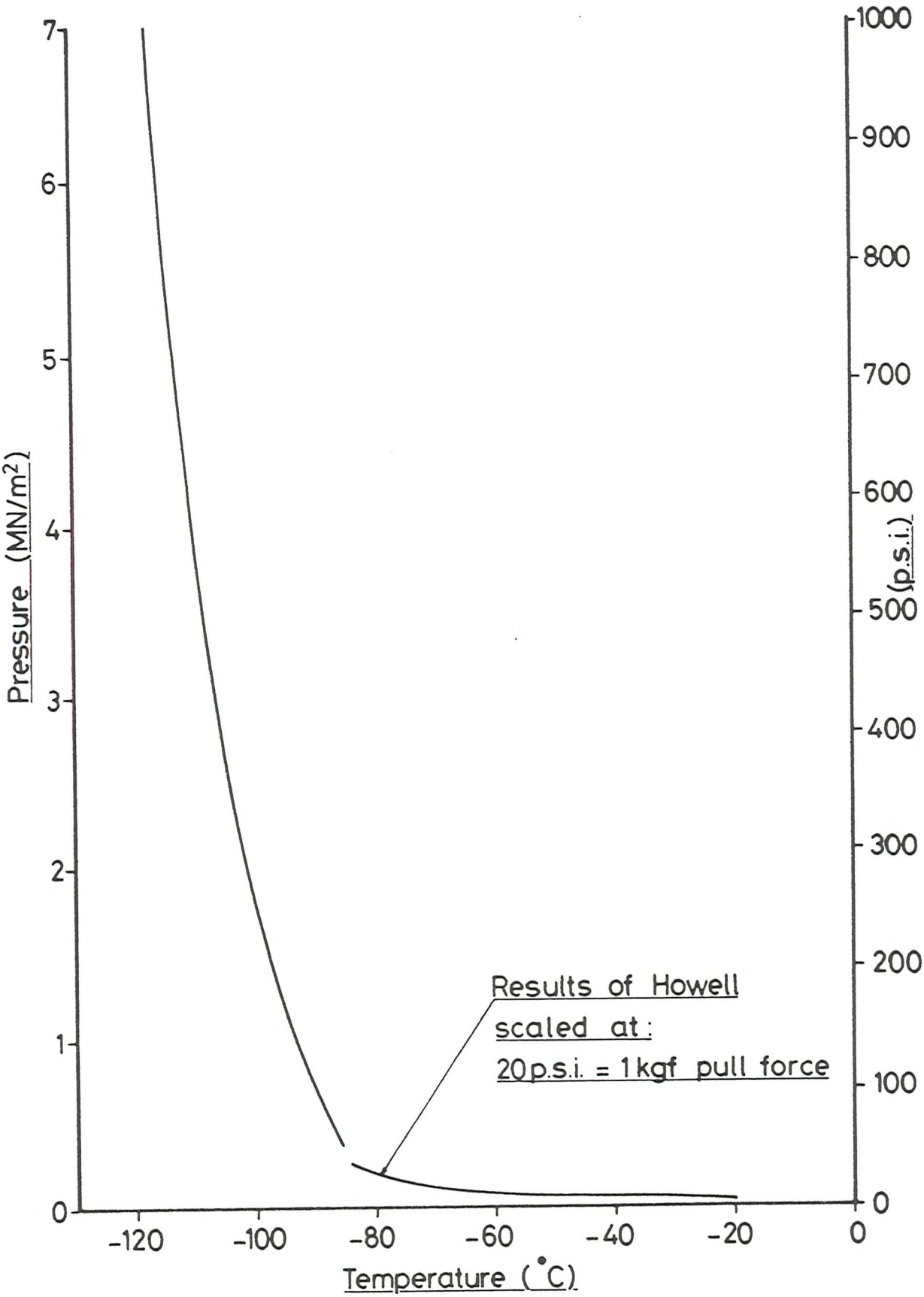

Fig. 2.7 Pressure test results of a 25 mm diameter Diesel plug

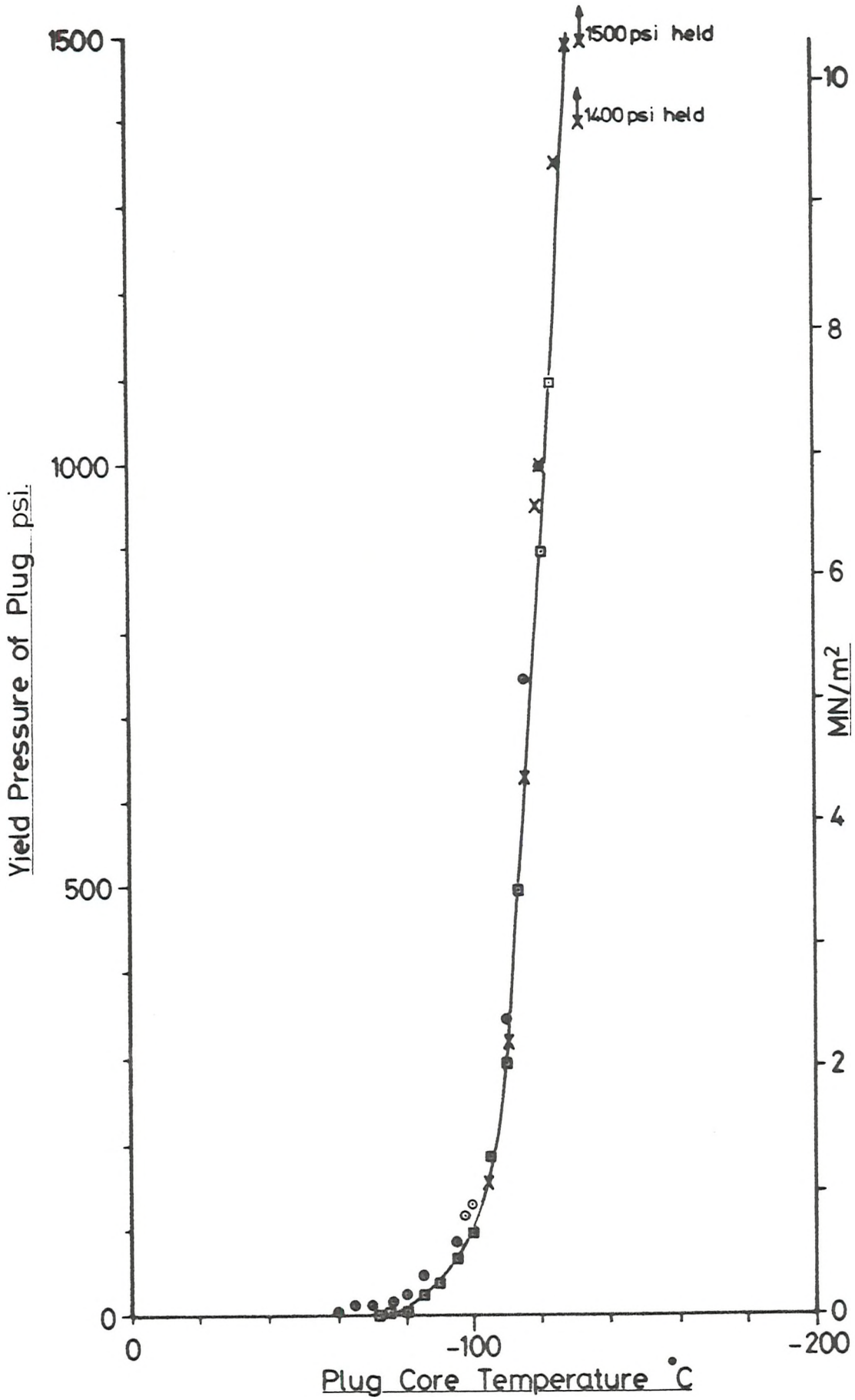

Fig. 2.8 Pressure holding capability v Plug core temperature for Statfjord crude oil

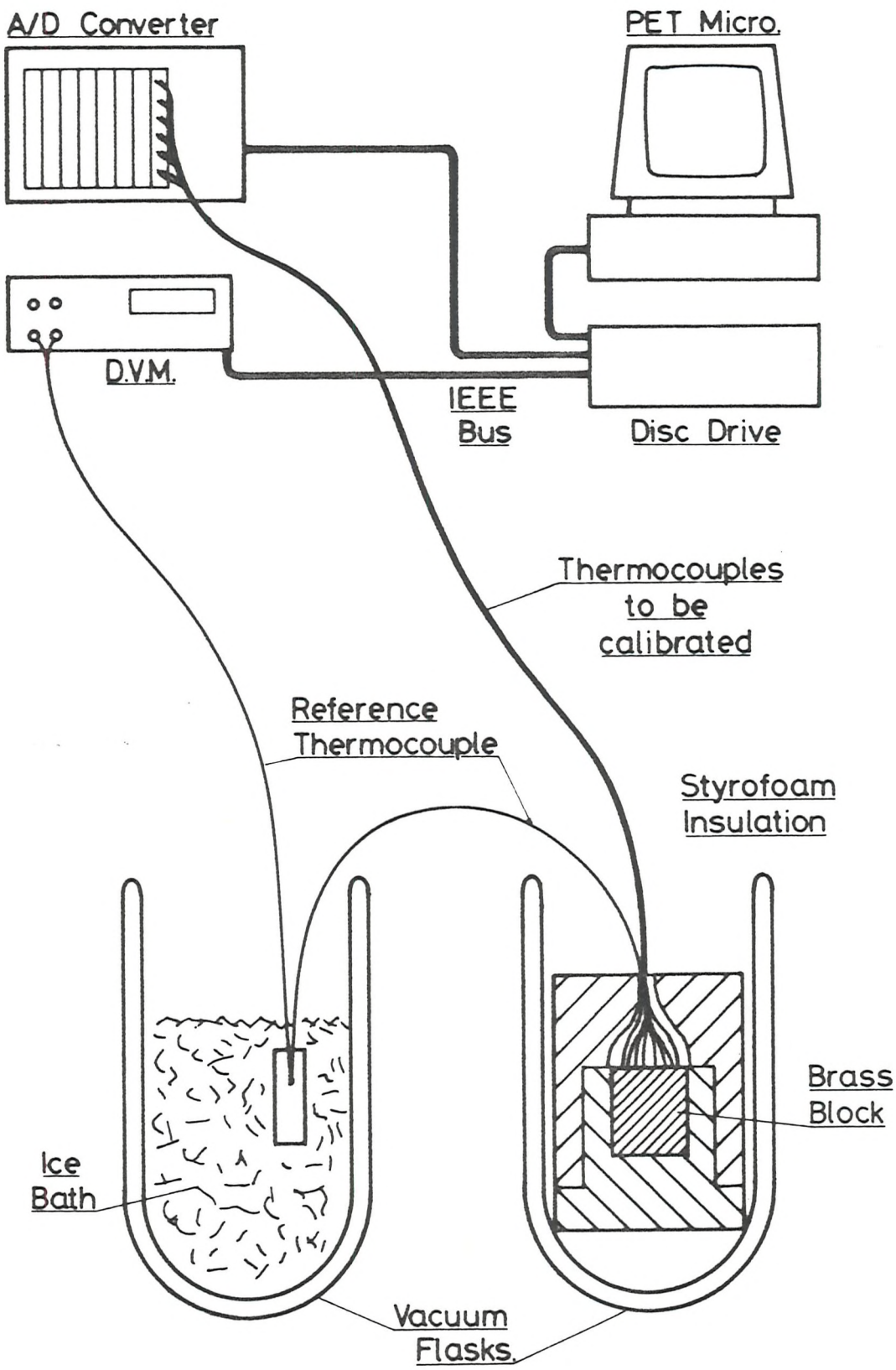

Fig. 3.1 Experimental setup for thermocouple calibration

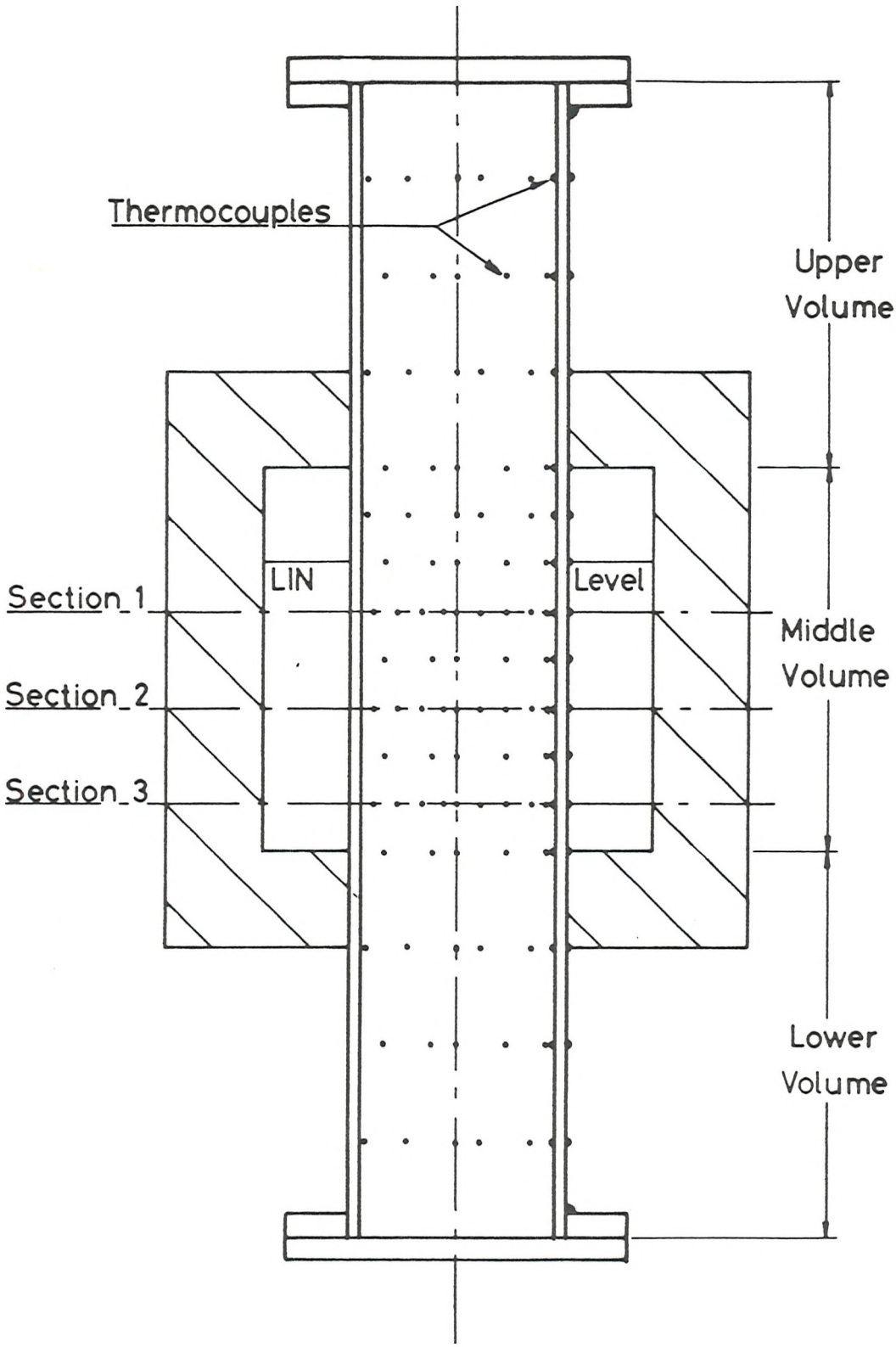

Fig. 4.1 General Arrangement of the 100 mm diameter vertical rig

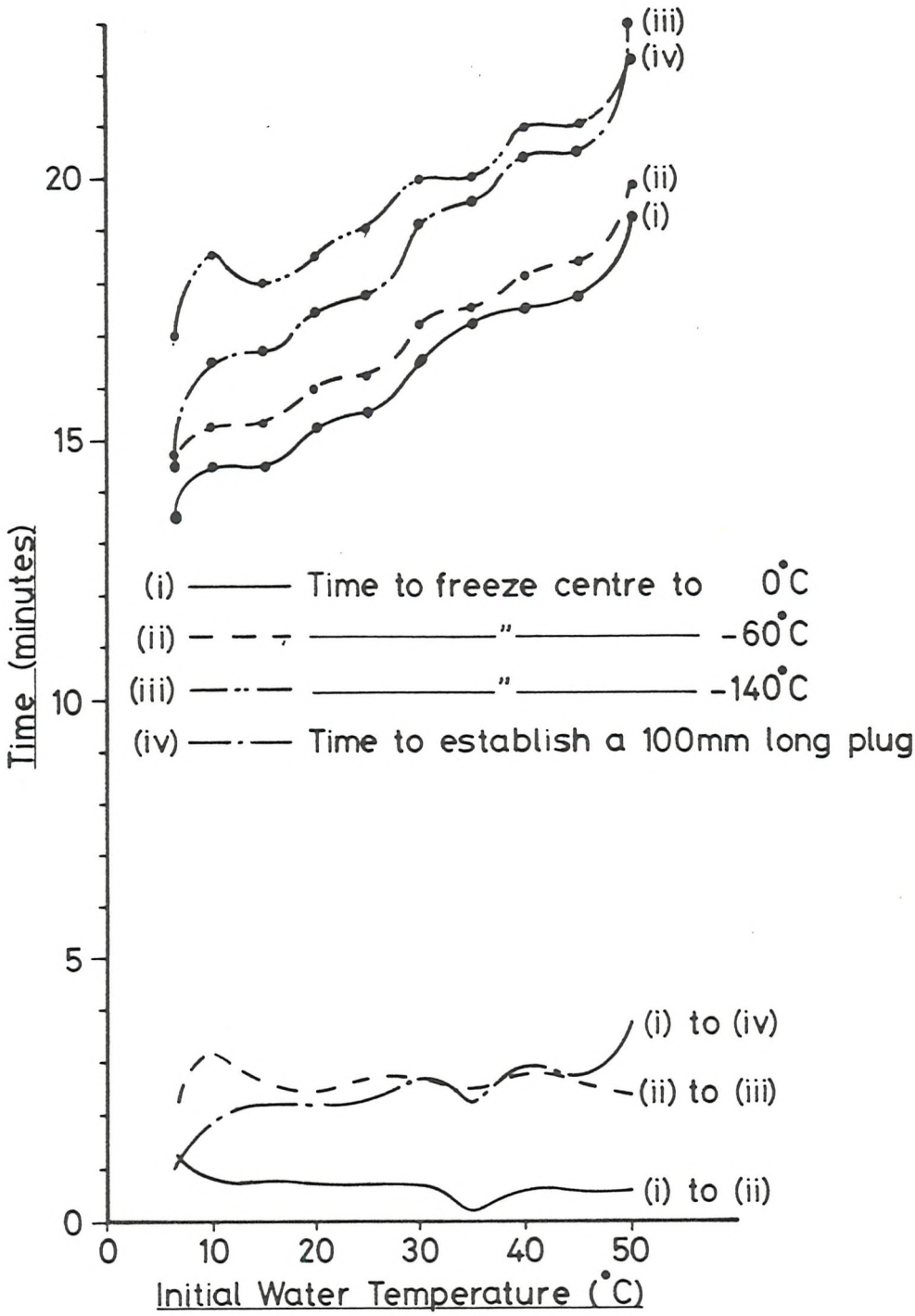

Fig. 4.2 Times to freeze for 100 mm diameter vertical rig without tank

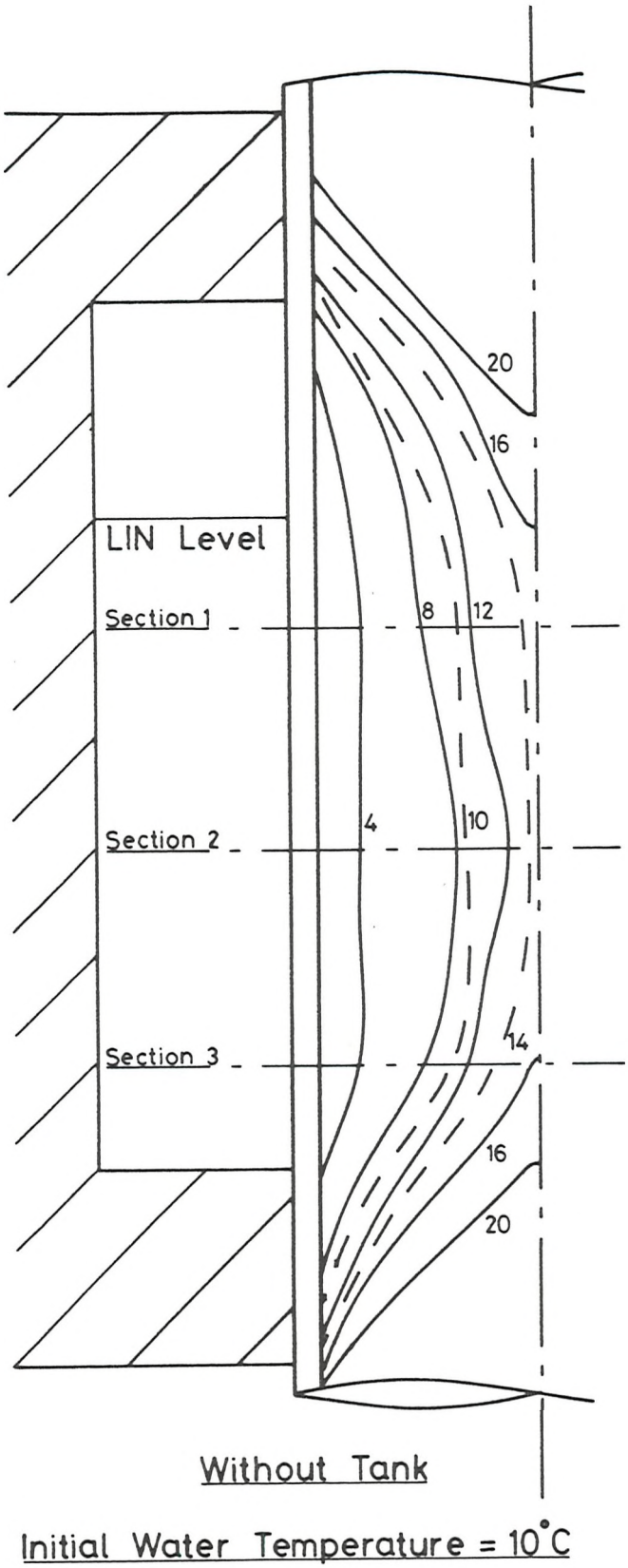

Fig. 4.3 Interface positions in 100 mm diameter vertical rig

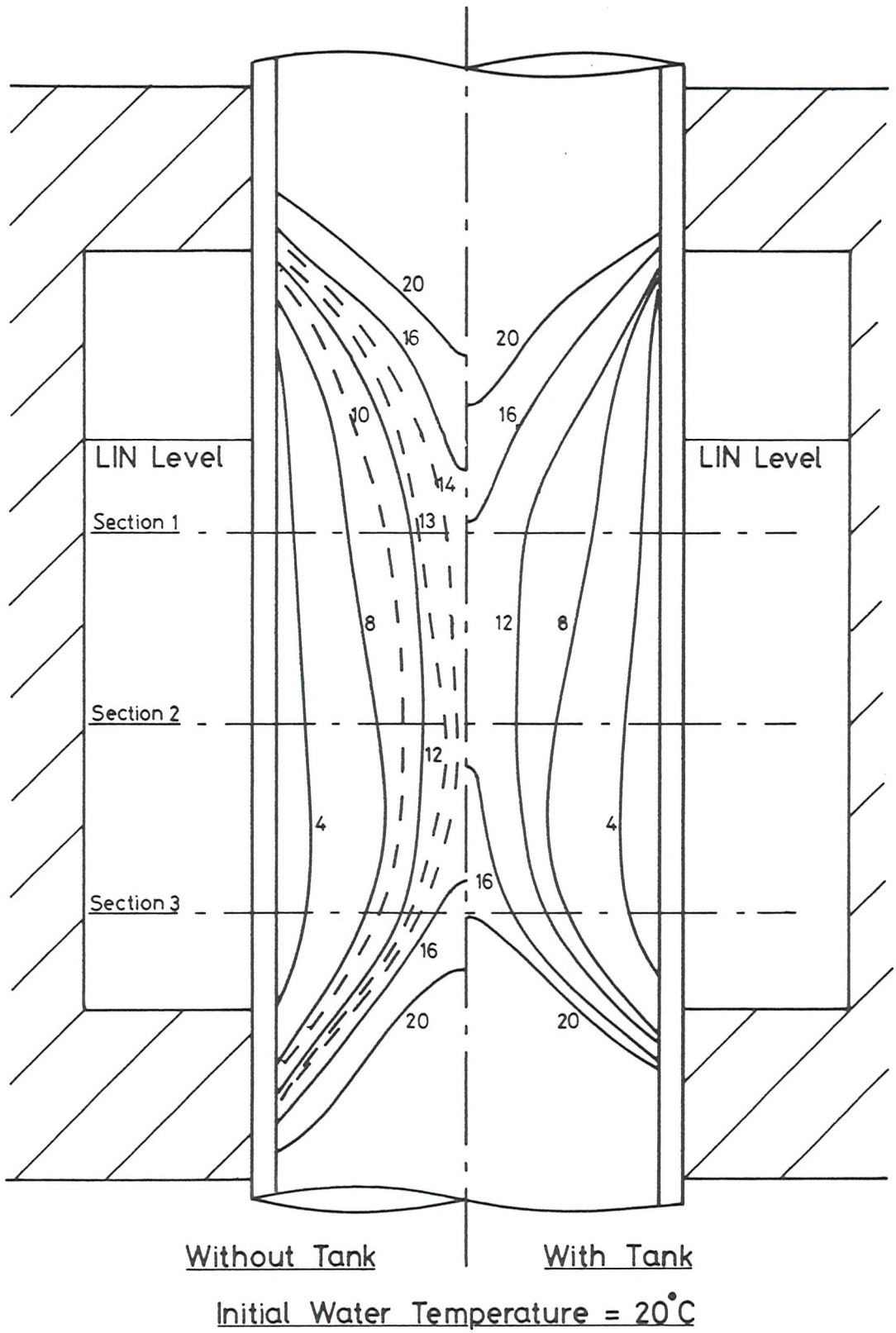

Fig. 4.4 Interface positions in 100 mm diameter vertical rig

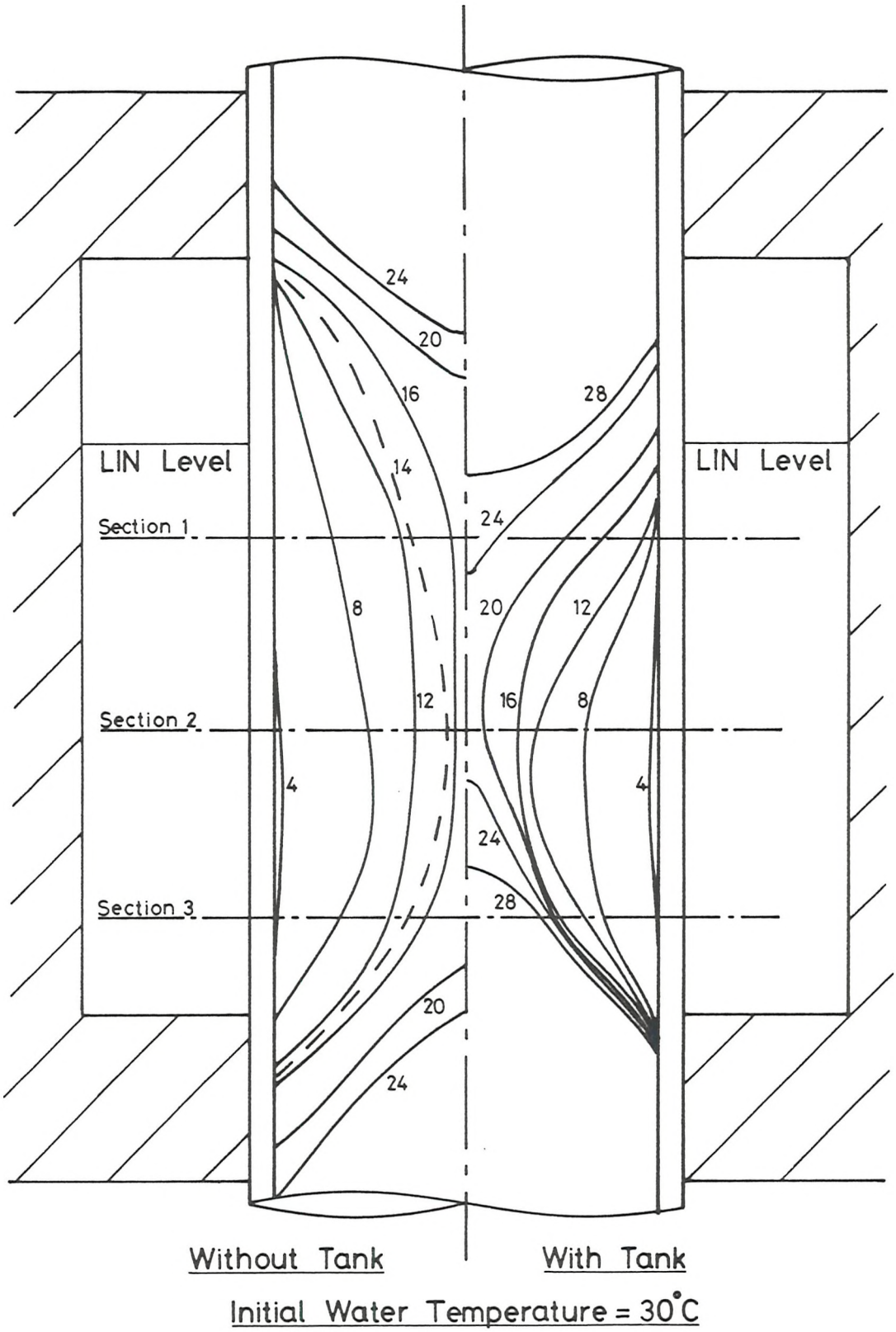

Fig. 4.5 Interface positions in 100 mm diameter vertical rig

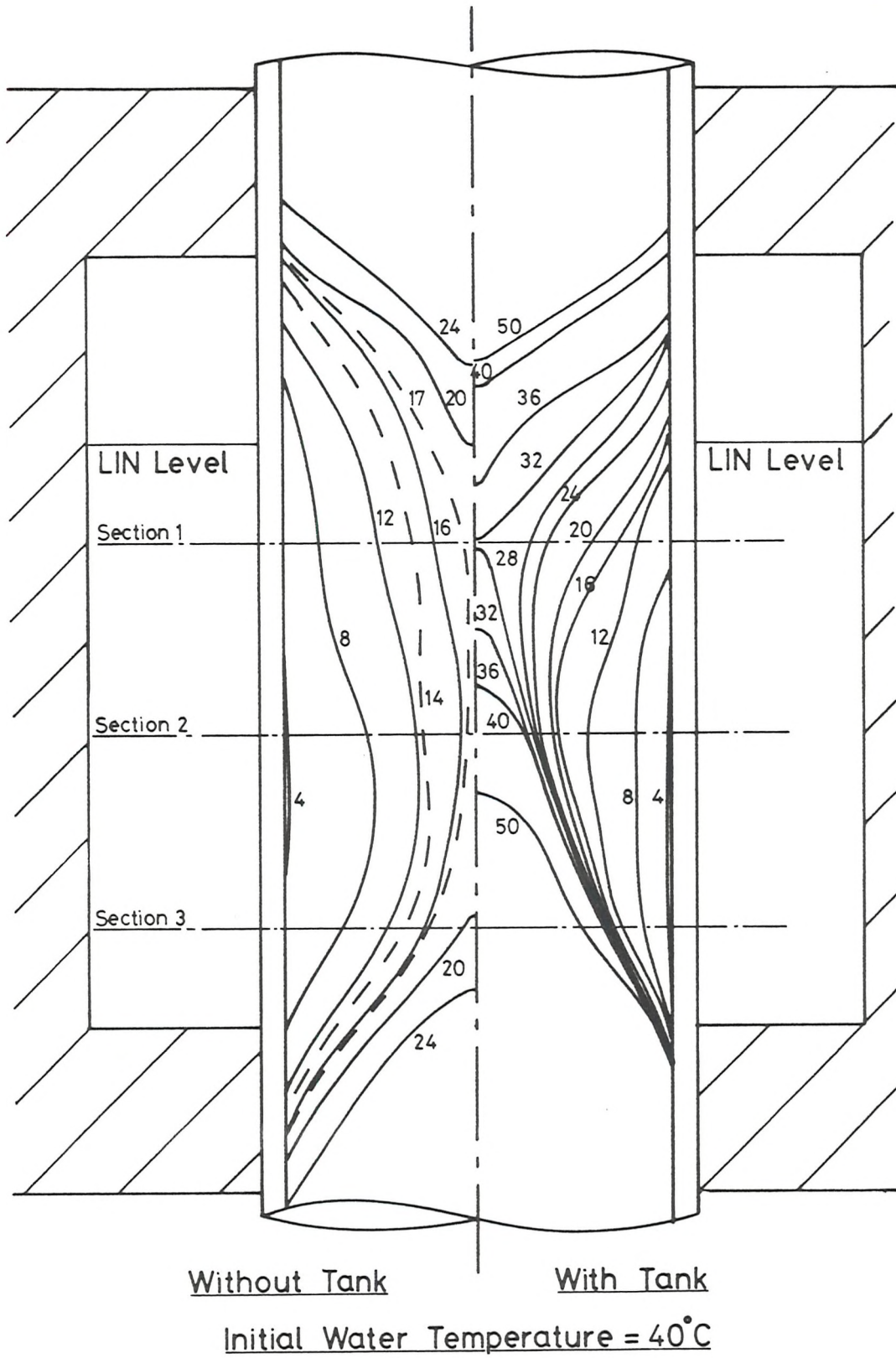

(a) (b)

Fig. 4.6 Interface positions in 100 mm diameter vertical rig

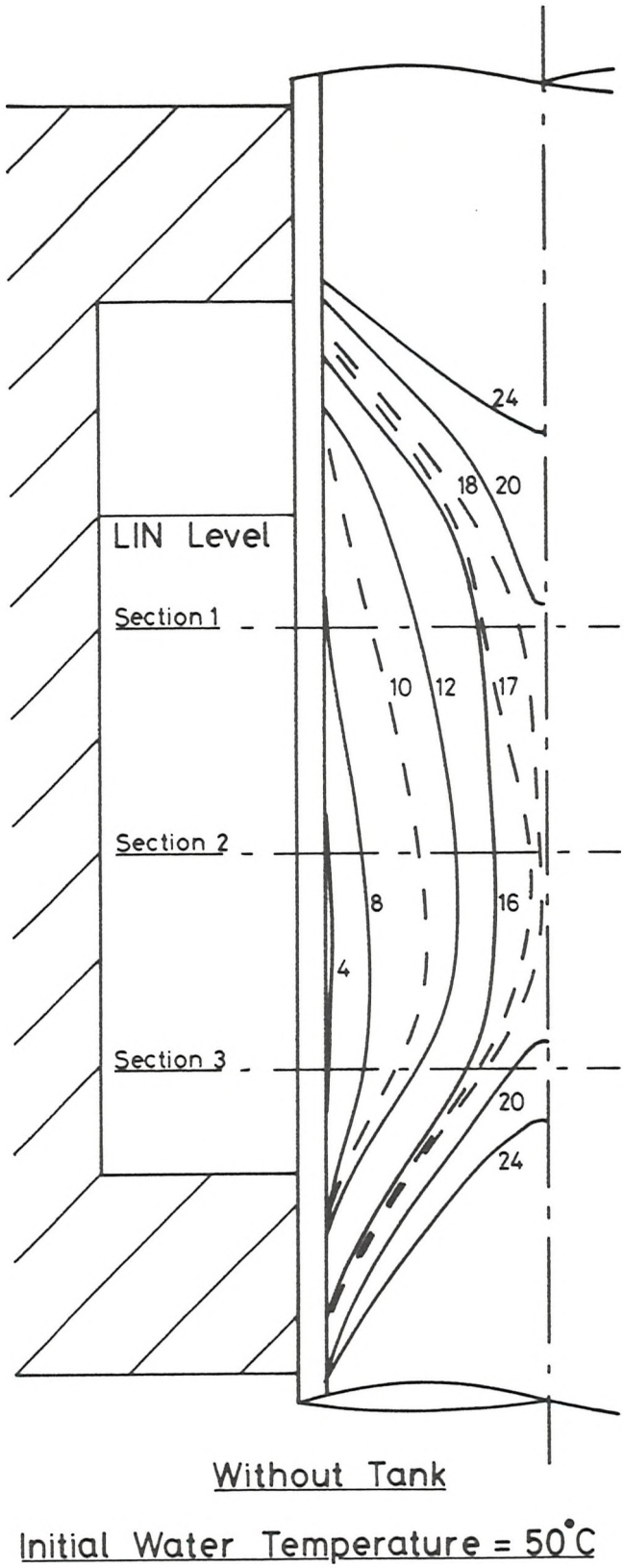

Fig. 4.7 Interface positions in 100 mm diameter vertical rig

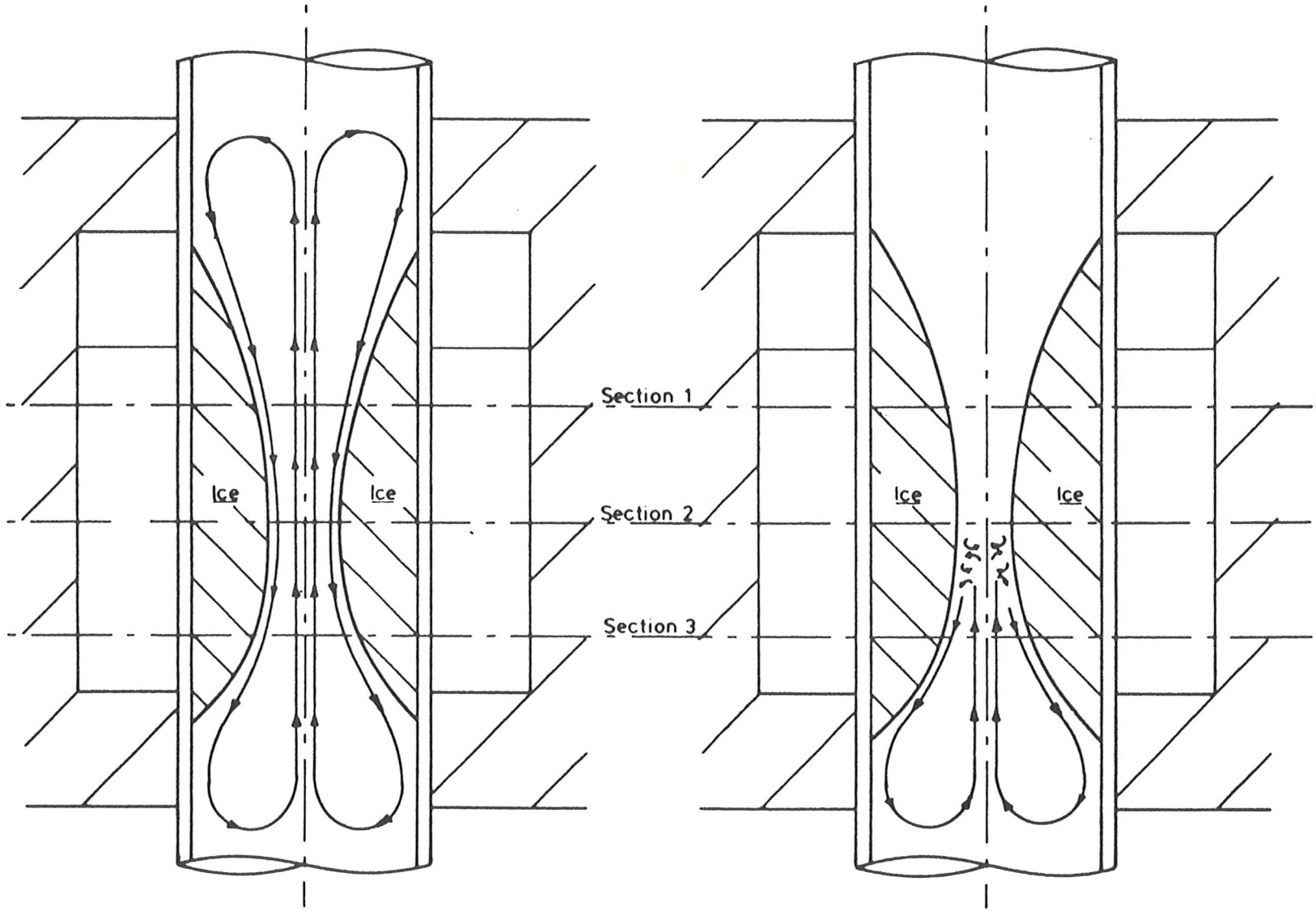

Phase One Convection

(a)

Fig. 4.8

Phase Two Convection

(b)

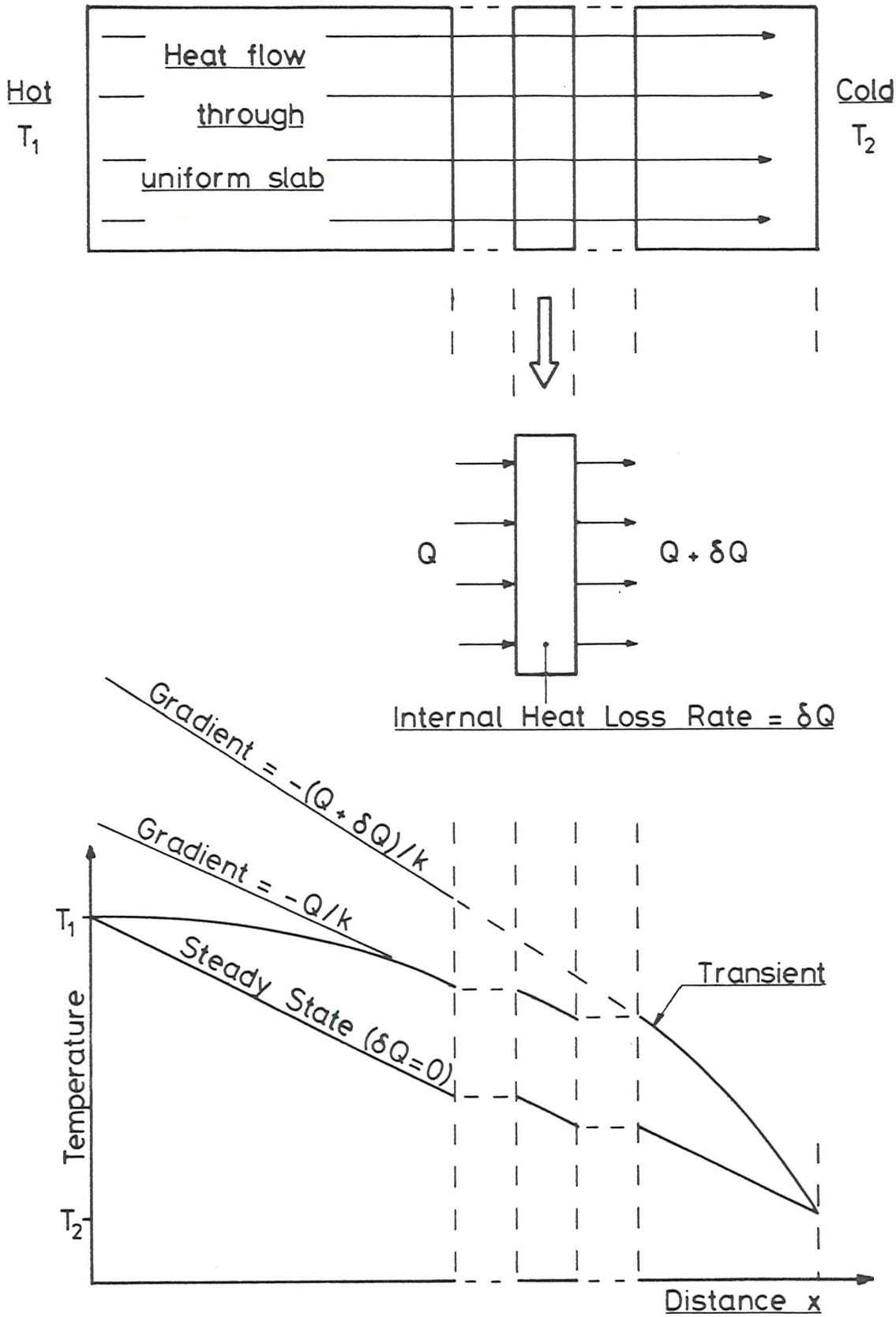

Fig. 4.9 Heat flow through a uniform slab

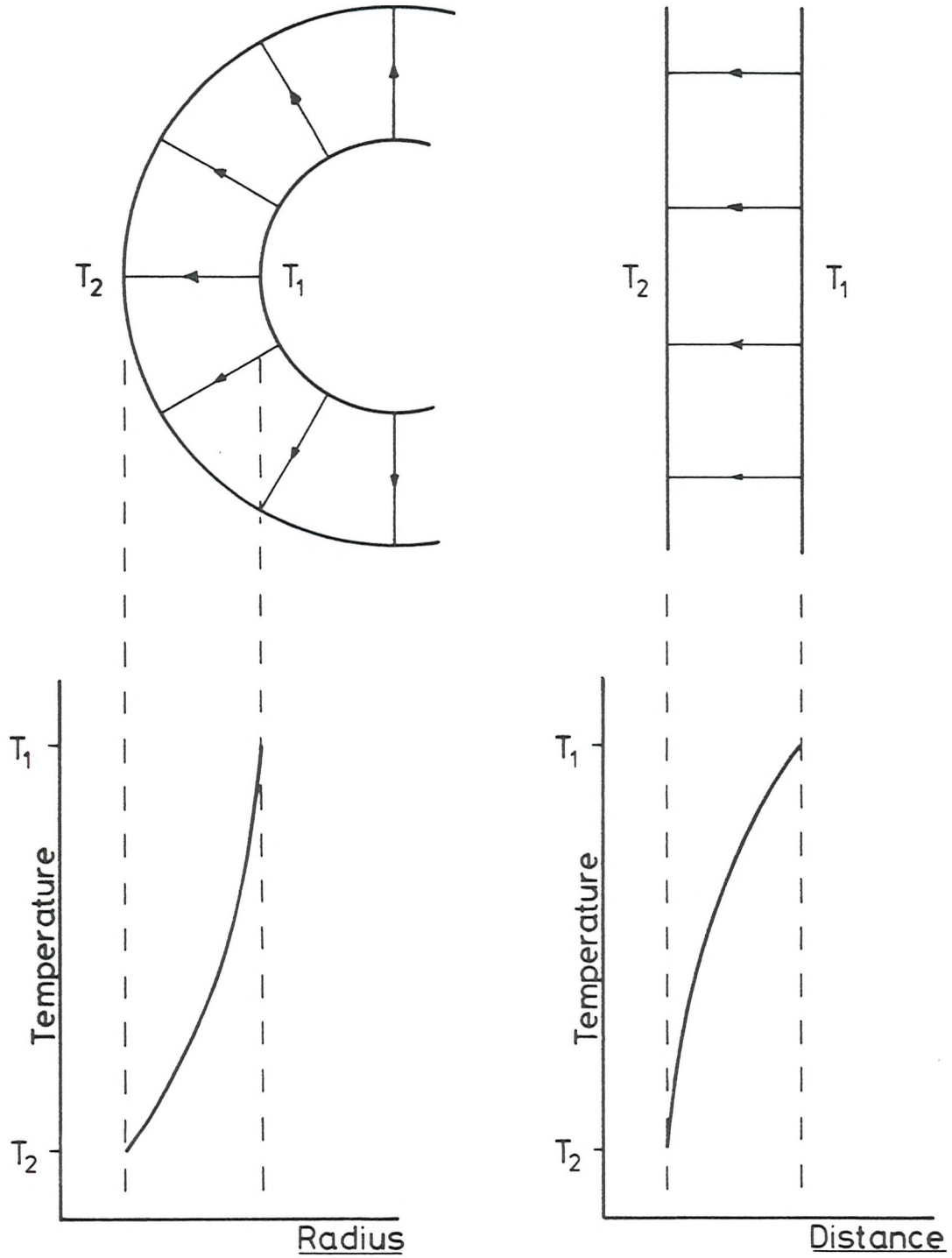

Steady State heat flow through a hollow cylinder.

(a)

Transient heat flow (cooling) through a uniform slab.

(b)

Fig. 4.10 'Convex' and 'Concave' Temperature Profiles

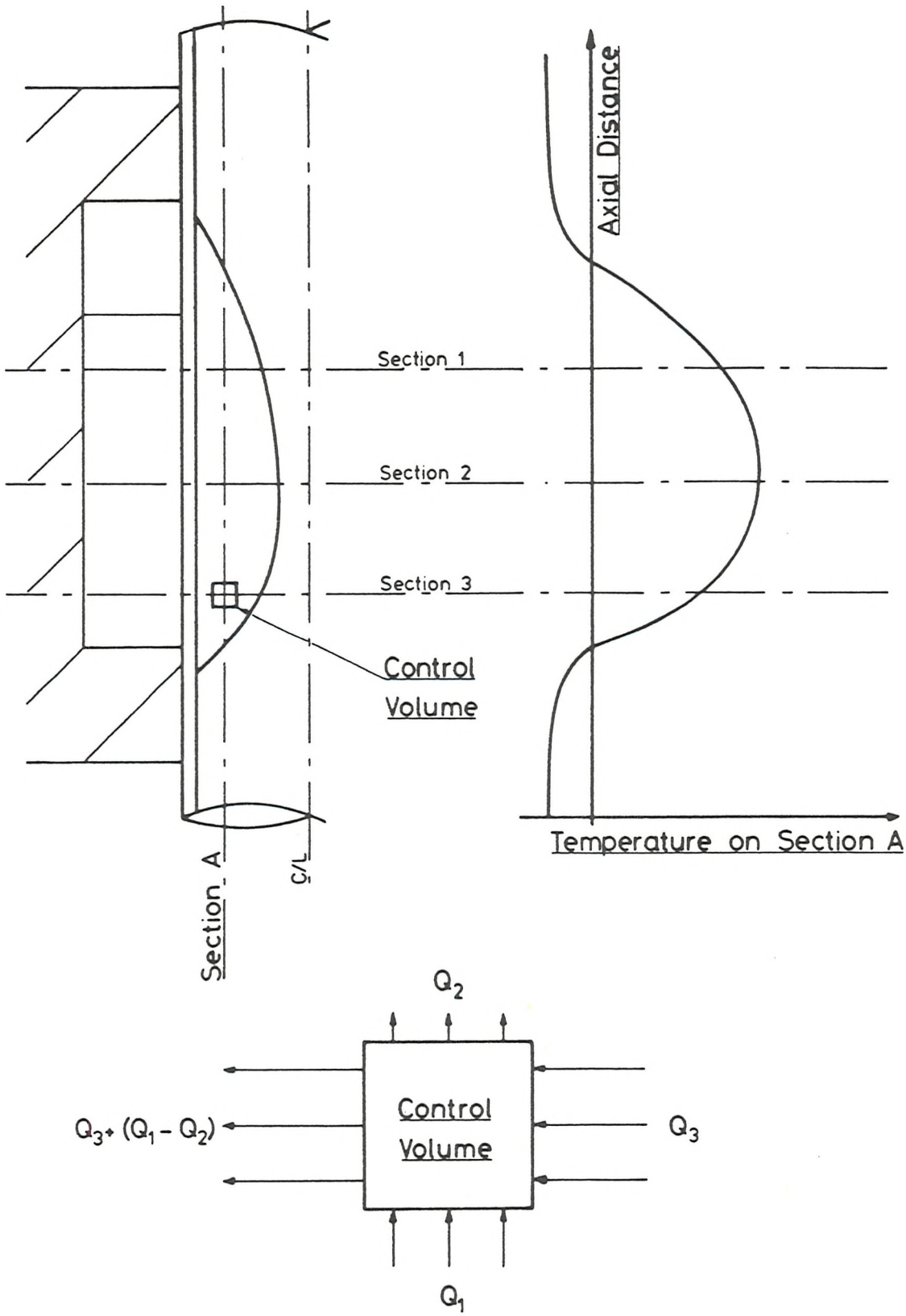

Fig. 4.11 Interaction of Longitudinal and Radial heat flow

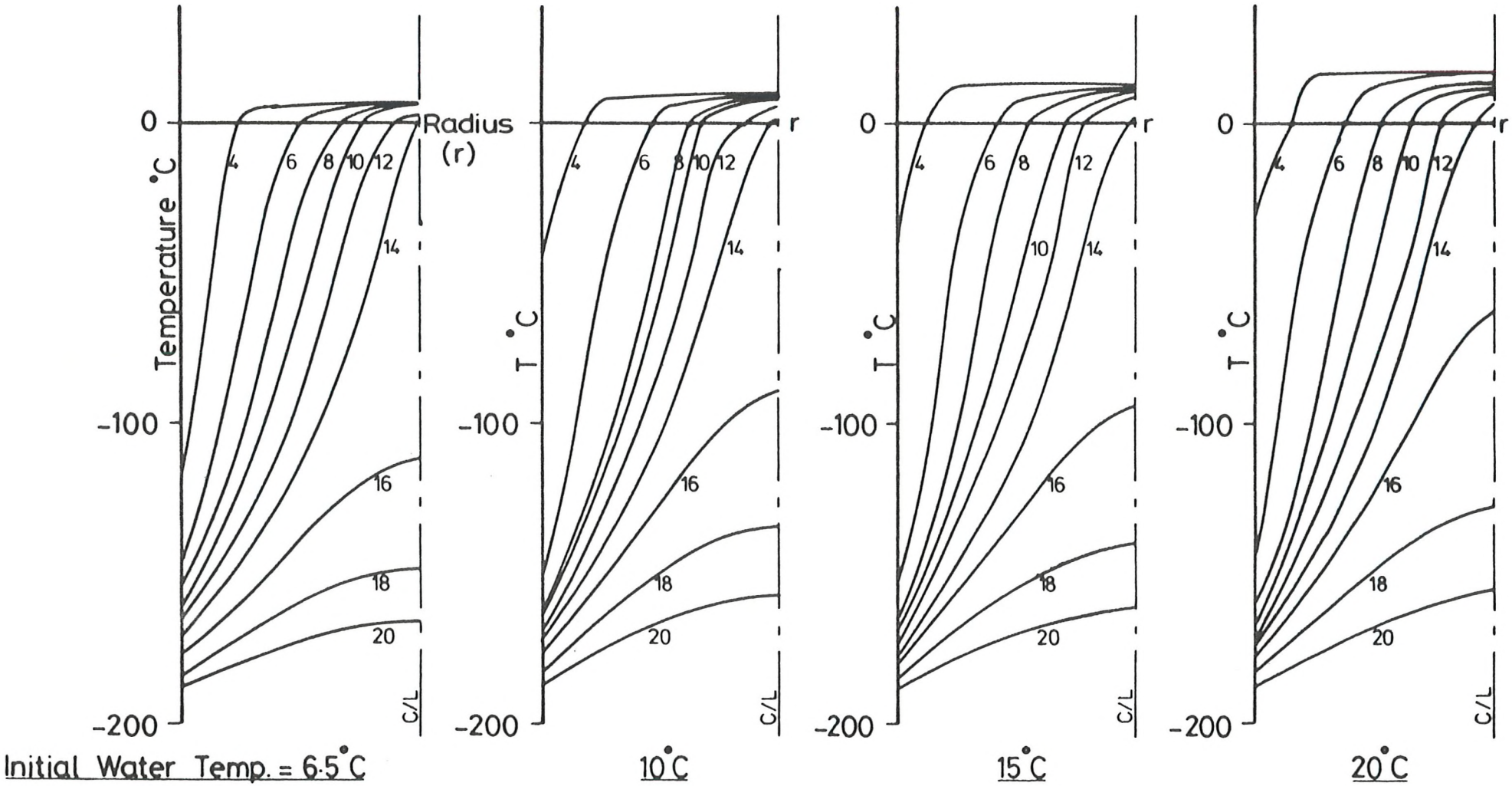
0
-100
-200
Temperature °C
Radius
(r)
r
T °C
4
6
8
10
12
14
16
18
20
C/L
Initial Water Temp. = 6·5°C
10°C
15°C
20°C
Radial Temperature Profiles on Section 2
(a)
(b)
(c)
(d)

Fig. 4.12

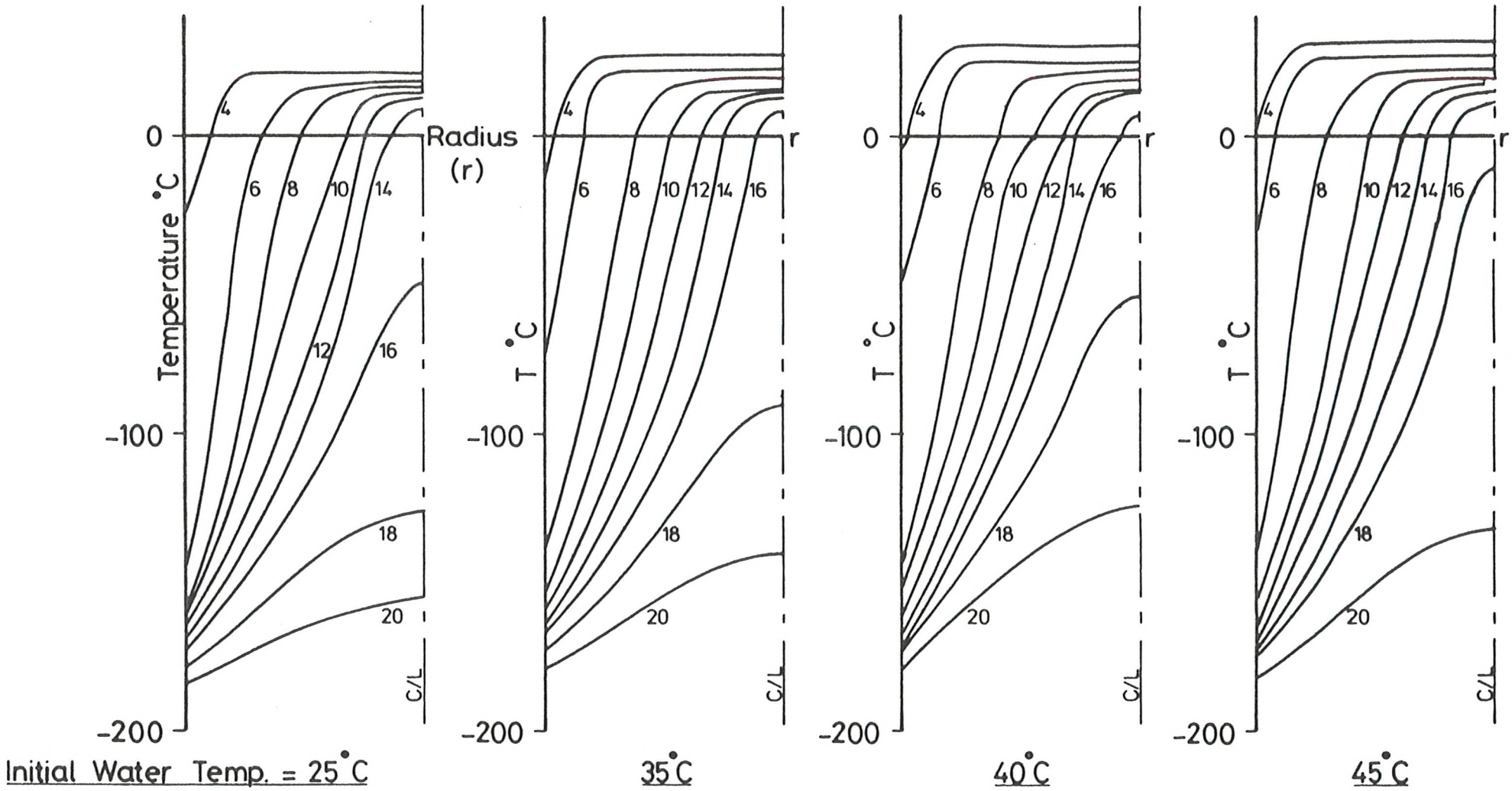

Radial Temperature Profiles on Section 2

Fig. 4.12 (e) (f) (g) (h)

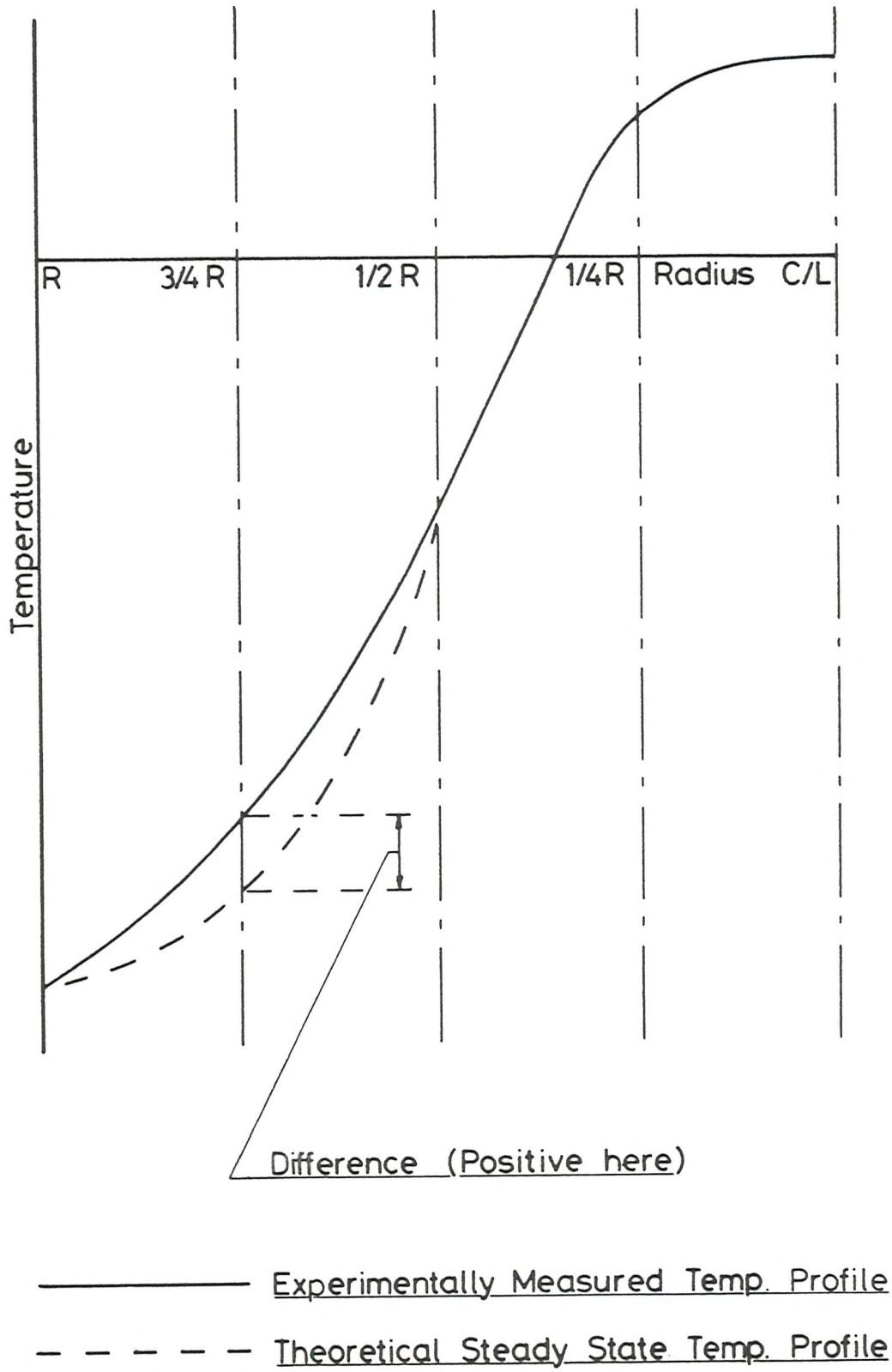

Fig. 4.13 Calculation of difference term in comparison of experimental and theoretical temperature profiles

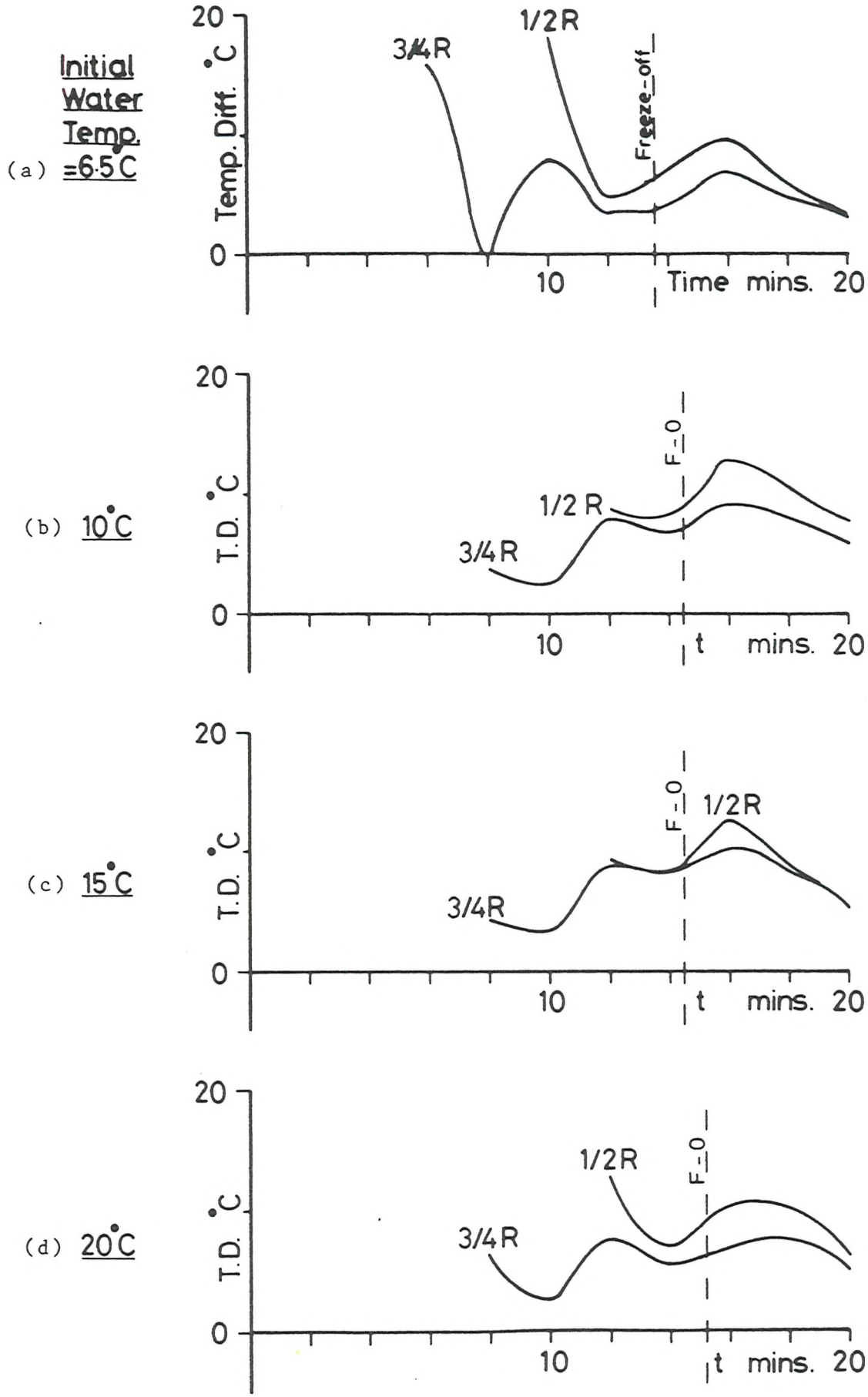

Fig. 4.14 Comparison of Experimental and Steady State Temperature Profiles.

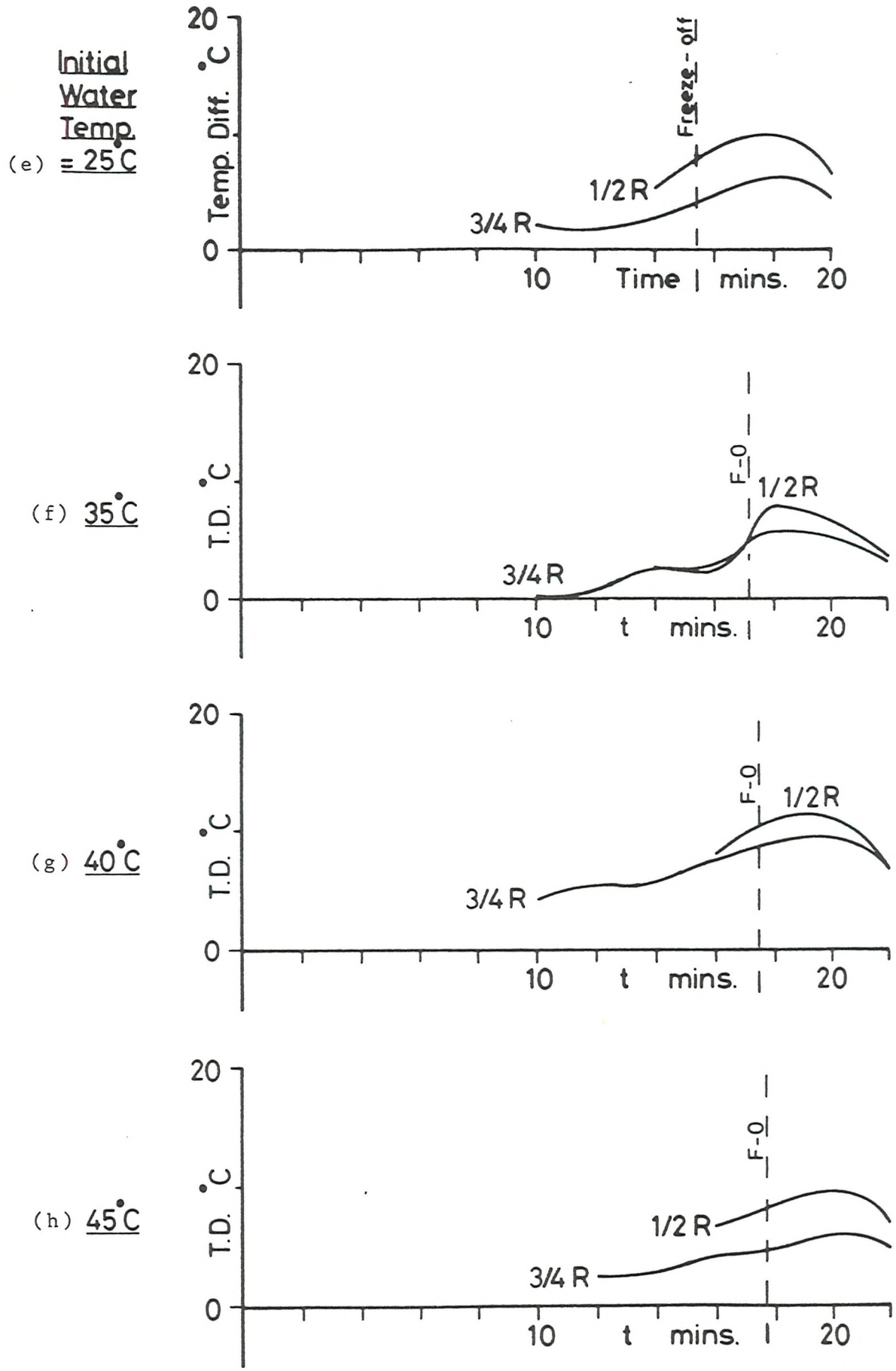

Fig. 4.14 Comparison of Experimental and Steady State Temperature Profiles.

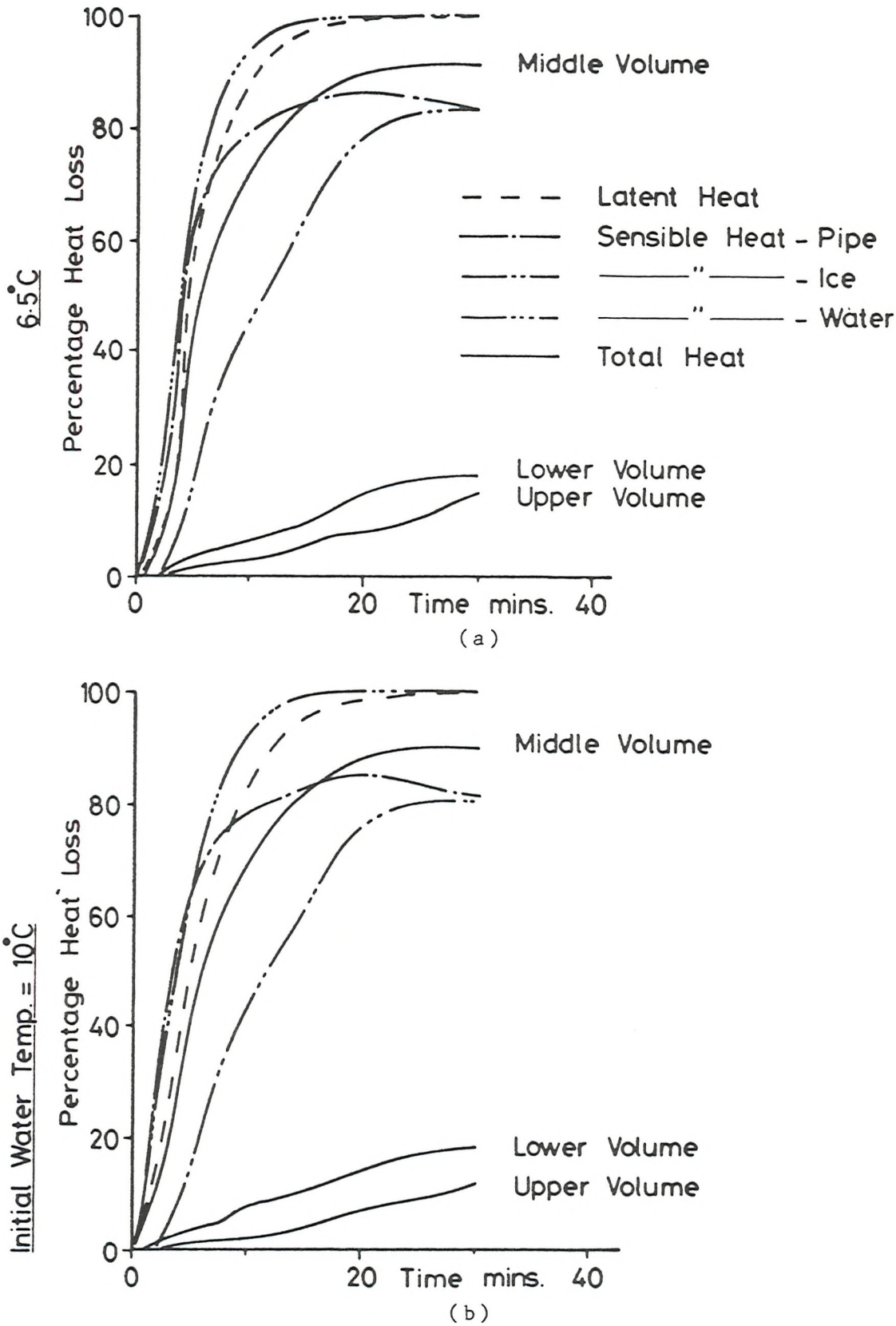

Fig. 4.15 Rate of energy loss during freezing of a 100 mm diameter vertical rig without tank

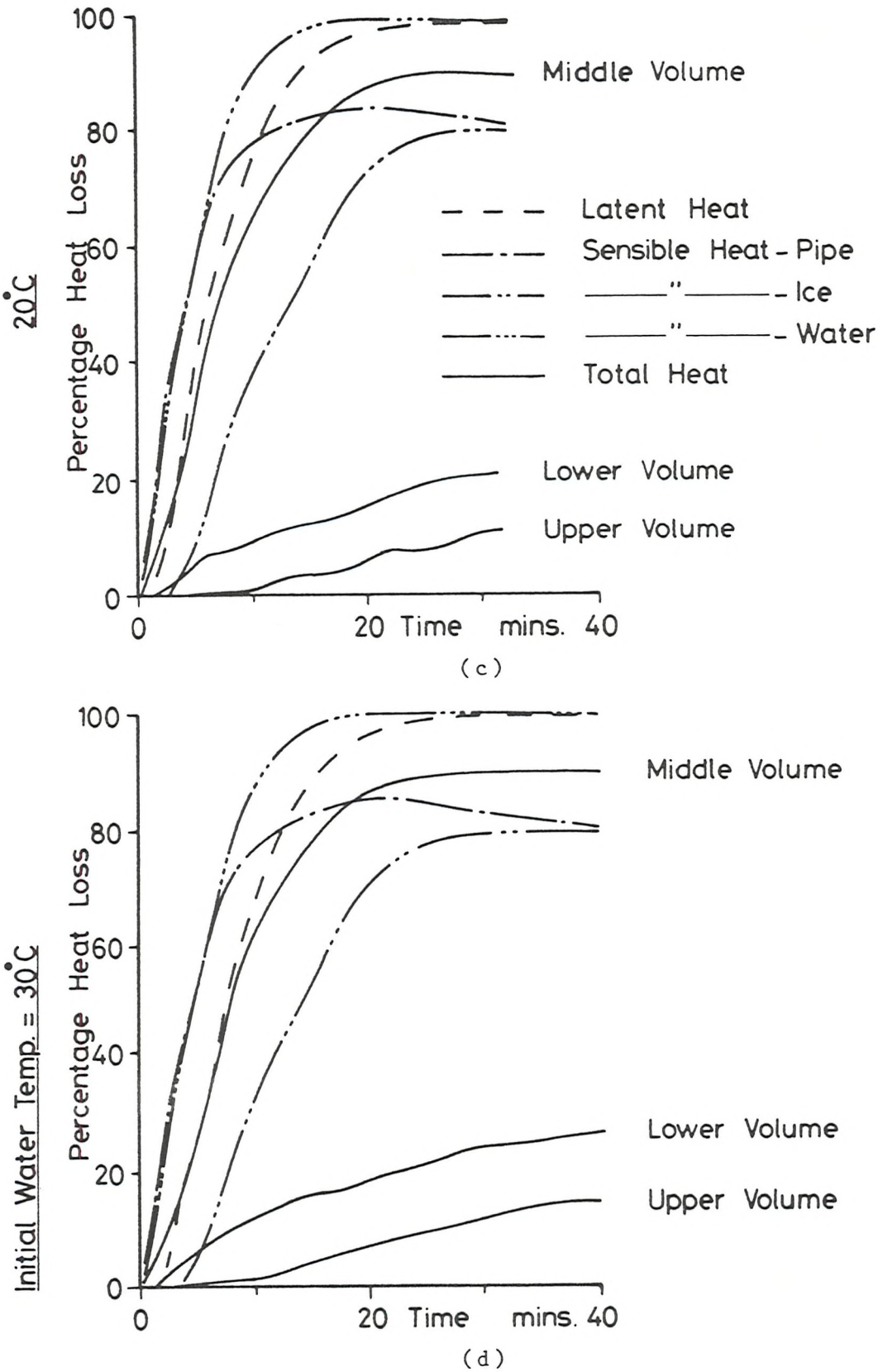

Fig. 4.15 Rate of energy loss during freezing of 100 mm diameter vertical rig without tank

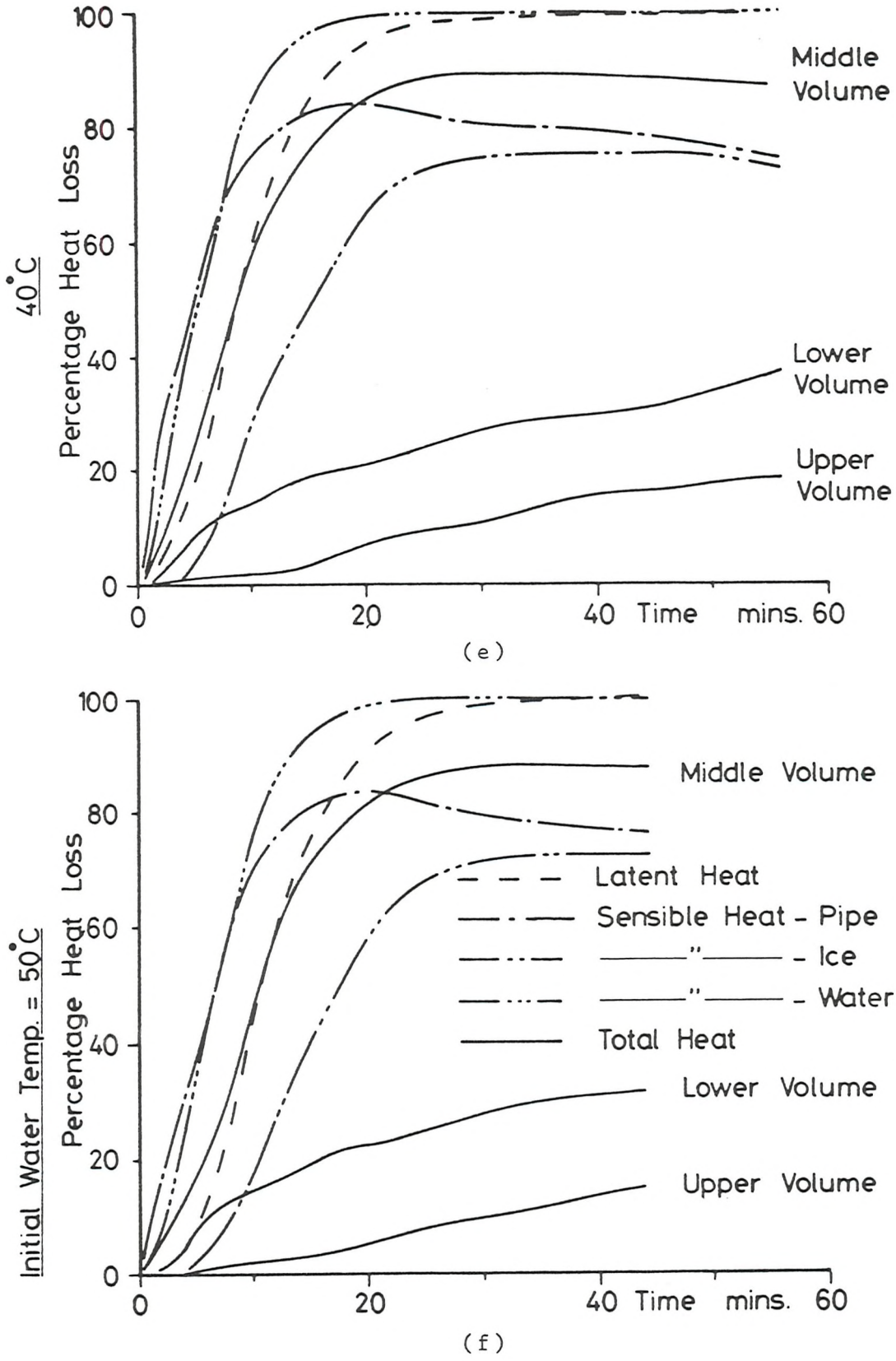

Fig. 4.15 Rate of energy loss during freezing of a 100 mm diameter vertical rig without tank

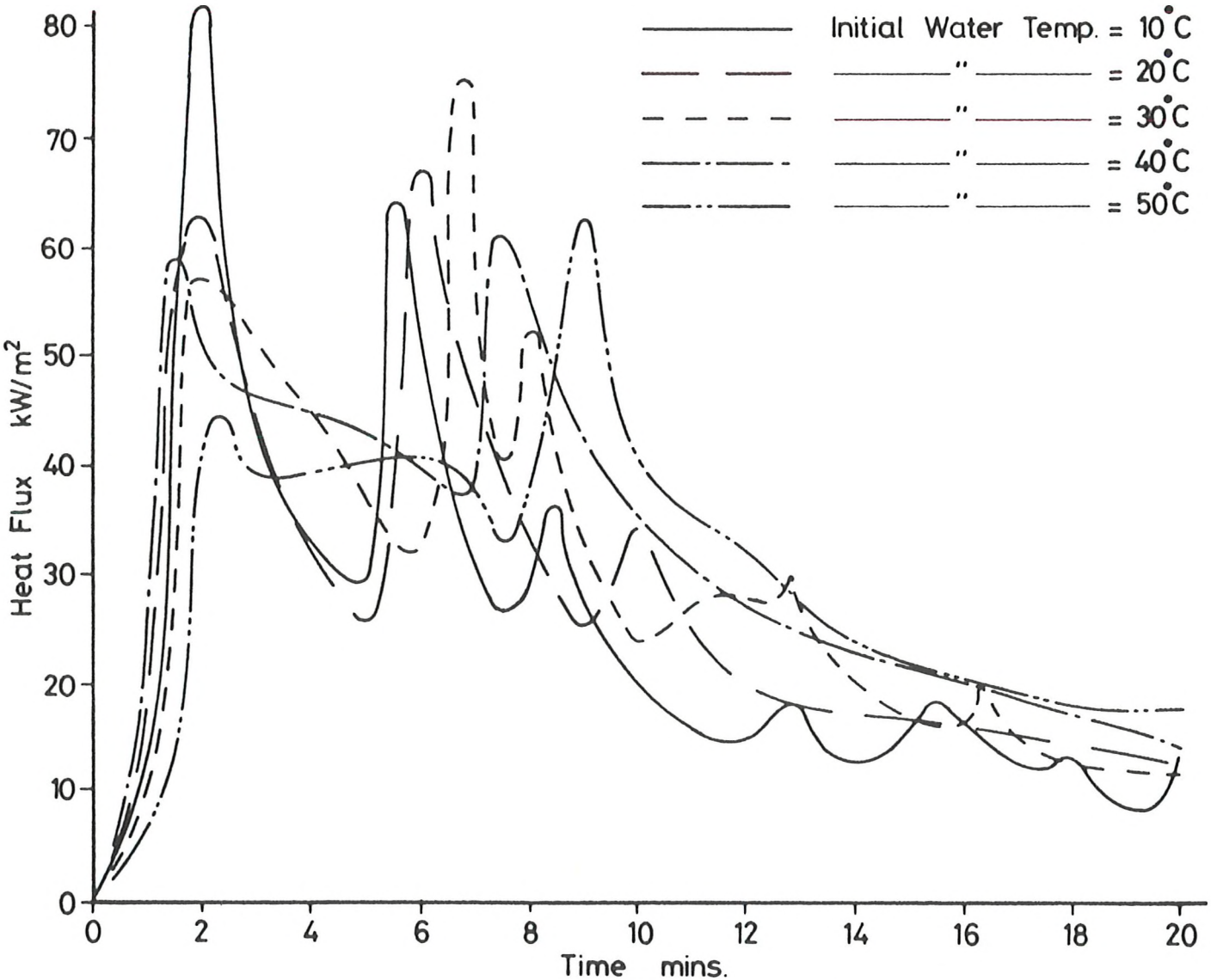

Average Heat Flux into Liquid Nitrogen.

Fig. 4.16

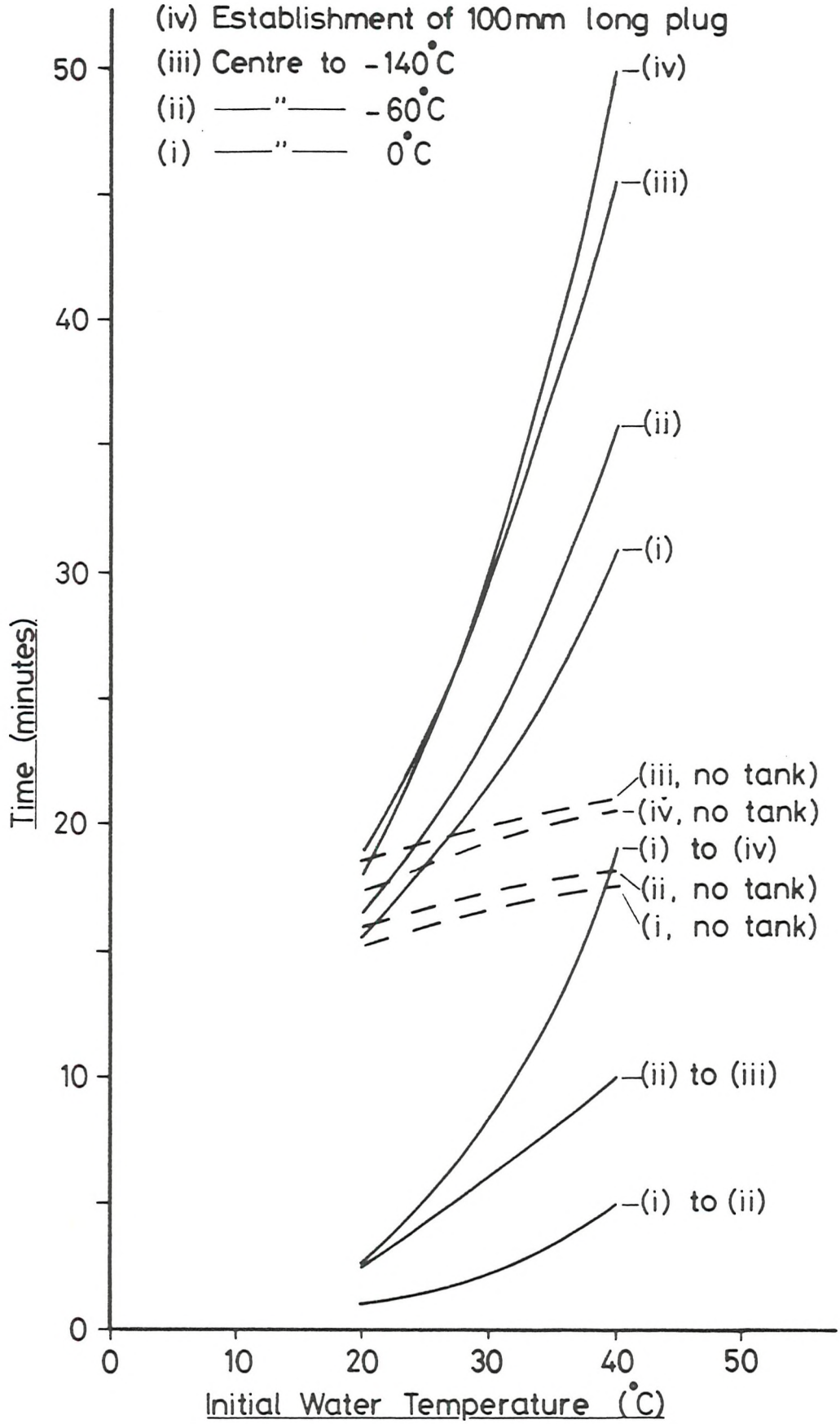

Fig. 4.17 Times to freeze for 100 mm diameter vertical rig with tank

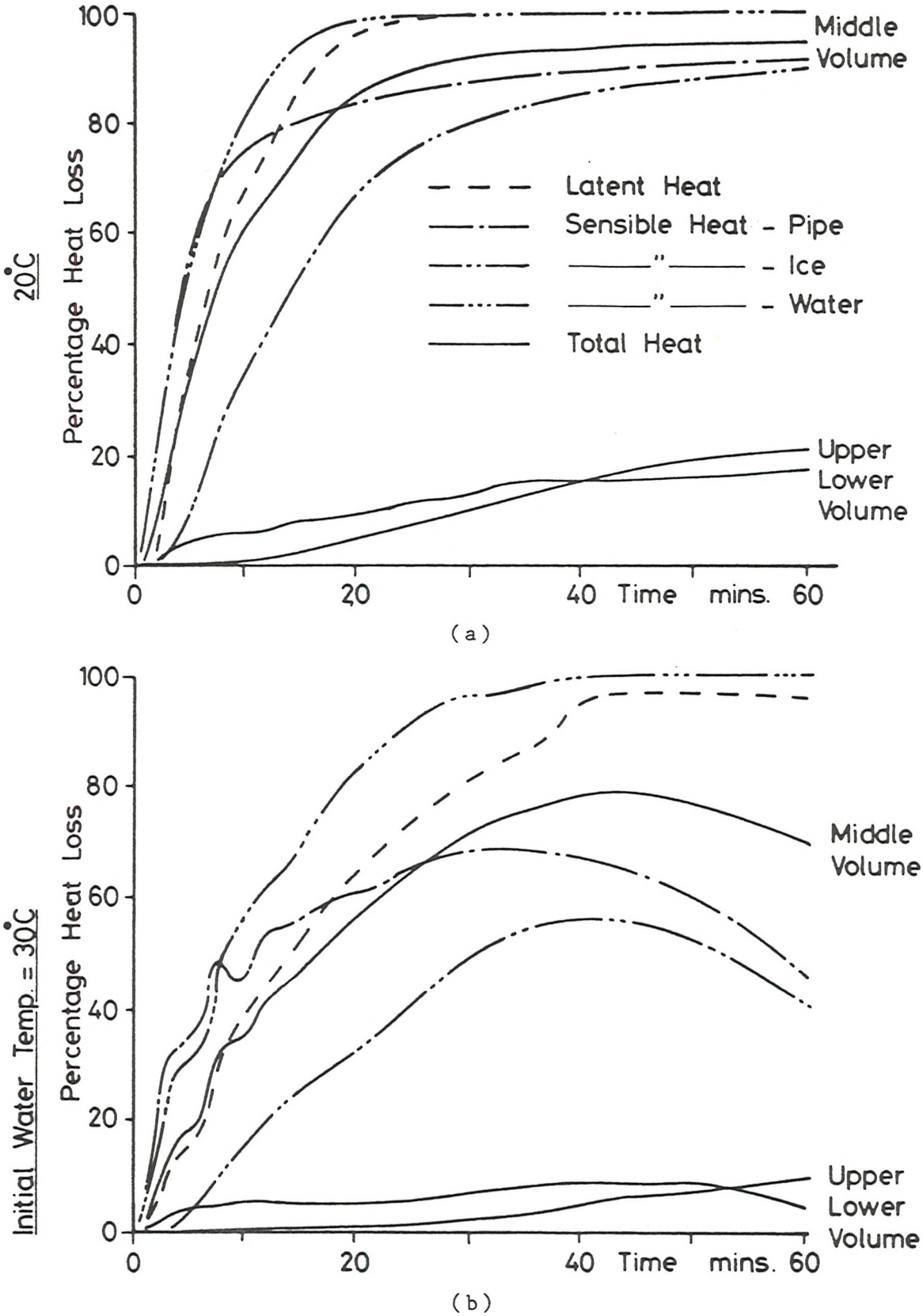

Fig. 4.18 Rate of energy loss during freezing of 100 mm diameter vertical rig with tank

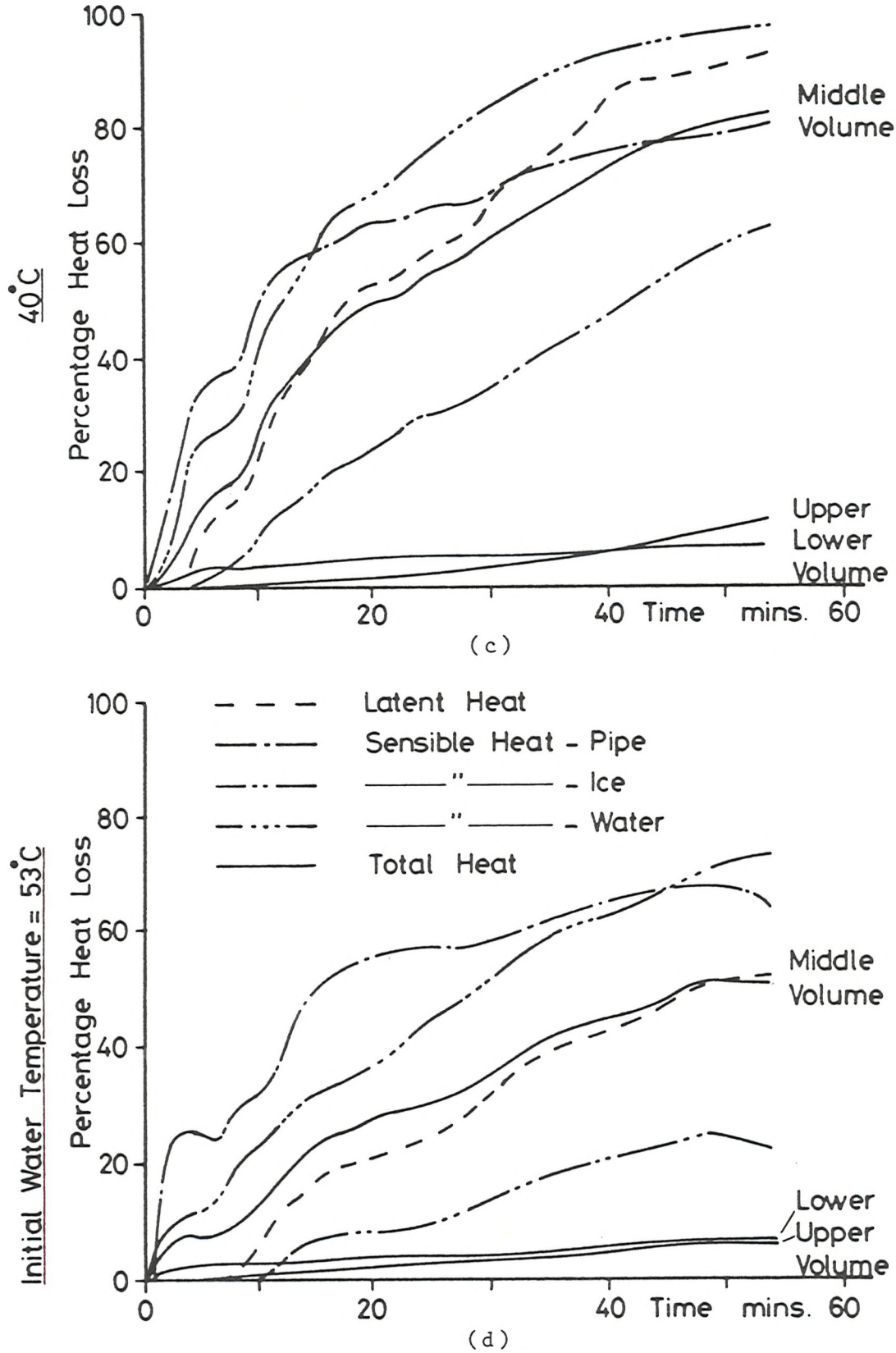

Fig. 4.18 Rate of energy loss during freezing of 100 mm diameter vertical rig with tank

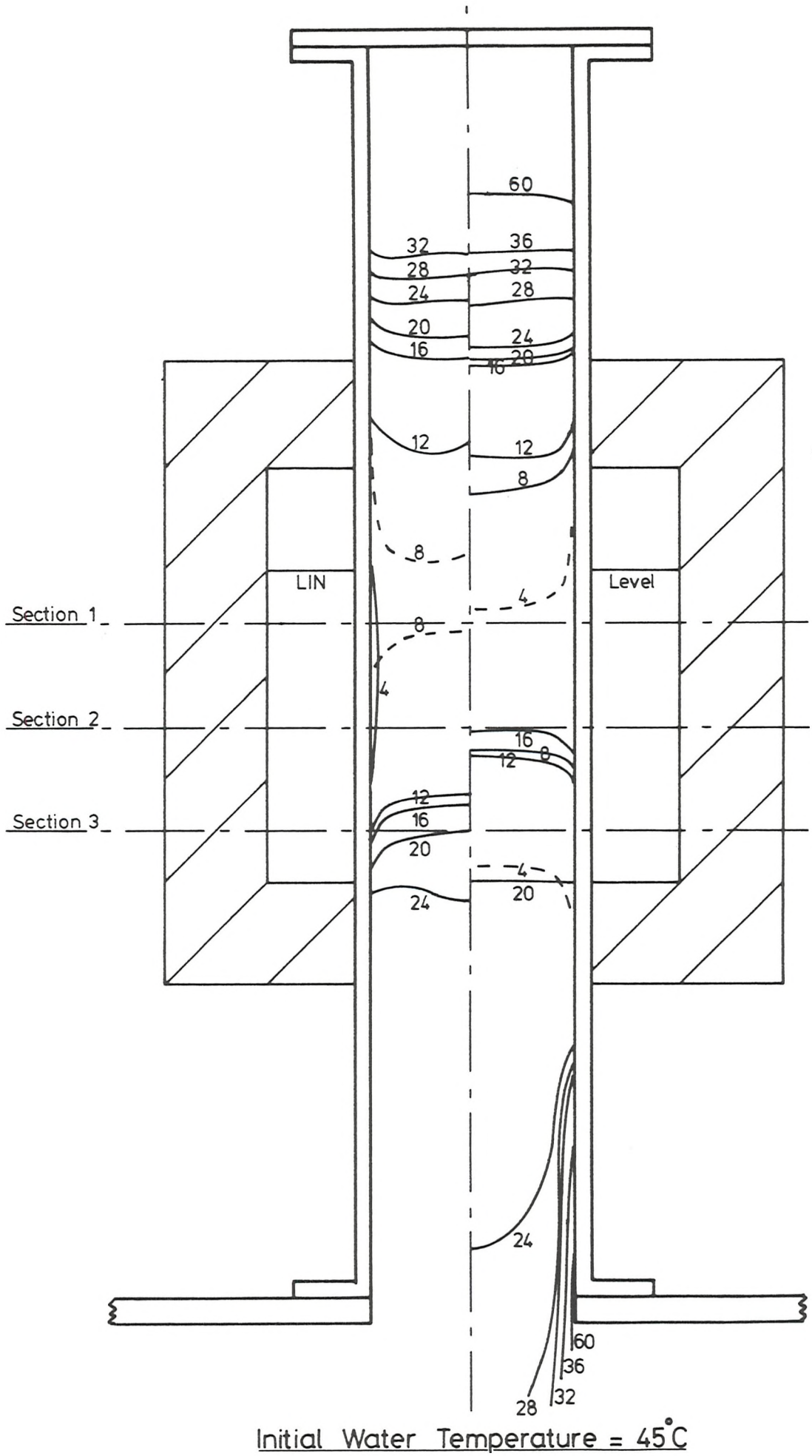

Fig. 4.19 Interface positions in 100 mm diameter vertical rig during two anomalous freezes

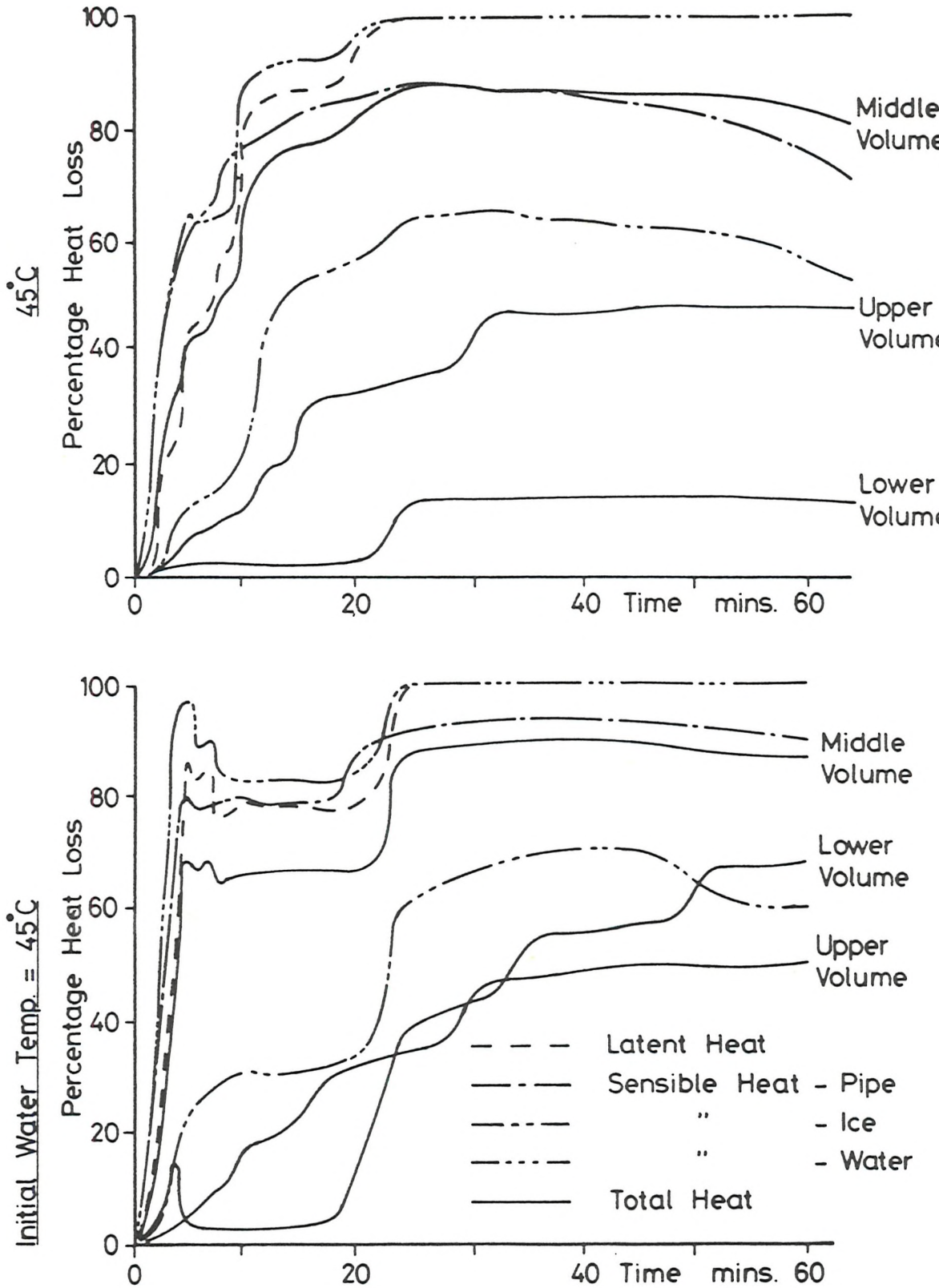

Fig. 4.20 Rate of energy loss during freezing of 100 mm diameter vertical rig with tank for two anomalous freezes

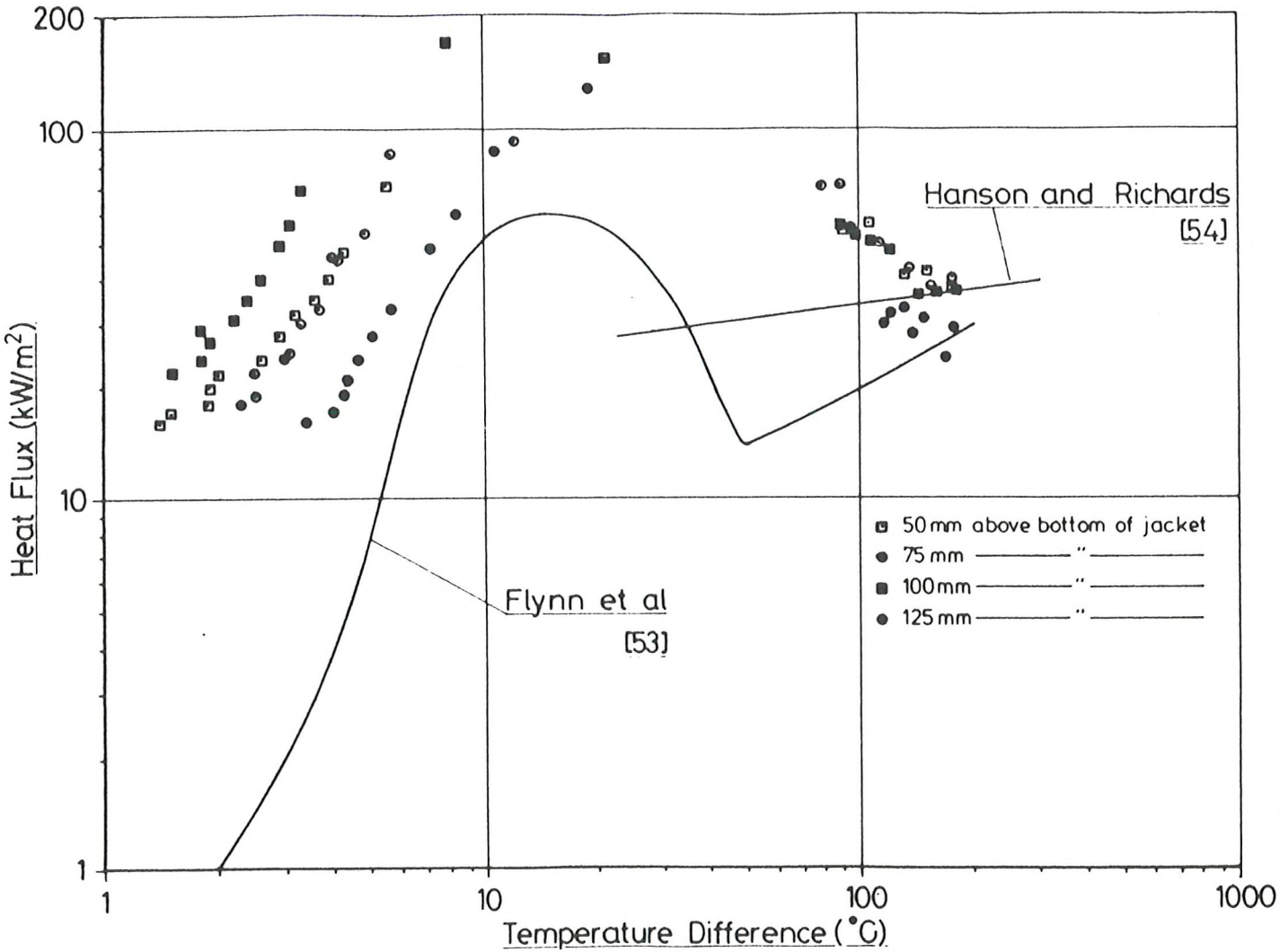

Fig. 4.21 Local heat flux v Surface to pool temperature difference

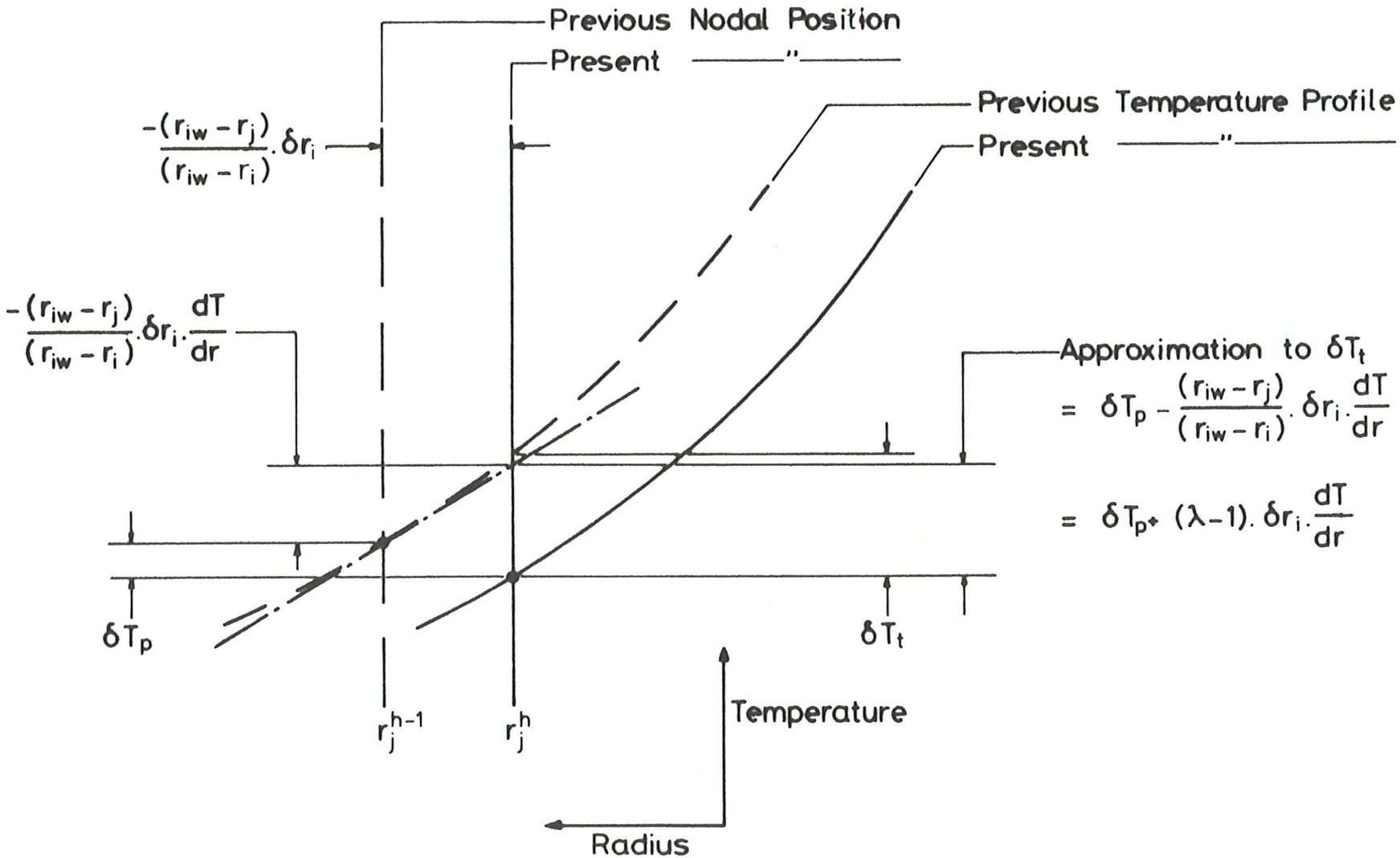

Fig. 5.1 Illustration of moving boundary approximation

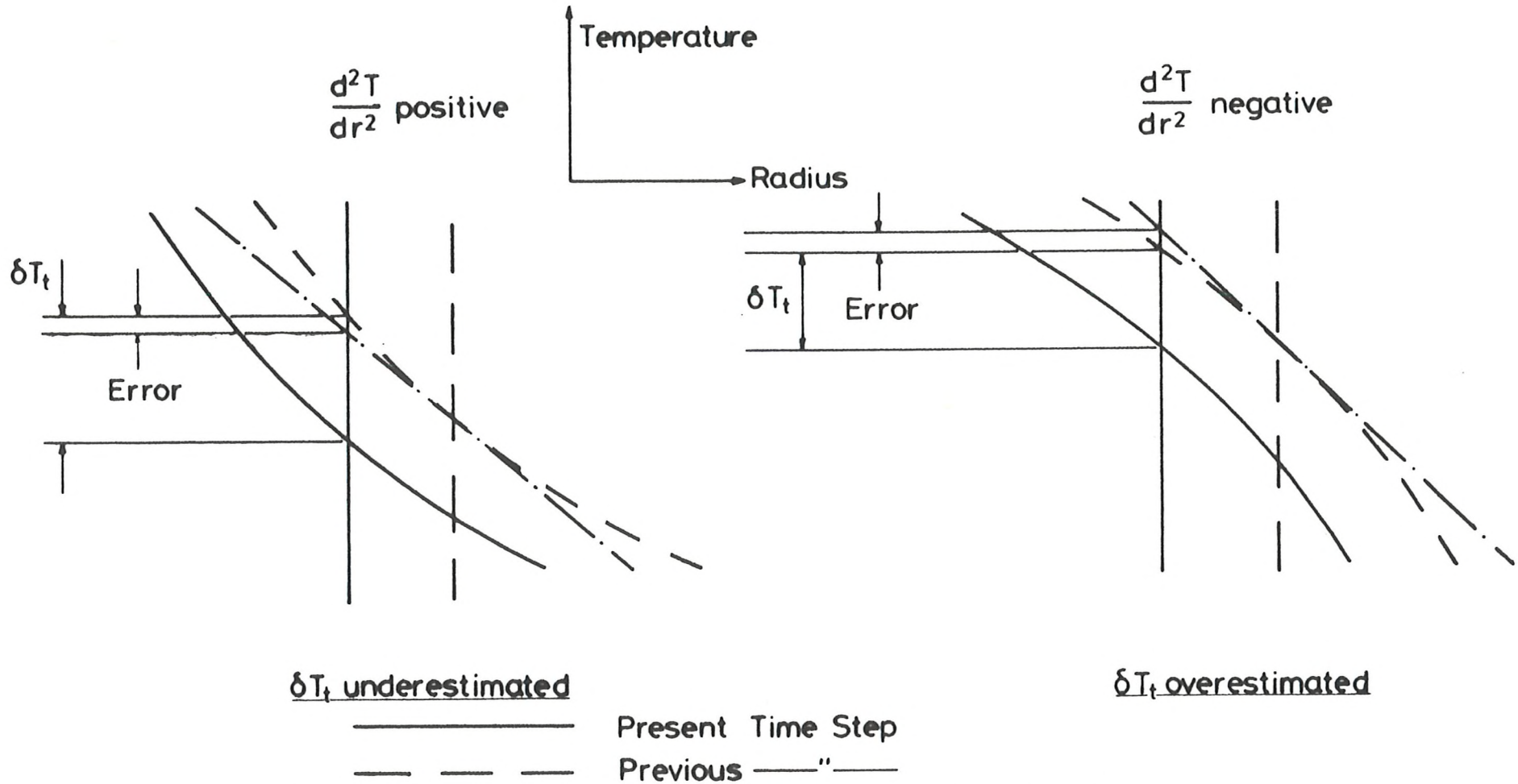

Fig. 5.2 Effect of positive and negative 2nd. order differentials of temperature with respect to time on the moving boundary approximation

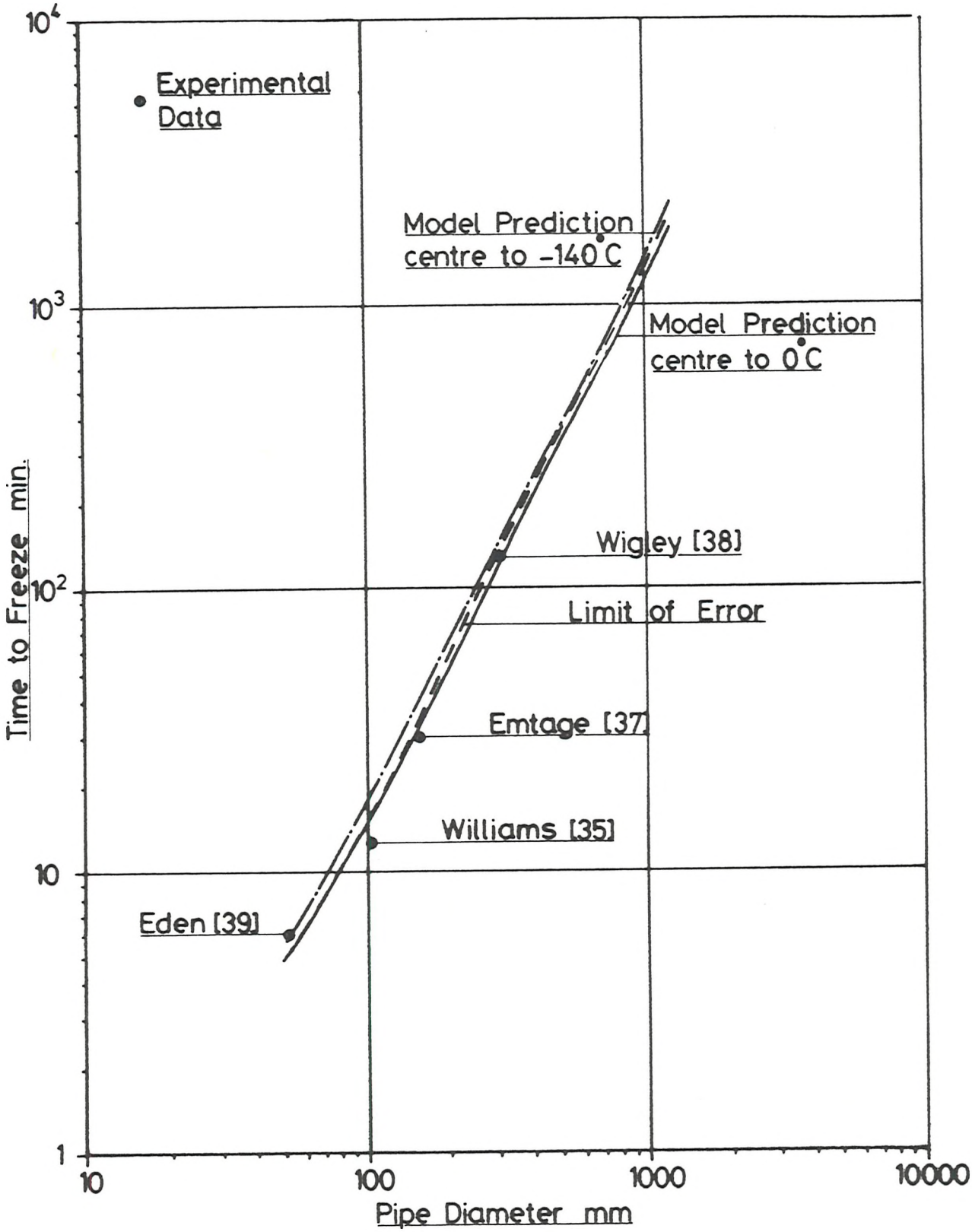

Fig. 5.3 Comparison between model prediction and experimental data for times to freeze varying pipe diameters

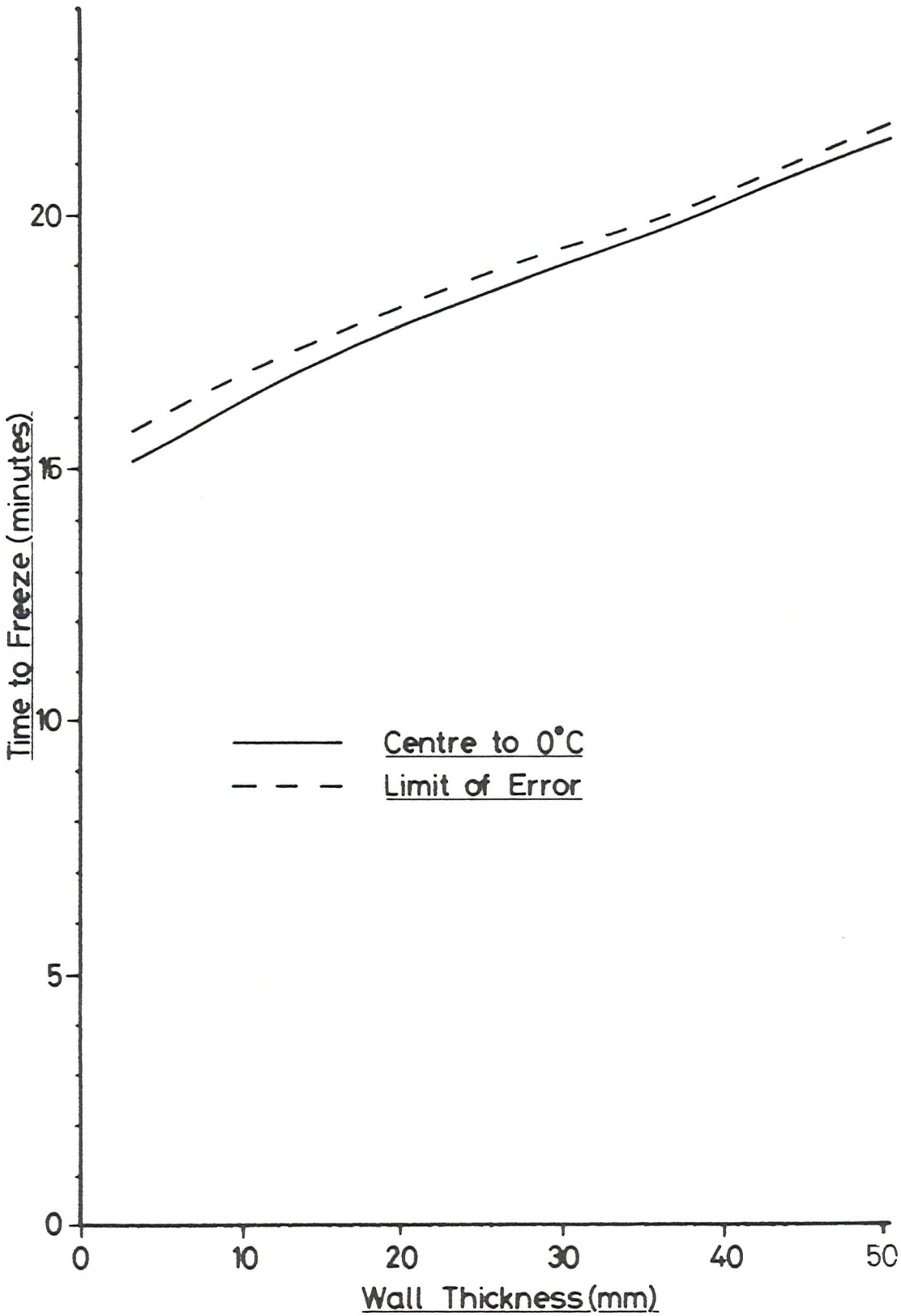

Fig. 5.4 Model prediction for the effect of pipe wall thickness on the time to freeze

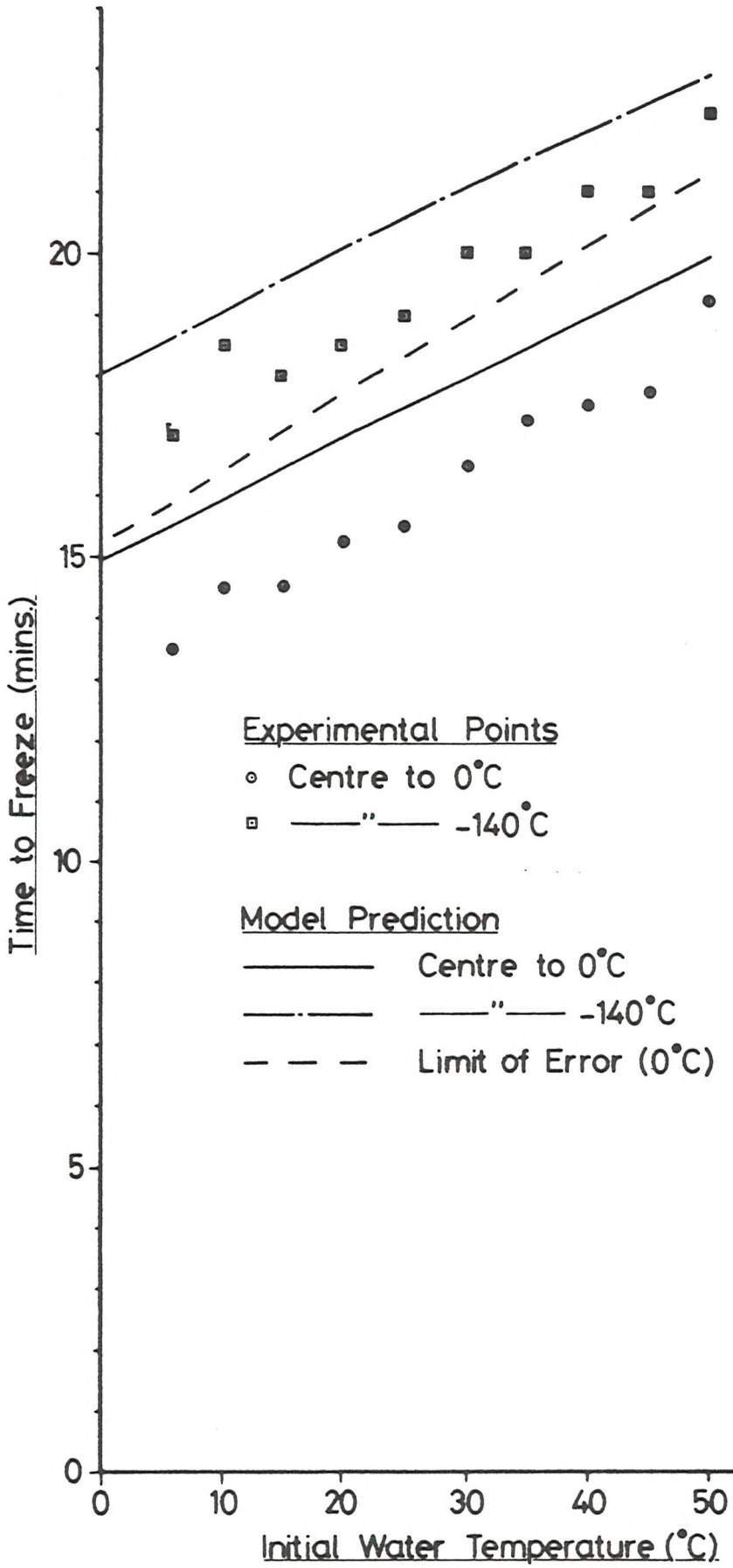

Fig. 5.5 Comparison between model prediction and experimental data for times to freeze a 100 mm diameter pipe with varying initial temperatures

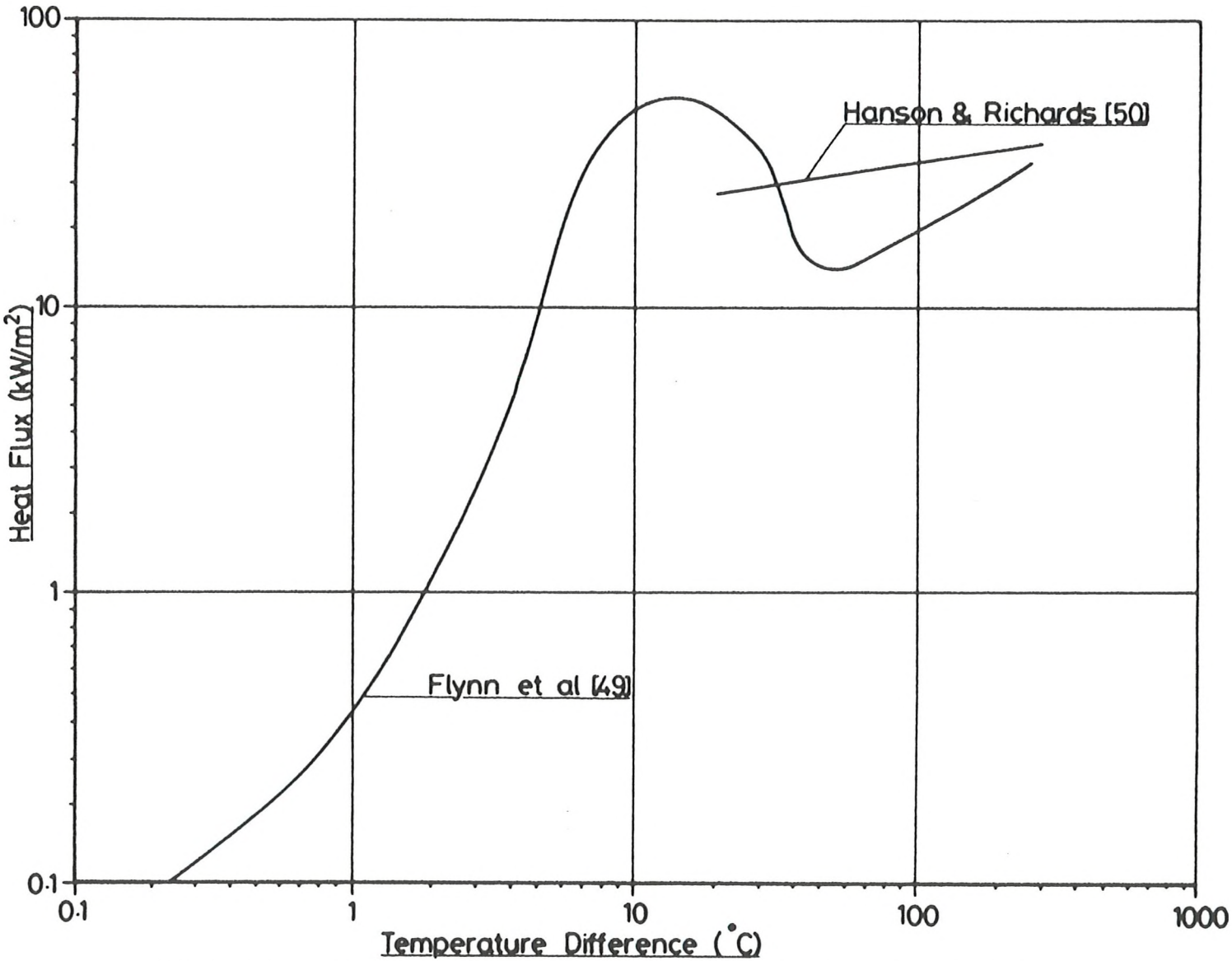

Fig. 5.6 Boiling Heat Transfer data for Liquid Nitrogen

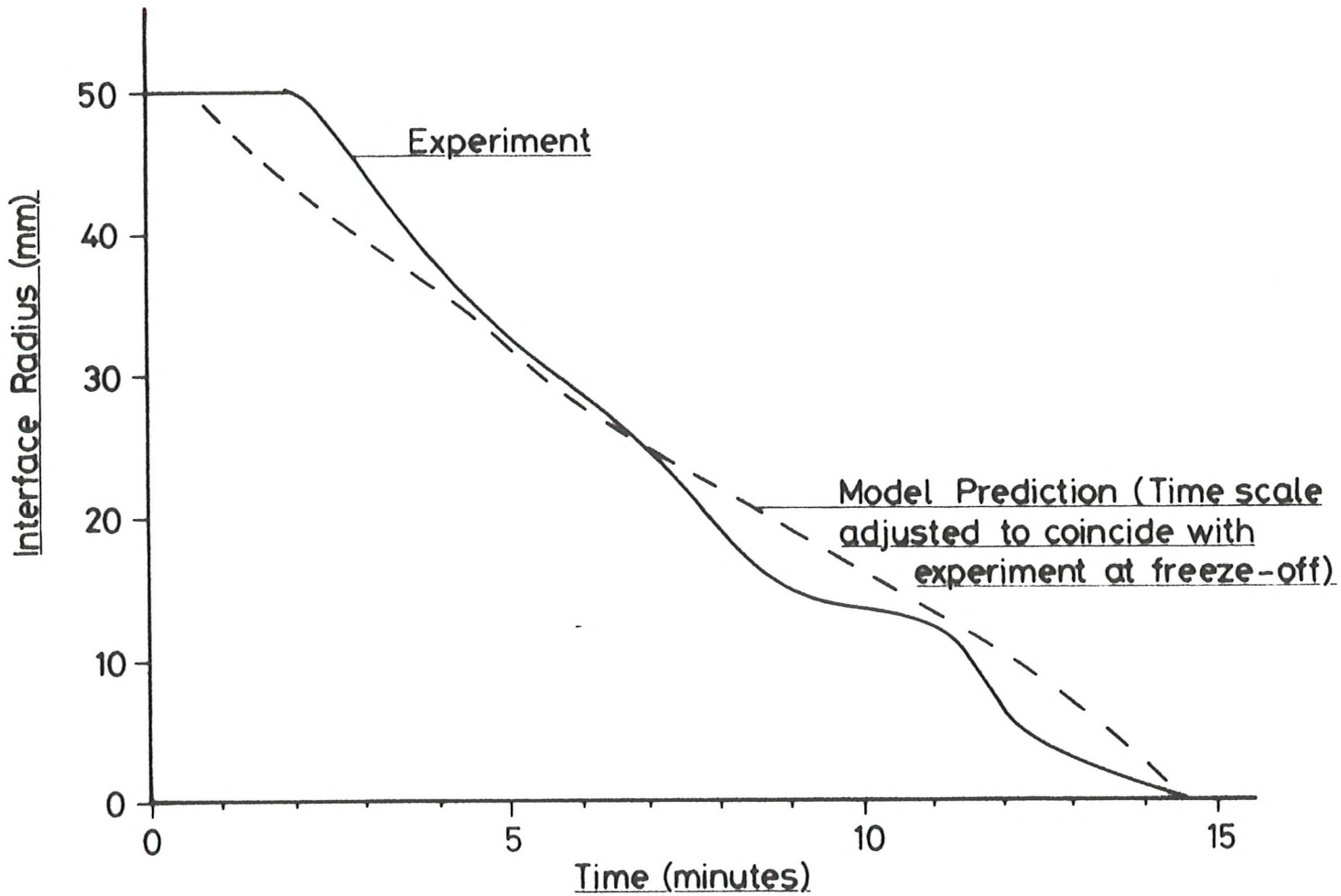

Fig. 5.7 Comparison between model prediction and experimental data for interface position during freezing

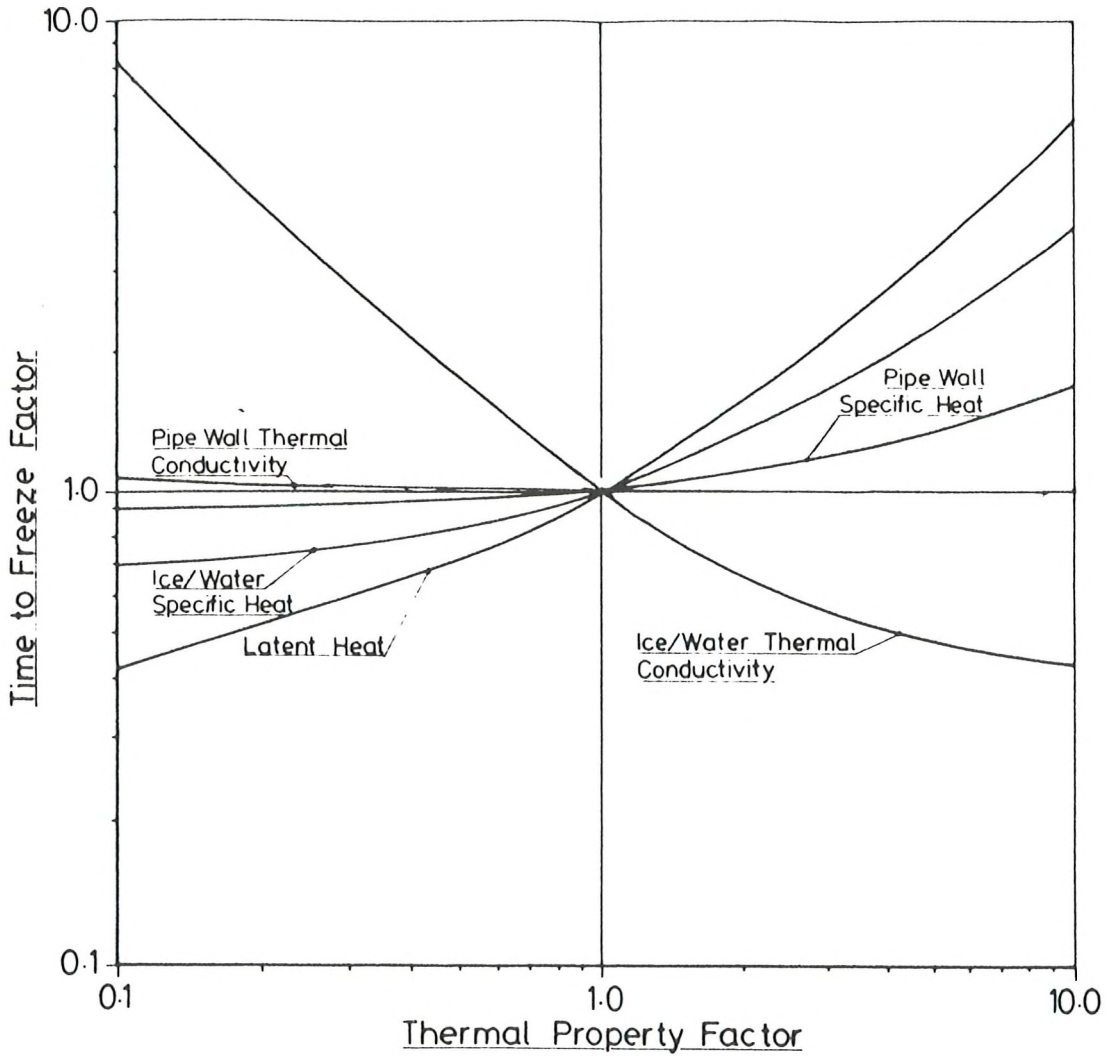

Fig. 5.8 Effect of varying thermal properties on the predicted time to freeze